JOURNAL OF RESEARCH

OF THE U.S. GEOLOGICAL SURVEY

U. OF I. LIB.
DOCUMENTS
APR 2 1973
CHICAGO CIRCLE

JANUARY-FEBRUARY 1973
VOLUME 1, NUMBER 1

Scientific notes and summaries of investigations in geology, hydrology, and related fields

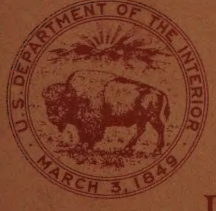

U.S. DEPARTMENT OF THE INTERIOR

UNITED STATES DEPARTMENT OF THE INTERIOR
ROGERS C. B. MORTON, Secretary
GEOLOGICAL SURVEY
V. E. McKelvey, Director

For sale by the Superintendent of Documents, U.S. Government Printing Office, Washington, D.C., 20402. Order by SD Catalog No. JRGS. Annual subscription rate $8.50 (plus $2.25 for foreign mailing). Single copy $1.50. Make checks or money orders payable to the Superintendent of Documents.

Send all subscription inquiries and address changes to the Superintendent of Documents at the above address.

Purchase orders should not be sent to the U.S. Geological Survey library.

Library of Congress Card No. 72-600241

The Journal of Research consists of six issues a year (January-February, March-April, May-June, July-August, September-October, November-December) published in Washington, D.C., by the U.S. Geological Survey. It contains papers by members of the Geological Survey on geologic, hydrologic, topographic, and other scientific and technical subjects.

The Journal supersedes the short-papers chapters (B, C, and D) of the former Geological Survey Research ("Annual Review") series of professional papers. The synopsis chapter (A) of the former Geological Survey Research series will be published as a separate professional paper each year.

Correspondence and inquiries concerning the Journal (other than subscription inquiries and address changes) should be directed to the Managing Editor, Journal of Research, Publications Division, U.S. Geological Survey, Washington, D.C., 20242.

Papers for the Journal should be submitted through regular Division publication channels.

The Secretary of the Interior has determined that the publication of this periodical is necessary in the transaction of the public business required by law of this Department. Use of funds for printing this periodical has been approved by the Director of the Office of Management and Budget through February 11, 1975.

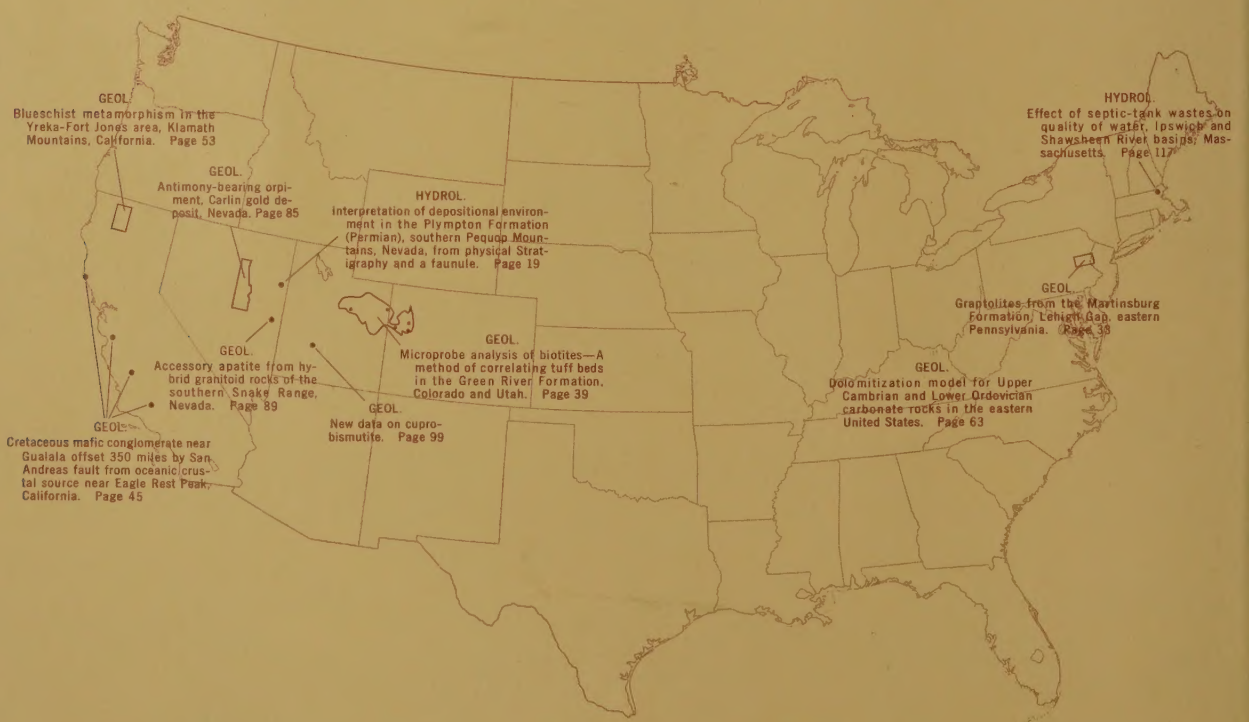
GEOL.
Blueschist metamorphism in the Yreka-Fort Jones area, Klamath Mountains, California. Page 53
GEOL.
Antimony-bearing orpiment, Carlin gold deposit, Nevada. Page 85
HYDROL.
Interpretation of depositional environment in the Plympton Formation (Permian), southern Pequop Mountains, Nevada, from physical Stratigraphy and a faunule. Page 19
GEOL.
Accessory apatite from hybrid granitoid rocks of the southern Snake Range, Nevada. Page 89
GEOL.
Microprobe analysis of biotites—A method of correlating tuff beds in the Green River Formation, Colorado and Utah. Page 39
GEOL.
New data on cuprobismutite. Page 99
GEOL.
Cretaceous mafic conglomerate near Gualala offset 350 miles by San Andreas fault from oceanic crustal source near Eagle Rest Peak, California. Page 45
HYDROL.
Effect of septic-tank wastes on quality of water, Ipswich and Shawsheen River basins, Massachusetts. Page 117
GEOL.
Graptolites from the Martinsburg Formation, Lehigh Gap, eastern Pennsylvania. Page 38
GEOL.
Dolomitization model for Upper Cambrian and Lower Ordovician carbonate rocks in the eastern United States. Page 63

GEOGRAPHIC INDEX TO ARTICLES

[See Contents for articles concerning areas outside the United States and articles without geographic orientation]

126

JOURNAL OF RESEARCH

of the

U.S. Geological Survey

Vol. 1 No. 1 Jan.—Feb. 1973

CONTENTS

Foreword, by V. E. McKelvey, Director, U.S. Geological Survey III
Abbreviations IV

GEOLOGIC STUDIES

Geologic implications of the Apollo 14 Fra Mauro breccias and comparison with ejecta from the Ries Crater, Germany ..... *E. C. T. Chao* 1
Interpretation of depositional environment in the Plympton Formation (Permian), southern Pequop Mountains, Nev., from physical stratigraphy and a faunule ..... *E. L. Yochelson and G. D. Fraser* 19
Graptolites from the Martinsburg Formation, Lehigh Gap, eastern Pennsylvania ..... *J. B. Epstein and W. B. N. Berry* 33
Microprobe analysis of biotites—A method of correlating tuff beds in the Green River Formation, Colorado and Utah ..... *G. A. Desborough, J. K. Pitman, and J. R. Donnell* 39
Cretaceous mafic conglomerate near Gualala offset 350 miles by San Andreas fault from oceanic crustal source near Eagle Rest Peak, Calif. ..... *D. C. Ross, C. M. Wentworth, and E. H. McKee* 45
Blueschist metamorphism in the Yreka-Fort Jones area, Klamath Mountains, Calif. ..... *P. E. Hotz* 53
Dolomitization model for Upper Cambrian and Lower Ordovician carbonate rocks in the eastern United States ..... *L. D. Harris* 63
Determination of gold in phosphates by activation analysis using epithermal neutrons ..... *J. J. Rowe* 79
Rapid determination of sulfur in rocks ..... *Leonard Shapiro* 81
Antimony-bearing orpiment, Carlin gold deposit, Nevada ... *A. S. Radtke, C. M. Taylor, and Chris Heropoulos* 85
Accessory apatite from hybrid granitoid rocks of the southern Snake Range, Nev. ..... *D. E. Lee, R. E. Van Loenen, and R. E. Mays* 89
New data on cuprobismutite ..... *C. M. Taylor, A. S. Radtke, and C. L. Christ* 99

HYDROLOGIC STUDIES

Chemical composition of a saline lake on Enderbury Island, Phoenix Island Group, Pacific Ocean ..... *D. W. Brown and R. A. Gulbrandsen* 105
A rapid method for the determination of radioactive cesium isotopes in water ..... *V. J. Janzer* 113
Effect of septic-tank wastes on quality of water, Ipswich and Shawsheen River basins, Massachusetts ..... *G. B. Morrill III and L. G. Toler* 117
The great Tunisian flood ..... *F. E. Clarke* 121

Recent publications of the U.S. Geological Survey ..... Inside of back cover

FOREWORD

Publication of the "Journal of Research of the U.S. Geological Survey" is an evolutionary advance in the publications program of the Geological Survey. The Journal is an outgrowth of the 13-year series of Geological Survey professional papers entitled "Geological Survey Research," also known informally as the "Annual Review" series.

The Geological Survey Research series was begun in 1960 as a means of more rapid publication of the results of Geological Survey research. Over a span of several years it evolved into a series of annual volumes containing four chapters each, one of which (chapter A) was an annual summary of results of Survey activities during the year, and the other three of which (chapters B, C, and D) were collections of short scientific papers. The short papers were primarily of two types—some were announcements of new discoveries or observations on problems of limited scope, whereas others were summaries of the conclusions of larger investigations that were to be published in greater detail later. An annual summary will continue to be published as a separate professional paper each year; short papers of the type that formerly appeared in chapters B, C, and D will now be published in the Journal of Research. The Journal will also contain listings of recently released Survey publications.

The Journal, which will be published six times a year, will enable the Survey to make the results of its research more readily available to readers. It will be easier to acquire because of its availability by subscription as well as on an individual-copy basis. Moreover, use of annual printing contracts will permit closer control of publication schedules.

The Journal shows more completely than any other Survey publication the wide range of research done by the Geological Survey. Papers will be drawn from all Divisions and all disciplines of the Survey, and thus will present a wide spectrum of subject matter in the earth sciences and related fields. This is in harmony with the interdisciplinary approach that is followed more and more in the study of problems in the natural sciences.

Just as the Journal has evolved from an earlier publication series, it is anticipated that it will continue to develop in style, format, and content in order better to meet future publications needs.

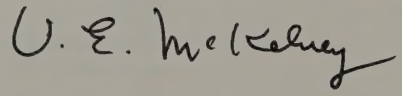

V. E. McKelvey
Director

ABBREVIATIONS

[Singular and plural forms for abbreviations of units of measure are the same]

A	angstrom units
A^3	cubic angstroms
a-c	alternating current
b.y.	billion years
cm	centimeters
cm^2	square centimeters
cm^3	cubic centimeters
cpm	counts per minute
cu ft	cubic feet
cu mi	cubic miles
eV	electron volts
emu	electromagnetic units
ft	feet
g	grams
gal	gallons
gpd	gallons per day
hr	hours
in.	inches
kb	kilobars
kg	kilograms
km	kilometers
km^2	square kilometers
km^3	cubic kilometers
kV	kilovolts
l	liters
lb	pounds
m	meters
m	molal (concentration)
m^2	square meters
m^3	cubic meters
MeV	million electron volts
mg	milligrams
ml	milliliters
mm	millimeters
mol	moles
mr	milliroentgens
mV	millivolts
m.y.	million years
μ	microns
μm	micrometers
μmhos	micromhos
n	neutrons
N	normal (concentration)
ng	nanograms
nm	nanometers
Oe	oersteds
pCi	picocuries
pH	pH (measure of hydrogen ion activity)
ppb	parts per billion
ppm	parts per million
rad	radiometric
rpm	revolutions per minute
sec	seconds
sq ft	square feet
sq mi	square miles
yr	years

Jour. Research U.S. Geol. Survey
Vol. 1, No. 1, Jan.–Feb. 1973, p. 1–18

GEOLOGIC IMPLICATIONS OF THE APOLLO 14 FRA MAURO BRECCIAS AND COMPARISON WITH EJECTA FROM THE RIES CRATER, GERMANY

By E. C. T. CHAO, Washington, D.C.

Work done in cooperation with the National Aeronautics and Space Administration under NASA contracts T-75412 and W13,130

Abstract.—On the basis of petrographic and laboratory and active seismic data for the Fra Mauro breccias, and by comparison with the nature and distribution of the ejecta from the Ries crater, Germany, some tentative conclusions regarding the geologic significance of the Fra Mauro Formation on the moon can be drawn. The Fra Mauro Formation, as a whole, consists of unwelded, porous ejecta, slightly less porous than the regolith. It contains hand-specimen and larger size clasts of strongly annealed complex breccias, partly to slightly annealed breccias, basalts, and perhaps spherule-rich breccias. These clasts are embedded in a matrix of porous aggregate dominated by mineral and breccia fragments and probably largely free of undevitrified glass. All strongly annealed hand-specimen-size breccias are clasts in the Fra Mauro Formation. To account for the porous, unwelded state of the Fra Mauro Formation, the ejecta must have been deposited at a temperature below that required for welding and annealing. Large boulders probably compacted by the Cone crater event occur near the rim of the crater. They probably consist of a similar suite of fragments, but are probably less porous than the formation. The geochronologic clocks of fragments in the Fra Mauro Formation, with textures ranging from unannealed to strongly annealed, were not reset or strongly modified by the Imbrian event. Strongly annealed breccia clasts and basalt clasts are pre-Imbrian, and probably existed as ejecta mixed with basalt flows in the Imbrium Basin prior to the Imbrian event. The Imbrian event probably occurred between 3.90 or 3.88 and 3.65 b.y. ago.

Prior studies of Apollo 14 breccias (Warner, 1972; Jackson and Wilshire, 1972; Wilshire and Jackson, 1972; Chao and others, 1972) show that thermally metamorphosed, strongly annealed breccias are dominant among the hand specimens returned from the Fra Mauro site on the moon. Associated with these are porous, friable feldspathic breccias. A prevalent view (LSPET, 1971; Wilshire and Jackson, 1972; Warner, 1972; McKay and others, 1972) is that the strongly annealed breccias are representative of the Fra Mauro Formation. The Fra Mauro Formation is postulated to represent a hot ejecta blanket from the Imbrium Basin, deposited at a high temperature. Citing the thermal blanketing effect after deposition, proponents of this theory infer that materials of the ejecta were annealed, some more than others. The high temperature would have reset the geochronological clock of most if not all of the Fra Mauro materials. Hence the annealing or the age of thermal metamorphism would date the Imbrian event. Other investigators (Dence and others, 1972; Chao and others, 1972) seriously question this view.

In order to interpret the Fra Mauro Formation correctly, three important questions must be answered: (1) Are the well-annealed hand-specimen-size breccias representative of the entire Fra Mauro Formation, or are they only clasts in the Fra Mauro Formation? (2) Were the breccias of the Fra Mauro Formation annealed and welded together after deposition of the Imbrian ejecta at the Fra Mauro site? (3) How should the ages determined on various lithic fragments in the Fra Mauro breccias be interpreted, and what is the age of the Imbrian event?

In order to answer these questions, this paper presents (1) a schematic geologic cross section of the Fra Mauro site based on photogeologic and active seismic onsite data, (2) a summary of the petrology of the breccias of the Fra Mauro Formation, (3) a summary of the nature and distribution of the ejecta of the Ries crater, illustrated by a geologic cross section and map, and a reconstruction of the development of this crater for comparison with the Imbrium Basin structure, and (4) an interpretation of age data and the age of the Imbrian event.

GEOLOGIC SETTING OF THE FRA MAURO SITE

The Fra Mauro Formation has been interpreted as an ejecta blanket excavated and ejected from the Imbrium Basin by the Imbrian impact event which produced the Imbrium multi-ring structure (Eggleton, 1970). This generally accepted interpretation is based principally on the ejecta topography; hummocky ejecta deposits can be traced more or less continuously from the rim of the Imbrium Basin to the Fra Mauro site. The

Apollo 14 landing site is within the type locality of the Fra Mauro Formation (Wilhelms, 1970).

The geology of the Fra Mauro site can be best illustrated by a schematic geologic cross section from the Neighbor crater just north of the LM (lunar module) landing site in the west to beyond Cone crater in the east (fig. 1). The profile of the cross section is from T. W. Offield (unpub. data). Areas of impact ejecta, mostly from Cone crater, are determined by field geologic data (Swann and others, 1971). The thickness of the regolith layer and the estimated thickness of the Fra Mauro Formation are based on the active seismic experiment data of Watkins and Kovach (1972). Neighbor crater is interpreted photogeologically as of Eratosthenian age (Eggleton, 1970) on the basis of its subdued and degraded morphology. Cone crater is much more recent, about 25 m.y. old (Ar^{38} cosmic ray exposure age, Burnett and others, 1972); thus a thin layer of regolith is shown over the ejecta of Neighbor crater and none over the Cone crater ejecta because of its young age.

Cone crater, which is about 320 m in diameter and about 70 m deep, has penetrated the regolith layer into the Fra Mauro Formation. Hence the boulders and coarse ejecta around Cone crater should essentially be from the Fra Mauro Formation.

According to Watkins and Kovach (1972), the regolith layer at the Fra Mauro site is 8.5 m thick and has a compressional wave velocity of 104 m/sec. It probably consists of a mixture of fines, fragments, and chunks of porous regolith microbreccias, which are compacted from fines by small impact events with an effective pressure of only a few kilobars (Chao and others, 1971; Warren and others, 1971). Ray materials, some from the Copernicus crater and others from more distant sources, are probably also present in the regolith.

The compressional wave velocity of the material that underlies the regolith is 299 m/sec. It is easily distinguishable from that of the regolith. The thickness of this layer is calculated to be between 16 and 76 m. Watkins and Kovach (1972) interpreted this layer as the Fra Mauro Formation. They contend that in order to account for such velocity the material must have a porosity of between 35 and 55 percent. Hence the Fra Mauro Formation must be highly porous.

The pre-Fra Mauro Formation material is probably also porous ejecta, with a compressive wave velocity of greater than 370 m/sec (Watkins and Kovach, 1972). The upper limit of compressive wave velocity and the depth of this layer are not given. Cone crater probably did not penetrate beyond the Fra Mauro Formation. Otherwise, some of the clasts from the Cone crater ejecta might belong to the pre-Fra Mauro materials.

Samples from both the regolith and the Cone crater ejecta were collected. Among the hand specimens returned from the Fra Mauro site, two are basalts, 14310 and 14053; the rest are breccias. The location from which 14310 was collected is uncertain. It may have been collected near station G near the Triplet craters (Swann and others, 1971). Specimen 14053 was collected near the rim of the Cone crater; hence it came from the Fra Mauro Formation.

Many of the hand specimens of gray, coherent breccias were collected from boulder fields. Some are from small to car-size boulders from the Cone crater ejecta. For example, samples 14312, 14314, 14315, 14318, and 14319 were collected at station H, in a boulder field of the Cone crater ejecta nearest to the LM site (Swann and others, 1971). Hand-specimen-size samples of white friable breccias (14063 and 14082) and the largest moderately coherent gray breccia (14312) were collected near the rim of Cone crater; 14082 was chipped off a car-size boulder at the Cone crater rim. Brownish-gray friable to coherent breccias such as 14042, 14047, 14049, 14055, and

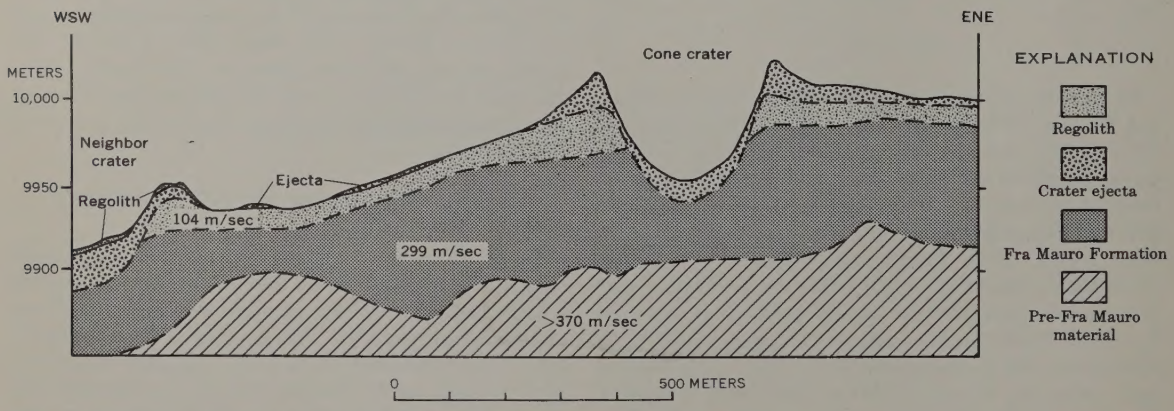

Figure 1.—Schematic geologic cross section of the Fra Mauro site. The section is drawn just north of the Apollo 14 lunar module landing site across Neighbor crater in the west to Cone crater in the east. Thickness of geologic units is principally based on active seismic data. Compressional wave velocities of some units are indicated on the cross section. The elevations shown in the vertical scale of the cross section are based on a reference elevation chosen to correspond to the mean radius of the moon of 1,738 km.

14301 were collected from areas mapped as regolith (Swann and others, 1971) east of the LM site.

DESCRIPTION OF FRA MAURO BRECCIAS

According to the genetic classification of Chao, Minkin, and Best (1972), the breccias from the Fra Mauro site can be divided into regolith microbreccias, Fra Mauro breccias, and spherule-rich microbreccias. Twenty-six hand-specimen-size breccias were so classified (table 1). The name Fra Mauro breccias was used because these samples were collected from the boulder field near the rim of Cone crater or from well-defined ejecta of the crater and hence they are derived from the Fra Mauro Formation. They also can be distinguished as different rock types from the regolith microbreccias. Among the hand specimens, the Fra Mauro breccias predominate over regolith microbreccias. Only two samples (14315 and 14318) are classified as spherule-rich microbreccias. Comparison of classification of the Apollo 14 breccias with that by Jackson and Wilshire (1972) has been given in a previous paper (Chao and others, 1972).

Table 1.—*Classification of Apollo 14 breccias based on the study of polished thin sections*

[Asterisk (*) indicates samples with fragment populations differing from others in same subgroup. From Chao, Minkin, and Best (1972)]

Classification	*Samples*
1. Regolith microbreccias:	
a. Unshocked, porous	14042, 14047, 14049, 14055, 14301*
b. Compact, nonporous	14313
c. Shocked	14307
2. Fra Mauro breccias:	
a. Unannealed or slightly annealed feldspatic breccias.	14063, 14082
b. Partly annealed breccias	14312
c. Strongly annealed (thermally metamorphosed) breccias:	
Unshocked	14006, 14270, 14311
Shocked	14066, 14171, 14303, 14304, 14305, 14306*, 14308, 14312*, 14314, 14319*, 14320
3. Spherule-rich microbreccias	14315*, 14318

Porous regolith microbreccias are poorly compacted and weakly lithified lunar fines. They generally consist chiefly of fine-grained mineral and lithic fragments and a large amount (about 50 volume percent) of glass particles. Their bulk chemical composition is generally very similar to or identical with that of the regolith. Except for a small but significant amount of exotic lithic and glass particles, and except for ray materials, most of the lithic fragments in the regolith are derived from underlying formation. In this paper, we are mainly concerned with the interpretation of the Fra Mauro breccias, rocks representative of the Fra Mauro Formation.

The Fra Mauro breccias are very complex and are characterized by a wide range of clast types and textures. The two principal types of Fra Mauro breccias are (1) a light-gray to grayish-white, generally friable, porous, unannealed to slightly annealed, highly feldspathic microbreccia, and (2) a gray, slightly or partly annealed (found principally among the coarse fines) to strongly annealed, highly coherent microbreccia. These two types are believed to be representative of the white and gray materials in the boulders near the rim of Cone crater. Most hand specimens of Fra Mauro breccias contain more than six types of lithic fragments, some as many as ten or more. Not only does the fragment population of a single Fra Mauro breccia vary, but the texture of the matrix which surrounds various clasts also varies in porosity and extent of annealing.

Principal lithic fragments

The principal categories of lithic fragments in the Fra Mauro breccias are (1) very fine grained hornfelsed noritic microbreccias and annealed fragment-laden glasses, (2) somewhat coarser grained micronorite hornfelses, (3) dark devitrified glasses, and (4) basalts. Other types of lithic fragments generally form less than a few percent of any single hand-specimen-size breccia. Most abundant among these less common types are vitrophyres, fine-grained anorthositic rocks, troctolitic rocks, and olivine-rich microbreccias. Some of the less common lithic types often occur as small inclusions in either the very fine grained hornfelsed noritic microbreccias or in annealed fragment-laden glasses or devitrified glasses. Some of the small breccia chips contain several types of breccia fragments of an earlier generation.

The very fine grained hornfelsed noritic microbreccias and annealed fragment-laden glasses may be roughly divided into three subtypes (1a, 1b, and 1c) on the basis of grain size of matrix (Chao and others, 1972). The extremely fine grained type (1c) is an annealed vuggy to vesicular impactite glass charged with fine xenocrysts and a few plagioclase-rich xenoliths. The two slightly coarser grained types (1a and 1b) probably have similar origin but are better annealed than those of type 1c. Their appearance is that of a vuggy hornfelsed noritic microbreccia with xenocrysts set in a granular crystalline matrix. The xenocrysts consist dominantly of plagioclase, clinopyroxenes, orthopyroxenes, and olivine, and subordinately of ilmenite, pink spinel, and nickel-iron. They are embedded in an annealed matrix consisting of lath-shaped to irregular grains of plagioclase, stubby and irregular grains of orthopyroxenes, and platy to granular ilmenite. The color of a noritic microbreccia fragment is directly related to the grain size and proportions of minerals in its annealed matrix, particularly ilmenite.

Micronorite hornfels fragments (type 2, Chao and others, 1972) are also hornfelsed fragmental rocks, but they are coarser and better recrystallized than the hornfelsed noritic microbreccias, and distinctions between fragments and matrix are more obscure. These fragments consist mainly of calcic plagioclase and inclusion-laden orthopyroxenes. They contain accessory olivine, ilmenite, a phosphate mineral, zircon, and a

distinct silica and potassium-rich mesostasis. This fine-grained mesostasis gives the rock a microporphyritic texture despite the fact that the amount of the mesostasis is small. Limited or large amounts of xenocrysts of plagioclase, pyroxene, and olivine, and a few xenoliths are also present. Some of the fragments are distinctly vesicular; most are vuggy.

A distinctive type of dark, devitrified glass with xenocrysts (type 3, Chao and others, 1972) is abundant in a few of the breccias. It contains abundant skeletal plagioclase crystals and crystallites, sparse ilmenite, and is more feldspathic than noritic in composition.

Basalt fragments (type 4, Chao and others, 1972) are rare in all Fra Mauro breccias except 14321. There are several types which differ in amounts of plagioclase, pyroxene, and ilmenite, and in textures. The most abundant type is a subophitic to ophitic basalt with pyroxene dominating over calcic plagioclase. These are commonly olivine bearing, and contain 1–5 percent ilmenite.

Fragment population and textures

Light-gray to grayish-white, friable, porous, largely unannealed, highly feldspathic microbreccias.—Samples 14063 and 14082 are representative of this type. Sample 14063 contains two main types of lithic fragments, brownish-gray devitrified glass (lithic type 3) and grayish-white micronorite hornfels (lithic type 2). The fragment populations measured from two thin sections are shown in table 2. Most large crystal or lithic fragments are free of evidence of mineral reactions. The rock is porous (38–51 percent porosity, table 2, see also figures 2 and 3). Because one of these samples, 14082, was chipped off from a car-size boulder near the Cone crater rim, this type of porous, largely unannealed feldspathic breccia is closely associated with the gray Fra Mauro breccias described below.

Figure 2.—A chip of slightly annealed grayish-white, friable, porous, feldspathic Fra Mauro breccia 14063. It contains fragments of well-recrystallized micronorite hornfels (right center) and dark-purplish-brown devitrified glass (center and lower center).

Gray, partly annealed, moderately coherent breccia.—In hand specimen size the only example of this type is 14321, the largest rock returned from the Fra Mauro site. It contains abundant black fragments of annealed extremely fine grained fragment-laden glass (lithic type 1c), and several types of basalt fragments (with subophitic olivine basalt similar to 14053 dominant) in a matrix of broken basaltic fragments (fig.

Table 2.—*Fragment population of some Apollo 14 Fra Mauro and spherule-rich breccias, in volume percent*

[From Chao, Minkin, and Best (1972)]

	Slightly annealed feldspathic		Partly annealed	Annealed	Spherule rich
	14063,13	14063,46	14321,241	14303,2	14315,8
Fine-grained hornfelsed noritic microbreccia (1a).	....	....	....	44.4	0.2
Very fine grained hornfelsed noritic microbreccia (1b).	0.8	3.1	....	11.1	16.8
Extremely fine grained annealed fragment-laden glass (1c).	....	....	59.3	....	2.6
Micronorite hornfels (2)	21.4	33.0	.3	....	.8
Feldspathic devitrified glass (3).	16.0	19.0	3.3	....	....
Basalt (4)	.6	.3	27.5	8.2	.4
Other lithic fragments	11.0	1.8	1.0	3.6	3.6
Devitrified glass spheroids	....	....	....	....	38.9
Undevitrified glass spheroids	....	....	....	....	1.9
Mineral fragments and matrix (<25μ).	50.3	42.9	8.2	32.6	34.8
Pores	(51)[1]	(38)[1]	(18)[1]	....	....

[1] The percentage of pores is excluded in mineral mode.

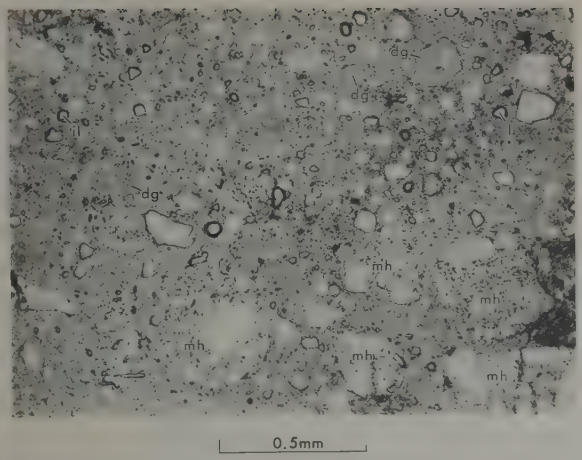

Figure 3.—Photomicrograph of part of polished thin section 14063,13, slightly annealed feldspathic Fra Mauro breccia, showing fragments of micronorite hornfels (mh, mottled light-gray fragments) and devitrified glass (dg, gray areas with high relief surrounded by thin black borders). Pores and open space are medium gray in low relief. Light areas in high relief are ilmenite (il). Reflected light.

4). A tentative estimate of the fragment population based on a large thin section is given in table 2.

Strongly annealed, coherent, gray breccias.—This is the most abundant group of hand specimens returned from the Fra Mauro site (table 1). They are generally light gray to gray. Except for vugs in annealed lithic or devitrified glass fragments within them, they are nonporous (fig. 5). In polished thin sections viewed in reflected light, fragment boundaries are distinguished only by changes in texture (fig. 6). Reaction rims around olivine and spinel are common (Wilshire and Jackson, 1972). Under high magnification, xenocrysts and surrounding matrix grains show interlocking textures.

The complexity of the strongly annealed breccias is evident from the wide range of fragment populations that they contain. Each sample contains a collection of annealed breccia fragments of multiple generations or sources. Hornfelsed noritic microbreccia fragments with strongly contrasting grain size of recrystallized matrix occur side by side (fig. 6). Preliminary study of thin sections shows that 14303, 14305, and 14311 are similar in fragment population, with fine-grained and very fine grained hornfelsed noritic microbreccia fragments (types 1a and 1b) dominant (see 14303 in table 2) and basalt fragments present in small but significant amounts.

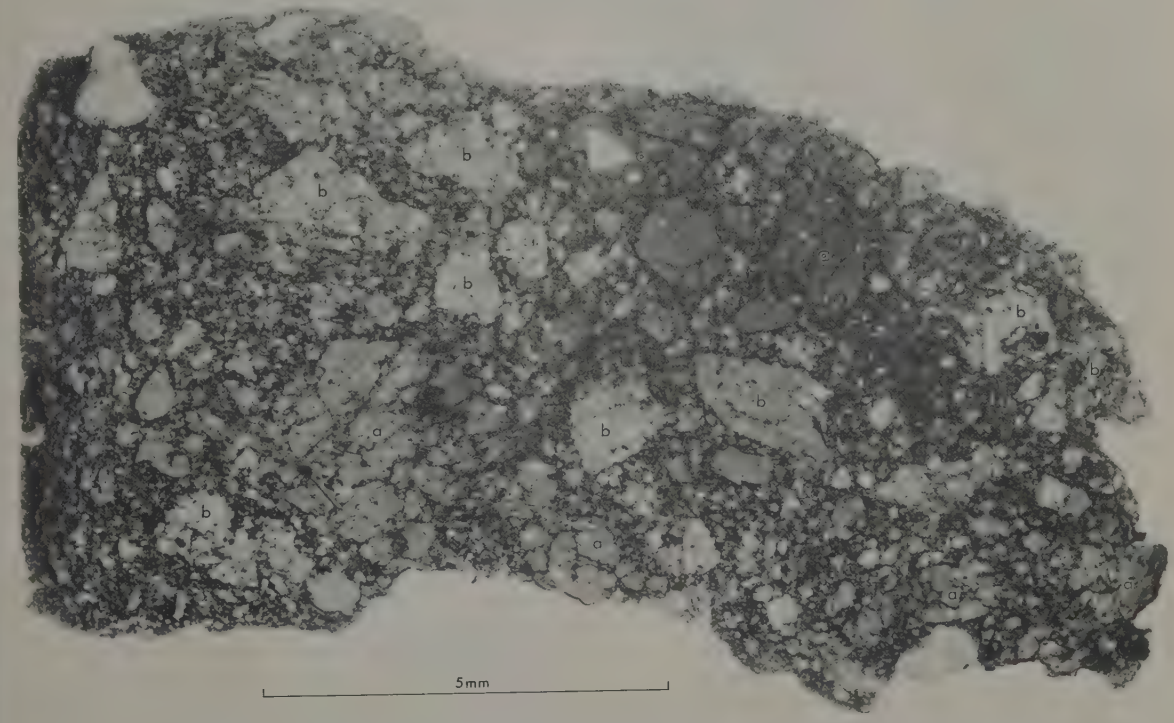

Figure 4.—Photomicrograph of polished thin section 14321,241-4, a partly annealed Fra Mauro breccia, showing the dominant fragments of basalt (b) and annealed extremely fine grained fragment-laden glass (a) in a granular matrix of moderate porosity. Reflected light.

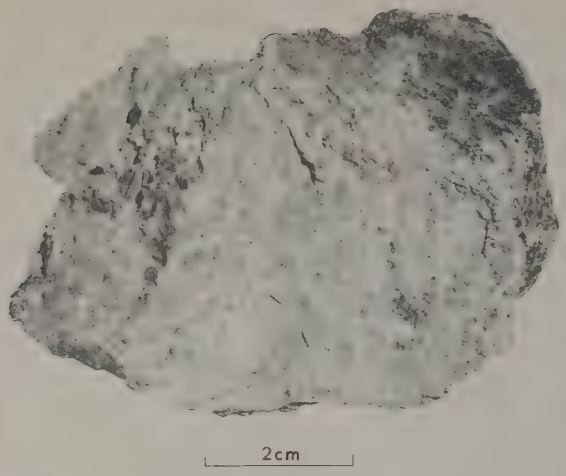

Figure 5.—Hand specimen of strongly annealed Fra Mauro breccia 14319, showing fragments of annealed very fine grained noritic microbreccias (gray) in a well-annealed lighter colored matrix. Dark fragment in upper left is an annealed extremely fine grained fragment-laden glass.

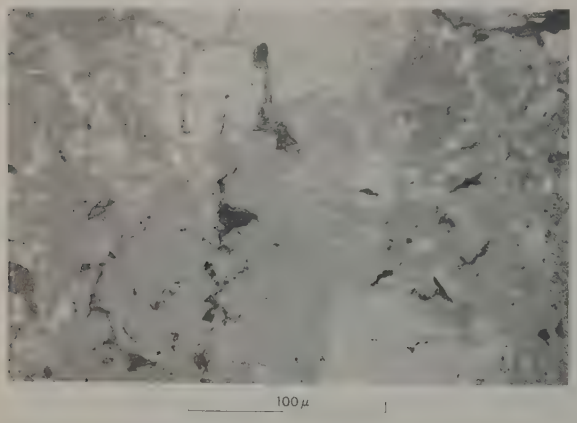

Figure 6.—Photomicrograph of an area in the upper right corner of specimen shown in figure 7, showing the details of the grain boundaries between different types of fragments. The texture is typical of a completely annealed breccia. The fragment of annealed fine-grained noritic microbreccia on the left is characterized by blebs and platy crystals of ilmenite. A fragment of annealed extremely fine grained fragment-laden glass is in the upper right center. Pyroxene fragments (light gray) are in upper center and lower right center; a plagioclase-rich gray fragment is in lower center. Dark areas are holes and fractures. Reflected light.

14312 and 14319 are similar to each other and distinct from the previous samples in fragment population. In these samples, fine-grained hornfelsed microbreccias (type 1a) are dominant, as in the first group, but basalts are very rare, and dark, devitrified pyroxene-dominant vitrophyric fragments generally free of xenocrysts are common. The fragment population of 14306 is unique. This sample contains fragments of fine-grained to very fine grained hornfelsed noritic microbreccias, similar to those in the other samples, but in addition dark extremely fine grained annealed fragment-laden glass is abundant, appreciable numbers of fragments of felsite (micrographite) are present, and basalt fragments are virtually absent (fig. 7).

Despite this complexity of textures of fragments, however, there appear to be only a few dominant types if bulk composition alone is considered. The predominant fragments in all the Fra Mauro breccias are noritic, troctolitic, or highly feldspathic (anorthositic gabbro). Basaltic rocks in which mafic minerals predominate over plagioclase are sparse, and ilmenite-rich rocks are extremely rare.

All the glass or glassy fragments in the well-annealed breccias are completely devitrified or annealed. Some are very well recrystallized. Undevitrified glass is very rare or absent. The amount of devitrified or annealed glass is generally less than 50 percent, less than the amount of mineral and crystalline rock fragments present.

Among the xenocrysts and crystalline rock fragments present in the well-annealed breccias, fragments with evidence of moderate to strong shock (such as vitrification and vesiculation) are generally lacking. Nearly all the well-annealed Fra Maura breccias are clasts made up of aggregates of crushed impact ejecta that have undergone only low shock. Effects of shock compression can be observed in many of the well-annealed hand-specimen-size breccias. They were probably produced by the Cone crater event.

Spherule-rich microbreccias.—Two microbreccias (14315 and 14318) are of this type and are characterized by abundant devitrified spherules and spheroids of varied composition, and by subrounded to rounded lithic fragments whose long dimensions are alined in a subparallel manner (particularly in 14315). The fragment population for 14315,8 is given in table 2. 14315 is nonporous and thoroughly indurated. 14318 contains fewer devitrified glass spheroids and more lithic fragments. How 14315 and 14318 are related to the Fra Mauro breccias is not clear.

Porosity and seismic velocity

Porosity of breccias reflects the degree of shock compaction (Chao and others, 1971) and annealing, and is reflected in the compressive seismic wave velocities. The compressive seismic wave velocity in Apollo 11 regolith microbreccia 10046 (26 percent porosity) measured by Anderson and others (1970) is 1.20 km/sec. The velocity in a similar microbreccia, 10065 (bulk density of 2.34 g/cm^3 and estimated porosity of about 22 percent), measured by Kanamori and others (1970) is 1.50 km/sec. The compressive seismic wave velocity in Apollo 14 regolith microbreccia 14313 (estimated porosity of 21 per-

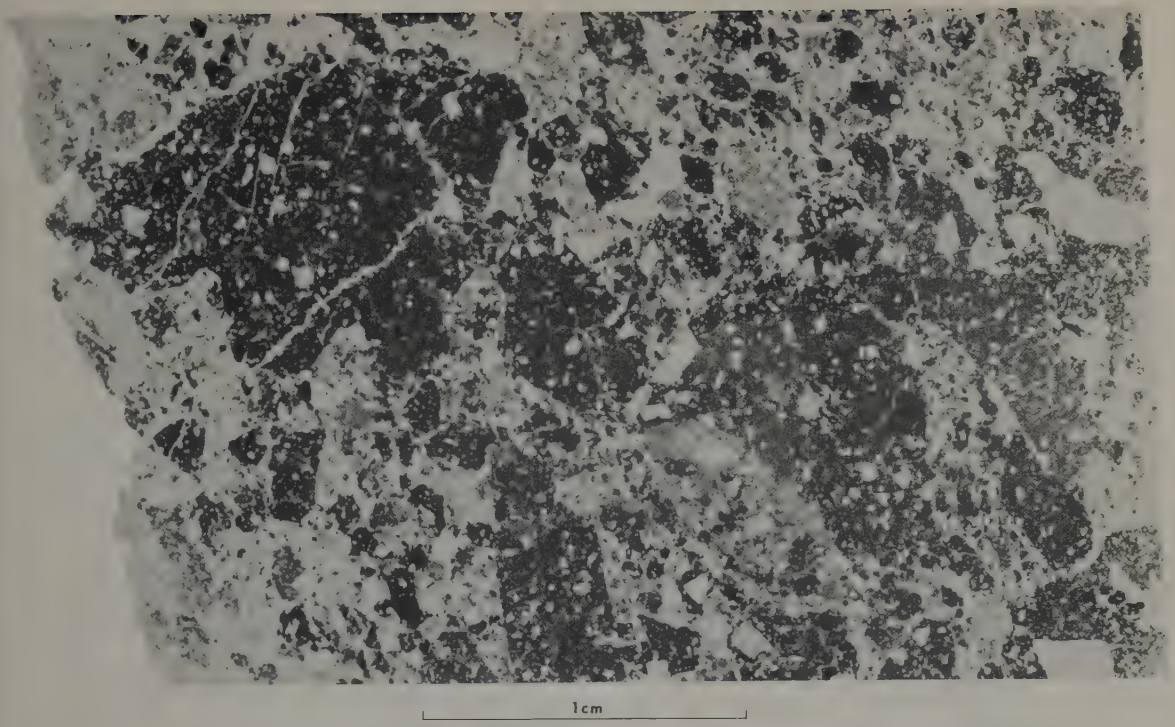

Figure 7.—Photomicrograph of polished thin section 14306,58, a strongly annealed Fra Mauro breccia. The black fragments are annealed very fine grained noritic microbreccias. The gray fragments are annealed fine-grained noritic microbreccias. The gradation in gray reflects the contrast in grain size. The sample is nonporous and strongly annealed. Transmitted plane-polarized light.

cent) is 2.25 km/sec (Mizutani and others, 1972). In contrast, Apollo 14 well-annealed Fra Mauro breccia 14311 has a much higher seismic velocity measured by the same authors, 5.65 km/sec. This seismic velocity is even higher than many of the Apollo 12 basalts measured (4.30 km/sec for 12052, 3.27 km/sec for 12065, Kanamori and others, 1971; 2.51–3.32 km/sec for 12063, 1.79–2.04 km/sec for 12018, Warren and others, 1971).

THE NATURE AND DISTRIBUTION OF THE EJECTA AND THE RECONSTRUCTED DEVELOPMENT OF THE RIES CRATER

Probably the best preserved terrestrial meteorite crater larger than 20 km in diameter is the Ries crater (Rieskessel) in southern Bavaria, Germany. The general structure and the stratigraphic section and basement crystalline rocks underlying the Ries are now fairly well known (Schmidt-Kaler, 1969; Dressler and others, 1969). Although partly eroded, the ejecta of the Ries are well preserved. A condensed summary of the reconstructed development of the Ries crater is given below. This summary includes the nature and distribution of the ejecta, their sequence of production and ejection trajectories. This summary is based on selected published literature and limited personal observations of the Ries ejecta material in the laboratory and during three short field trips in 1961, 1964, and 1971.

The geologic literature of the Ries crater is voluminous. A review of this literature up to 1969 citing earlier reviews by Löffle, Kranz, Preuss, and Barthel was made by Preuss (1969). A collection of many of the recent investigations in geology, stratigraphy, geophysics, and petrology concerning the Ries, including a geologic map (1:100,000), was published in a single volume of Geologica Bavarica (no. 61, 1969). A separate brief review has been published by Dennis (1971).

Geologic setting

The Ries crater is on the Schwabian-Frankian Alb, a low cuesta or plateau that extends east-northeasterly across Bavaria. The Alb is underlain by gently southeastwardly dipping Mesozoic sedimentary rocks (fig. 8) which in turn unconformably overlie basement crystalline rocks of Hercynian and pre-Hercynian age. The basement

Figure 8.—Geologic map of the Ries crater. Compiled from large-scale geologic maps and the 1:100,000 geologic map by Hüttner, Schmidt-Kaler, and Treibs (1969).

crystalline rocks consist of fine-grained to medium-coarse-grained granodiorite, dioritic and granitic rocks, granitic gneisses, amphibolites, and dark lamprophyres and other dike rocks. They have been described by Dressler and others (1969). According to Schmidt-Kaler (1969), Wirth (1969), and Preuss (1969), the reconstructed Ries sedimentary section consists of 700 to nearly 1,000 m of chiefly Mesozoic sedimentary rocks. In ascending order, these rocks consist of (1) Rotliegendes sandstones and shales (Permian?, 30 to 200 m) and some limestones in the upper part (Muschelkalk about 50 m), (2) Triassic Keuper sandstones and shales (about 250 m), (3) Lias (Black Jura) bluish-gray shales (about 30 m), (4) Dogger (Brown Jura) shale and oolitic and pisolitic ferruginous sandstone (about 140 m), and (5) Malm (White Jura) limestones consisting of thin-bedded limestone followed by massive limestone (about 300 m). Both geologic and geophysical data show that the bottom of the Ries crater lies within the basement crystalline rocks. Hence the crater has penetrated a minimum of several hundred meters of Mesozoic sedimentary rocks. After the crater was formed, the crater depression was filled with upper Miocene fossiliferous lacustrine deposits of shales and limestones having a maximum estimated thickness of about 350 m (Angenheister and Pöhl, 1969). Hence, based on the geology and the potassium-argon ages determined on Ries glass (Gentner and Wagner, 1969), the Ries crater was formed in late Miocene time about 14.5 m.y. ago. Since that time the crater and its ejecta have been partly eroded. Pleistocene loess and other periglacial deposits cover parts of the structure.

Nature of ejecta

Because of the distinctive lithologies of the various Mesozoic formations and the basement crystalline rocks, four types of ejecta can be recognized on the basis of the dominant lithic types in the ejecta: (1) suevite, a breccia rich in fragmental glass and containing lithic fragments predominantly of crystalline rock, (2) crystalline rock breccia, consisting of fractured and brecciated blocks of granitic rocks, amphibolites, and other metamorphic basement crystalline rocks, (3) "Bunte breccia," a mixed breccia of predominantly variegated shale and sandstone, limestone, and some crystalline rocks, and (4) "Gries," an intensely shattered and finely brecciated limestone. The nature of these four types of ejecta is summarized below.

Suevite, a term traced to Sauer (1901), is a poorly sorted, unstratified, brownish-gray, moderately indurated breccia deposit. The rock is soft, somewhat compacted, and moderately coherent because of cementation in many instances by secondary minerals. It resembles tuff-breccia but contains abundant strongly shocked granitic rock fragments and abundant glass particles and "bombs" (fig. 9). This unique rock type is found only in the vicinity of the Ries and nowhere else in Germany. Petrographic descriptions of suevite have been

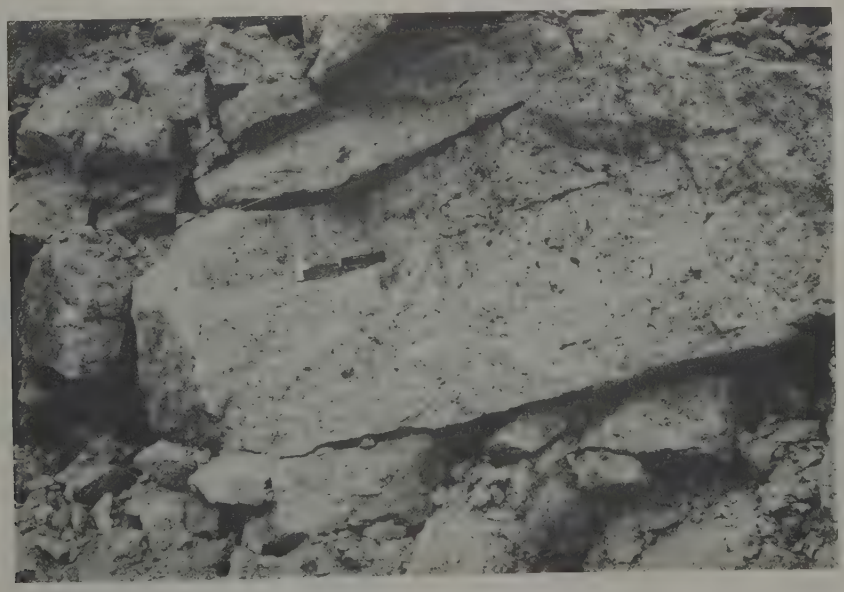

Figure 9.—Suevite, west side of quarry wall in Otting, Ries, Germany. Dark fragments are glass. White fragments are granitic rocks, and many are strongly shocked. The lack of bedding is characteristic. The area selected for fragment count is outlined by strings.

given by Sauer (1901), Oberdorfer (1905), and Ackermann (1959) from the volcanic point of view. Suevite was reinterpreted by Shoemaker and Chao (1961) and Chao and Littler (1963) as impact ejecta on the basis of the shock effects in fragments and the occurrence of coesite and stishovite in strongly shocked fragments of granitic rocks. Additional evidence of shock or meteorite impact origin of suevite was reported later by Chao (1967, 1968), Engelhardt and Stöffler (1968), and Engelhardt and others (1968, 1969). Hence the impact origin of the Ries crater has been firmly established.

In suevite the fragment size varies from less than a millimeter to a little more than 25 cm (Chao, unpub. data). Glass bombs are as much as 25 cm. Most bombs appear to have cooled quickly and show no sign of recrystallization or annealing, although small clusters of trichites of pyroxene are present in some samples. A small number show more extensive devitrification. There is no mineral reaction of any kind between adjacent fragments. Except for a thin veneer of small particles, most fragments adjacent to the glass bombs do not stick to the glass.

Other than glass, most of the fragments in suevite are mineral fragments and fragments of granitic crystalline rocks. Some of the lithic fragments are coated by glass whose composition may be similar to or different from the rock fragment; thus the glasses coating such fragments are not products of in-place melting of the enclosed fragment. The predominant crystalline rock types in suevite appear to vary with respect to their geographic location in the ejecta deposits, perhaps reflecting the proximity to the sources of the basement crystalline rocks. Suevite also contains small amounts of shale, sandstone, and limestone fragments; a few of these show evidence of fusion and thermal metamorphism.

Fragment population data on suevite are sparse. Some estimates of the proportions of glass "bombs" in suevite were reported by Ackermann (in Engelhardt and others, 1969), and a fragment count of sedimentary fragments in suevite was done by Barani (in Engelhardt and others, 1969). Fragment counts, by a method similar to the Rosiwal method, of those fragments in suevite larger than 1 cm were made on outcrops of suevite in several quarries in the Ries by the author in 1971. The lithology of each rock fragment and the degree of shock of granitic fragments were determined with a 20× hand lens. These fragment counts were obtained from outcrop areas of about 1 m^2. Hand samples of breccias containing only fragments finer than 1 cm from the same outcrops were collected. Fragment population study of these samples in thin sections has yet to be completed.

A preliminary fragment count (table 3) indicates that the Ries suevite contains a very high percentage (50–75) of glass fragments. Where the glass fragment content is high, fragments of strongly shocked crystalline rock predominate over moderately shocked fragments. Fragment count of a sample of suevite from St. George's Church in Nördlingen shows that as the percentage of glass fragments decreases, the quantities of the moderately shocked granitic fragments and sedimentary rock fragments from the overlying Mesozoic section increase notably.

Table 3.–*Fragment population, in percent of fragments larger than 1 cm, determined for suevite from the Ries crater area, Germany*

	Locality				
	Otting	Hainsfarth	Bollstadt	Aufhausen	St. George's Church
Vesicular glass.	74.7	70.0	67.9	62.4	51.5
Granodiorite, moderately shocked.	4.2	1.0	....	.9	4.8
Granodiorite, strongly shocked.	9.0	4.0	5.7	7.3	2.4
Granite gneiss, moderately shocked.	.6	9.0	3.8	3.7	5.4
Granite gneiss, strongly shocked.	4.2	9.0	13.2	18.3	....
Glass-coated fragments.	4.8	2.0	1.9	2.8	6.1
Shales, sandstones.	1.8	5.0	5.7	3.7	19.4
Limestones	....	....	1.9	.9	7.9
Metamorphic rocks.	.6	....	Trace	....	2.4

Crystalline rock breccias consist of intensely shattered and highly fractured house-size or larger blocks of basement crystalline rocks (monomict) and breccias of mixed varieties of crystalline rocks (polymict; see Stöffler in Engelhardt and others, 1969). The monomict breccias are generally deeply weathered and highly friable. The intense shattering is the only shock effect observed; evidence of shock strong enough to produce plastic deformation is generally absent (see also Stöffler in Engelhardt and others, 1969). The polymict crystalline rock breccias, such as those from Meyer's Keller (about 2 km south of Nördlingen), contain many lithic fragments that show a somewhat greater degree of shock (see also Stöffler in Engelhardt and others, 1969). Some of these breccias also contain mixed bunte breccias, but the degree of mixing between crystalline rock breccias and bunte breccias appears to be very limited. Most of the polymict breccias are slightly to moderately coherent. Because of weathering, they are highly friable and crumbly. Fragment size is seriate rather than bimodal. The maximum degree of shock effects observed so far in fragments in crystalline rock breccias is low to moderate (classification presented in Chao, 1968). The presence of vesiculated rocks or glasses has not been reported from any crystalline rock breccias so far. There is no evidence of annealing or welding of fragments.

Bunte breccia is weakly to moderately coherent, variegated, mixed breccia, consisting predominantly of variegated shales and sandstones of Keuper, Lias, and Dogger, and limestones of Malm. Descriptions of bunte breccias have been summarized

by Hüttner (1969) and by W. Schneider (in Engelhardt and others, 1969). Although the proportions of kinds of sedimentary rocks vary, and a small number of basement crystalline rock fragments are commonly present, bunte breccias consist of fragments derived principally from the lower part of the Mesozoic section (fig. 10). According to Schneider (in Engelhardt and others, 1969) fragments from the lower part of the Mesozoic section tend to be more abundant in the upper part of the bunte breccias and those from the upper part of the Mesozoic section tend to be abundant in the lower part, similar to an inverted section. He also noted that blocks of older Mesozoic sedimentary rocks are more abundant near the crater rim and that fragments from the upper Mesozoic section are more abundant in bunte breccias farther away from the rim. Bunte breccias in general are free of fragments that have undergone any optically detectable shock effects.

The Gries consists chiefly of light-gray to yellowish-white intensely shattered, highly fractured and brecciated limestone derived largely from Malm. A description of the nature and occurrences of Gries was given by Hüttner (1969). Figure 11 shows some detail of a quarry wall in this type of material. Besides intense shattering, calcite in thin sections of such limestones shows abundant shock-induced lamellar twinning. Because of the lack of experimental shock data on calcite, the shock undergone by most of the brecciated limestones can only be estimated, but the shock effects are clearly all of low degree.

Relative abundance and distribution of the Ries ejecta materials

The best exposures showing the relationships of the different types of Ries ejecta are in quarries and roadcuts. The ejecta deposits were also exposed in a 2-m deep trench for an oil pipeline extending from north of Nördlingen to Gansheim (Treibs, 1965). The areal distribution of the ejecta is shown on the geologic map (fig. 8). The vertical distribution is illustrated in the geologic cross section from Hainsfarth in the northeast to beyond Eglingen in the southwest (fig. 12).

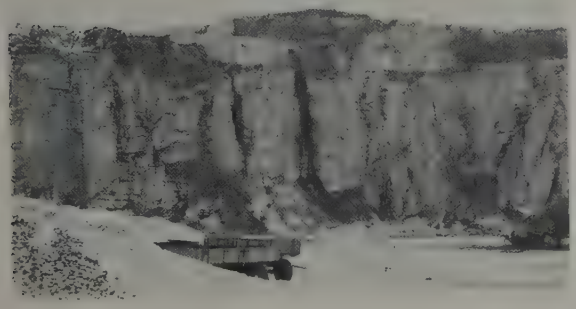

Figure 10.—North wall of Harburg-N quarry, showing large blocks of Jurassic limestone (light) in loosely cemented bunte breccia overlying flat-lying to gently dipping Jurassic limestone of the crater wall. The contact is marked by a striated surface (Schliff-Fläche). Bulldozer in lower right provides scale.

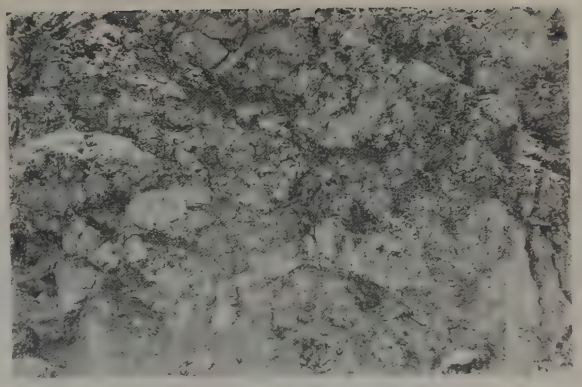

Figure 11.—Fractured, brecciated, and shattered limestone of the Gries (limestone breccia) exposed in a quarry wall near Wörnitzstein. Bedding structures in the limestone have been obliterated. Hammer in lower right provides scale.

The total amount and the relative abundance of the different types of Ries ejecta can be roughly estimated because (1) the reconstructed thickness of the sedimentary section is available, (2) the position of the undisturbed crystalline rocks corresponding to the bottom of the crater cavity has been estimated to be 1 to 1.4 km below the normal unconformity contact (Angenheister and Pöhl, 1969), and (3) the diameter of the crater is known (average 23 km). Thus, the calculated total amount of Ries ejecta is about 400 km^3, of which 155 km^3 are crystalline rock breccias and suevite and 245 km^3 are sedimentary rock breccias (bunte breccias and Gries). It is evident from the geologic map (fig. 8) that the bulk of the fallback and fallout breccias are the crystalline breccias and suevite, whereas the throwout breccias are dominated by the sedimentary rock breccias. The crystalline rock breccias and suevite occur within a distance about equal to one crater radius of the rim of the crater. The sedimentary rock breccias are distributed about a crater diameter or more beyond the crater rim.

Within the crater, suevite, as fallback breccia, occurs below the upper Miocene lacustrine sediments and above fractured or brecciated basement crystalline rocks. This is demonstrated by rocks from drill holes at Deiningen and Wörnitzostheim (Förstner, 1967) and by geophysical data (Angenheister and Pöhl, 1969). Although the thicknesses of suevite penetrated by the two drill holes are about 40 m and 85 m, respectively, the maximum thickness of suevite underlying the Ries lake deposits is estimated to range from 300 to 400 m (Angenheister and Pöhl, 1969). This estimate has not been verified by drilling.

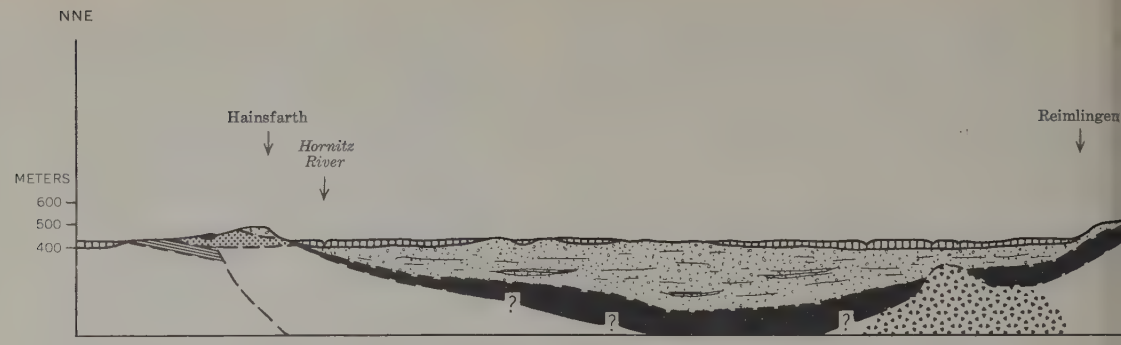

Figure 12.—Geologic cross section of the Ries from near Hainsfarth in the northeast to beyond Eglingen in the southwest. The profile is bas 1:100,000 topographic maps (AMS M642). The surface geology is from figure 8. Most of the subsurface geology is from geophysical (Angenheister and Pöhl, 1969; Reich and Horrix, 1955) and extrapolation from the drill holes at Deiningen and Wörnitzostheim (Förs 1967). Small suevite bodies near Eglingen have been slightly exaggerated in size. Bunte and limestone breccias extend nearly twice as fa from the crater rim as the scattered overlying suevite fallout breccias. Some of the former overlie Paleocene-Eocene(?) sand, which i thin to show in the cross section. The general limit of the crater cavity is marked by the dashed line.

The thickness of suevite deposits that occur outside of the crater rim ranges from a few meters to about 20 m. Suevite in many cases occurs in steep contact with bunte breccias or limestone breccias. As observed along the trench of the pipeline (Treibs, 1965) and in the Otting and Hainsfarth quarries (fig. 13) suevite overlies bunte breccia. This relationship has also been observed in other localities by other investigators (Hüttner, 1969; Engelhardt and others, 1969). The fact that suevite overlies the bunte breccias indicates that it was the last to settle or deposit and that it must have been produced in the late stage of cratering and have had a high-angle trajectory.

Shattered and fractured crystalline blocks and mixed crystalline rock breccias occur in isolated outcrops both within and outside the rim of the crater. Those that occur within the crater, such as that of Wennenberg, may be a part of a horseshoe-shaped crystalline rock wall that is buried beneath the surface sediments (Reich and Horrix, 1955). The other outcrops of crystalline rock breccias within the crater are located largely outside of this horseshoe ridge. This raised crystalline rockwall may be part of the brecciated and fractured basement rock which in most places underlies a blanket of suevite inside the crater. If so, instead of a central hill, the Ries structure has a horseshoe-shaped raised central ridge (now buried). Dislodged blocks and breccias of crystalline rocks also occur outside the crater rim but not far away from the rim. Areas of scattered crystalline rocks that extend farthest away from the rim are located near Stillnau and Hochstein southward from the rim and near Mündling, Sulzdorf, and Itzing in the southeastern part of Vorries.

Bunte breccias are best exposed high above the crater wall from quarries such as at Harburg-N, where large blocks of inverted and rotated Malm limestone were enclosed in the bunte breccia (fig. 10).

Although some outcrops of bunte breccias occur within the crater, most are outside the crater and far beyond outcrops of suevite and the crystalline rock breccias (fig. 12). In many localities bunte breccias were deposited on the flat-lying limestones of the crater wall, above a distinctly striated surface known as Schliff-Fläche similar to surfaces produced by glaciation (Wagner, 1964; Hüttner, 1969). The striated or grooved surfaces are generally flat, and the direction of striae or grooves is basically radial with respect to the crater (Wagner, 1964). Such surfaces were probably produced by gouging and scraping of fragments at the base of the bunte breccia as the large volume of brecciated rock moved laterally and radially away out of the crater. If so, the angles of trajectory of the bunte breccias were flat to low, and the bunte breccias were deposited before the suevite which was ejected at high angles. Such lateral movement of breccias is also strong evidence against a simple overturning of the stratigraphic section.

Deposits of brecciated and shattered limestone are most extensive to the southwest and southeast of the crater, outside the rim. They overlie the eroded surface of white Jurassic limestones, and in places occur on Paleocene and Eocene(?) sand (fig. 12). They are among the farthest throwout ejecta from the Ries (shown as an undifferentiated unit from bunte breccia, in fig. 8).

Rare veins of fine-grained clayey to sandy bunte breccia materials occur in shattered and brecciated limestone such as at Holheim (east quarry) and at the Schwalbenberg quarry near Fünfstetten. These veins were probably produced by injection of crushed rock along fractures when the crater was formed.

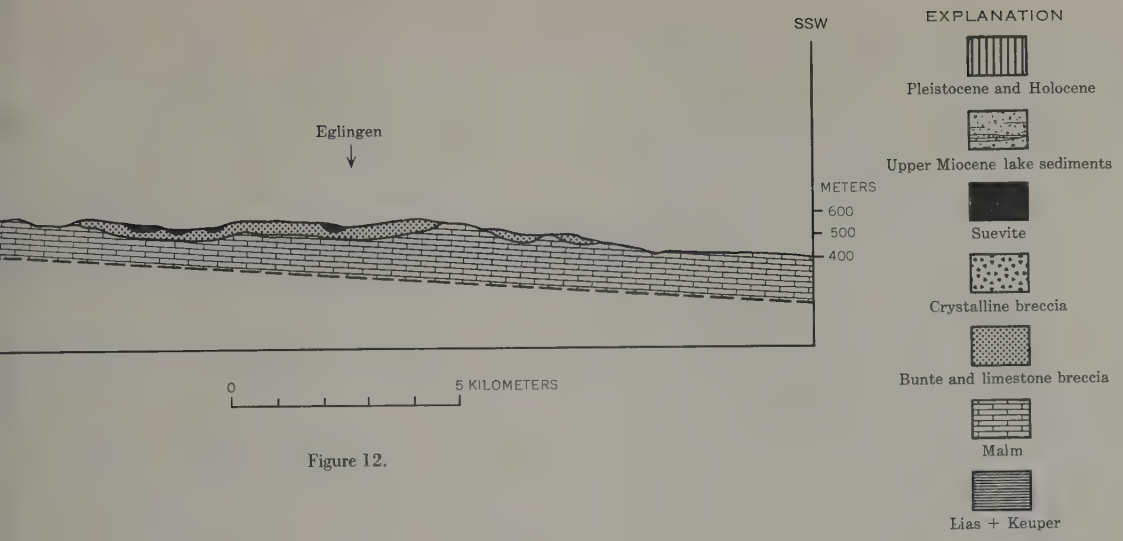

Figure 12.

Reconstructed development of the Ries crater

On the basis of the nature and the lateral and vertical distribution of the four types of Ries ejecta, the cratering event that produced the Ries structure may be reconstructed as outlined below. The entire sequence described occurred within a few seconds or perhaps even a fraction of a second.

1. The impacting body (probably a tough meteoritic body) penetrated at least 700 m of the Mesozoic section of the Schwabian-Frankian Alb; the crater bottom lies within the basement crystalline rocks.

2. Before the impacting body reached the basement crystalline rocks, the Mesozoic sedimentary rocks in the upper part of the section were compressed, crushed, dislodged, and ejected at low angles radially outward from the center of the crater. Movement of this material produced the slickensided surfaces above the crater wall. The deposits of this material are the bunte breccias and Gries and they occur farther out from the crater center than the other types of Ries ejecta deposits. The fragments are only weakly shocked, and the shock-induced temperatures must have been very low.

3. As the impacting body continued to penetrate, the compression of the target materials and the impacting body increased, and the shock-induced temperature in the immediate region appears to have exceeded the melting temperatures at just about the time that the impacting body penetrated the basement crystalline rocks. This is the moment when the peak transient pressure and shock-induced temperature were reached and when the particles of molten crystalline rocks and fragments of strongly shocked crystalline rocks were formed. Deposits of these materials are the suevites, and their distribution indicates that the fragments were ejected at high angles. Crystalline rock farther from the immediate area of penetration of the impacting body was moderately to weakly shocked and compressed; then it was fractured, brecciated, and dislodged and pushed up and, in part, beyond the crater rim to form deposits of throwout breccias.

Two modes of ejecta transport that have been proposed for impact cratering apparently were not important in the Ries event. These are: (1) jetting upon first contact between the impacting body and the target materials (suggested by small-scale hypervelocity impact experiments by Gault and others, 1968) and (2) base surge (suggested by underwater nuclear explosion, Young, 1965).

In laboratory hypervelocity experiments using principally lexan projectiles impacting in sand, Gault and others (1968) presented evidence of the occurrence of the highest temperature ejected phase by jetting upon contact. In the Ries event, however, producing a large amount of melt or glass by jetting upon contact is not consistent with the time sequence of development of suevite, the Ries ejecta deposit that contains the hottest ejecta. Suevite could not have been produced until the impacting body had penetrated, or the impact momentum had been transferred into, the basement crystalline rocks where the apparent origin of shock is located. The Ries impact event is probably similar to that proposed by Shoemaker (1960) in his analysis of the penetration mechanics of Meteor Crater in Arizona, where the meteorite-impact penetration by hydrodynamic flow was accomplished by lateral deflection of material at the leading end of the still fast-moving system of compressed rock and meteorite. The depth of penetration of the impacting body is directly proportional to the square root of the ratio of the density of the impacting body and the target material (cited by Shoemaker, 1960). Hence the impacting body producing the Ries structure should have been dense; probably an iron meteorite.

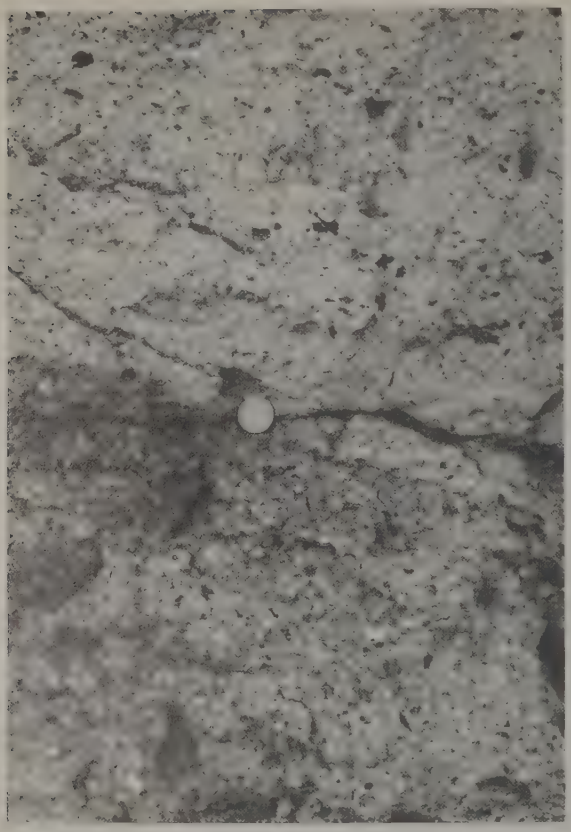

Figure 13—Weathered lighter colored suevite overlying slightly darker bunte breccia. Coin (2 cm in diameter) marks the contact. Glass (dark spots) is only found in suevite. Dark spots in bunte breccia below are gray and purple shale of Lias and Keuper, respectively. Hainsfarth quarry, north of Hainsfarth, Ries, Germany.

The phenomenon of base surge was first observed in the Baker underwater nuclear test at Bikini in 1947. According to Young (1965) the primary base surge of this test occurred 11 seconds after the detonation of the nuclear device. The primary base surge was produced by spillout, caused principally by gaseous (steam) expansion (G. A. Young, oral commun., 1972). The secondary base surge of this same test was the result of lateral displacement produced by the fallback of the ejected water column. Once produced, a base surge behaves more or less as a density current. Base surge has also been observed in cratering events of high-energy chemical explosives and underground detonation of nuclear devices (Young, 1965; R. B. Colton, written commun., 1963). The base-surge deposit of the Sedan nuclear event consists of dust a few millimeters thick, and the dust was so fine that its distribution was controlled by a southerly wind (R. B. Colton, written commun., 1963). The phenomenon of base surge has also been observed in recent volcanic eruptions (Moore, 1967). All these observed instances of base-surge transport have one thing in common—gaseous expansion—and all involve fluid- or gas-entrained materials that are only a small fraction of the total ejecta. None of the four major types of ejecta of the Ries can be identified as base-surge deposits. Although a small fraction of the rocks may be vaporized in a meteorite-impact event, meteorite impact (particularly on the outgassed moon) is not an effective process for the production of a lot of gases by vaporization of rocks. Because the occurrence of a base surge depends principally on gaseous expansion, it should not be surprising to find that base-surge deposits are not a part of impact-originated ejecta. Base surge produced by fallback also would be hardly significant.

INTERPRETATION OF THE FRA MAURO FORMATION

The data presented here suggest that the Fra Mauro Formation, as a whole, consists of unwelded, porous ejecta, slightly less porous than the regolith. It contains hand-specimen and larger size clasts of strongly annealed breccias, partly to slightly annealed breccias, basalts, and perhaps spherule-rich breccias. These clasts are embedded in a matrix of porous aggregate dominated by mineral and breccia fragments and probably largely free of undevitrified glass. Large boulders occurring near the rim of Cone crater are probably blocks of indurated materials of the Fra Mauro Formation. They are probably less porous than the underlying formation and could have been compacted into large blocks by the Cone crater event.

To account for the porous, unwelded state of the Fra Mauro Formation, the ejecta must have been deposited at a temperature below that required for welding and annealing. All strongly annealed hand-specimen-size breccias are clasts in this ejecta deposit. The strongly annealed breccia clasts and the basalt clasts are pre-Imbrian. They probably existed in an ejecta deposit, mixed perhaps with basalt flows, at the site of the Imbrian Basin prior to the Imbrian event.

Major lines of evidence for these interpretations are as follows:

1. Onsite active seismic data indicate that the Fra Mauro Formation has a compressive wave velocity much lower than that of porous regolith microbreccias, and almost as low as that of regolith material. This means that the material of the Fra Mauro Formation is more porous than porous regolith microbreccia and only slightly less porous than regolith. The seismic velocity of strongly annealed, nonporous Fra Mauro breccias such as 14311 is 5.65 km/sec, much greater than that of the formation as a whole and greater even than that of most of the basalts measured. If 14311 were representative of the whole Fra Mauro Formation, the seismic velocity of the formation as a whole would be more than an order of magnitude greater than it is. The low porosity of the formation

cannot be accounted for by fracturing of the annealed breccias. The returned clasts of strongly annealed Fra Mauro breccias are not intensely fractured. They are subrounded and coherent, neither bounded by angular fracture surfaces nor intensely shattered. Thus, the seismic data are not consistent with the view that the Fra Mauro Formation was deposited hot by the Imbrian event and that the annealing of the breccias occurred at the Fra Mauro site in this hot debris blanket. (Warner, 1972; Wilshire and Jackson, 1972; McKay and others, 1972).

2. Largely unannealed, very friable and porous feldspathic microbreccias, such as 14063, evidently coexist with strongly annealed breccias, resembling 14303 and 14311, in car-size boulders on the rim of the Cone crater. The difference in porosity and in degree of annealing between these two types of breccias is striking. If the strongly annealed breccias were annealed after deposition at the Fra Mauro site, it would be difficult to explain why the coexisting unannealed feldspathic breccias were not also strongly annealed.

3. The hand-specimen-size Fra Mauro breccias have a wide range of distinctive fragment populations and probably are products of different impact events in different source areas. Many contain fragments showing a wide range of annealed textures and fragments of breccias of still earlier generations. It is unlikely that a single impact event would produce an ejecta deposit that differed so radically in fragment population over very short distances, as would be required if the annealed breccias had been annealed at the Fra Mauro site.

4. The hottest ejecta deposit from the Ries crater, the suevite, shows little or no annealing after deposition. Suevite is characterized by a large amount of glass particles and significant amounts of strongly shocked fragments. Thus it had appreciable sources of internal heat. In contrast, the annealed breccias of the Fra Mauro Formation contain only small amounts of strongly shocked fragments and small amounts of material that was demonstrably hot glass when the breccia was formed. Without glasses and strongly shocked fragments as an internal source of heat, it is unlikely that these latter represent hot ejecta deposits.

5. By extrapolation, the distribution of the different types of ejecta deposits produced by the Ries event may be compared to the probable distribution of ejecta deposits produced by the Imbrian event. Such a comparison is informative in spite of the hazard that some drastic modification may be necessary because of the difference in size (Ries, 23 km in diameter; Imbrium, about 900 km in diameter) and the low gravity and the lack of atmospheric aerodynamic drag on the moon. The ejecta at the Fra Mauro site is about 450 km from the Carpathian Mountains, the southern rim of the Imbrium Basin, about one crater radius away. By analogy with the Ries crater, the ejecta at the Fra Mauro site should be equivalent to the bunte breccias and limestone breccias of the Ries, not to the suevite. If so, the Fra Mauro Formation at the Apollo 14 site was derived from the upper part of the stratigraphic section of the site of the Imbrian event and was probably transported at low-angle trajectories. The corresponding deposits from the Ries do not contain abundant strongly shocked material and were deposited at low temperatures, far below the temperatures necessary for annealing of the fragments within the ejecta. They were not products of jetting, nor were they transported laterally by base surge.

AGE OF FRAGMENTS IN FRA MAURO BRECCIAS AND AGE OF THE IMBRIAN EVENT

Several basalt samples (among them 14310, 14073, and 14053) have been dated both by the Rb-Sr and the ^{40}Ar-^{39}Ar methods. In addition, fragments from several breccias have been investigated by the ^{40}Ar-^{39}Ar method. The Rb-Sr or the ^{40}Ar-^{39}Ar age of an unmodified basalt is the age of crystallization or solidification of the basalt, but both shock and thermal metamorphism can modify isotopic ratios and cause the age dating methods to give younger ages than the age of crystallization. The age of thoroughly thermally annealed breccia or basalt should date the age of the thermal metamorphism. An example of one such thoroughly annealed and reequilibrated breccia is 12013 (Turner, 1970). The ^{40}Ar-^{39}Ar release pattern in this sample has a well-defined plateau; hence it is readily interpreted as the age of thermal metamorphism. Complex ^{40}Ar-^{39}Ar release patterns have been obtained for many fragments from Apollo 14 breccias, however, and these are not understood and the ages they yield cannot be interpreted at this time.

Age of basalt fragments

The age of 14310, a fine-grained feldspathic basalt, has been determined by Rb-Sr and ^{40}Ar-^{39}Ar methods to be 3.88 b.y. (Papanastassiou and Wasserburg, 1971; Wasserburg and others, 1972). Unfortunately, sample 14310 is not well documented and its location is uncertain. It has tentatively been located at station G (Swann and others, 1971). The Rb-Sr and ^{40}Ar-^{39}Ar age of another fragment of very similar basalt, 14073, is also 3.88 b.y. (Papanastassiou and Wasserburg, 1971; Wasserburg and others, 1972), and this sample was definitely collected at station G (Swann and others, 1971). These basalt fragments could have been excavated from the Fra Mauro Formation by either the center or the south crater of Triplet. However, it is also possible that both samples could be from ray ejecta from an unknown source and be unrelated to the Fra Mauro Formation.

A pyroxene-dominant basalt, 14053, was collected from station C2 from the Cone crater ejecta. Its Rb-Sr and ^{40}Ar-^{39}Ar age is 3.92–3.95 b.y. (Papanastassiou and Wasserburg 1971; Turner and others, 1971; Wasserburg and others, 1972; Schaeffer and others, 1972).

Two chips from an olivine-bearing pyroxene-dominant basalt (14072,6) collected from station C at the Cone crater rim were also dated by the ^{40}Ar-^{39}Ar method (York and others, 1972). Both have well-defined plateaus in their gas-release patterns indicating ages of 4.0 b.y.

Several fragments of basalt from the partly annealed Fra Mauro breccia 14321 have been investigated by the ^{40}Ar-^{39}Ar method by several laboratories. A basalt clast from 14321,191 gave an age of 3.95 b.y. (Papanastassiou and Wasserburg, 1971). Three basalt clasts from 14321,184 gave ^{40}Ar-^{39}Ar plateau ages of 3.90, 3.95, and 3.99 b.y. (York and others, 1972). A 72-mg sample consisting of multiple fragments of basalt clasts from 14321,144 gave an age of 3.92 b.y. (Turner and others, 1971). However, this multiple sample of basalt has a complex ^{40}Ar-^{39}Ar release pattern that is not easily interpreted, suggesting that the basalt clasts from 14321 may not all be of the same type or have the same thermal history.

Evidently we have two main groups of basalts, one group represented by the feldspathic basalts 14310 and 14073 yielding ages of 3.88 b.y., the other group represented by pyroxene-dominant basalts 14053, 14072, and clasts from 14321 yielding plateau ^{40}Ar-^{39}Ar ages of 3.90 to 4.0 b.y. Basalts of the latter group were all collected from the Cone crater rim and should have come from the Fra Mauro Formation. Basalts of the former group may or may not be derived from the Fra Mauro Formation.

Age of fragments in well-annealed breccias

Two clasts, one of basalt and one of annealed microbreccia, from sample 14303,13, a well-annealed Fra Mauro breccia, have been investigated by the ^{40}Ar-^{39}Ar method (Kirsten and others, 1972). The basalt clast shows a complex gas-release pattern but gives a high-temperature plateau age (800°–1,000°C) of 3.91±0.04 b.y. (Schaeffer and others, 1972). The gas-release pattern of the annealed microbreccia fragment shows a narrow plateau followed by a strong drop at temperatures above 800°C; the plateau age is reported to be 3.78±0.14 b.y. Perhaps these complex gas-release patterns and age differences between fragments indicate that annealing in sample 14303 has not proceeded to the same degree as in sample 12013, so that an age for the thermal metamorphism of the hand specimen cannot easily be determined. A breccia clast (No. 17) from 14066,21, another hand sample of well-annealed Fra Mauro breccia, was dated at 4.0 b.y. by the Rb-Sr method (Cliff and others, 1972). Again, the meaning of this age depends on the degree of reequilibration caused by the thermal metamorphism.

Age of fragments in slightly to partly annealed breccias

The ages of clasts in unannealed nonregolith breccias should reflect the last dominant event that these clasts underwent prior to incorporation in the unannealed breccias. The least annealed Fra Mauro breccia is probably 14063. Two separate clasts from 14063,37 have been studied by the ^{40}Ar-^{39}Ar method by Derek York (oral commun., 1972). The petrology of these clasts has not been described, but both gave well-defined plateau ages of 3.95 b.y. This suggests that some of the source materials of 14063 are 3.95 b.y. old. Since they have been largely unaffected by the Imbrian impact, their ages are useful as indicators of the maximum age of the Imbrian event.

Various chips of breccias from coarse fines 14167,6 and 14257,12 (Sutter and others, 1971) and from 14321 (Turner and others, 1971) have been investigated by the ^{40}Ar-^{39}Ar method. The gas-release patterns were complex; their origins are not understood and their age significance cannot be determined at present.

Age of the Imbrian event

The age of the youngest basalt clast from the Fra Mauro Formation should set an upper limit on the date of the Imbrian event. The youngest dated basalt clast clearly derived from the Fra Mauro material is from 14321, and its age is 3.90 b.y. Whether 14310 or 14073 are also from the Fra Mauro Formation is unknown. If they are, then the maximum age of the Imbrian event is 3.88 b.y.

The minimum age of the Imbrian event can be determined by geological reasoning. The Imbrian event must have occurred before 3.65 b.y., the age of the ilmenite basalt which filled Mare Tranquillitatis, for the Imbrian sculpture affected the basin wall of Mare Tranquillitatis but not the ilmenite basalts that filled it. Hence, the best estimate of the age of the Imbrian event that can be made with the data available at present is between 3.90 or 3.88 and 3.65 b.y.

ACKNOWLEDGMENTS

I thank my colleagues, Odette B. James, and Newell Trask for their helpful review of this paper. I am particularly indebted to Odette B. James for discussion of many aspects of this paper. I appreciate the assistance of Judith B. Best in the preparation of the map and geologic cross sections and some of the photomicrographs.

REFERENCES CITED

Ackermann, Wilhelm, 1959, Geologisch-petrographische Untersuchungen im Ries: Germany, Geol. Landesanst., Geol. Jahrb., v. 75 (1958), p. 135–182.

Anderson, O. L., Scholz, Christopher, Soga, Naohiro, Warner, Nicholas, and Schreiber, Edward, 1970, Elastic properties of a micro-breccia, igneous rock and lunar fines from Apollo 11 mission, *in* Apollo 11 Lunar Sci. Conf., Houston, Tex., 1970, Proc., V. 3, Physical properties: New York, Pergamon Press (Geochim. et Cosmochim. Acta Supp. 1), p. 1959–1973.

Angenheister, Gustav, and Pöhl, Jean, 1969, Die seismischen Messungen im Ries von 1948–1969: Geologica Bavarica, no. 61, p. 304 -326.

Burnett, D. S., Huneke, J. C., Podosek, F. A., Russ, G. P., III, Turner, G., and Wasserburg, G. J., 1972, The irradiation history of lunar samples [abs.], *in* Lunar Sci. Conf., 3d, Houston, Tex., 1972, Revised abs.: Houston, Tex., Lunar Science Institute, p. 105–107.

Chao, E. C. T., 1967, Shock effects in certain rock-forming minerals: Science, v. 156, no. 3772, p. 192–202.

—— 1968, Pressure and temperature histories of impact metamor-

phosed rocks—Based on petrographic observations, *in* French, B. M., and Short, N. M., eds., Shock metamorphism of natural materials—1st Conf., Greenbelt, Md., 1966, Proc.: Baltimore, Md., Mono Book Corp., p. 135–158.

Chao, E. C. T., Boreman, J. A., and Desborough, G. A., 1971, The petrology of unshocked and shocked Apollo 11 and Apollo 12 microbreccias, *in* Lunar Sci. Conf., 2d, Houston, Tex., 1971, Proc., V. 1, Mineralogy and petrology: Cambridge, Mass., MIT Press (Geochim. et Cosmochim. Acta Supp. 2), p. 797–816.

Chao, E. C. T., and Littler, Janet, 1963, Additional evidence for the impact origin of the Ries basin, Bavaria, Germany [abs.]: Geol. Soc. America Spec. Paper 73, p. 127.

Chao, E. C. T., Minkin, J. A., and Best, J. B., 1972, Apollo 14 breccias—General characteristics and classification, *in* Lunar Sci. Conf., 3d, Houston, Tex., 1972, Proc., v. 1, Mineralogy and petrology: Cambridge, Mass., MIT Press (Geochim. et Cosmochim. Acta Supp. 3), p. 645–659.

Cliff, R. A., Lee-Hu, C., and Wetherill, G. W., 1972, K, Rb, and Sr measurements in Apollo 14 and 15 material [abs.], *in* Lunar Sci. Conf., 3d, Houston, Tex., 1972, Revised abs.: Houston, Tex., Lunar Science Institute, p. 146–147.

Dence, M. R., Plant, A. G., and Traill, R. J., 1972, Impact-generated shock and thermal metamorphism in Fra Mauro lunar samples [abs.], *in* Lunar Sci. Conf., 3d, Houston, Tex., 1972, Revised abs.: Houston, Tex., Lunar Science Institute, p. 174–176.

Dennis, J. G., 1971, Ries structure, southern Germany, a review: Jour. Geophys. Research, v. 76, no. 23, p. 5394–5406.

Dressler, Burkhard, Graup, Günther, and Matzke, Klaus, 1969, Die Gesteine des kristallinen Grundgebirges im Nördlingen Ries: Geologica Bavarica, no. 61, p. 201–228.

Eggleton, R. E., 1970, Geologic map of the Fra Mauro region of the Moon, *in* Offield, T. W., and Eggleton, R. E., Geologic maps of the Fra Mauro region of the Moon: U.S. Geol. Survey Misc. Geol. Inv. Map I-708, sheet 2, scale 1:250,000.

Engelhardt, Wolf von., Hörz, F., Stöffler, D., and Bertsch, W., 1968, Observations on quartz deformation in the breccias of West Clearwater Lake, Canada, and the Ries basin, Germany, *in* French, B. M., and Short, N. M., eds., Shock metamorphism of natural materials—1st Conf., Greenbelt, Md., 1966, Proc.: Baltimore, Md., Mono Book Corp., p. 475–482.

Engelhardt, Wolf von, and Stöffler, D., 1968, Stages of shock metamorphism in the crystalline rocks of the Ries basin, Germany, *in* French B. M., and Short, N. M., eds., Shock metamorphism of natural materials—1st Conf., Greenbelt, Md., 1966, Proc.: Baltimore, Md., Mono Book Corp., p. 159–168.

Engelhardt, Wolf von, Stöffler, Dieter, and Schneider, Werner, 1969, Petrologische Untersuchungen im Ries: Geologica Bavarica, no. 61, p. 229–295.

Förstner, U., 1967, Petrographische Untersuchungen des Suevits aus den Bohrungen Deiningen und Wörnitzostheim im Ries von Nördlingen: Contr. Mineralogy and Petrology, v. 15, p. 281–308.

Gault, D. E., Quaide, W. L., and Oberbeck, V. R., 1968, Impact cratering mechanics and structures, *in* French, B. M., and Short, N. M., eds., Shock metamorphism of natural materials—1st Conf., Greenbelt, Md., 1966, Proc.: Baltimore, Md., Mono Book Corp., p. 87–99.

Gentner, Wolfgang, and Wagner, G. A., 1969, Altersbestimmungen an Riesgläsern und Moldaviten: Geologica Bavarica, no. 61, p. 296–303.

Hüttner, Rudolf, 1969, Bunte Trümmermassen und Suevit: Geologica Bavarica, no. 61, p. 142–200.

Hüttner, Rudolf, Schmidt-Kaler, Hermann, and Treibs, Walter, 1969, Anmerkungen zur geologischen Übersichtskarte (Beilage 1): Geologica Bavarica, no. 61, p. 451–454.

Jackson, E. D., and Wilshire, H. G., 1972, Classification of the samples returned from the Apollo 14 landing site [abs.], *in* Lunar Sci. Conf., 3d, Houston, Tex., 1972, Revised abs.: Houston, Tex., Lunar Science Institute, p. 418–420.

Kanamori, Hiroo, Mizutani, H., and Hamano, Y., 1971, Elastic wave velocities of Apollo 12 rocks at high pressures, *in* Lunar Sci. Conf., 2d, Houston, Tex., 1971, Proc., V. 3, Physical properties: Cambridge, Mass., MIT Press (Geochim. et Cosmochim. Acta Supp. 2), p. 2323–2326.

Kanamori, Hiroo, Nur, Amos, Chung, D. H., and Simmons, Gene, 1970, Elastic wave velocities of lunar samples at high pressures and their geophysical implications, *in* Apollo 11 Lunar Sci. Conf., Houston, Tex., 1970, Proc., V. 3, Physical properties: New York, Pergamon Press (Geochim. et Cosmochim. Acta Supp. 1), p. 2289–2293.

Kirsten, T., Deubner, J., Horn, P., Kaneoka, I., Kiko, J., Schaeffer, O. A., Thio, S. K., 1972, The rare gas record of Apollo 14 and 15 samples, *in* Lunar Sci. Conf., 3d, Houston, Tex., 1972, Proc. V. 2: Cambridge, Mass., MIT Press (Geochim. et Cosmochim. Acta Supp. 3). [In press]

LSPET (Lunar Sample Preliminary Examination Team), 1971, Preliminary examination of lunar samples from Apollo 14: Science, v. 173, no. 3998, p. 681–693.

McKay, D. S., Clanton, U. S., Heiken, G. H., Morrison, D. A., and Taylor, R. M., 1972, Vapor phase crystallization in Apollo 14 breccias and size analysis of Apollo 14 soils [abs.], *in* Lunar Sci. Conf., 3d, Houston, Tex., 1972, Revised abs.: Houston, Tex., Lunar Science Institute, p. 529–531.

Mizutani, H., Fujii, N., Hamano, Y., Osako, M., and Kanamori, H., 1972, Elastic wave velocities and thermal diffusivities of Apollo 14 rocks [abs.], *in* Lunar Sci. Conf., 3d, Houston, Tex., 1972, Revised abs.: Houston, Tex., Lunar Science Institute, p. 547–549.

Moore, J. G., 1967, Base surge in recent volcanic eruptions: Bull. Volcanol., v. 30, p. 337–363.

Oberdorfer, R., 1905, Die vulkanischen Tuffe des Ries bei Nördlingen: Ver. vaterl. Naturkunde Württemberg, Jahresh., v. 61, p. 1–40.

Papanastassiou, D. A., and Wasserburg, G. J., 1971, Rb-Sr ages of igneous rocks from the Apollo 14 mission and the age of the Fra Mauro Formation: Earth and Planetary Sci. Letters, v. 12, no. 1, p. 36–48.

Preuss, Ekkehard, 1969, Einführung in die Ries-Forschung: Geologica Bavarica, no. 61, p. 12–24.

Reich, Hermann, and Horrix, W., 1955, Geophysikalische Untersuchungen im Ries und Vorries und deren geologische Deutung: Germany, Geol. Landesanst., Geol. Jahrb. Beihefte, Heft 19, 119 p.

Sauer, Adolf, 1901, Petrographische Studien an den Lavabomben aus dem Ries: Ver. vaterl. Naturkunde Württemberg, Jahresh., v. 57, p. lxxxviii.

Schaeffer, O. A., Husain, L., Sutter, J., and Funkhouser, J., 1972, The ages of lunar material from Fra Mauro and the Hadley Rille–Appenine Front area [abs.], *in* Lunar Sci. Conf. 3d, Houston, Tex., 1972, Revised abs.: Houston, Tex., Lunar Science Institute, p. 675–677.

Schmidt-Kaler, Hermann, 1969, Versuch einer Profildarstellung für das Rieszentrum vor der Kraterbildung (Beilage 5): Geologica Bavarica, no. 61, p. 38–40.

Shoemaker, E. M., 1960, Penetration mechanics of high velocity meteorites, illustrated by Meteor crater, Arizona: Internat. Geol. Cong., 21st, Copenhagen, 1960, Rept., pt. 18, p. 418–434.

Shoemaker, E. M., and Chao, E. C. T., 1961, New evidence for the impact origin of the Ries basin, Bavaria, Germany: Jour. Geophys. Research, v. 66, p. 3371–3378.

Sutter, J. F., Husain, L., and Schaeffer, O. A., 1971, ^{40}Ar-^{39}Ar ages from Fra Mauro: Earth and Planetary Sci. Letters, v. 11, no. 4, p. 249–253.

Swann, G. A., Trask, N. J., Hait, M. H., and Sutton, R. L., 1971, Geologic setting of the Apollo 14 samples: Science, v. 173, no. 3998, p. 716–719.

Treibs, W., 1965, Beitrag zur Kenntnis der Geologie des Rieses und östlichen Vorries nach Beobachtungen in Rohrgraben der Rhein-Donau-Ölleitung: Geologica Bavarica, no. 55, p. 310–316.

Turner, G., 1970, ^{40}Ar-^{39}Ar age determination of lunar rock 12013: Earth and Planetary Sci. Letters, v. 9, no. 2, p. 177–180.

Turner, G., Huneke, J. C., Podosek, F. A., and Wasserburg, G. J., 1971, ^{40}Ar-^{39}Ar ages and cosmic ray exposure ages of Apollo 14 samples: Earth and Planetary Sci. Letters, v. 12, no. 1, p. 19–35.

Wagner, G. H., 1964, Kleintektonische Untersuchungen im Gebiet des Nördlinger Ries: Geol. Jahrb., v. 81, p. 519–600.

Warner, J. L., 1972, Apollo 14 breccias–Metamorphic origin and classification [abs.]. *in* Lunar Sci. Conf., 3d, Houston, Tex., 1972, Revised abs.: Houston, Tex., Lunar Science Institute, p. 782–784.

Warren, N., Schreiber, E., Scholz, C., Morrison, J. A., Norton, P. R., Kumazawa, M., and Anderson, O. L., 1971, Elastic and thermal properties of Apollo 11 and Apollo 12 rocks, *in* Lunar Sci. Conf., 2d, Houston, Tex., 1971, Proc., V. 3. Physical properties: Cambridge, Mass., MIT Press (Geochim. et Cosmochim. Acta Supp. 2), p. 2345–2360.

Wasserburg, G. J., Turner, G., Tera, F., Podosek, F. A., Papanastassiou, D. A., and Huneke, J. C., 1972, Comparison of Rb-Sr, K-Ar, and U-Th-Pb ages; lunar chronology and evolution [abs.], *in* Lunar Sci. Conf., 3d, Houston, Tex., 1972, Revised abs.: Houston, Tex., Lunar Science Institute, p. 788–790.

Watkins, J. S., and Kovach, R. L., 1972, Apollo 14 active seismic experiment: Science, v. 175, no. 4027, p. 1244–1245.

Wilhelms, D. E., 1970, Summary of lunar stratigraphy–Telescopic observations: U.S. Geol. Survey Prof. Paper 599-F, 47 p.

Wilshire, H. G., and Jackson, E. D., 1972, Petrology and stratigraphy of the Fra Mauro Formation at the Apollo 14 site: U.S. Geol. Survey Prof. Paper 785, 26 p.

Wirth, E., 1969, Ein Profil vom Malm bis ins Rotliegendes südöstlich des Rieses–Kurzprofit der Erdölaufschlussbohrung Daiting 1: Geologica Bavarica, no. 61, p. 41–42.

York, D., Kenyon, W. J., and Doyle, R. J., 1972, ^{40}Ar-^{39}Ar ages of Apollo XIV and XV samples [abs.], *in* Lunar Sci. Conf., 3d, Houston, Tex., 1972, Revised abs.: Houston, Tex., Lunar Science Institute, p. 822–824.

Young, G. A., 1965, The physics of the base surge: White Oak, Md., U.S. Naval Ordnance Laboratory Rept. NOLTR 64–103, 284 p.

Jour. Research U.S. Geol. Survey
Vol. 1, No. 1, Jan.–Feb. 1973, p. 19–32

INTERPRETATION OF DEPOSITIONAL ENVIRONMENT IN THE PLYMPTON FORMATION (PERMIAN), SOUTHERN PEQUOP MOUNTAINS, NEVADA, FROM PHYSICAL STRATIGRAPHY AND A FAUNULE

By ELLIS L. YOCHELSON and GEORGE D. FRASER,
Washington, D.C., Denver, Colo.

Abstract.—Field mapping in the southern part of the Pequop Mountains has shown the presence of a major structural high which has profoundly affected the stratigraphy of Pennsylvanian and Lower Permian beds; lesser effects of this high persisted into the later Permian. Within the Park City Group (Permian), the Plympton Formation, overlying the Kaibab Limestone, is divided informally into five parts. The uppermost Plympton has yielded silicified fossils. The faunule studied is characterized by the scaphopod *Plagioglypta* and by bellerophontacean and neritacean gastropods, suggestive of a middle Permian age. Specimens are worn, and several lines of evidence suggest that this is a high-energy beach deposit associated with a residual high. The interpretation supplements the field evidence of a hiatus between the Plympton and the overlying Gerster Formation. Other occurrences of elements of the faunule in the equivalent Phosphoria rock complex are noted, but only a few were probably deposited in a high-energy beach environment. A new species of *Naticopsis* that has the color pattern preserved is named and described.

This paper is a combination of specific paleontological information regarding a silicified scaphopod faunule found locally at the top of the Plympton Formation and general stratigraphic information about a larger part of the thick Permian section in the southern Pequop Mountains, northeast Nevada (fig. 1). The paper compares environmental interpretations based on the independent laboratory study of the fossils with environmental interpretations based on field study of the physical stratigraphy. The two studies complement and reinforce each other; both indicate high-energy beach or shallow-water conditions and a local disconformity at the top of the Plympton where the fossils were found. The stratigraphic study suggests further that an ancient positive area, which was transverse to the present mountains and which had its south flank in the area of this report, controlled Late Pennsylvanian–Early Permian stratigraphic patterns and exerted a lesser modifying effect on subsequent depositional patterns throughout latest Paleozoic and earliest Mesozoic time.

The outcrop of silicified mollusks discussed (USGS locality 23819-PC) is at the top of the Plympton Formation on the northwest side of the hill 700 feet north of the water tank in sec. 3, T. 31 N., R. 65 E., Spruce Mountain 4 quadrangle, Nevada (fig. 2). That 15-minute quadrangle includes nearly all the southern Pequop Mountains. The railroad tunnel through a pass in the northern part of the quadrangle, 28 miles west of Wendover, Nev., is a convenient dividing line between the southern and northern Pequop Mountains, as those terms are used in this report.

The parts of this report relating primarily to identification and interpretation of the silicified mollusks are by Yochelson; the new species is named by him. The parts relating to physical stratigraphy and its interpretation are by Fraser. Fraser was aided in his fieldwork (1965–71) by H. A. Waldrop (1966), M. T. Naney (1968), and G. P. Eager (1970–71). Fieldwork included geologic mapping of the quadrangle, section measuring, and special phosphate studies in the basal part of the Plympton Formation; these activities are part of a continuing program of Federal land classification by the U.S. Geological Survey.

RECURRENT STRUCTURAL CONTROL OF STRATIGRAPHIC CHANGES

In the southern Pequop Mountains, obvious stratigraphic changes occur in the upper part of the Pennsylvanian and lower part of the Permian section, thousands of feet below the Plympton Formation and seemingly unrelated to it. Nevertheless, these older changes are so great and the structures which caused them so large that one suspects that subtle changes higher in the section and in nearly the same geographic area are related in some way to the older events.

Early stratigraphic studies in the area by Steele (1960), Robinson (1961), and Bissell (1964) indicated a great difference between the Lower Permian sections in the southern and northern Pequop Mountains. Mapping in the southern area shows additional changes and suggests that most or all of them were caused by an east- or southeast-trending Pennsylvanian–Permian positive area that began a conspicuous rise in Late Pennsylvanian (Virgilian) time. Limestone and chert boulders, cobbles, and pebbles derived from Ely Limestone of Pennsyl-

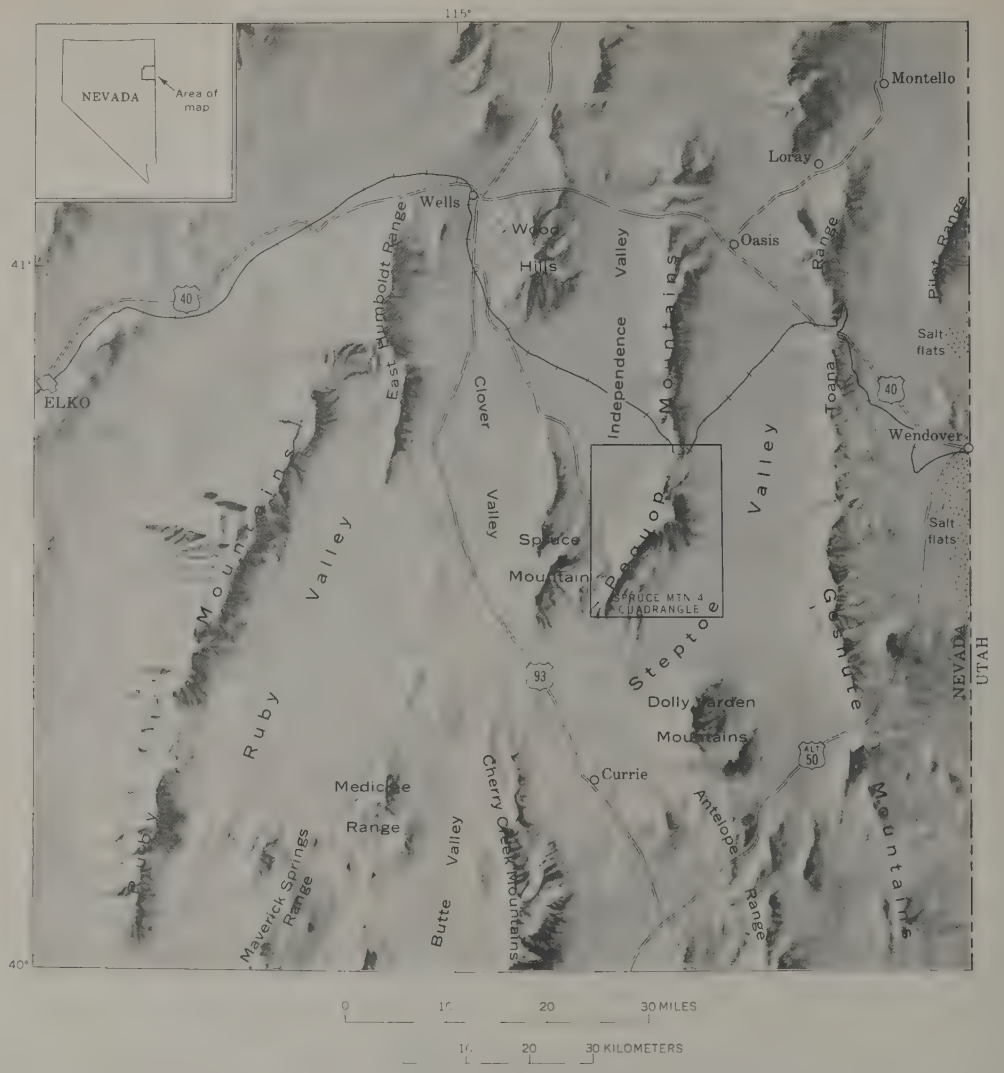

Figure 1.—Index map showing location of Spruce Mountain 4 quadrangle in southern Pequop Mountains, northeast Nevada.

vanian age were shed southward into a local basin where an unusually thick and complete deposit of Pennsylvanian and Permian limestone is preserved. No unconformity has been found in the basin, and the one on the positive area does not coincide with the systemic boundary.

By a combination of erosion and transgressive overlap on the south flank of the positive area (fig. 2), the total thickness of Pennsylvanian-Permian rock was reduced northward by about 5,000 feet in 6 miles. About 2,200 feet of nonconglomeratic Upper and Middle Pennsylvanian rock was eroded in this small area. In the same area, the conglomeratic overlap unit, mostly Permian limestone, thins northward from 1,390 feet to 250 feet and changes to a thin tongue of nearly pure conglomerate. The overlying Rib Hill(?) Sandstone thins abruptly northward and loses most of its diagnostic sandstone to become the basal (upper Wolfcampian) part of the type Pequop Formation of Steele (1960; Robinson, 1961). These major stratigraphic changes, which introduce many nomenclature problems, require a more detailed explanation (G. D. Fraser and R. C. Douglass, unpub. data).

The indicated positive area extended at least 23 miles north of the quadrangle boundary, where a thin basal conglomerate

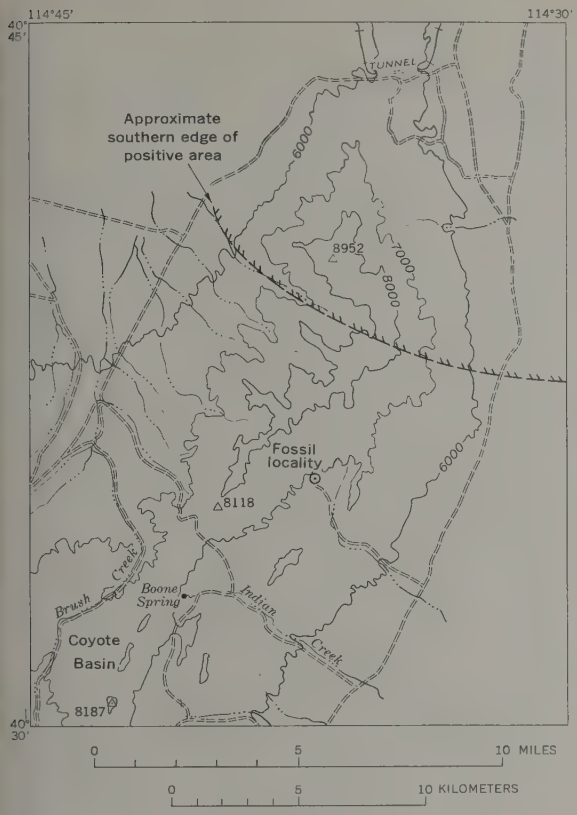

Figure 2.—Map of Spruce Mountain 4 quadrangle in southern Pequop Mountains, showing principal access roads and molluscan fossil locality. Southern edge of positive area refers only to Late Pennsylvanian-Early Permian structure. Contour interval 1,000 feet.

of the Pequop Formation rests unconformably on Mississippian rocks near the highway on the east side of the northern Pequop Mountains (fig. 1; Thorman, 1970, fig. 4). In that area, about 7,000 feet of the section exposed in the southern Pequop Mountains is missing. Fraser's investigations show further that the south flank of the positive area was not eroded evenly, but it is not known what fraction of the unusually thick Pennsylvanian section in the southern basin may never have been deposited on the crest of the positive area. After prolonged erosion, the positive area was inundated by the Early Permian (Leonardian) sea and deeply covered by limestone and the limited amount of sandstone composing the Pequop Formation.

Diffuse and ill-defined versions of the ancient structures were recurrently active, and their subdued late-stage effects can be found in many units younger than the Pequop Formation. The Loray(?) Formation of Steele (1960) and formations in the Park City Group thin northward erratically, apparently onto the same positive area. Conglomerates have been found locally at the base of the Kaibab Limestone, within and at the top of the Plympton Formation, at the base of the Gerster Formation, and at the base of the Thaynes Formation (Lower Triassic). Doubtless, the Permian-Triassic hiatus (Hose and Repenning, 1959, p. 2189; Collinson, 1968, p. 33) and perhaps some older disconformities were regional events, which however, were locally exaggerated on positive areas and damped out in basins, on structures similar to those described here.

The recurrent southerly margin of the uplift, where successive formations thinned and patches of conglomerate accumulated, seems to have shifted progressively southward in response either to a structural shift or to the broadening effect of thousands of feet of sediment on the uplift. The late-stage uplift probably was marked only by scattered ephemeral shoals or low islands, because late-stage conglomerates, unlike the earlier ones, are thin and discontinuous and contain no boulders and few cobbles. Several thick Pennsylvanian and Lower Permian units, but none of the younger formations within or above the Park City Group, pinch out or change to different formations within the Spruce Mountain 4 quadrangle.

Brief examination of the stratigraphic section in the mountains west of Montello, Nev. (fig. 1), suggests approximate geographic limits on the width of the positive area and indicates a deeper basin on the north side of the positive area, at least in Late Permian and Early Triassic time. In the basin, at least the lowest and highest formations within the Park City Group are much thicker and contain far more chert than they do to the south, so that a different stratigraphic nomenclature, more like that of the western phosphate field, may be required. The tectonic breccia everywhere present in the Plympton Formation of the southern Pequop Mountains was not found near Montello; only the lowest conglomerate of that formation extends northward from the southern Pequops to the vicinity of Montello. A very thick Lower Triassic section is present in both areas, but no conglomerate was found at its base near Montello. A pre-Thaynes (pre-*Meekoceras* zone) "flat-clam" and shale unit, not present in the southern Pequops, confirms a deeper basin on the north and a shorter hiatus between Permian and Triassic deposition.

PARK CITY GROUP

The Park City Group (Hose and Repenning, 1959) can be extrapolated into the southern Pequop Mountains and homotaxis maintained if it can be shown that the underlying Arcturus Group of Bissell (1964) is equivalent to the Arcturus Formation. Field studies indicate that the Arcturus Group of Bissell is characterized in the southern Pequop Mountains by intertonguing facies relationships (lithosomes) similar to those described in other areas by Stevens (1965). Everywhere in the quadrangle the Pequop lithosome is dominant; on the south flank of the positive area, the Pequop Formation commonly is

the only mappable unit below the Park City Group and above the conglomeratic tongue of pre-Rib Hill rock noted above. These observations confirm generally the regional correlations by previously cited authors; although different stratigraphers may use different boundaries and names for the local facies, there can be little doubt about homotaxis.

As used here, the Park City Group contains only the original three formations of Hose and Repenning (1959): Kaibab Limestone (oldest), Plympton Formation, and Gerster Limestone. The Indian Canyon Formation of Hodgkinson (1961) is included here as approximately the upper half of the Plympton (see below, parts 4 and 5 of the Plympton Formation) because in the field one could not map the base of the Indian Canyon consistently and because its lithology is chiefly a Plympton lithology. As noted by Hose and Repenning (1959, p. 2182), the upper part of the Plympton Formation is more variable than the lower part. Mudstone, siltstone, or sandstone is common in the upper half. In the Pequop Mountains, abundant dolomite and chert, algal structures, conglomeratic lenses, phosphorite or phosphatic black chert, and a molluscan rather than a brachiopod fauna tie the lower to the upper Plympton and clearly separate both from limestone formations above and below. For structural mapping and phosphate studies, Fraser found it convenient to split the Plympton only at the base of the tectonic breccia (see below, part 2 of the Plympton Formation), which is about 200 feet above the base.

In the Medicine Range (fig. 1), Collinson (1968, p. 32) included the probable Indian Canyon equivalent in a more inclusive Gerster Formation, even though he too considered the Indian Canyon equivalent to be part of the type Plympton. The brachiopod fauna used by Collinson to make this reasonable assignment cannot be used in the Pequop Mountains, where a molluscan fauna and other Plympton attributes persist to the base of the Gerster Formation, where there is an abrupt change.

Kaibab Limestone

In the southern Pequop Mountains, the Kaibab is mostly light-gray, resistant, and thick-bedded coarsely bioclastic crinoidal limestone or dolomitic limestone. The basal part, generally darker, thinner bedded, and finer grained, grades downward into the less resistant Pequop Formation or Loray(?) Formation of Steele (1960), whichever lithosome is present locally. A thin basal chert-pebble conglomerate was found in only one small area near the railroad tunnel. Light- to dark-gray bedded and nodular chert is common in middle and upper parts of the formation, particularly in northern areas, but chert is less abundant than in the Plympton. Large silicified productoid brachiopods are locally present near the base, and poorly preserved *Composita* occur where darker and thinner beds are present at the top. The formation thins irregularly northward from 300 to 150 feet or less locally.

Plympton Formation

The Plympton is mainly dolomite, bedded chert, and dolomitic mudstone or siltstone. Generally it is more iron stained, more fractured, less resistant, finer grained, and supports less vegetation than the limestone formations. The Plympton can be divided informally into five parts:

1. A basal zone about 200 feet thick, mostly brown to black chert interbedded with subordinate gray, yellow, or reddish-brown mudstone and capped in most areas by about 35 feet of light-gray sugary limestone or dolomite. The chert contains thin beds of impure and commonly pelletal phosphorite, especially near base and top, and rare low-spired gastropods, spicules, and fossil hash. Thin algal mats are present very locally at the top of the carbonate caprock where the flat faults of part 2 have not cut too deeply into the section.

2. A brown-weathering tectonic breccia[1] 2 to 200 feet thick with an average thickness of about 75 feet. The breccia is composed of coarse dark chert fragments as much as 2 feet in diameter and subordinate carbonate-rock fragments, all cemented by calcite.

3. Interbedded light-gray thin- to thick-bedded medium-crystalline to finely crystalline dolomite, dolomitic limestone, bedded gray to brown chert, and yellowish-gray dolomitic mudstone, totaling about 300 feet stratigraphically. This part has a thin lenticular but widespread chert-pebble conglomerate at its base in areas north of Indian Creek. The bed may mark an intraformational disconformity that helped to localize the tectonic breccia zone. The conglomerate is locally coarse and about 10 feet thick in some northern areas. One or more thin beds of phosphorite or black phosphatic chert are also present in areas both north and south of Indian Creek. Local beds of shell fragments and ghost structures of large pelecypods(?) are

[1] The breccia indicates a stratigraphically localized and fold-generated zone of bedding-plane slip present wherever the Plympton is exposed in the quadrangle. The movement zone never cuts up-section through part 3 of the Plympton but does cut down-section on the stretched limbs of some folds. In these areas, flat normal faults are indicated, and 1,500 feet or more of the stratigraphic section may be missing; part 1 of the Plympton, all of the Kaibab, all of the Loray(?) Formation of Steele where that lithosome was deposited, and part of the Pequop Formation are cut out; part 3 of the Plympton rests on structurally truncated Pequop Formation with only a screen of the tectonic breccia between. A parallel deeper slip zone, localized by weak beds directly below the Kaibab, is also involved in these unusual structures but generally is covered and rarely can be mapped.

The brittle and conspicuous Kaibab acts as a marker bed to reveal large tectonic lenses similar to boudins on the crests and troughs of folds and broad tectonic gaps on the stretched flanks of the folds. Needless to say, the stratigraphic anomalies created by this incipient diapirism are many. In Fraser's opinion, some of the so-called younger-over-older thrusts, common in the eastern Great Basin but rare elsewhere, are not explicable by gravitational gliding tectonics; they are explicable in terms of bedding faults and flat normal faults controlled by folding in a thick and differentially plastic carbonate section.

present north of Indian Creek. Numerous geodelike chert rosettes (Hodgkinson, 1961, p. 181), ¼- to 3-inch ovoids, characterize this and most other parts of the Plympton in all areas. Many rosettes are partly filled with secondary quartz and calcite. Although the scattered rosettes are variable in size, in some beds where they are abundant the size is consistent, and originally they might have been organic in origin.

4. Interbedded yellowish- to reddish-brown-weathering gray platy dolomitic siltstone, thin-bedded gray dolomite, and bedded chert, about 300 feet thick and mostly covered. The base of part 4 is probably the base of the Indian Canyon Formation of Hodgkinson (1961), which is a locally mappable member of the Plympton but not, in Fraser's opinion, a separate formation.

5. A highly variable and partly covered zone, generally about 200 feet thick, of interbedded thin- to thick-bedded dolomite, dolomitic limestone, chert, dolomitic mudstone, thin local beds of phosphatic black chert, siltstone, yellowish-brown quartzitic sandstone, and lenticular or disseminated chert-pebble conglomerate or gritstone locally scattered through at least the upper 100 feet of section. North of Indian Creek, near the fossil locality discussed below, the extreme top of the formation has the following stratigraphic sequence, in ascending order: light-gray thin- to medium-bedded dolomite or dolomitic limestone; 10 feet or more of yellowish-brown quartzitic sandstone; a thin 1- to 5-foot zone or zones of silicified molluscan coquina or pelecypod fragments, and as much as 10 feet of fine to coarse well-rounded chert-pebble conglomerate. Because of erosional truncation or extremely local deposition patterns, any of the rock types may form the uppermost beds in the formation. A thick silicified algal mat was found directly below the pelecypod fragments in one area. No evaporites were found in the quadrangle (compare Hose and Repenning, 1959, p. 2182).

Much of the Plympton is covered, but parts 2 and 3 commonly form ridges, and platy brown scree slopes derived from part 4 are locally conspicuous. Apparent thickness is variable because the formation localizes flat faults 200 feet above the base and, less commonly, at the top. Stratigraphic thickness probably ranges from about 1,000 to 1,200 feet. The upper part is differentially bevelled by pre-Gerster erosion north of Indian Creek, where the disconformity at the top of the formation is most conspicuous.

Gerster Formation

The Gerster is a light-gray resistant limestone, which is thin to thick bedded and which contains variable gray to brown nodular and bedded chert in less abundant quantities than in the Plympton. Much of the formation is a brachiopod coquina, but near the base of the formation, this may be reduced locally to a fossil hash containing thin lenticles of fine-grained conglomerate or gritstone. Thickness ranges from at least 376 feet to less than 140 feet. Rapid northward thinning was observed south of Indian Creek on the east side of the range. The formation is generally but variably thin north of Indian Creek. Erosional unconformities at the base, and particularly at the top, may explain reddish and purplish tints in those parts of the formation. A prolonged Permian-Triassic hiatus in this area may also explain the rapid thickness changes and the general thinness of the formation as compared with most other parts of the eastern Great Basin.

THAYNES FORMATION

The thick Lower Triassic section is assigned here entirely to the Thaynes Formation. The well-known *Meekoceras* zone, generally marking the base of the Thaynes in other areas, is present here in all areas where the base of the formation is exposed; other Early Triassic fossils have been found at the extreme top of the formation. Details of the formation are not discussed here. The Thaynes is about 3,300 feet thick in the southern part of the area, but generally most of it is covered. A rarely exposed thin lenticular chert-pebble conglomerate is widespread at the base. The coarsest known conglomerate is found in areas north of Indian Creek.

The Thaynes is the youngest marine formation in the area and the only known Mesozoic unit. Jurassic rocks have been reported from the Currie area, some distance south of the Pequop Mountains (fig. 1).

INTERPRETATION OF ENVIRONMENT AT THE TOP OF THE PLYMPTON FORMATION

In many areas north of Indian Creek, the top of the Plympton can be interpreted on the field evidence as indicative of a very shallow water environment peripheral to low islands and including some beach or tidal-flat deposits. Limy muds, silts, sands, and gravels mixed with molluscan shells were commonly reworked, and the youngest beds were locally truncated by erosion.

The silicified scaphopod-bellerophontid faunule discussed in detail below is a rare and extremely limited development in a much more extensive deposit of silicified pelecypod fragments, a thin coquina which is part of a still more extensive chert-pebble conglomerate. All this material is much more abundant north of Indian Creek than it is to the south, and the associated brown quartzite was found only north of Indian Creek. Exposures of this upper facies of the Plympton are best on the east side of the range.

During Gerster time the water was deeper, no coarse conglomerates were deposited, and productid brachiopods were the characteristic fossils. Locally, at the base of the Gerster the brachiopods were ground to a fossil hash and mixed with silicified molluscan debris derived from the underlying Plympton. Grits and fine-grained local lenticular conglomerates in the base of the Gerster appear to be largely reworked shells.

ONE PLYMPTON FOSSIL OCCURRENCE

A large collection (USGS locality 23819-PC, fig. 2) of silicified molluscan material was obtained from a limestone in part 5 of the Plympton Formation just below the conglomerate that marks the top of the formation. In the rocks collected from locality 23819-PC, the fossils have been completely replaced by silica, but there is no additional silica in the form of nodules. The original collection was not weighed, but it is estimated that about 50 pounds of limestone was treated with hydrochloric acid. The residue consisted exclusively of replaced organic remains. Excess silica is not present to cement the individual fossils together, as at several other Permian localities that contain a similar fossil assemblage. Part of the residue, after acid solution of the matrix, is shown in figure 3. The assemblage was washed in running water to remove any mud and to dissolve calcium chloride but was little disturbed by that process. It is apparent that several sedimentary grade sizes are present.

The following fossils have been recovered from the insoluble residue of rock collected at locality 23819-PC:

Scaphopoda:
  Plagioglypta canna (White) (abundant)
Gastropoda:
  Euphemites imperator Yochelson (abundant)
  Euphemites or *Euphemitopsis* fragment (one specimen)
  Knightites (*Retispira*) *modesta* (Girty) (one complete specimen and four fragments)
  Naticopsis (*?Naticopsis*) *rosewateri* n. sp. (abundant)
  Neritacean gastropod, new genus (three specimens)
Pelecypoda:
  ?Permophorus sp. indet. (one specimen)
  Crassitellid pelecypod indet. (two specimens)

As noted above, except for quantitatively insignificant minor additions, the fauna is limited to more than 100 examples each of three forms: a scaphopod, *Plagioglypta* (fig. 4); a large bellerophontacean gastropod, *Euphemites* (fig. 5); and a neritacean gastropod, *Naticopsis* (*?Naticopsis*) *rosewateri* n. sp. (fig. 7). In the shell debris, almost all pieces large enough to identify are assigned to the first two taxa.

Plagioglypta canna (White) is a well-known form, though the type specimens have never been redescribed or reillustrated. *Knightites* (*Retispira*) *modesta* (Girty) was reillustrated by Yochelson (1960, p. 275, pl. 56, figs. 15–19) in the same publication in which *Euphemites imperator* was described (Yochelson, 1960, p. 247). The new species of *Naticopsis* is described in the systematics part of this paper; the remaining material, including the new genus, is inadequate for description or meaningful illustration.

Sedimentary character of the fossil remains

The scaphopod shells show one remarkable feature which apparently has not been reported previously. Some examples have a smaller specimen lodged within a larger. Occasional specimens have two smaller shells nested or telescoped. The rare Middle Ordovician genus *Polylopia* often has multiple nestings of shells (Yochelson, 1968a). Hyolithids at some localities may be found nested; the resulting nonbiologic assemblage is often misinterpreted, and the name *Biconulites* is based on such a misinterpretation. However, both *Polylopia* and "*Biconulites*" are tubes with a closed apex. Even the telescoped orthoconic cephalopods, perhaps best known from the Maquoketa Shale (Upper Ordovician) of Iowa (Tasch, 1955), are septate. Geometrically, all these fossils are quite unlike the scaphopod tube which is open at both anterior and posterior. Flume or wave-tank studies of the currents required to cause the nestings of these various forms of fossils might provide useful data for paleoecologic interpretations.

A few of the scaphopod tubes are at an oblique angle to the bedding plane (fig. 6); at first glance, the tubes might be interpreted as being in life position. However, several of these show a smaller specimen jammed within a larger, and accordingly they cannot have lived in the bottom as they are now presently seen. Most specimens are parallel to bedding, and some scaphopods appear to be current oriented, but without preference for the larger or smaller ends; observations on orientation are based on insoluble residues from each block, and there might have been some slight movement of the material during the etching and subsequent washing.

Most of the bellerophontacean gastropods are 3.5–4.0 cm wide, very few being smaller than 3.0 cm. Thus, they do not resemble a sample of a life population in which small specimens are far more common than large individuals (compare with Yochelson, 1960, p. 221, fig. 2). The specimens show no orientation, but as their shape is somewhat spherical, the lack of orientation is not surprising. Most *Plagioglypta* are short segments of the long tube, generally 2–5 cm long. Few juvenile specimens are present. Specimens as long as 10 cm are present, though rare. Comparison with material from other localities suggests that some of these individuals may have attained a length of about 20 cm during life.

Many of the specimens are not well preserved. Although in part this is the result of fracture of the thick silicified shells, damage of this sort is the exception rather than the rule. Rather, almost all the bellerophontaceans and scaphopods show evidence of erosion by mechanical wear. In most *Euphemites* and *Plagioglypta*, the shell is 2 to 3 mm thick, so that wear of the thin marginal edge is obvious.

In addition to wear, about 5 percent of bellerophontacean shells also show a large number of elongate holes, such as have been ascribed to the action of boring barnacles (Tomlinson, 1969). The percentage of long-dead shells which accumulated on the bottom may be underrepresented in the sample because the bored shells are weaker and therefore more easily destroyed than those unbored. None of the scaphopod shells show indication of borings.

About half the rock volume is composed of *Plagioglypta* and *Euphemites*. The interstices are filled mainly with worn shell

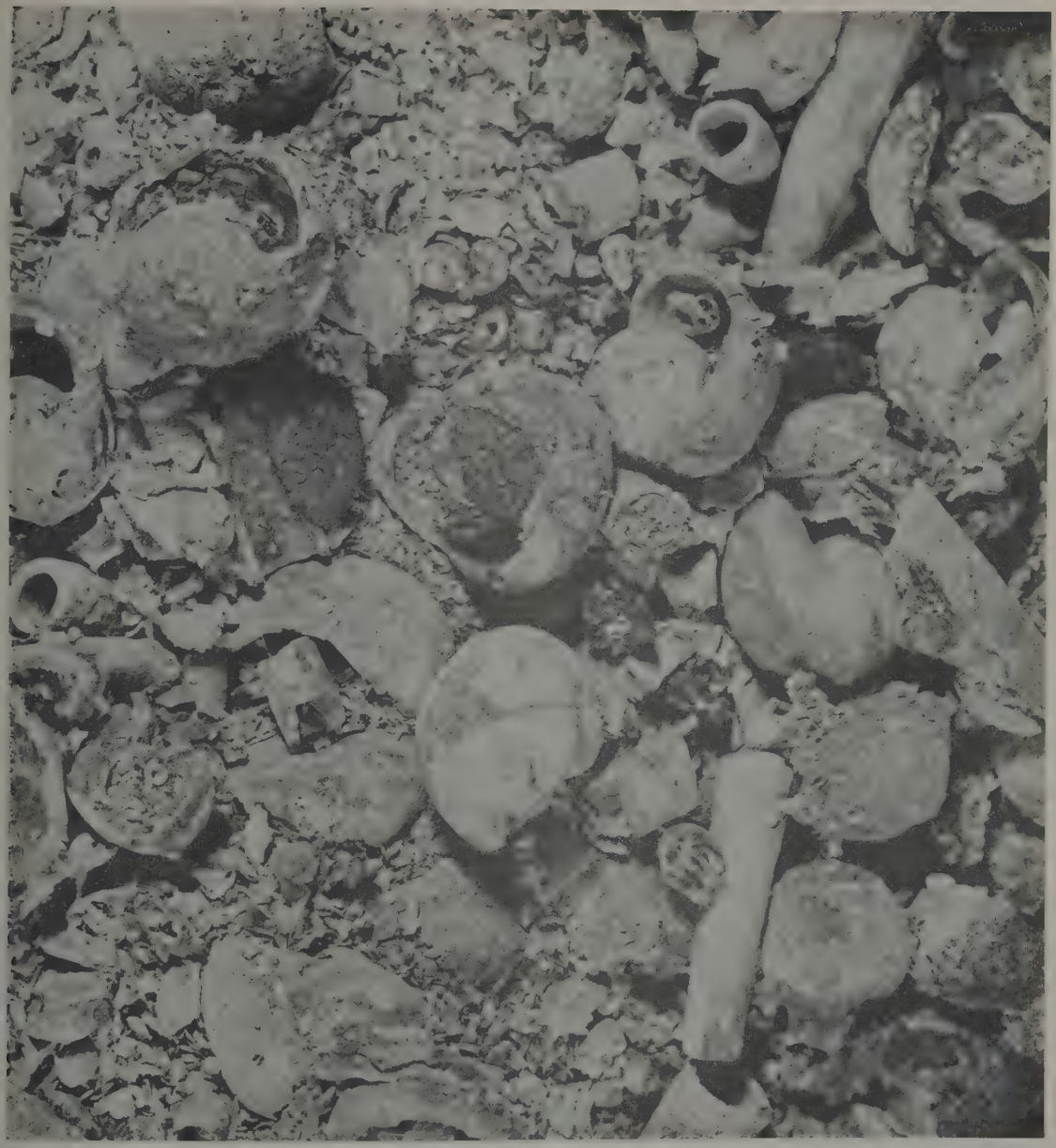

Figure 3.—Part of the insoluble residue from collection 23819-PC in which a large number of *Euphemites* are present in varying states of preservation. Scaphopods are obvious on the right side of the photograph but are scattered in both horizontal and vertical position within the residue. Natural size.

fragments which range in size from about 1 cm in maximum diameter down to the smallest fragments that can still be identified as organic. The individual particles of the shell coquina thus are held together with a minor amount of calcium carbonate cement.

Scattered randomly through the shell fragments are neritacean gastropods. Most of these range from 0.5 to 1 cm in width, but a few are wider than 1 cm. Individuals less than 0.5 cm are virtually unknown; were this a life population they should be the most common size. Several hundred specimens

Figure 4.—*Plagioglypta canna* (White) in several orientations. Most specimens are worn, are nested, or show both features. The specimen near the center has two tubes telescoped within the outermost specimen. Natural size.

have been recovered, or about as many as the *Euphemites* and *Plagioglypta* combined. Some of these neritaceans are also worn, but collectively they are better preserved than the larger fossils. Many specimens retain a conspicuous color pattern which would likely have been removed had any significant part of the shell thickness been worn away, for the color is confined to the outer layer of the shell.

Interpretation of the faunule

Every obvious feature of the fossils supports their interpretation as a death assemblage gathered together under conditions of relatively strong water movement. The wear of most large fossils, the high percentage and large size of shell debris, and the telescoping of the *Plagioglypta* tubes all indicate a high-energy environment. From this one-spot locality, it is impossible to determine the geometry of the deposit, but similar assemblages elsewhere in the Permian of the west are variable and laterally discontinuous over distances of a few feet. Accumulation of the fossils at or near the strandline is a reasonable conclusion.

Specimens have probably been moved a few feet to a maximum of a few tens of feet vertically. On modern beaches after heavy storms, unworn shells are found of mollusks that lived at shallow depths. Most wear was probably accomplished by movement back and forth, with only limited transport. The amount of lateral transport can only be guessed, but the large volume of fossils still identifiable, even though worn, would seem to imply a short time of such transport. If transported for extended distances, it might be expected that the bellerophontacean shell would be breached and specimens worn so that only the columella remained, whereas, in fact, most are complete shells. A short violent stage of transport is in keeping with interpretation of storm-driven waves moving up a relatively steep outer beach slope; it is somewhat less in keeping with their moving up a long, very gently sloping mudflat.

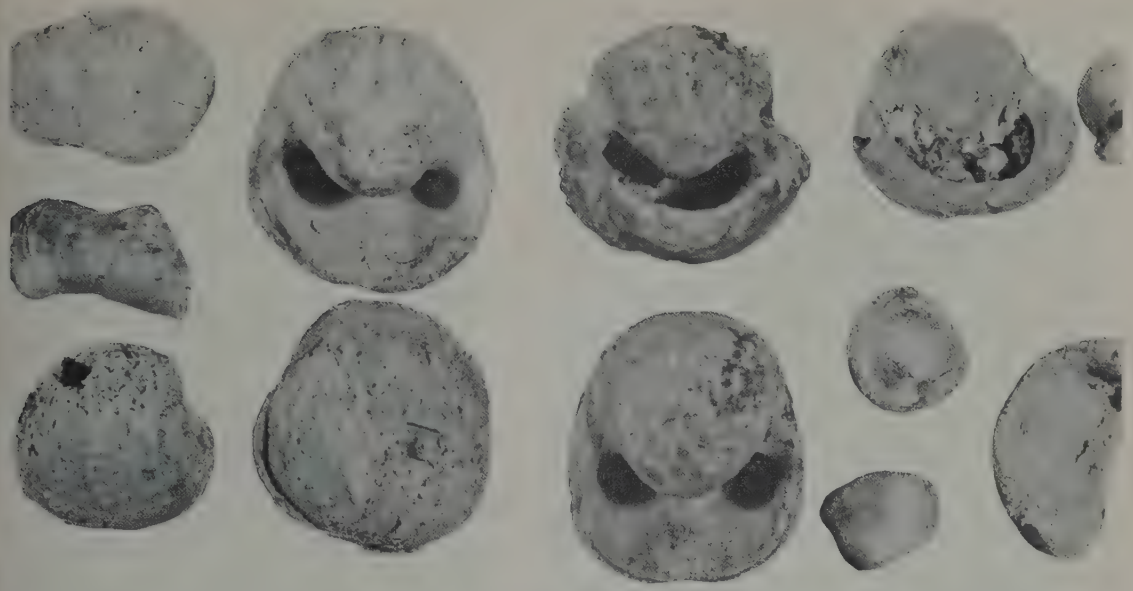

Figure 5.—*Euphemites imperator* Yochelson in several orientations. Although a few specimens preserve spiral ornament, most are worn on the outer surface and the aperture. The specimen in the lower left is bored, and the fragment above it is that of a worn columella; other shell fragments are shown in the lower right. Natural size.

Living neritacean gastropods occupy a variety of habitats, but they are particularly characteristic of shores, many forms living between the tide lines and some in the spray zone above high-tide level. It may be that the *Euphemites* and *Plagioglypta* shells were swept shoreward, there to be mixed with the neritaceans. Some transport of the neritaceans must certainly have taken place, as indicated by shell wear, but it was far less than that affecting the other specimens.

Speculations on feeding habits of the fossils support the general picture built up from the physical evidence. By comparison with living Neritacea, one may confidently assume that the fossil forms were microherbivores. Within this broad niche, the most likely method of feeding was scraping algae from hard surfaces, rather than clinging to algal fronds or digesting of algal mats. The bellerophontaceans probably were also herbivores. The large size of specimens precluded life on algal fronds. It seems more likely that they lived on algal mats rather than on the shoreline, but no evidence directly supports this assertion. Thus, one can speculate that the bellerophontaceans in the faunule were large specimens from a very shallow water sand-algal mat environment, which were transported to a nearshore bottom area and then perhaps were moved along a beach.

Limited data are available on the habits of living scaphopods. Morton (1959, p. 225, fig. 1) described a species in some detail, noting that it burrowed in "fairly clean sand of medium grade," at an oblique angle to the substrate. Dinamani (1964b) described another species which lives with the shell at an even more acute angle to the upper surface of the substrate. Trueman (1968, p. 27), in a detailed discussion of the burrowing process, concluded that in contrast to the pelecypods, the scaphopods are only able to burrow shallowly and obliquely. Both Morton (1959) and Dinamani (1964a) discussed the role of captacula, highly specialized tentacles, in feeding. Although there are some differences in the accounts, they agree on the importance of these structures in trapping benthonic foraminifers; the radula of living North Atlantic species seems to be well suited for crushing foram shells (John Kraeuter, oral commun., 1971). Dinamani (1964a) suggested that organic detritus also forms an important part of the diet and noted that stirring of the sediment by the probing foot is reflected on the surface, another indication of the extreme shallowness of burrowing. From these data, one would be inclined to guess that large specimens such as are found at the Pequop Mountains locality lived in a sand bottom rather than in mud. If water movement were sufficiently strong to move sand grains, the tubes would be readily dislodged.

Ever since the work of Nicol (1944), which compared a *Plagioglypta*-bearing faunule with two others in the Kaibab Limestone of Arizona, it has been traditional to assume that an abundance of scaphopods is suggestive of restricted water circulation and hypersaline conditions. Lateral and vertical facies changes do support such an assumption at the locality studied by Nicol and in places within the slightly older Arcturus Formation (Permian) of the Ely, Nev., district. In other areas, evidence is equivocal, and the assumption of

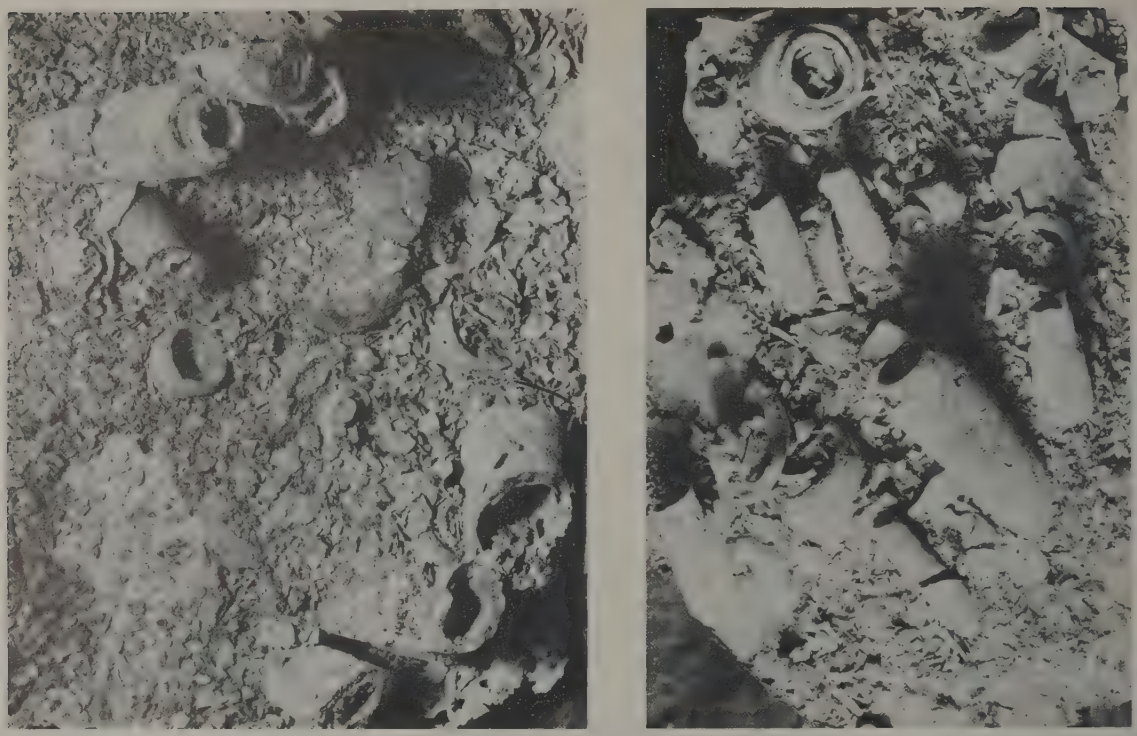

Figure 6.—View from above of two limestone blocks, partly etched, showing nested scaphopod tubes standing at various angles to the horizontal bedding plane. Natural size.

hypersalinity may be in error. At the Pequop locality, the interpretation of the fossils as an exceedingly shallow water deposit laid down by strong currents is difficult to reconcile with a restricted basin, though such a hydrographic situation is certainly possible. No evaporites have been found in the Plympton Formation in the Pequop Mountains, but evaporites have been found in the upper part of the formation 100 miles to the southeast (Hose and Repenning, 1959, p. 2182).

The evidence of a storm bed—the wear of fossils and the mixing of forms from slightly different environments—seems clear. The changes observed in the regional pattern of stratigraphy indicate moderately pronounced relief and a hiatus at the top of the Plympton Formation. The two fundamentally different approaches thus complement each other.

Age of the faunule

In spite of its limited variety, this faunule is readily dated as late Leonardian-early Wordian in age, in terms of the western Texas Permian section. An important fossil for dating is *Euphemites imperator;* this is the first known occurrence of the species since its description from localities in western Texas (Yochelson, 1960).

Knightites (*Retispira*) *modesta* is known from western Texas as well as from the Kaibab Limestone in Arizona. It also occurs in Montana in the Franson Member of the Park City Formation at Big Sheep Canyon (USGS locality 18581-PC) and at Cedar Creek (loc. 10829-PC), probably in the upper member of the Shedhorn Sandstone. The very abundant *Naticopsis* does not appear to be represented in collections from the Permian of western Texas, and the other rare gastropods and pelecypods add no information on the age of the deposit.

Mr. S. D. Olmore, University of Utah, has recently contributed a collection from the "*Bellerophon* limestone horizon" within the Harrisburg Gypsiferous Member of the Kaibab Limestone in the East Mormon Mountains; except for several small *Bellerophon*, only *Plagioglypta canna* (White) has been collected. The locality (22282-PC) is in the NW¼SW¼, sec. 13, T. 10 S., R. 69 E., Nevada, approximately 200 miles almost due south of the Pequop Mountains locality. This new occurrence of exceptionally well preserved material provides an intermediate point between the Pequop Mountains and

Relief Spring, Ariz. White (1874, p. 23) described *Dentalium canna* originally from both that locality and Salt Lake, N. Mex. *Plagioglypta canna* is conventionally used in the sense of specimens known from the Kaibab Plateau region; a type locality has never been designated.

Paleozoic scaphopods have received little study in the United States from the standpoint of either their biology or stratigraphic occurrence; in part, this is because their relatively simple shell shows only a limited number of characters. Accordingly, it is impossible to document conclusively the range of even such a well-known species as *Plagioglypta canna* (White). Nevertheless, the common occurrence of this taxon in certain facies of the Kaibab Limestone and Franson Member of the Park City suggests that it is an excellent guide to rocks of upper Leonardian-lower Wordian equivalents. This supposition can be tested when the scaphopods of the American standard Permian section are studied in detail.

DISTRIBUTION OF THE PERMIAN PLAGIOGLYPTA FACIES IN THE NORTHWESTERN UNITED STATES

The *Plagioglypta* faunule from the southern Pequop Mountains is similar to category 6 of Yochelson (1968b, p. 592), who summarized the fossil collections within the Phosphoria rock complex by their principal faunal components. Some useful data might be gathered by comparing these occurrences. As any attempt to generalize inevitably leads to loss of precision, one must immediately note that of the several dozen occurrences of *Plagioglypta* included in category 6, only about half a dozen are closely comparable to the Pequop occurrence. Locality details and other pertinent matters concerned with the Phosphoria fossils are given in Yochelson (1968b; see also Yochelson, 1968c) and need not be repeated here. Bretsky and Bermingham (1970) summarized the paleoecologic setting of reported Paleozoic scaphopods, but they did not review the occurrences in the Phosphoria rock complex in any detail.

Although a great deal of effort has gone into interpretation and reconstruction of the Phosphoria sea (McKelvey and others, 1959; Sheldon, 1963; Cressman and Swanson, 1964; Sheldon and others, 1967), many details still remain to be worked out. If the Permian phosphate deposits of the Western United States are the result of deposition from upwelling waters, studies of position of shoreline may be important. Further, the general nature of the shoreline slope could be critical, for a steep gradient is more likely to promote local upwelling than a shallow shelf area some miles wide. As indicated, a steep gradient is more likely to produce a storm-tossed beach deposit.

Viewed in this aspect, only two areas where *Plagioglypta* occur are particularly comparable. The first area is on the south side of the Uinta Mountains in Utah at Coulter Ranger Station (USGS loc. 10019-PC, 19406-PC) and at Split Mountain (19407-PC). The second is in the disturbed belt of southwestern Wyoming at Deadline Ridge (13350-PC; 18633-PC). At these localities, observation of fossil assemblages is inhibited because secondary silicification has changed the matrix to a mass composed of solid chert.

Several attempts to collect silicified faunules in both areas met with quite limited success and make the Pequop Mountains material all the more meaningful, for none of this Phosphoria matrix can be disaggregated. No information is available on what factors might govern silicification of fossils and oversilicification of the matrix. As a consequence of this strong secondary silicification, the Phosphoria localities are now chert. There appears little merit in equating these local deposits with the Rex Chert Member of the Phosphoria Formation, rather than the Franson Member of the Park City. Whatever the conditions of Rex deposition may have been, they do not appear to have been nearshore. The point is raised here simply to caution the unwary as to the potential effects of secondary silicification.

Orientation of fossils, degree of sorting from a life population, amount of wear, and the general character of preservation are features which fall between the interests of the stratigraphic paleontologist and the sedimentologist.

With those qualifications clearly understood, one would judge that, at the localities in southwestern Wyoming, fossils show deposition near the strandline in the most striking manner; therefore, presumably quite strong currents were involved. In the Uinta Mountains area, the evidence of high-energy deposition is not quite so obvious. The Pequop Mountains locality seems intermediate in character, but much closer to the environment of deposition of the southwestern Wyoming fossils. A locality near Big Timber in eastern Montana (USGS loc. 18843-PC) may be similar in depositional environment to that of the Uinta Mountains, but the fossils are not silicified, and observations on wear and orientation cannot be made so readily.

At the presumed beach localities in the Phosphoria rock complex that have been noted above, pelecypods are abundant and bellerophontacean gastropods are rare. The only previously known locality that approaches the faunal composition of the Pequop Mountains faunule is at Cedar Creek, Mont. (10528-PC); we have not investigated this locality and do not know if it represents a beach. In that collection, *Plagioglypta* and the bellerophontaceans *Bellerophon* and *Knightites* are present in about equal numbers, along with a few pelecypods (*Permophorus*).

At a few other localities, such as Hidden Pastures (18581-PC) and Sappington Canyon (18588-PC) in south-central Montana and Blind Stream (19408-PC) and Dry Bread Hollow (19415-PC) in the Uinta Mountains and northern Utah, respectively, the faunules consist predominantly of *Plagioglypta* and pelecypods. None of the material at these four localities shows obvious evidence of transport. The available material does not show a large amount of wear, though some specimens may have been discarded before being examined by Yochelson (1968b). Although these assemblages may be similar to *Plagioglypta*-bellerophontacean faunules, so

little is known of the ecological requirements of the organisms that it may be premature to assume that they lived under the same general conditions.

For the sake of completeness, it is appropriate to mention a slab from La Marche Gulch (12629-PC) in central Montana, which contains only large *Plagioglypta*, and collections from Cinnabar Mountain (12695-PC; 18844-PC) in extreme southeastern Montana, which has yielded *Bellerophon* and *Euphemites* but no *Plagioglypta*. *Plagioglypta* have been collected at other localities reported by Yochelson (1968c), but they appear to have a somewhat different aspect than those outlined above.

SYSTEMATIC PALEONTOLOGY

Class GASTROPODA
Order NERITOPSIDA Cox and Knight
Superfamily NERITACEA Rafinesque
Family NERITOPSIDAE Gray
Subfamily NATICOPSINAE Miller
Genus NATICOPSIS M'Coy
Subgenus NATICOPSIS M'Coy

Naticopsis (?Naticopsis) rosewateri Yochelson n. sp.

Figure 7, *a–t*

Description.—Elongate neritiform gastropods with a thickened but quite restricted inductura. Nucleus unknown. Shell exceedingly low spired, the upper part of the early growth stages seemingly relatively lower than that of the penultimate whorl. Suture obscure. Whorl profile that of a flattened ovoid, the short upper segment being only gently inclined and almost ramplike before curving abruptly downward to the outer face; periphery at or just above midwhorl, the whorl segment above it being more flattened than the part below; lower part of whorl profile a smooth curve following the arc of a circle and continuing this curvature to the base of the columella. Outer lip unknown; basal lip simple and smoothly curved. Shell surface smooth; growth lines unknown. Shell presumably has a thin outer layer and a thick inner layer. Inductura distinct and clearly set off from underlying shell, limited to a narrow zone parallel to the aperture and extending through less than one-eighth the circumference of the body whorl; inductura thin at the upper part of the aperture and at its farthest lateral extension, raised and nearly bosslike adjacent to the middle part of the aperture; not quite so thick near the lower part of the aperture and in early growth stages, but in later growth stages thicker and bounded by a distinct ridge. Inductura appears to be partially filling a shallow columellar depression. Ornamented by light and dark color bands, the dark bands being crescentic in early stages and elongating at later stages to form a variable zigzag pattern.

Discussion.—Conventionally, the Neritacea are placed within the Archaeogastropoda. Morton and Yonge (1964, p. 2) have formally raised this superfamily to the rank of order, basing this change on anatomical distinctions between present-day Neritacea and all other forms assigned to the Archaeogastropoda. There is no reason to challenge this new classification, and the rather mysterious appearance of the neritacean stock in the Devonian, without any obvious ancestral forms, provides slight additional support for this view. Although no rules of priority apply at the ordinal level, it should be noted that Cox and Knight (1960, p. 263) earlier had differentiated as a suborder a group termed by them Neritopsina.

The common late Paleozoic genus *Naticopsis* has never been subjected to monographic treatment. Because it has a relatively simple shell form and lacks many of the features, such as elaborate ornament, which are of use in distinguishing members of other gastropod groups, *Naticopsis* has been divided into subgenera on the basis of features of shell shape (Yochelson, 1953), the limits of which are more or less subjective. This new species differs in shape from typical *Naticopsis* in being somewhat narrower. However, it is more similar to that form than it is to any of the other subgenera currently recognized; questioned placement on the subgeneric level is better practice at this time than any ill-founded attempt to characterize yet another subgenus.

Naticopsis (*?Naticopsis*) *rosewateri* is distinguished by its somewhat peculiar whorl profile, being elongate but flattened above. In apertural view, as in figure 7, *f* or *k*, the shell appears compressed, whereas in the adapertural view it appears more inflated. This is clearly an optical illusion, heightened possibly because the outer lip is broken back, but it is the best expression of the low spire and the elongate whorl profile.

North American late Paleozoic species of *Naticopsis* have been listed by Yochelson and Saunders (1967, p. 139–144), who supplied the pertinent references to literature. Among the named Permian taxa, *N. remex* is based on indeterminate material, and *N. diminuta* is incorrectly assigned to genus, for it has a denticulate aperture. *N. transversa* has prominent colabral ornament and may not belong to this genus. *N. deformis*, *N. gracilis*, and *N. oblatus* are all relatively wider than this new form. *N. apachensis* and *N. oblatus* are more similar than other named forms, but each has a teardrop-shaped profile with virtually no development of an inclined upper surface. The difficulty in distinguishing species emphasizes the need for some scheme to describe more quantitatively the overall shape of the whorl profile. Though *N.* (*?N.*) *rosewateri* appears to be distinctive, several of the forms distinguished from it may be synonymous with others listed above.

Preservation of the *Naticopsis* is better than that of the other fossils in the faunule, but it leaves something to be desired. Many specimens have the early whorls worn, as in figure 7, *r*, so that the species appears even lower spired than it actually is. A few specimens are crushed, as on the side of the specimen in figure 7, *j*, or near the base of the aperture (fig. 7, *k*). All specimens have the outer lip broken back so that the aperture is not known in detail. Undoubted growth lines are not preserved, even though striations shown in figure 7, *n*,

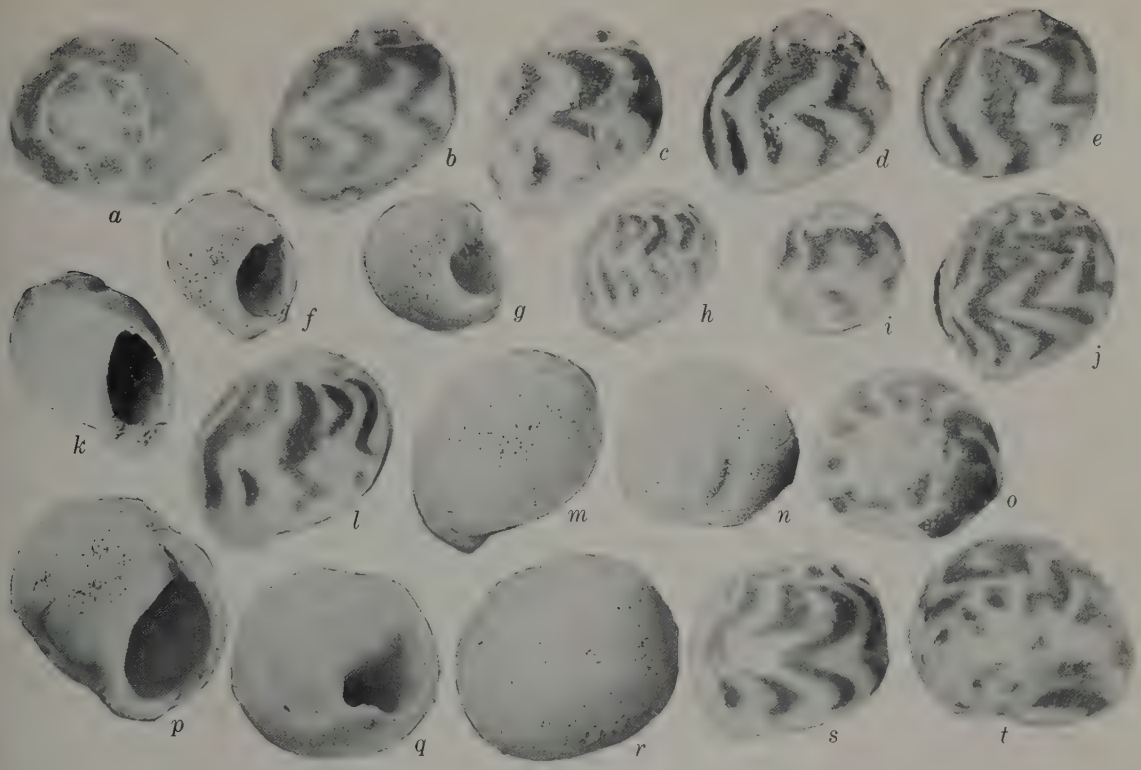

Figure 7.—*Naticopsis* (*?Naticopsis*) *rosewateri* n. sp. All illustrations × 3. *f*, *g*, *k*, *m*, *n*, and *p*–*r* coated with ammonium chloride; for other illustrations the specimens were moistened to accentuate the dark color bands. *a*, *b*, top and side views of paratype, USNM 183540; *c*, side view of paratype, USNM 183541; *d*, side view of paratype, USNM 183542; *e*, slightly oblique side view of paratype, USNM 183543; *f h*, apertural view, oblique basal view to emphasize inductura, and side view of paratype, USNM 183544; *i*, side view of paratype, USNM 183545; *j*, side view of paratype, USNM 183546, *k*–*o*, apertural view, side views, and top views of paratype, USNM 183547; *p*–*t*, apertural view, oblique basal view, side views, and top view of holotype, USNM 183548.

might suggest that the apertural lip was nearly orthocline. The lack of growth lines does not seem to be a factor of poor preservation but rather a reflection of an originally highly polished shell surface.

The color pattern preserved on so many individuals is certainly the most eye-catching feature of this species. What the original colors may have been is not known and cannot be surmised. Color patterns preserved in silicified Permian specimens are not common, but they do occur at some localities. Any consideration of the mechanism of silicification must take into account the retention of this pattern during the replacement process. It does not persist through the shell but is limited to the thinner outer shell layer.

As demonstrated by the specimens illustrated in figure 7, there is a high degree of individual variation in the precise details of light and dark stripes that follow a general zigzag pattern. As it is likely that the zigzag stripes were used for camouflage by complicating predator recognition of the shell shape, evolutionary theory supports the notion that there would not be rigorous natural selection toward a precise unvarying form. Variation in this pattern, as shown for example in figure 7, *c*, *e*, and *s*, is not uncommon. Even the early stages (fig. 7, *h* and *i*) do not have a definite pattern.

During the early days of conchology, many varieties were named among elaborately patterned modern forms. Further study has shown that some populations are highly variable in many details of coloration and that this feature is of limited taxonomic significance, even if only the general pattern is considered. In fossils, the preservation of color pattern is such a special event—even at this locality more than half the specimens lack the pattern—that such patterns should not be used as a feature for distinguishing species.

The specific name acknowledges a debt of long standing to Dr. Joseph Rosewater, of the National Museum of Natural History, for his assistance, in ways too numerous to detail, in my attempts to draw comparisons between features of Paleozoic gastropods and those of the modern fauna.

Types.—Holotype, USNM 183548; figured paratypes, USNM 183540–183547.

REFERENCES CITED

Bissell, H. J., 1964, Ely, Arcturus, and Park City Groups (Pennsylvanian-Permian) in eastern Nevada and western Utah: Am. Assoc. Petroleum Geologists Bull., v. 48, no. 5, p. 565–636.

Bretsky, P. W., and Bermingham, J. J., 1970, Ecology of the Paleozoic scaphopod genus *Plagioglypta* with special reference to the Ordovician of eastern Iowa: Jour. Paleontology, v. 44, no. 5, p. 908–924.

Collinson, J. W., 1968, Permian and Triassic biostratigraphy of the Medicine Range, northeastern Nevada: Earth Sci. Bull., v. 1, no. 4, p. 25–44.

Cox, L. R., and Knight, J. B., 1960, Suborders of Archaeogastropoda: Malacological Soc. London Proc., v. 33, p. 262–264.

Cressman, E. R., and Swanson, R. W., 1964, Stratigraphy and petrology of the Permian rocks of southwestern Montana: U.S. Geol. Survey Prof. Paper 313-C, p. 275–569, pls. 14–25.

Dinamani, P., 1964a, Feeding in *Dentalium conspicuum:* Malacological Soc. London Proc., v. 36, p. 1–5.

—— 1964b, Burrowing behavior of *Dentalium:* Biol. Bull., v. 126, p. 28–32.

Hodgkinson, K. A., 1961, Permian stratigraphy of northeastern Nevada and northwestern Utah: Brigham Young Univ. Geology Studies, v. 8, p. 167–196.

Hose, R. K., and Repenning, C. A., 1959, Stratigraphy of Pennsylvanian, Permian, and Lower Triassic rocks of Confusion Range, west-central Utah. Am. Assoc. Petroleum Geologists Bull., v. 43, no. 9, p. 2167–2196.

McKelvey, V. E., and others 1959, The Phosphoria, Park City, and Shedhorn formations in the western phosphate field: U.S. Geol. Survey Prof. Paper 313–A, p. 1–47, pls. 1–3.

Morton, J. E., 1959, The habits and feeding organs of *Dentalium entalis:* Marine Biol. Assoc. United Kingdom Jour., v. 38, p. 225–238.

Morton, J. E., and Yonge, C. M., 1964, Classification and structure of the Mollusca, *in* Wilber, K. W., and Yonge, C. M., Physiology of the Mollusca: New York, Academic Press, v. 1, p. 1–58.

Nicol, David, 1944, Paleoecology of three faunules in the Permian Kaibab Formation at Flagstaff, Arizona: Jour. Paleontology, v. 18, no. 6, p. 553–557.

Robinson, G. B., Jr., 1961, Stratigraphy and Leonardian fusulinid paleontology in central Pequop Mountains, Elko County, Nevada: Brigham Young Univ. Geology Studies, v. 8, p. 93–145.

Sheldon, R. P., 1963, Physical stratigraphy and mineral resources of Permian rocks in western Wyoming: U.S. Geol. Survey Prof. Paper 313-B, p. 49–273, pls. 4–13.

Sheldon, R. P., Cressman, E. R., Cheney, T. M., and McKelvey, V. E., 1967, Paleotectonic investigations of the Permian System in the United States—Middle Rocky Mountains and northeastern Great Basin: U.S. Geol. Survey Prof. Paper 515–H, p. 159–170.

Steele, Grant, 1960, Pennsylvanian-Permian stratigraphy of east-central Nevada and adjacent Utah, *in* Intermtn. Assoc. Petroleum Geologists, Guidebook to the geology of east-central Nevada, 11th annual field conference, 1960: Salt Lake City, Utah Geol. and Mineralog. Survey, p. 91–113.

Stevens, C. H., 1965, Pre-Kaibab Permian stratigraphy and history of Butte basin, Nevada and Utah: Am. Assoc. Petroleum Geologists Bull., v. 49, no. 2, p. 139–156.

Tasch, Paul, 1955, Paleoecologic observations on the orthoceratid coquina beds of the Maquoketa at Graf, Iowa: Jour. Paleontology, v. 29, no. 3, p. 510–518.

Thorman, C. H., 1970, Metamorphosed and nonmetamorphosed Paleozoic rocks in the Wood Hills and Pequop Mountains, northeast Nevada. Geol. Soc. America Bull., v. 81, no. 8, p. 2417–2448.

Tomlinson, J. T., 1969, The burrowing barnacles (Cirripedia: Order Acrothoracica): U.S. Natl. Mus. Bull. 296, 162 p.

Trueman, E. R., 1968, The burrowing process of *Dentalium* (Scaphopoda): Zool. Soc. London Jour., v. 154, p. 19–27.

White, C. A., 1874, Preliminary report upon invertebrate fossils collected by expeditions of 1871, 1872, and 1873, with descriptions of new species: U.S. Geog. Explor. W. 100th meridian (Wheeler), 27 p.

Yochelson, E. L., 1953, *Jedria*, a new subgenus of *Naticopsis:* Washington Acad. Sci. Jour., v. 43, no. 3, p. 65.

—— 1960, Permian Gastropoda of the southwestern United States* * *–3. Bellerophontacea and Patellacea: Am. Mus. Nat. History Bull., v. 119, art. 4, p. 207–294, pls. 46–57.

—— 1968a, On the nature of *Polylopia:* U.S. Geol. Survey Prof. Paper 593-F, p. F1-F7, pl. 1.

—— 1968b, Biostratigraphy of the Phosphoria, Park City, and Shedhorn Formations: U.S. Geol. Survey Prof. Paper 313-D, p. 571–660.

—— 1968c, Charts showing distribution and abundance of fossils in the Phosphoria, Park City, and Shedhorn Formations in Wyoming, Idaho, Utah, and Montana: U.S. Geol. Survey open-file report, 8 sheets.

Yochelson, E. L., and Saunders, B. W., 1967, A bibliographic index of North American late Paleozoic Hyolitha, Amphineura, Scaphopoda, and Gastropoda: U.S. Geol. Survey Bull. 1210, 271 p.

Jour. Research U.S. Geol. Survey
Vol. 1, No. 1, Jan.–Feb. 1973, p. 33–37

GRAPTOLITES FROM THE MARTINSBURG FORMATION, LEHIGH GAP, EASTERN PENNSYLVANIA

By JACK B. EPSTEIN and WILLIAM B. N. BERRY[1]
Beltsville, Md., Berkeley, Calif.

Work done in cooperation with the Pennsylvania Department of Environmental Resources, Bureau of Topographic and Geologic Survey

Abstract.—Graptolites collected from the uppermost part of the Martinsburg Formation (Pen Argyl Member) at and near the contact with the overlying Shawangunk Formation at Lehigh Gap, Pa., indicate that the uppermost Martinsburg is as young as Edenian to early Maysvillian (upper subzone [*Climacograptus spiniferus* subzone] of zone 13 [*Orthograptus truncatus intermedius* zone]). The Martinsburg gradationally overlies the Jacksonburg Limestone of late Middle Ordovician age, suggesting a lower age limit for the Martinsburg.

The Martinsburg Formation in easternmost Pennsylvania and northwestern New Jersey consists predominantly of 9,800 to 12,800 feet of slate, graywacke, and graywacke siltstone. Three members were defined by Drake and Epstein (1967), namely a middle graywacke-bearing member (Ramseyburg) separating lower (Bushkill) and upper (Pen Argyl) slate-dominated members. The distribution of these is shown in figure 1.

The upper age of the Martinsburg in eastern Pennsylvania has generally been given as early Maysvillian (for example, Twenhofel and others, 1954) based on shelly fossils identified by Ulrich (in Stose, 1930, p. 648–649) from the Shochary Ridge area west of Lehigh River. The Shochary Sandstone and what is here called the Ramseyburg Member were originally thought to be contiguous units by Behre (1933). Reconnaissance by A. A. Drake, Jr., and J. B. Epstein (see Epstein and others, 1972) suggests that the rocks in Shochary Ridge may be separated from the Martinsburg of the slate belt to the east by a fault of large displacement. The abundant shelly fauna in the sandstone in Shochary Ridge (named the Shochary Sandstone by Willard and Cleaves, 1939) has not been found in sandstone of the Ramseyburg Member of the slate-belt Martinsburg. Only very sparse brachiopod and crinoid debris have been found in the Ramseyburg during the past decade of mapping in eastern Pennsylvania by members of the U.S. Geological Survey.

[1] Department of Paleontology, University of California.

Previously, few fossils have been found in the slate-belt Martinsburg that yielded a precise age determination. Beerbower (1956) found the trilobite *Triarthrus beckii* just below the contact of the Martinsburg and Shawangunk Formations at Delaware Water Gap in New Jersey. *Triarthrus* ranges from Barnveldian through Edenian (Twenhofel and others, 1954; see fig. 2 for stage names used in this report). The fossil was collected from the upper part of the Ramseyburg Member, whose contact with the overlying Pen Argyl Member is truncated by the Shawangunk 0.75 mile southwest of the gap (fig. 1). Willard and Cleaves (1939, p. 1184) found poorly preserved fossils at Lehigh Gap—identification was not possible. Schuchert (1916, p. 548), however, reported *Diplograptus foliaceus* var. *vespertinus* Ruedemann (=*Glyptograptus vespertinus* (Ruedemann), suggestive of zone 13) from the Martinsburg (Pen Argyl Member) from within 75 feet of the overlying Shawangunk. Unspecified fossils in the Ramseyburg Member north of Klecknersville, Pa., were believed to be of probable Trenton age (late Middle Ordovician?) by Ulrich (in Stose, 1930, p. 638), but Behre (1933, p. 142) maintained that their poor state of preservation shed doubt on the age determination.

More recently, Aldrich (1967) discovered *Glyptograptus* cf. *G. teretiusculus* (Hisinger) and a variety of *Orthograptus calcaratus* Lapworth in the Bushkill Member of the Martinsburg Formation near Seemsville, Pa. These graptolites also occur in the Normanskill Shale and the Canajoharie Shale in New York (Ruedemann, 1947; Berry, 1962; Riva, 1969) and are, therefore, indicative of the zone 12-lower subzone of zone 13 interval.

NEW GRAPTOLITE COLLECTIONS FROM LEHIGH GAP—UPPER AGE LIMIT OF THE MARTINSBURG FORMATION

Graptolites have been found at four localities in the Pen Argyl Member of the Martinsburg Formation in the Palmerton quadrangle immediately south of Lehigh Gap (fig. 3). The Pen Argyl is nearly 6,000 feet thick in the Lehigh Valley.

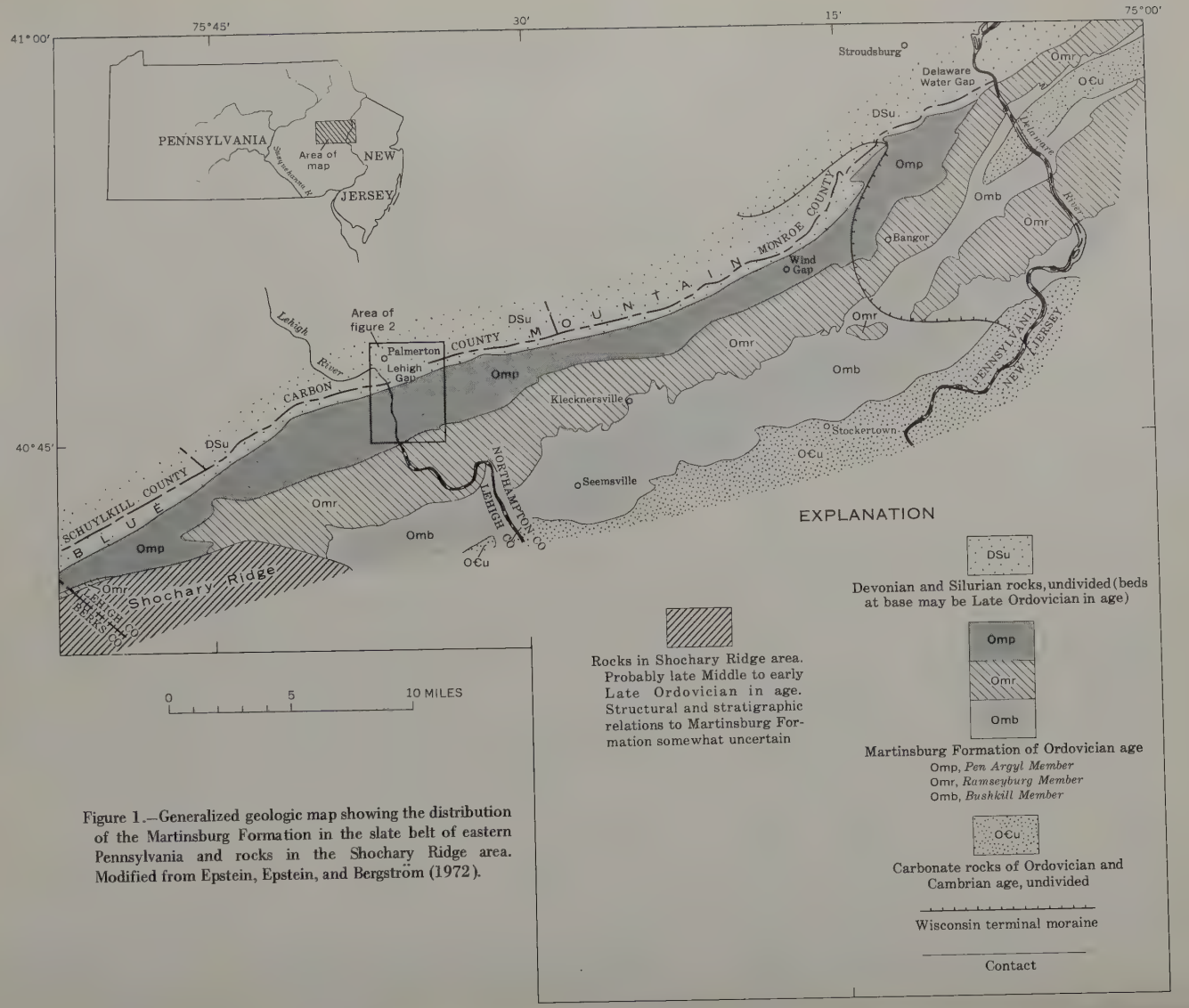

Figure 1.—Generalized geologic map showing the distribution of the Martinsburg Formation in the slate belt of eastern Pennsylvania and rocks in the Shochary Ridge area. Modified from Epstein, Epstein, and Bergström (1972).

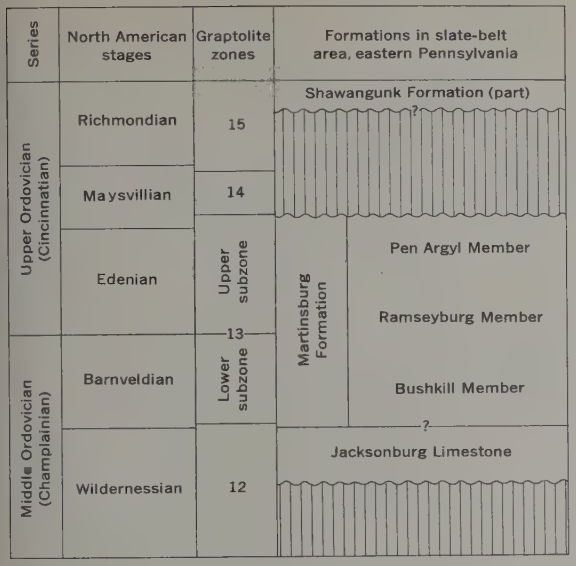

Figure 2.—Age of the Martinsburg Formation in the slate belt of eastern Pennsylvania and upper Middle and Upper Ordovician stages and graptolite zones used in this report. Many of the reports cited in this paper present age determinations in reference to either the Trenton Group or "Trentonian" stage. Conodont faunas in the type areas of the "Trentonian" and Edenian (Bergström and Sweet, 1966; Schopf, 1966; Sweet and Bergström, 1970) indicate that the upper part of the Trenton Group is Edenian, so that "Trenton" is Wildernessian through early Edenian in age.

The graptolites collected at each locality and the structural setting are listed in table 1. The stratigraphic and structural positions of the graptolite localities are shown in the cross section in figure 3. Stratigraphic and structural details are given in Epstein and Epstein (1969).

The association of *Climacograptus spiniferus*, *C. typicalis*, and *Dicranograptus nicholsoni* var. *minor* with orthograptids of the *O. quadrimucronatus* and *O. truncatus* groups in collections from the Pen Argyl Member is indicative of the upper subzone of zone 13 of Berry (1970). The upper subzone of zone 13 (the *Climacograptus spiniferus* subzone of the *Orthograptus truncatus intermedius* zone) is equivalent to the *Climacograptus spiniferus* zone of Riva (1969). Riva (1969) indicated that the *Climacograptus spiniferus* zone is in the lower part of the Utica Shale in the Mohawk Valley, N.Y. He (Riva, 1969) correlated the lower part of the Utica Shale in the Mohawk Valley with the Cobourg Limestone in the Trenton Group. Sweet and Bergström (1971) correlated the Cobourg Limestone with the entire Edenian and the lower part of the Maysvillian in the Cincinnati area on the basis of their conodont studies. The upper part of the Martinsburg Formation in eastern Pennsylvania (the Pen Argyl Member) may thus be correlated with at least a part of the Edenian-Maysvillian interval. If the youngest rocks in Shochary Ridge west of the Lehigh River are Maysvillian in age as suggested by Stose (1930), then the upper part of the Martinsburg in the slate belt could be about the same age. However, modern paleontologic studies of Shochary Ridge rocks have not been undertaken as yet to prove the Maysvillian correlation.

LOWER AGE LIMIT OF THE MARTINSBURG FORMATION

The Martinsburg Formation grades down into the Jacksonburg Limestone in easternmost Pennsylvania. Miller (1937) indicated that the uppermost part of the Jacksonburg Limestone is correlative with the Sherman Fall Formation (Barnveldian in age) in New York and Ontario. Twenhofel and others (1954) correlated the uppermost part of the Jacksonburg with the lower part of the Sherman Fall. Barnett (1965), on the basis of conodont studies, concluded that the Jacksonburg probably correlates with the Rockland, Kirkfield, and lower Shoreham Formations. Barnett's (1965) conclusions are supported by conodont collections made by J. B. Epstein near Stockertown, Pa. (fig. 1). J. W. Huddle, of the U.S. Geological Survey, identified the conodonts (written commun., 1970; USGS loc. 6974-CO and 6975-CO) and cited the presence of *Phragmodus undatus* Branson and Mehl which suggests that the beds bearing it in the Jacksonburg Limestone are no older than the Rockland Formation. The Rockland is in the upper part of the Wildernessian Stage (Cooper, 1954). Thus, precise dating of the top of the Jacksonburg and the transitional beds in the basal Martinsburg remains to be established, but it seems likely that the basal Martinsburg is late Wildernessian to early Barnveldian (or late zone 12 to lower subzone of zone 13) in age.

SUGGESTIONS FOR FUTURE COLLECTING IN THE SLATE BELT

The graptolite-bearing rocks of the Pen Argyl Member have several characteristics in common that may aid in future discovery of other fossil localities in the eastern Pennsylvania slate belt. In general, bedding and cleavage are nearly parallel at the localities from which the graptolites were obtained. In areas where cleavage is at an appreciable angle to the bedding, the slate will not split parallel to bedding. Thus, bedding surfaces are not exposed as in the case where bedding and cleavage are subparallel. Cleavage is poorly developed at locality 1 which is regarded as a pressure-shadow area (Epstein and Epstein, 1969, p. 166–167). Other pressure-shadow areas near the contact with the Shawangunk Formation may be good sites for inspection. They include exposures in the Delaware Water Gap and at the Yards Creek hydroelectric project near Blairstown, N.J. (Epstein and Epstein, 1969, p. 135, fig. 3).

The graptolites from most of the localities are dark brown and stand out against the lighter colored, weathered slate that bears them. Weathered outcrops that fulfill the near-parallel

bedding-cleavage requirement are excellent sites for examination for future collecting. As the weathering took place primarily prior to Wisconsin glaciation (Epstein and Hosterman, 1969), outcrops south and west of the Wisconsin terminal moraine (fig. 1) are generally more favorable for finding graptolites.

CONCLUSIONS

The faunal evidence suggests that the Martinsburg Formation in the eastern Pennsylvania slate belt ranges in age from late Middle Ordovician at its base to an age in the span of Edenian-Maysvillian (the upper subzone of zone 13 of Berry, 1970) at the top. This dates the youngest beds exposed beneath the Taconic unconformity in this part of eastern Pennsylvania. Berry (1970) has previously discussed the significance of the graptolite collections from the Pen Argyl Member near Lehigh Gap, Pa., in his reevaluation and refinement of graptolite zone 13 in New York and Pennsylvania.

ACKNOWLEDGMENTS

We wish to acknowledge P. B. Myers, Jr., Lehigh University, who first discovered graptolites in the Lehigh Gap area (loc. 3, fig. 3), and J. W. Huddle for identifying the conodonts from the Jacksonburg Limestone. We give our sincere thanks to A. A. Drake, Jr., U.S. Geological Survey, for his exchange of ideas on the stratigraphy on the Martinsburg Formation.

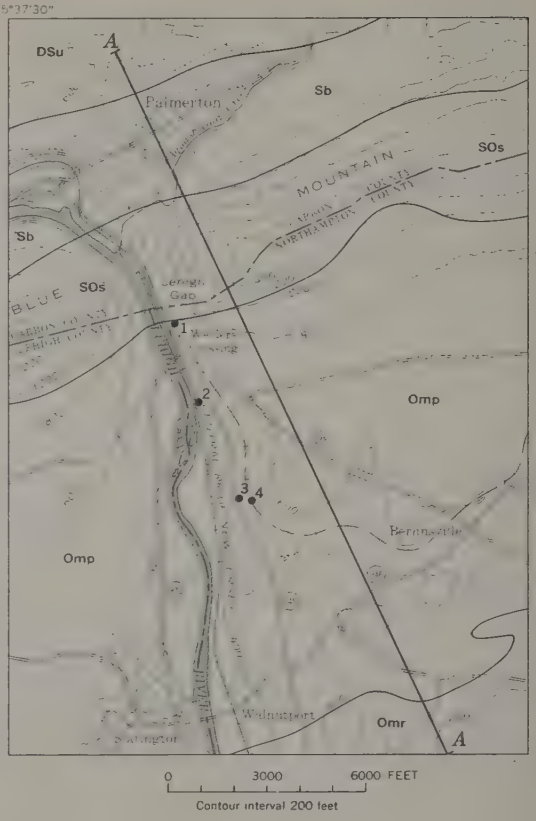

Figure 3.

Table 1.—*Ordovician graptolites in the Pen Argyl Member of the Martinsburg Formation near Lehigh Gap, Pa.*

Locality	Description	Graptolites
1.	Abandoned railroad cut. Slightly weathered argillite, cleavage poorly developed. Samples 80 to 100 feet below contact with overlying Shawangunk Formation. Locality described by Epstein and Epstein (1969, p. 180–181).	*Climacograptus spiniferus* Ruedemann
2.	Railroad cut. Weathered slate in cleavage arch, cleavage and bedding nearly parallel. Sample about 2,400 feet below contact with overlying Shawangunk Formation.	*Climacograptus* cf. *C. bicornis* var. *longispina* T. S. Hall *C. spiniferus* Ruedemann *C. typicalis* J. Hall *Diplograptus* sp. *Orthograptus truncatus* cf. var. *pertenuis* (Ruedemann)
3.	Shale pit. Weathered slate in vertical beds, cleavage and bedding nearly parallel. Samples collected from 300-foot interval about 3,000 feet below the Shawangunk Formation.	*C. spiniferus* Ruedemann *C. typicalis* J. Hall *Dicranograptus nicholsoni* var. *minor* Bulman *Diplograptus mohawkensis* Ruedemann *Leptograptus* sp. *Orthograptus quadrimucronatus* cf. var. *approximatus* (Ruedemann) *O. truncatus* var. *intermedius* (Elles and Wood)
4.	Same as at locality 3 but from abandoned railroad cut above locality 3.	*Climacograptus spiniferus* Ruedemann *C. typicalis* J. Hall *Diplograptus mohawkensis* Ruedemann? *Diplograptus* sp. *Orthograptus quadrimucronatus* cf. var. *approximatus* (Ruedemann) *Orthograptus* sp. (of the *O. truncatus* group)

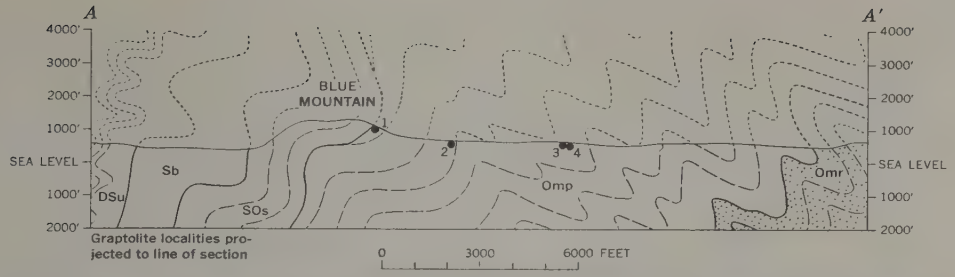

Figure 3.–Generalized geologic map and section showing graptolite localities in the Lehigh Gap area, Pennsylvania. DSu, Devonian and Upper Silurian rocks, undivided; Sb, Bloomsburg Red Beds; SOs, Shawangunk Formation; Omp, Pen Argyl Member of Martinsburg Formation; Omr, Ramseyburg Member of Martinsburg Formation. Base from U.S. Geological Survey, Palmerton, Pa., 7½-minute quadrangle, 1960.

REFERENCES CITED

Aldrich, M. J., Jr., 1967, Cambrian dolomite in the Martinsburg Formation, eastern Pennsylvania: Pennsylvania Acad. Sci. Proc., v. 41, p. 133–140.

Barnett, S. G., III, 1965, Conodonts of the Jacksonburg Limestone (Middle Ordovician) of northwestern New Jersey and eastern Pennsylvania: Micropaleontology, v. 11, no. 1, p. 59–80.

Beerbower, J. R., 1956, The Ordovician-Silurian contact, Delaware Water Gap, New Jersey: Pennsylvania Acad. Sci. Proc., v. 30, p. 146–149.

Behre, C. H., Jr., 1933, Slate in Pennsylvania: Pennsylvania Geol. Survey, 4th ser., Bull. M16, 400 p.

Bergström, S. M., and Sweet, W. C., 1966, Conodonts from the Lexington Limestone (Middle Ordovician) of Kentucky, and its lateral equivalents in Ohio and Indiana: Bulls. Am. Paleontology, v. 50, no. 229 p. 271–441.

Berry, W. B. N., 1962, Stratigraphy, zonation, and age of Schaghticoke, Deepkill, and Normanskill shales, eastern New York: Geol. Soc. America Bull., v. 73, p. 695–718.

——1970, Review of late Middle Ordovician graptolites in eastern New York and Pennsylvania: Am. Jour. Sci., v. 269, p. 304–313.

Cooper, G. A., 1954, Chazyan and related brachiopods: Smithsonian Misc. Colln., v. 127, pts. 1 and 2, 1245 p.

Drake, A. A., Jr., and Epstein, J. B., 1967, The Martinsburg Formation (Middle and Upper Ordovician) in the Delaware Valley, Pennsylvania-New Jersey: U.S. Geol. Survey Bull. 1244-H, p. H1–H16.

Epstein, J. B., and Epstein, A. G., 1969, Geology of the Valley and Ridge province between Delaware Water Gap and Lehigh Gap, Pennsylvania, *in* Subitzky, Seymour, ed., Geology of selected areas in New Jersey and eastern Pennsylvania and guidebook of excursions: New Brunswick, N.J., Rutgers Univ. Press, p. 132–205.

Epstein, J. B., Epstein, A. G., and Bergström, S. M., 1972, Significance of Lower Ordovician exotic blocks in the Hamburg klippe, eastern Pennsylvania, *in* Geological Survey Research 1972: U.S. Geol. Survey Prof. Paper 800-D, p. D29–D36.

Epstein, J. B., and Hosterman, J. W., 1969, Residual clay deposits in rocks of Early and Middle Devonian age near Kunkletown, Pennsylvania, *in* Geological Survey Research 1969: U.S. Geol. Survey Prof. Paper 650-D, p. D94–D105.

Miller, R. L., 1937, Stratigraphy of the Jacksonburg Limestone: Geol. Soc. America Bull., v. 48, p. 1687–1717.

Riva, John, 1969, Utica and Canajoharie Shales in the Mohawk Valley, *in* Bird, J. M., ed., New England Intercollegiate Geological Conf., 61st Ann. Mtg., Oct. 10–12, 1969, Guidebook for field trips in New York, Massachusetts, and Vermont, 7 p. (paged separately).

Ruedemann, Rudolf, 1947, Graptolites of North America: Geol. Soc. America Mem. 19, 652 p.

Schopf, T. J. M., 1966, Conodonts of the Trenton Group (Ordovician) in New York, southern Ontario, and Quebec: New York State Mus. and Sci. Ser. Bull. 405, 105 p.

Schuchert, Charles, 1916, Silurian formations of southeastern New York, New Jersey, and Pennsylvania: Geol. Soc. America Bull., v. 27, p. 531–554.

Stose, G. W., 1930, Unconformity at the base of the Silurian in southeastern Pennsylvania: Geol. Soc. America Bull., v. 41, p. 629–658.

Sweet, W. C., and Bergström, S. M., 1970, Stratigraphic significance of conodonts from the Lexington Limestone and Kope Formation in the Cincinnati region [abs.]: Geol. Soc. America Abs. with Programs, v. 2, no. 3, p. 242–243.

—— 1971, The American Upper Ordovician standard XIII–A revised time-stratigraphic classification of North American upper Middle and Upper Ordovician rocks: Geol. Soc. America Bull., v. 82, p. 613–628.

Twenhofel, W. H., and others, 1954, Correlation of the Ordovician formations of North America: Geol. Soc. America Bull., v. 65, p. 247–298.

Willard, Bradford, and Cleaves, A. B., 1939, Ordovician-Silurian relations in Pennsylvania: Geol. Soc. America Bull., v. 50, p. 1165–1198.

Jour. Research U.S. Geol. Survey
Vol. 1, No. 1, Jan.–Feb. 1973, p. 39–44

MICROPROBE ANALYSIS OF BIOTITES—A METHOD OF CORRELATING TUFF BEDS IN THE GREEN RIVER FORMATION, COLORADO AND UTAH

By GEORGE A. DESBOROUGH, JANET K. PITMAN,
and JOHN R. DONNELL, Denver, Colo.

Abstract.—Quantitative electron microprobe analyses of biotite grains for iron, magnesium, and titanium from tuff beds in the lacustrine Green River Formation (Eocene) of Colorado and Utah provide a tentative method of identification and a permissive stratigraphic correlation of tuffs. Tuff beds that have been identified and correlated by stratigraphic means were sampled at five localities in Colorado and Utah to determine if microprobe analyses of biotite could be used as a method of correlation. Although most of the original phenocrysts and glass shards of these pyroclastic beds have undergone extensive postdepositional alteration, biotite seems to have been unaffected. The iron, magnesium, and titanium contents of the biotite do not uniquely characterize individual tuff beds, but when the proportions of these elements are compared in a continuous stratigraphic sequence of beds, correlation of individual tuffs or groups of tuffs is possible over areas exceeding several hundred square miles. The method may be used for detailed correlation of pyroclastic beds where stratigraphic, faunal, and radiometric methods have been unsatisfactory.

Biotites from certain thin, persistent tuff beds in the lacustrine Green River Formation (Eocene) of Colorado and Utah have been studied by electron microprobe analysis in an effort to provide a method of characterizing these beds. This information might facilitate the correlation of stratigraphic sequences from one depositional basin to another, particularly in those areas where lacustrine and fluviatile facies of the Green River Formation interfinger and coalesce.

This report gives results of analyses for iron, magnesium, and titanium in biotites from tuff beds of the Green River Formation in Colorado and Utah. The study consisted of two parts: (1) Well-known tuff beds in the Mahogany ledge, Parachute Creek Member, were used as a model to test the consistency in chemical composition of the biotites from tuff beds at one locality with biotites of the same beds at other localities; and (2) biotites from two stratigraphic sequences of unknown tuffs were analyzed to determine if correlation between the sequences might be made from the chemical composition of biotite in each bed.

Upper-Tertiary tuffs that are widely distributed in western North America have been successfully correlated by means of quantitative electron microprobe analysis of "fresh" glass (Smith and Westgate, 1969; Izett and others, 1970). However, the Eocene ash beds of the Green River Formation were subjected to such intensive postdepositional alteration that the original glass shards were converted to zeolites (primarily analcime), quartz, and carbonates (Bradley, 1964). Therefore, we studied only biotites in the tuffs, because they apparently have undergone only minimal alteration. Unaltered hornblende occurs in a few tuffs, but only in trace amounts.

For the sequence of tuffs studied, the radiometric age difference between the oldest and youngest bed is approximately 5 m.y. (R. L. Mauger, written commun, 1971). The precision of K/Ar dating is about ±0.9 m.y. for beds 45 m.y. old; this amount prevents correlation of individual tuffs by absolute age in sequences such as those shown in figures 1 and 2.

Microprobe analysis of biotites, which was used as a method of correlation, was found to be valuable in distinguishing individual beds in a sequence of beds for which stratigraphic, faunal, and radiometric dating methods of identification have not been particularly successful.

ANALYTICAL METHODS

Tuff samples were prepared for analysis by one of three methods. Biotites from selected tuff beds were concentrated in bromoform (method 1), or were separated by electromagnetic techniques (method 2). These grains were mounted in epoxy and polished with diamond pastes. Rock slabs of the tuffs showing biotite were polished in a similar manner (method 3). For one tuff bed, the arithmetic means of iron, magnesium, and titanium in biotite separated by each of the three methods are the same within one standard deviation; therefore, because of the considerable time saving involved, most of the biotite grains analyzed were prepared by polishing rock slabs.

Three chemically homogeneous biotite concentrates, whose iron, magnesium, and titanium content had previously been determined by wet chemical analysis, were used as quantitative standards. Each standard contains the following weight percentage of iron, magnesium, and titanium calculated as an oxide:

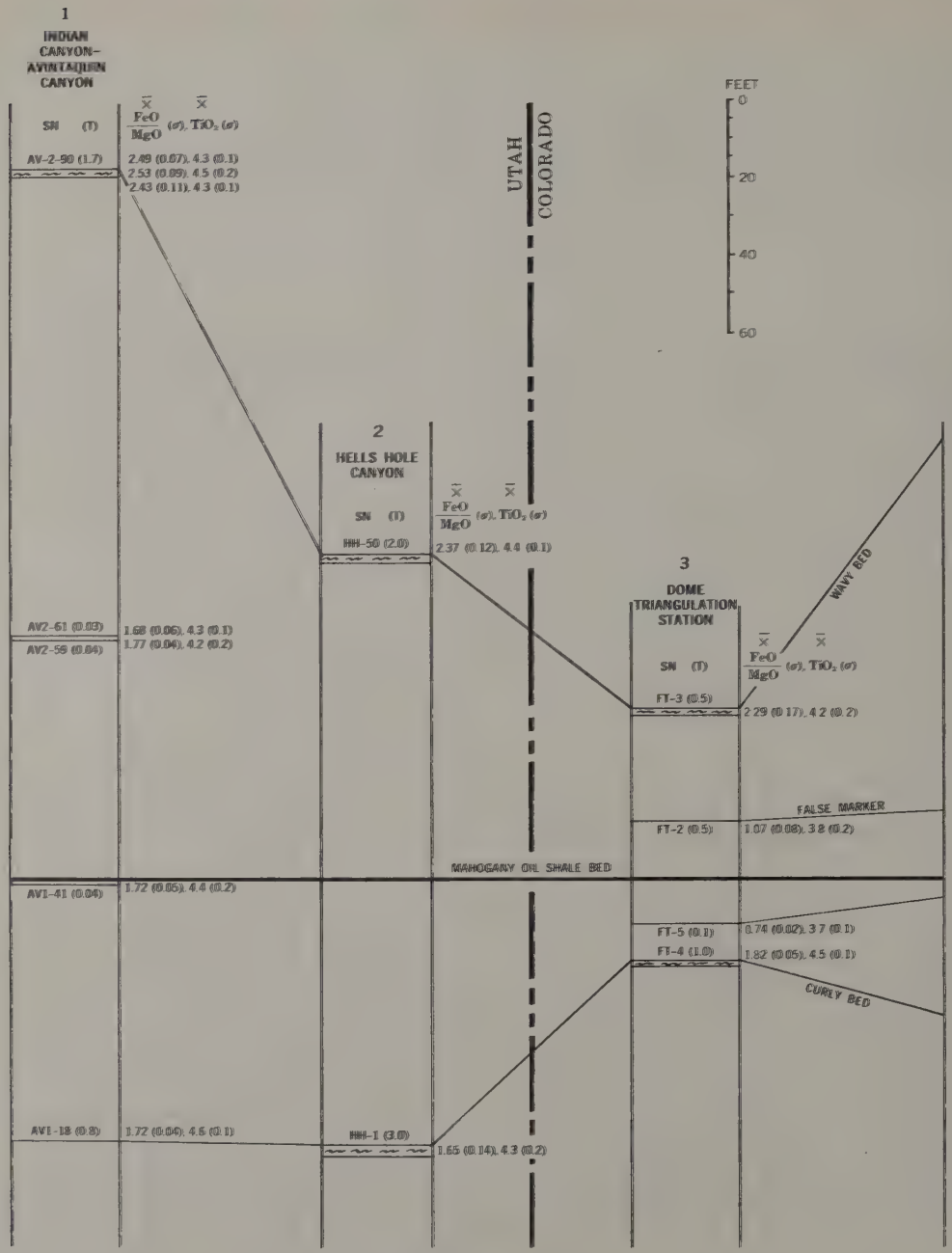

Figure 1.–Correlation of biotitic tuff beds in the Mahogany ledge, Parachute Creek Member, Green River Formation, in Colorado and Utah, showing sample number (SN); thickness of bed in feet (T); and the arithmetic mean ($\bar{x}$) in weight percent, and standard deviation (σ) for FeO/MgO and TiO_2 as determined by microprobe analysis. Localities correspond to those in table 1.

MAP SHOWING LOCATION OF STRATIGRAPHIC SECTIONS

Figure 1.

Table 1.—*Mean weight percentage* ($\bar{X}$) *and standard deviation* (σ) *for* FeO, MgO, *and* TiO_2 *in biotite of selected tuff beds in the Mahogany ledge, Parachute Creek Member, Green River Formation, in Colorado and Utah*

[Locality numbers correspond to those on figure 1]

Bed name	1 Indian Canyon–Avintaquin Canyon, Utah Sec. 14, T. 5 S., R. 4 W.			2 Hells Hole Canyon, Utah Sec. 17, T. 10 S., R. 25 E.			3 Dome triangulation station, Colo. Sec. 7, T. 5 S., R. 10 W.			4 Fourteen Mile Creek, Colo. Sec. 12, T. 3 S., R. 97 W.			5 Savage quarry, Logan Peak, Colo. Sec. 36, T. 7 S., R. 97 W.		
	FeO $\bar{X}$ (σ)	MgO $\bar{X}$ (σ)	TiO_2 $\bar{X}$ (σ)	FeO $\bar{X}$ (σ)	MgO $\bar{X}$ (σ)	TiO_2 $\bar{X}$ (σ)	FeO $\bar{X}$ (σ)	MgO $\bar{X}$ (σ)	TiO_2 $\bar{X}$ (σ)	FeO $\bar{X}$ (σ)	MgO $\bar{X}$ (σ)	TiO_2 $\bar{X}$ (σ)	FeO $\bar{X}$ (σ)	MgO $\bar{X}$ (σ)	TiO_2 $\bar{X}$ (σ)
Wavy	[1]22.9(0.4)	9.2(0.2)	4.3(0.1)	22.0(0.5)	9.3(0.3)	4.4(0.1)	22.1(0.7)	9.7(0.5)	4.2(0.2)	21.3(1.4)	9.2(0.3)	4.2(0.2)	21.7(0.7)	10.2(0.6)	[1]4.0(0.2)
	[2]22.7(0.4)	9.0(0.2)	4.5(0.2)	.....	.....	.....	.....	.....	.....	.....	.....	.....	.....	.....	.....
	22.5(0.4)	9.3(0.5)	4.3(0.1)	.....	.....	.....	.....	.....	.....	.....	.....	.....	.....	.....	.....
Unnamed	21.0(0.4)	12.5(0.5)	4.3(0.1)	.....	.....	.....	.....	.....	.....	.....	.....	.....	.....	.....	.....
Do.	19.5(0.4)	11.0(0.3)	4.2(0.2)	.....	.....	.....	15.3(0.5)	14.3(0.3)	3.8(0.2)	.....	.....	.....	14.3(0.8)	14.7(0.6)	4.1(0.1)
False marker	.....	.....	.....	.....	.....	.....	.....	.....	.....	20.8(0.9)	10.5(0.4)	4.3(0.2)	16.8(0.8)	12.4(0.5)	3.5(0.1)
Mahogany marker	.....	.....	.....	.....	.....	.....	.....	.....	.....	.....	.....	.....	.....	.....	.....
Unnamed	19.6(0.4)	11.4(0.3)	4.4(0.2)	.....	.....	.....	12.6(0.2)	17.0(0.4)	3.7(0.1)	13.1(0.2)	17.2(0.2)	3.9(0.1)	.....	.....	.....
Do.	.....	.....	.....	.....	.....	.....	.....	.....	.....	15.5(0.8)	13.6(0.5)	4.6(0.2)	.....	.....	.....
Do.	.....	.....	.....	.....	.....	.....	.....	.....	.....	19.4(0.4)	11.2(0.3)	4.3(0.1)	.....	.....	.....
Curly	19.1(0.4)	11.1(0.2)	4.6(0.1)	19.0(0.67)	11.6(0.8)	4.3(0.2)	20.2(0.3)	11.1(0.2)	4.5(0.1)	19.4(0.4)	11.2(0.3)	4.3(0.1)	19.5(0.7)	10.8(0.5)	4.3(0.2)

[1] Magnetic concentrate.

[2] Bromoform concentrate.

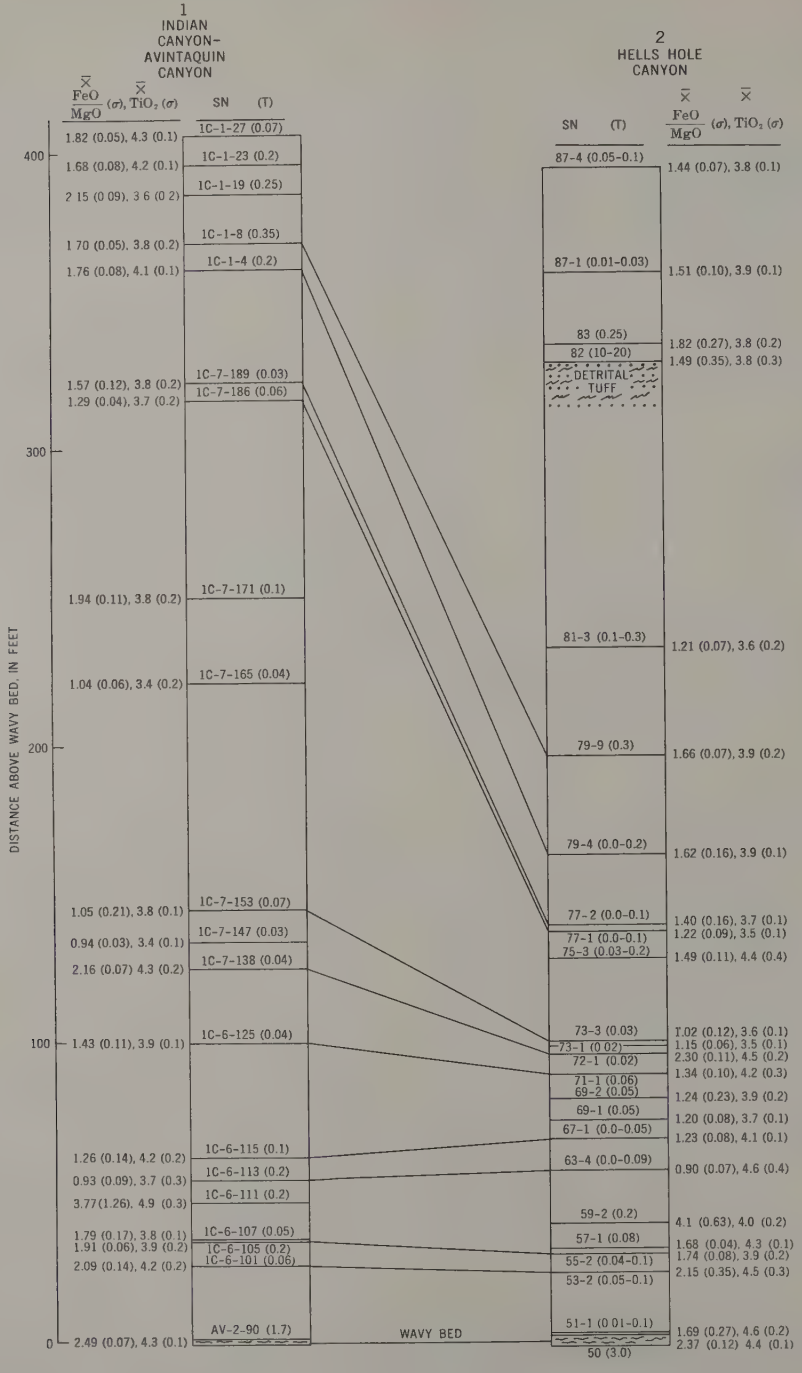

Figure 2.—Correlation based on microprobe analysis of biotitic tuffs above the wavy bed, Parachute Creek Member, Green River Formation, in the Uinta Basin, showing sample number (SN); thickness of bed in feet (T); and the arithmetic mean ($\bar{X}$) in weight percent, and standard deviation (σ) for FeO/MgO and TiO_2. Localities are shown on figure 1.

	FeO	MgO	TiO_2
1	31.39	2.93	1.45
2	34.71	1.24	3.85
3	11.00	19.90	1.58

Because iron in the divalent and trivalent state cannot be distinguished by microprobe analysis, all iron is reported as FeO. Measurements of X-ray intensities (counts) of the $K\alpha$ lines for the elements were recorded before and after analysis of the samples. Calibration curves were constructed by plotting elemental weight percentage against accumulated counts. These procedures corrected for background and instrument drift. All analyses were performed at 10 kV with 2×10^{-4} amperes emission current, 2×10^{-8} amperes sample current, an integrated beam current, and electron beam size of 5–10 μm.

Twenty-five biotite grains per sample were analyzed for iron, magnesium, and titanium with two to four measurements obtained for each grain. A mean weight percentage and a standard deviation for FeO, MgO, TiO_2 and FeO/MgO were calculated for each grain. For each sample, a mean weight percentage and a standard deviation were computed for each element and for the FeO/MgO ratio from results calculated for each of the individual grains. This method permitted an FeO/MgO ratio to be computed for a sample as well as allowing equal emphasis to the ratio of each grain. High compositional homogeneity among individual biotite grains in each sample was indicated by the small variation in counts.

STRATIGRAPHY

The Parachute Creek Member of the Green River Formation underlies large areas of the Piceance Creek basin in Colorado and the Uinta Basin in Utah. This interval is well known because of detailed studies of the rich oil shale. The lower part of the member is composed of oil shale, interbedded with thin, persistent tuff beds ranging in thickness from 0.5 inches to 3 feet. Certain rich oil shale units within the Parachute Creek Member are used as key stratigraphic markers. The Mahogany ledge is one of the thickest and richest of these units. Within the Mahogany ledge is a thin, persistent, exceedingly rich bed known as the Mahogany bed; it serves as an excellent stratigraphic marker and is laterally persistent for several hundred miles along the outcrop (Donnell, 1961).

The upper part of the Parachute Creek Member consists of marlstone, siltstone, and some tuffaceous sandstone. In this rock sequence, the volume of clastic material varies considerably, and as a result the thickness of the stratigraphic intervals between individual beds may vary significantly over short distances. Donnell (1961) has described and mapped beds of the Green River Formation in the Piceance Creek basin, and Cashion (1967) has studied time-equivalent beds in the Uinta Basin. These investigations as well as other subsequent studies provide the stratigraphic information upon which this report is based.

Numerous tuff beds are in the Parachute Creek Member, but only a few have been widely correlated (Donnell, 1961; Cashion, 1967; Cashion and Donnell, 1972). Many of the tuffs do not have sufficient thickness, lateral extent, or unique lithologic characteristics to permit field identification over large areas. Several of the tuffs contain biotite suitable for our study; however, many tuff beds throughout the sequence studied are nonbiotitic and have not been discussed in this report. Among the key tuff beds that have been widely recognized and that have been studied for this report is the wavy bed. This tuff marks the base of the "tuff zone," Parachute Creek Member (Dane, 1955), and is equivalent to the "wavy bedded analcitized tuff" (Cashion, 1967, pl. 3; Donnell, 1961, pl. 53). The wavy bed is an excellent time-stratigraphic marker and is present throughout the southern part of the Piceance Creek basin and the Uinta Basin.

RESULTS OF ANALYSES

In the first part of the present study, well-known tuff beds below the wavy bed were sampled from five localities in Colorado and Utah. Figure 1 shows the stratigraphic positions of these beds at each of the localities. Microprobe analyses of biotites from corresponding beds are listed in table 1. The chemical data indicate that the biotite from any specific tuff bed has almost the same chemical composition as the biotite from the same bed at a different locality. The biotite composition among tuff beds is sufficiently different to permit some tuffs to be distinguished from others. The arithmetic means for the weight percentages of FeO, MgO, and TiO_2 for a particular bed may be distinctly different from those of other beds within a sequence. However, samples of an individual tuff bed but from various localities have the same mean within 1½ standard deviations.

The lateral consistency in composition shown by the analyses indicates that postdepositional alteration had little or no effect on biotites in any of the tuff beds, regardless of the geographic locality, and that detrital biotite has not been added to any of the tuffs studied. Because the contents of FeO, MgO, and TiO_2 in the biotite grains of a single tuff sample follow a normal distribution about a mean, it is assumed that little if any mixing of ash from more than one source occurred.

In the second part of the study, biotites from stratigraphic sequences of tuff beds above the wavy bed at two localities were analyzed. Correlations of these tuffs between localities by use of other methods have been unsuccessful. Stratigraphic positions and the mean FeO/MgO ratio and TiO_2 content for biotites in these tuffs are reported in figure 2. The mean FeO/MgO ratio and mean TiO_2 contents of individual tuffs may not be distinctive taken alone; however, they can be used with confidence in correlating a sequence of tuff beds. For example, the mean FeO/MgO ratio of samples IC-6-113 and 63-4 (fig. 2) is about 0.9, in a sequence of beds having ratios from 1.2 to 4.1. Samples IC-7-138 and 72-1 have a mean

FeO/MgO of 2.2 in a sequence with ratios ranging from 1.0 to 1.4. Correlations might be made on one bed with such distinctive FeO/MgO ratios, but the chemical composition of adjacent beds in a stratigraphic sequence establishes a pattern which remains relatively constant at localities 1 and 2. This pattern may allow one to determine if some beds are absent or if they are unrecognizable.

CONCLUSIONS

Microprobe analysis may provide a quantitative method of identifying tuff beds within a sequence of biotite-bearing beds in the absence of other stratigraphic controls, and it is useful in extending correlations over relatively long distances without detailed stratigraphic measurements between localities.

ACKNOWLEDGMENTS

The authors acknowledge the following individuals for their cooperation in providing measured stratigraphic sections and field consultation: J. R. Dyni and W. B. Cashion for Indian Canyon–Avintaquin Canyon, Utah; W. B. Cashion for Hells Hole Canyon, Utah; and R. B. O'Sullivan for Fourteen Mile Creek, Colo. R. L. Mauger provided unpublished K/Ar radiometric dates. We thank Jacquie Tripp for aid in sample preparation and data reduction. We appreciate helpful suggestions provided by Charles Maxwell, W. B. Cashion, J. R. Dyni, and W. J. Mapel on the manuscript.

REFERENCES CITED

Bradley, W. H., 1964, Geology of the Green River Formation and associated Eocene rocks in southwestern Wyoming and adjacent parts of Colorado and Utah: U.S. Geol. Survey Prof. Paper 496-A, 86 p.

Cashion, W. B., 1967, Geology and fuel resources of the Green River Formation, southeastern Uinta Basin, Utah and Colorado: U.S. Geol. Survey Prof. Paper 548, 48 p.

Cashion, W. B., and Donnell, J. R., 1972, Chart showing correlation of selected key units in the organic-rich sequence of the Green River Formation, Piceance Creek Basin, Colorado, and Uinta Basin, Utah: U.S. Geol. Survey Oil and Gas Inv. Chart OC-65.

Dane, C. H., 1955, Stratigraphic and facies relationships of the upper part of the Green River formation and the lower part of the Uinta formation in Duchesne, Uintah, and Wasatch Counties, Utah: U.S. Geol. Survey Oil and Gas Inv. Chart OC-52.

Donnell, J. R., 1961, Tertiary geology and oil-shale resources of the Piceance Creek basin between the Colorado and White Rivers, northwestern Colorado: U.S. Geol. Survey Bull. 1082-L, p. 835–891.

Izett, G. A., Wilcox, R. E., Powers, H. A., and Desborough, G. A., 1970, The Bishop Ash bed, a Pleistocene marker bed in the Western United States: Quaternary Research, v. 1, no. 1, p. 121–132.

Smith, D. G. W., and Westgate, J. A., 1969, Electron probe technique for characterising pyroclastic deposits: Earth and Planetary Sci. Letters, v. 5, p. 313–319.

Jour. Research U.S. Geol. Survey
Vol. 1, No. 1, Jan.–Feb. 1973, p. 45–52

CRETACEOUS MAFIC CONGLOMERATE NEAR GUALALA OFFSET 350 MILES BY SAN ANDREAS FAULT FROM OCEANIC CRUSTAL SOURCE NEAR EAGLE REST PEAK, CALIFORNIA

By DONALD C. ROSS, CARL M. WENTWORTH, and EDWIN H. McKEE,
Menlo Park, Calif.

Abstract.—Upper Cretaceous mafic conglomerate and quartz-plagioclase arkose that crop out on the southwest side of the San Andreas fault near Gualala, Calif., may have been eroded from a gabbroic terrane that now lies about 350 miles to the southeast, on the opposite side of the San Andreas fault. The plagioclase arkose near Gualala contains little or no K-feldspar, and the conglomerate is characterized by quartz-bearing mafic rocks that lack K-feldspar–volcanic rocks, diabase, and diorite to gabbro. Hornblendes from these clasts yield K/Ar ages of 141±4, 175±7, and 186±7 m.y. The arkose and conglomerate appear to have been eroded from a chert-poor ophiolite (oceanic crust) sequence that, according to paleocurrent evidence, lay east of the present San Andreas fault. Near Eagle Rest Peak, 350 miles southeast of Gualala, similar mafic quartz-bearing volcanic rocks, diabase, and gabbro are exposed in a small structurally isolated area that abuts the San Andreas fault on the southwest. These rocks yield hornblende K/Ar ages of 134±4, 165±4, and 207±10 m.y. They may also be the source of two small fault slivers of similar mafic rocks, which yield hornblende K/Ar ages between 144 and 172 m.y. These slivers now lie 100 and 200 miles to the northwest along the San Andreas fault at Gold Hill and Logan.

Upper Cretaceous sedimentary rocks near Gualala, Calif., offer a possible key to a Late Cretaceous tie across the San Andreas fault because of their unusual mafic composition and present separation from their source by that fault. Studies of basement rocks along the San Andreas fault by Ross (1970, 1972) and of the Cretaceous and Tertiary sedimentary rocks near Gualala by Wentworth (1966, 1968) have led to proposals that these unusual sedimentary rocks were eroded from a terrane of oceanic crust, a remnant of which is preserved as the gabbroic rocks in the western San Emigdio Mountains, now offset about 350 miles from Gualala by the San Andreas fault. In contrast, Cretaceous and lower Tertiary arkose and granitic conglomerate associated with the mafic sedimentary rocks were probably derived from Salinian granitic basement.

This report provides additional petrographic data on the mafic and granitic clasts in the two types of Gualala conglomerates, records seven K/Ar mineral dates from those clasts and the possible mafic source terrane, and discusses the limitations that these data place on the characteristics of the basement source areas of the two conglomerates.

THE SEDIMENTARY SEQUENCE NEAR GUALALA

The conglomerates occur scattered throughout a tripartite stratigraphic sequence of marine sandstone, mudstone, and conglomerate. The sequence consists of two intertonguing Upper Cretaceous facies, one of K-feldspar arkose and granitic conglomerate and one of plagioclase arkose and mafic conglomerate, which together are overlain by K-feldspar arkose and granitic conglomerate of Paleocene and Eocene age (fig. 1). The entire sequence, including the conglomerate, was deposited at bathyal depths by turbidity currents, as indicated by sedimentary structures and by interbedding of sandstone and conglomerate beds, some of which contain abundant shallow-water megafossils, with mudstone beds containing deepwater foraminifers. The foraminifers indicate that both the K-feldspar and the plagioclase arkoses were deposited contemporaneously during late Campanian and (or) early Maestrichtian time.

The orientation of the more regular cross-laminations and of some linear structures in the plagioclase arkose and in the younger (Tertiary) K-feldspar arkose suggests that the two lithologies were supplied from opposite sides of a northwest-trending basin (fig. 1). The source of the Cretaceous K-feldspar arkose, which lacks mesoscopic paleocurrent indicators, is assumed to be the same as that of the Tertiary arkose because the two rocks are similar in composition and contain the same kinds of granitic conglomerate clasts. The currents that deposited both the plagioclase and K-feldspar parts flowed northwestward for the most part, suggesting deposition in a northwest-trending basin. However, some northward and northeastward directional components in the K-feldspar arkose and contrasting westward and southwestward components in the plagioclase arkose suggest that the two lithologies were supplied from opposite sides of the northwest-trending basin.

Conglomerate occurs scattered throughout the two units and, like the sandstone, has distinctly contrasting compositions in the two lithologies. The conglomerate associated with the plagioclase arkose is characterized by a gabbroic suite, which is the sole component of conglomerate in the Anchor

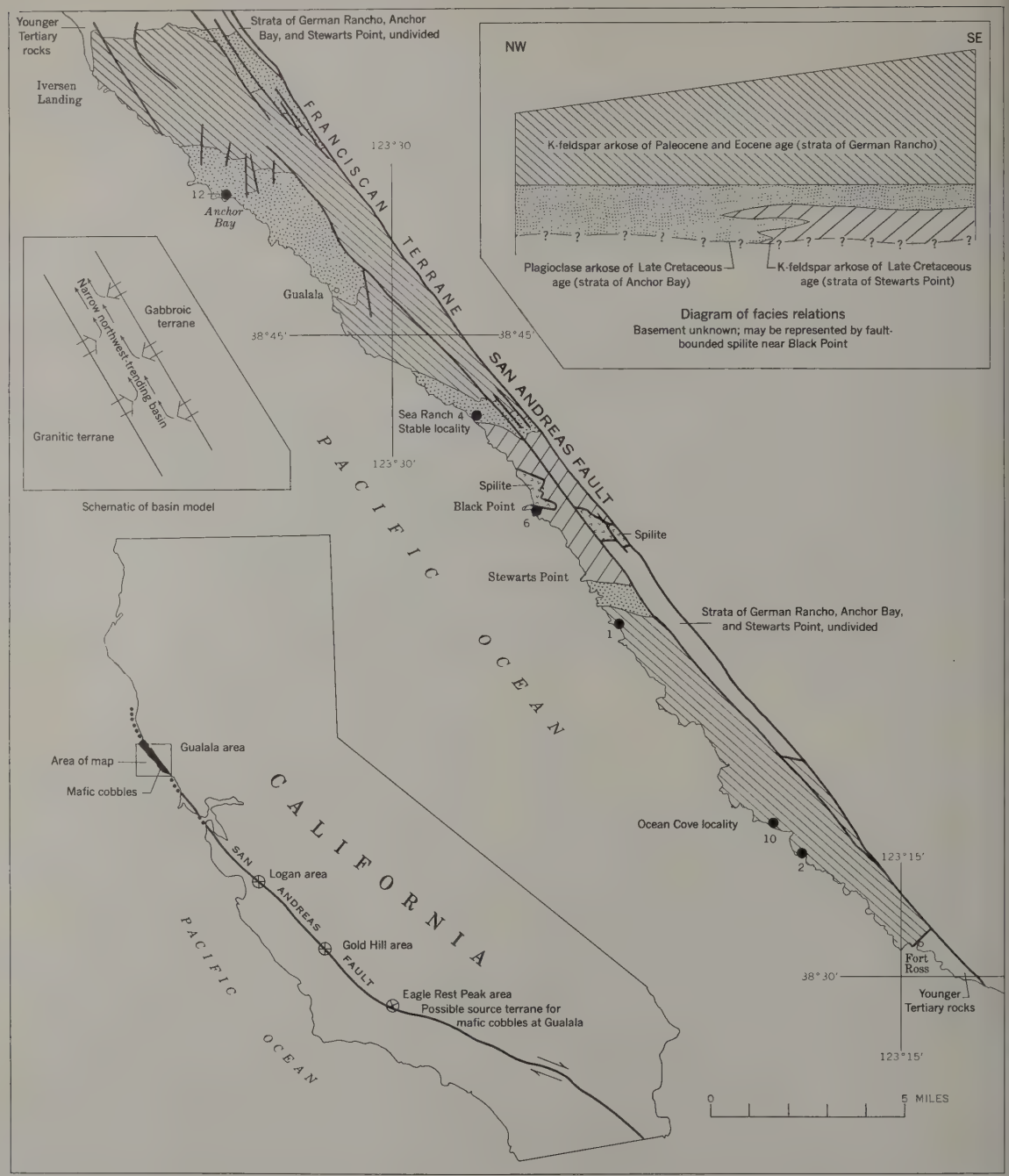

Figure 1.—Index map, generalized geologic map, basin model, and diagram of facies relations in the Gualala area, California. Dots indicate sample localities of modally analyzed conglomerate clasts; number of modes shown for each locality.

Bay area, and is diluted in the Sea Ranch Stable locality by resistant siliceous volcanic clasts at least superficially similar to those present throughout the sedimentary section in the Coast Ranges. Conglomerate in the K-feldspar arkose lacks gabbroic clasts entirely and is characterized by granitic clasts, which are accompanied by abundant siliceous volcanic clasts in the Cretaceous part and by various metamorphic clasts in the Tertiary part. The conglomerate beds consist of coarse pebbles, cobbles, and sparse boulders and occur both scattered in the sequence and to a greater extent concentrated in sequences a few feet to hundreds of feet thick. The samples discussed in this report were collected from most of the major occurrences of conglomerate in the section exposed along the sea cliffs.

CONGLOMERATE CLASTS FROM THE K-FELDSPAR ARKOSE

Four localities where conglomeratic layers in the K-feldspar arkose are particularly well exposed are shown on figure 1. These localities are dominated by granitic clasts ranging in size from small pebbles to boulders more than 1 foot in diameter. Clasts of marble, felsic gneiss, mica schist, amphibolite, quartzite, and volcanic rocks are also present in the conglomerates, but this report will concentrate on the granitic debris. The granitic clasts range from white alaskite to quartz diorite with 15 to 20 percent dark minerals and from fine- to coarse-grained varieties. Quartz is generally abundant, plagioclase is oligoclase to andesine, biotite is yellow and brown, and green hornblende commonly is intensely altered. These clasts form a rather prosaic suite of granitic rocks ranging from quartz monzonite to quartz diorite.

The northernmost locality, near Black Point (fig. 1), is part of Wentworth's (1968) strata of Stewarts Point of Cretaceous age, whereas the other three localities to the south are part of his strata of German Rancho of Paleocene and Eocene age. Although only a limited number of samples were studied, the same range of rock types and compositions is found in both age groups. The limited modal data plotted on figure 2, however, suggest that the Cretaceous strata may have a higher percentage of felsic rock types.

Clasts from both the Cretaceous and the Paleocene and Eocene strata define a somewhat linear, nearly horizontal modal field (fig. 2), showing that the quartz content is relatively constant throughout the compositional range. Another diagnostic feature of these clasts is the rarity or complete absence of metallic opaque minerals even in rocks containing as much as 15 percent biotite and hornblende. Several percent of garnet was found in some clasts.

CONGLOMERATE CLASTS FROM THE PLAGIOCLASE ARKOSE

Two of the best exposures of the conglomeratic layers in the plagioclase arkose, the Anchor Bay and Sea Ranch Stable localities (fig. 1), were extensively sampled. The clasts are dominantly fine- to medium-grained gabbro and diorite, fine-grained diabase, and quartz-bearing mafic volcanic rock. The absence of K-feldspar in most specimens, even some that are relatively light colored and rich in quartz, is characteristic. Olivine-bearing ultramafic clasts are present but extremely rare. Some of the gabbroic rocks are gneissic, but metamorphic clasts appear to be lacking. The modal plot (fig. 2) is mostly of quartz diorite and gabbro specimens, with minor representation of diabase. Additional diabase and mafic volcanic specimens would not markedly alter the modal field but would add points on the plagioclase-quartz tieline in the range of 0 to 20 percent quartz.

The most abundant clast type, and consequently the most extensively sampled, at both the Anchor Bay and Sea Ranch Stable localities is quartz diorite-quartz gabbro, which ranges from fine to medium grained; coarse-grained types are also present but rare. Dark-mineral content, and hence color, varies considerably, but more of these rocks look like average diorite and gabbro, even though many contain abundant quartz. The complete absence of K-feldspar is particularly surprising in the lighter colored clasts, some of which have rather large masses of quartz. Plagioclase is in the andesine-labradorite range and is in part intensely altered. The dark minerals, which range from 10 to 40 percent, consist dominantly of hornblende, with lesser biotite, and minor clinopyroxene as cores of some hornblende. Fresh biotite is rare in these rocks, but a few traces of unchloritized reddish-brown biotite remain. Hornblende is also intensely altered, but most rocks preserve a little relatively fresh hornblende that is pleochroic from moderate greenish yellow to light olive and grayish green.

Clasts of medium- to coarse-grained gabbro rich in amphibole and clinopyroxene that have well-developed bladed plagioclase crystals are abundant at the Sea Ranch Stable locality but are virtually absent in the Anchor Bay area. These rocks are in part diabasic and grade to coarser anorthositic gabbro. Plagioclase is as calcic as bytownite in some of these specimens.

Finer grained rocks with typical diabasic texture are also present. These rocks are in part quartz bearing, seem to have about the same composition as the gabbros, and may be gradational in grain size with the gabbros. Some contain both clinopyroxene and amphibole, others only amphibole. The most distinctive feature of these rather prosaic dark diabases is that some contain 10 percent of quartz or more.

Another locally abundant rock type is a dense, dark-gray rock with a pilotaxitic mat of plagioclase laths as much as 1 mm long set in a groundmass of amphibole, chlorite, epidote, and some interstitial quartz. Varieties of these volcanic rocks also have small quartz phenocrysts as large as 1 mm across as well as plagioclase and amphibole phenocrysts of about the same size. The variety of gabbroic rocks suggests that there are all gradations from these dense pilotaxitic volcanic types, through diabasic types, to medium- to coarse-grained anorthositic gabbro of possible cumulate origin.

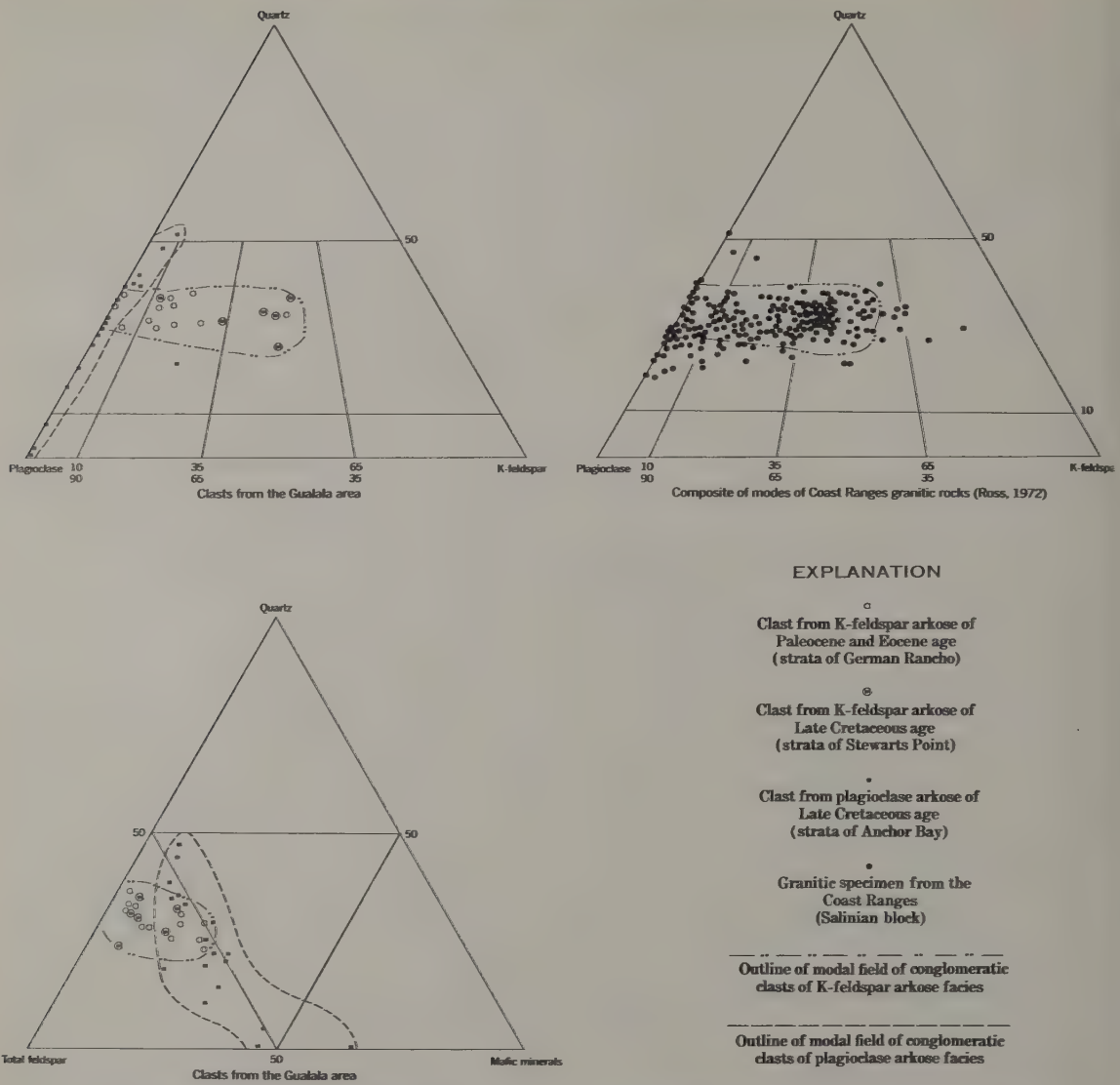
Quartz
50
Plagioclase 10 35 65
90 65 35
K-feldspar
Clasts from the Gualala area
Quartz
50
10
Plagioclase 10 35 65
90 65 35
K-feldspa
Composite of modes of Coast Ranges granitic rocks (Ross, 1972)
Quartz
50
50
Total feldspar
50
Mafic minerals
Clasts from the Gualala area
EXPLANATION
Clast from K-feldspar arkose of Paleocene and Eocene age (strata of German Rancho)
Clast from K-feldspar arkose of Late Cretaceous age (strata of Stewarts Point)
Clast from plagioclase arkose of Late Cretaceous age (strata of Anchor Bay)
Granitic specimen from the Coast Ranges (Salinian block)
Outline of modal field of conglomeratic clasts of K-feldspar arkose facies
Outline of modal field of conglomeratic clasts of plagioclase arkose facies

Figure 2.—Modal plots of conglomerate clasts from the Gualala area and of granitic rocks in the California Coast Ranges.

SOURCE OF THE CONGLOMERATE CLASTS IN THE K-FELDSPAR ARKOSE

The basement terrane that supplied the K-feldspar arkose and associated conglomerate must have had an abundance of relatively quartz-rich granitic rocks ranging from quartz monzonite to quartz diorite. In addition, significant amounts of calcareous, micaceous, and siliceous metamorphic rocks were present, and mafic plutonic rocks were rare. Such conditions are easily satisfied throughout much of the Cordilleran batholithic belt, but the nearest and most obvious source area is the Salinian block of the California Coast Ranges. The general basement rock types in the Salinian block (Ross, 1972) are similar to those in the clasts of the K-feldspar arkose facies. More specifically, as shown by figure 2, the modal field of the conglomerate clasts bears a close correspondence to the composite plot of modes for specimens from the granitic rocks of the Salinian block. The Salinian modal trend is unusual

because it is more horizontal than the modal trend of most other granitic suites in the Cordilleran batholithic belt (Ross, 1972), which strengthens the case for correlation.

The physical and petrographic qualifications of the Salinian block as a source for the conglomerate clasts of the K-feldspar arkose facies are convincing. Coupled with this is the paleocurrent evidence that the K-feldspar arkose material was derived from southwest of the Gualala basin. In addition, a K/Ar age of 82±3 m.y. (table 1) was obtained from hornblende separated from a clast at the Ocean Cove locality (fig. 1). This age lies within the 70- to 90-m.y. determinations that have been made on numerous biotites and hornblendes from the Salinian block of the California Coast Ranges (Curtis and others, 1958; Evernden and Kistler, 1970; Huffman, 1970). Together, these factors strongly indicate that the Salinian block granitic terrane is the source for the K-feldspar arkose and associated granitic conglomerate.

SOURCE OF THE CONGLOMERATE CLASTS IN THE PLAGIOCLASE ARKOSE

The basement source that supplied the sediment for the plagioclase arkose and mafic conglomerate was rich in gabbro, diorite, diabase, and dark volcanic rocks, all characterized by the common presence of quartz, and was virtually devoid of K-feldspar-bearing rocks. The sediment must have been derived from a terrane virtually free of granitic rocks, for any granitic rock present would have been concentrated to some degree in the weathering cycle at the expense of the less stable gabbroic rocks (Goldich, 1938). Such a quartz-bearing mafic terrane is not easy to locate in the region—in fact, no such basement terrane large enough to supply cubic miles of gabbroic sedimentary debris now exists anywhere in the western Cordilleran batholithic belt. The difficulty is further compounded by paleocurrents that indicate that the sediments were derived from northeast of the Gualala basin, where the presently exposed basement is the Franciscan Formation, an unsuitable source terrane for the clasts of the plagioclase arkose. As Wentworth pointed out in 1968, the search for a suitable source area should probably focus on the area of the San Emigdio Mountains far to the southeast across the San Andreas fault. Ross later (1970) noted that the bulk of the San Emigdio basement was relatively rich in K-feldspar-bearing granitic rocks, which were not suitable as a source terrane for the gabbroic suite of the plagioclase arkose facies. However, the Eagle Rest Peak area (fig. 1; Ross, 1970, fig. 1), which may be structurally separate from the rest of the San Emigdio basement, contains a suite of gabbro, diabase and hornfels (in part quartz bearing), quartz diorite-quartz gabbro, anorthositic gabbro, minor pyroxenite and serpentine, and virtually no K-feldspar-bearing rock. Though the few square miles of present gabbroic exposures are not large enough to have supplied the cubic miles of plagioclase arkose at Gualala, this may be all that is left of what was originally a much larger gabbroic terrane, because the Eagle Rest Peak area abuts against the San Andreas fault. Added to this tantalizing possible correlation are similar gabbroic blocks at Gold Hill

Table 1.—*Hornblende mineral ages*

[Potassium measurements were made on an I. L. flame photometer with a lithium internal standard. Argon measurements were made using standard techniques of isotope dilution. Ages were calculated using these constants: K^{40} decay constants: $\lambda_\epsilon = 0.585\times10^{-10}$ year^{-1}; $\lambda_\beta = 4.72\times10^{-10}$ year^{-1}. Abundance ratio: $K^{40}/K = 1.19\times10^{-4}$ atom percent. Analysts: Potassium measurements, Lois Schlocker; argon measurements and age calculation, E. H. McKee, except ABc-4 and DR-1169A by J. C. Von Essen]

Sample	K_2O (percent)	Ar^{40}_{rad} (moles/g$\times10^{-11}$)	$\frac{Ar^{40}_{rad}}{Ar^{40}_{total}}$	Calculated age (m.y.)
Gualala area:				
Anchor Bay:				
ABc-1	0.207	5.608	0.09	175±8
ABc-4	.098	2.135	.52	141±4
ABi-1	.250	7.20	.54	186±7
Ocean Cove:				
OC-3	.198	1.99	.22	82±3
Eagle Rest Peak area:				
DR-1169A	.204	4.202	.55	134±4
DR-1182C	.190	4.82	.26	165±6
DR-1189C	.107	3.46	.41	207±10

Location and description of samples:

Gualala area:

Anchor Bay: Gualala 7½-minute quadrangle, Mendocino County, Calif., lat 38°48′ N., long 123°35′ W. Clasts from plagioclase arkose facies.

ABc-1, Hornblende quartz diorite-quartz gabbro (andesine-labradorite 49 percent, hornblende 25, quartz 22, biotite 2, opaque minerals 2).

ABc-4, Hornblende quartz gabbro (labradorite 50 percent, hornblende 40, quartz 10, minor biotite, clinopyroxene, and opaque minerals).

ABi-1, Hornblende quartz diabase (andesine 59 percent, hornblende 26, quartz 11, opaque minerals 4).

Ocean Cove: Plantation 7½-minute quadrangle, Sonoma County, Calif., lat 38°33′ N., long 123°19′ W. Clast from K-feldspar arkose facies.

OC-3, Biotite granodiorite (oligoclase(?) 43 percent, K-feldspar 12, quartz 34, biotite 8, pale-green hornblende 3).

Eagle Rest Peak area:

DR-1169A: Eagle Rest Peak 7½-minute quadrangle, Kern County, Calif., lat 34°56′ N., long 119°13′ W. Hornblende-quartz gabbro (labradorite, grayish-green hornblende, quartz, abundant opaque minerals, minor clinopyroxene).

DR-1182C: Santiago Creek 7½-minute quadrangle, Kern County, Calif., lat 34°56′, long 119°15′ W. Hornblende-quartz gabbro (labradorite, grayish-green hornblende, quartz, minor biotite, and opaque minerals).

DR-1189C: Eagle Rest Peak 7½-minute quadrangle, Kern County, Calif., lat 34°56′ N., long 119°14′ W. Hornblende-rich pegmatite composed of andesine, euhedral green hornblende in crystals as long as 20 mm ($n_\alpha = 1.636\pm$, $n_\gamma = 1.651\pm$), and quartz. Occurs as dikes or "sweated out" patches in gabbro-pyroxenite suite that is comparable to the anorthositic gabbro at Gold Hill and Logan (Ross, 1970).

and Logan (fig. 1) that seem to be slivers of this basement terrane strewn out along the San Andreas fault.

In appearance and petrography, the anorthositic gabbro at Eagle Rest Peak is strikingly similar to the bladed coarse anorthositic gabbro of the Sea Ranch Stable locality. Also, the presence in both areas of similar quartz diorite-quartz gabbro is noteworthy. In addition, fine-grained dark diabasic rocks and finer grained volcanic varieties are common to both the Gualala and Eagle Rest Peak areas.

Ross (1970, p. 3656), postulated, largely on the basis of earlier work by Hammond (1958), that the Eagle Rest Peak area was a remnant of a pile of volcanic and diabasic rocks intruded by a gabbro-pyroxenite sequence, which in turn was intruded by a quartz diorite-quartz gabbro mass. Such an assemblage would furnish a suitable source terrane for the clasts of the plagioclase arkose and mafic conglomerate of Gualala. Though the percentage of conglomerate clasts of the various rock types has not been determined in the plagioclase arkose facies of Gualala, the dominant rock types are probably gabbro, quartz diorite-quartz gabbro, diabase, and volcanic rocks; one ultramafic clast was found.

To test further the compatibility of the Eagle Rest Peak and Gualala terranes, K/Ar determinations were made on several hornblendes from both terranes (table 1). Figure 3 summarizes these data from the clasts of the plagioclase arkose facies of the Gualala area and the possible parent area of Eagle Rest Peak, and from previously published hornblende ages on similar rocks that may be fault slivers caught between Gualala and Eagle Rest Peak (Ross, 1970). The age range is wide but grossly similar in both terranes. Although these sparse data by no means prove that the Eagle Rest Peak area is the source area for the Gualala clasts, they at least permit that possibility. Hornblende ages from the hornblende quartz gabbro of both areas seem to group at about 135 to 140 m.y. and about 165 to 175 m.y. The diabase clast from Gualala and the gabbro pegmatite from Eagle Rest Peak give expectably older, somewhat comparable hornblende ages. Virtually the same range of ages was found in both areas.

It is interesting to speculate on the meaning of the rather wide range of hornblende ages from these terranes (fig. 3), which we would have expected to have a much more restricted age range. Two distinct ages of hornblende quartz gabbro are at least suggested by the radiometric data, and the Eagle Rest Peak basement would permit two such ages; the two dated localities are separated by a fault but are only 2 miles apart and are petrographically similar. Furthermore, the possible intermediate slivers (Ross, 1970) at Gold Hill and Logan bridge the time gap between the two Eagle Rest Peak specimens. However, in such a spread of ages in what looks like a related suite of similar rocks, the younger ages may reflect argon loss. The intrusive age of the hornblende quartz gabbro is more likely somewhere in the range of 165 to 175 m.y., or even older.

The hornblende determinations from a diabase clast and gabbro pegmatite in the range of 180 to 220 m.y. push the

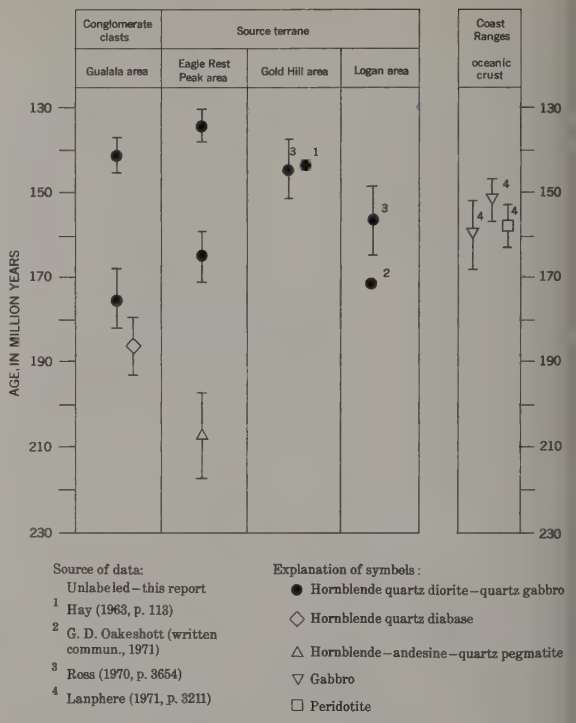

Figure 3.—Comparison of K/Ar ages of hornblendes from conglomerate clasts of the Gualala area, granitic rocks of the Eagle Rest Peak, Gold Hill, and Logan areas, and oceanic crust in the California Coast Ranges.

possible age of these gabbroic terranes down into the very earliest Jurrassic or even into the Triassic. Whatever the true age and range of ages of these gabbroic terranes, we can at least say that a similar range of ages at both Eagle Rest Peak and Gualala supports the view that these two terranes could be related. Furthermore, this range of ages is distinctly different from anything in the Salinian block or in the "Sierran basement" of the Transverse Ranges. The only other somewhat comparable ages from plutonic rocks in this region are from gabbros in the California Coast Ranges that Lanphere (1971, p. 3211) has dated as about 155 m.y. (fig. 3).

OCEANIC CRUSTAL ORIGIN OF THE GABBROIC ROCKS AND CLASTS

The gabbroic and related clasts in the conglomerates of the plagioclase arkose in the Gualala area require a very special and unusual source terrane. The rarity of granitic and metamorphic debris in these conglomerates rules out virtually any present-day basement exposures as a source of the more than 20 cu mi of plagioclase arkose and conglomerate (Wentworth, 1968, p. 136). The gabbroic and related rocks at Eagle Rest Peak are a petrographically suitable source, but what we see now is only a

small remnant of a terrane large enough to father the observed sedimentary product. Wentworth (1968, p. 36) suggested that the source terrane could have been several hundred square miles in area, as the minimum volume of the Gualala plagioclase arkose and conglomerate would cover an area of 100,000 sq mi to a depth of 1 foot.

The type of terrane that best qualifies as a source for the Gualala mafic debris is ophiolitic oceanic crust. Ross (1970, p. 3660) has already speculated that the Eagle Rest Peak locality might be a remnant of ophiolitic oceanic crust. The quartz-bearing gabbro-diabase-volcanic assemblage with minor ultramafic rocks, both at Gualala and Eagle Rest Peak, is compatible with the rock types in ophiolitic oceanic crust as described from various localities in California by Bailey, Blake, and Jones (1970). The K/Ar ages on hornblendes from the gabbroic rocks of Gualala and Eagle Rest Peak are also grossly compatible with K/Ar ages determined by Lanphere (1971, p. 3211) from gabbros from suspected oceanic crust in the California Coast Ranges (fig. 3). The major obstacles to such an identity are the paucity of ultramafic rocks or serpentine and the absence of chert in both the Gualala and Eagle Rest Peak areas. The absence or rarity of some of the members of the common ophiolitic suite at Eagle Rest Peak can be accounted for by assuming that a somewhat nonrepresentative sample of oceanic crust is preserved in the rather limited area now exposed. But this argument is not sufficient to account for the absence of these rocks at Gualala, where many cubic miles of sedimentary debris attest to a large mafic source area.

The lack of chert in the Gualala beds may not pose a serious problem. Though chert is considered one of the "trinity" in the ophiolite suite along with serpentinite and pillow lava, Maxwell (1969, p. 489) noted that it is not everywhere present. Bailey, Blake, and Jones (1970, p. C73) in ten columnar sections of ophiolitic successions in the California Coast Ranges showed no chert in five of the sections. Thus it seems reasonable that chert could be missing from rather wide terranes of oceanic crust, and therefore its absence at Gualala does not preclude derivation of the plagioclase arkose from an oceanic crustal source.

The general absence of ultramafic rock or serpentine clasts in the conglomerates could have resulted from weathering and disaggregation of such rocks in the source area, rather than from their absence there, although the disposition of any resultant finer serpentine sediment is unknown at present. Maxwell (1969, p. 490), in a review of ophiolitic sequences, noted that ultramafic rocks make up 65 to 85 percent of the Tethyan ophiolitic sequences. If this percentage is representative of ophiolitic oceanic crustal sequences, then one might expect considerable ultramafic debris in the Gualala beds if they were derived from an ophiolitic sequence. However, in the suspected ophiolite sequences in the California Coast Ranges that might be expected to represent the kind of terrane that furnished the Gualala debris, Bailey, Blake, and Jones (1970) noted that much of the ultramafic part of the sequence is serpentinized. Such rocks might not survive to become well-rounded clasts in the relatively mature Gualala conglomerates.

The rarity of ultramafic clasts may also be due to their selective alteration and dissaggregation in the weathering and transportation processes attendant to the production of the Gualala conglomerates. The stability series of Goldich (1938) shows that the susceptibility to weathering of the dark-minerals series olivine-pyroxene-amphibole-biotite parallels their order of crystallization in the well-known Bowen reaction series. Thus olivine and pyroxene are highly susceptible to weathering and are less stable than amphibole or biotite. As the biotite and hornblende are almost universally highly altered in the Gualala clasts—at least in part owing to weathering—we consider clasts rich in olivine and pyroxene less likely to survive, even though they may have been abundant in the source area.

It seems reasonable that from a chert-poor ophiolitic sequence, gabbro, quartz gabbro-quartz diorite, diabase, and dense crystallized volcanic rocks (those with little or no glass) could be concentrated in a relatively mature conglomerate. Even though the fit is far from perfect, and regardless of the presence or absence of ultramafic rocks or serpentine in the source area, oceanic crust seems to be the most plausible source for these gabbroic terranes. It is virtually impossible to find a gabbroic continental basement area lacking granitic rocks along the western margin of North America that is large enough to supply the mafic debris of the Gualala area.

SUMMARY AND CONCLUSIONS

Mafic conglomerate and quartz-plagioclase arkose of Late Cretaceous age near Gualala, Calif., may well have been eroded from a gabbroic oceanic crustal terrane that is now offset about 350 miles southeastward from Gualala by the intervening San Andreas fault. This tentative conclusion has resulted from study of basement rocks along the San Andreas fault by Ross (1970, 1972) and study of the Cretaceous and Tertiary sedimentary rocks near Gualala by Wentworth (1966, 1968), in the context of abundant evidence of large right-lateral slip on the San Andreas fault. The character of the Gualala conglomerates is thus a possible key to a Late Cretaceous tie across the San Andreas fault.

Two distinct clastic lithologies near Gualala, one consisting of quartz-plagioclase arkose with mafic conglomerate and one of quartz–K-feldspar–plagioclase arkose with granitic conglomerate, are inferred from paleocurrent indicators to have been derived from opposite sides of a northwest-trending depositional basin. The Salinian granitic terrane southwest of the Gualala rocks seems an adequate source for the K-feldspar arkose facies. But the apparent lack of an adequate source for the plagioclase arkose facies in the Franciscan terrane northeast of and across the San Andreas fault from the Gualala rocks led Wentworth (1968) to suggest right-lateral offset of the source to at least southeast of the Diablo Range (270 miles). Possible spilitic basement with Franciscan affinities beneath granitic sediment derived from the south and west

further led him to suggest offset of the Gualala block from an original position near the presumed intersection of the San Andreas fault and the Sierran-Franciscan basement contact 350 miles to the southeast along the fault. This evidence in turn suggests a source for the mafic conglomerate near the west end of the San Emigdio Mountains.

Ross (1970) concluded that two very similar bodies of quartz gabbro and anorthositic gabbro located about 100 miles apart along the San Andreas fault at Gold Hill and Logan probably were once part of a single gabbroic terrane. Similar rocks in a small gabbroic terrane 100 miles farther to the southeast at the west end of the San Emigdio Mountains near Eagle Rest Peak suggest that the Gold Hill and Logan bodies have been sliced by the San Andreas fault from a once larger gabbroic terrane there.

The mafic Gualala conglomerates contain clasts of the distinctive anorthositic gabbro common to the three localities mentioned above, as well as quartz diorite-quartz gabbro and dark, dense, fine-grained volcanic and diabasic rocks similar to rocks in the Eagle Rest Peak terrane. We conclude that a large area of oceanic crustal material exposed near Eagle Rest Peak in Late Cretaceous time may have yielded the gabbroic sediment rich in quartz and lacking K-feldspar that formed the plagioclase arkose of the Gualala section. Subsequent right-lateral slip on the San Andreas fault then carried the sediment about 350 miles away from the source and also carried two slices of the gabbroic basement terrane to their present intermediate positions at Gold Hill and Logan.

REFERENCES CITED

Bailey, E. H., Blake, M. C., Jr., and Jones, D. L., 1970, On-land Mesozoic oceanic crust in California Coast Ranges, *in* Geological Survey Research 1970: U.S. Geol. Survey Prof. Paper 700-C, p. C70–C81.

Curtis, G. H., Evernden, J. F., and Lipson, J., 1958, Age determinations of some granitic rocks in California by the potassium-argon method: California Div. Mines Spec. Rept. 54, 16 p.

Evernden, J. F., and Kistler, R. W., 1970, Chronology of emplacement of Mesozoic batholithic complexes in California and western Nevada: U.S. Geol. Survey Prof. Paper 623, 42 p.

Goldich, S. S., 1938, A study in rock-weathering: Jour. Geology, v. 46, p. 17–58.

Hammond, P. E., 1958, Geology of the lower Santiago Creek area, San Emigdio Mountains, Kern County, California: California Univ., Los Angeles, unpub. M.S. thesis, 108 p.

Hay, E. A., 1963, Age and relationships of the Gold Hill pluton, Cholame Valley, California, *in* Geology of Salinas Valley and the San Andreas fault: Am. Assoc. Petroleum Geologists, Pacific Sec. Guidebook, p. 113–115.

Huffman, O. F., 1970, Miocene and post-Miocene offset on the San Andreas fault in central California: Geol. Soc. America Abs. with Programs, v. 2, no. 2, p. 104–105.

Lanphere, Marvin, 1971, Age of Mesozoic oceanic crust in the California Coast Ranges: Geol. Soc. America Bull., v. 82, no. 11, p. 3209–3212.

Maxwell, J. C., 1969, "Alpine" mafic and ultramafic rocks—The ophiolite suite: A contribution to the discussion of the paper, "The origin of ultramafic and ultrabasic rocks" by P. J. Wylie: Tectonophysics, p. 489–494.

Ross, D. C., 1970, Quartz gabbro and anorthositic gabbro-markers of offset along the San Andreas fault in the California Coast Ranges: Geol. Soc. America Bull., v. 81, p. 3647–3662.

—— 1972, Petrographic and chemical reconnaissance of some granitic and gneissic rocks near the San Andreas fault from Bodega Head to Cajon Pass, California: U.S. Geol. Survey Prof. Paper 698, 93 p.

Wentworth, C. M., Jr., 1966, The Upper Cretaceous and lower Tertiary rocks of the Gualala area, northern Coast Ranges, California: Stanford Univ., unpub. Ph. D. thesis, 197 p.

—— 1968, Upper Cretaceous and lower Tertiary strata near Gualala, California, and inferred large right lateral slip on the San Andreas fault: Stanford Univ. Pubs. Geol. Sci., v. 11, p. 130–143.

Jour. Research U.S. Geol. Survey
Vol. 1, No. 1, Jan.–Feb. 1973, p. 53–61

BLUESCHIST METAMORPHISM IN THE YREKA–FORT JONES AREA, KLAMATH MOUNTAINS, CALIFORNIA

By PRESTON E. HOTZ, Menlo Park, Calif.

Abstract.—Blueschist is plentiful in the Yreka–Fort Jones area, eastern Klamath Mountains, adjacent to a belt of serpentinite that marks the boundary between two fundamental lithologic units, an eastern belt of early Paleozoic sedimentary and metamorphic rocks, and a western greenstone-chert assemblage of late Paleozoic and Triassic(?) age. The blueschists, which contain lawsonite and glaucophane or crossite, occur with phyllitic quartzite and siliceous phyllite of the Stuart Fork Formation, which is overthrust northwestward on the greenstone-chert terrane. The blueschist facies metamorphism probably was synchronous with Middle and Late Jurassic metamorphism of the Stuart Fork Formation. The blueschist-serpentinite terrane possibly marks the site of collision between the eastern Klamath plate and an oceanic western Paleozoic and Triassic plate.

Although blueschist facies metamorphic rocks occur at many places adjacent to the Klamath Mountains in the Coast Ranges of northern California and southwestern Oregon (Blake and others, 1967; Blake, 1969; Coleman and Lanphere, 1971), they are unusual within the Klamath Mountains province. They were first reported in this province by Masson (1949), who discovered an outcrop of glaucophane-lawsonite rock north of Fort Jones in Siskiyou County, Calif. Recent mapping by the writer in the Hornbrook, Yreka, and Fort Jones 15-minute quadrangles has shown that blueschist is plentiful in this region. Blueschist and ultramafic rock occur near the boundary between two distinctive lithologic belts: the western Paleozoic and Triassic belt and the eastern Klamath belt, as defined by Irwin (1960, 1966). The former, lying to the northwest, comprises a greenstone-chert assemblage; the latter, to the southeast, Paleozoic sedimentary and metamorphic rocks. (See fig. 1.)

The only other occurrences of blueschist that have been found in the Klamath Mountains are south of Cecilville, Calif. (Davis, 1968) (fig. 2), and an isolated occurrence in the southern part of the Helena quadrangle (Cox, 1956).

GEOLOGIC SETTING

In the Yreka–Fort Jones area a belt of ultramafic rocks as much as 2½ miles wide trends northeast-southwest and separates the western Paleozoic and Triassic belt from the eastern Klamath belt. At its northeast end it narrows to a few feet and is overlapped by Upper Cretaceous sedimentary rocks. It extends southward beyond the area of figure 1 and apparently is continuous with a large ultramafic body in the southeastern Klamath Mountains (fig. 2). The ultramafic rocks have not been studied in detail, but at most places they are highly sheared serpentinites. In some places where they are less sheared, harzburgite and dunite can be recognized. Minor amounts of fine-grained gabbro are associated with the serpentinite.

The serpentinite is bordered on its east side by a narrow belt of fine-grained epidote amphibolite. Southward the serpentinite interfingers with amphibolite and schistose micaceous marble. The ages of the amphibolite and marble are unknown, but these rocks are lithologically similar to the Salmon Hornblende Schist and Abrams Mica Schist of the southern Klamath Mountains, whose metamorphic age is Devonian (Lanphere and others, 1968). A thrust fault separates the amphibolite from sedimentary rocks of the Duzel and Gazell Formations which include phyllitic calcareous siltstone, calcareous quartz wacke, quartzite (quartz arenite), recrystallized chert, and lenticular bodies of marble. These sedimentary rocks are part of a northeast-trending oblong belt more than 30 miles long and 12 miles wide that contains the only known Ordovician and Silurian strata in the Klamath Mountains (Churkin and Langenheim, 1960; Churkin, 1965; Potter and Boucot, 1971; Wells and others, 1959; Zdanowicz, 1971).

West of the serpentinite are rocks of the western Paleozoic and Triassic belt, including a belt of highly deformed phyllitic quartzite and siliceous phyllite and closely associated blueschist facies rocks thrust over a greenstone-chert assemblage. The siliceous rocks lithologically resemble the Stuart Fork Formation of the southern Klamath Mountains (Davis and Lipman, 1962), which Davis (1968) regards as a metamorphic equivalent of the western Paleozoic and Triassic belt. Meager paleontologic data indicate that rocks in this subprovince range from late Paleozoic to Late Triassic. Northeast of Yreka a limestone lens in the greenstone-chert assemblage has yielded Late Permian (Ochoan) fossils (Elliott, 1971, p. 13).

Stuart Fork Formation

The Stuart Fork Formation was named by Davis and Lipman (1962, p. 1548) for excellent exposures along the

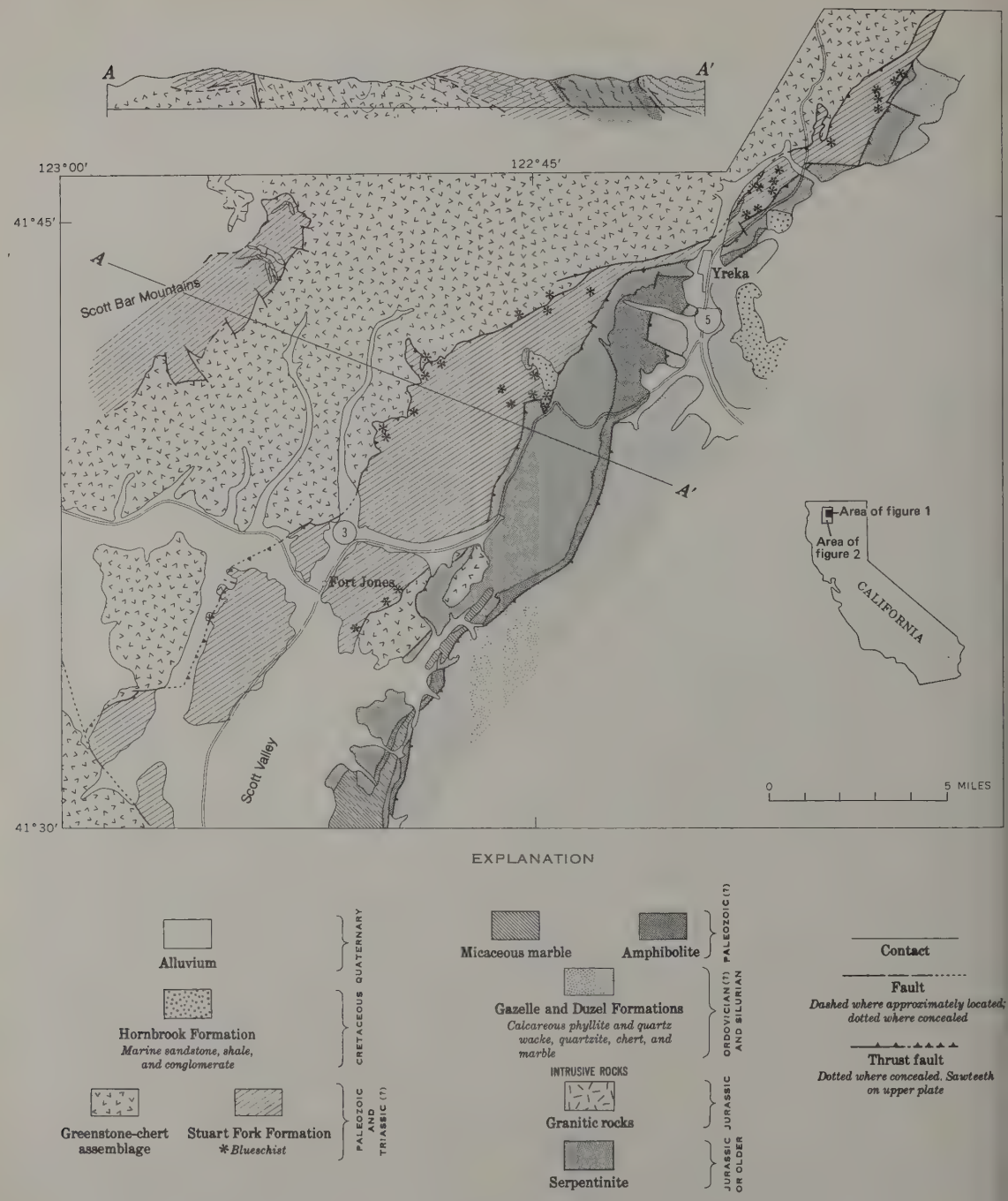

Figure 1.—Geologic map of the Yreka–Fort Jones area, California, and cross section along line *A*–*A*′.

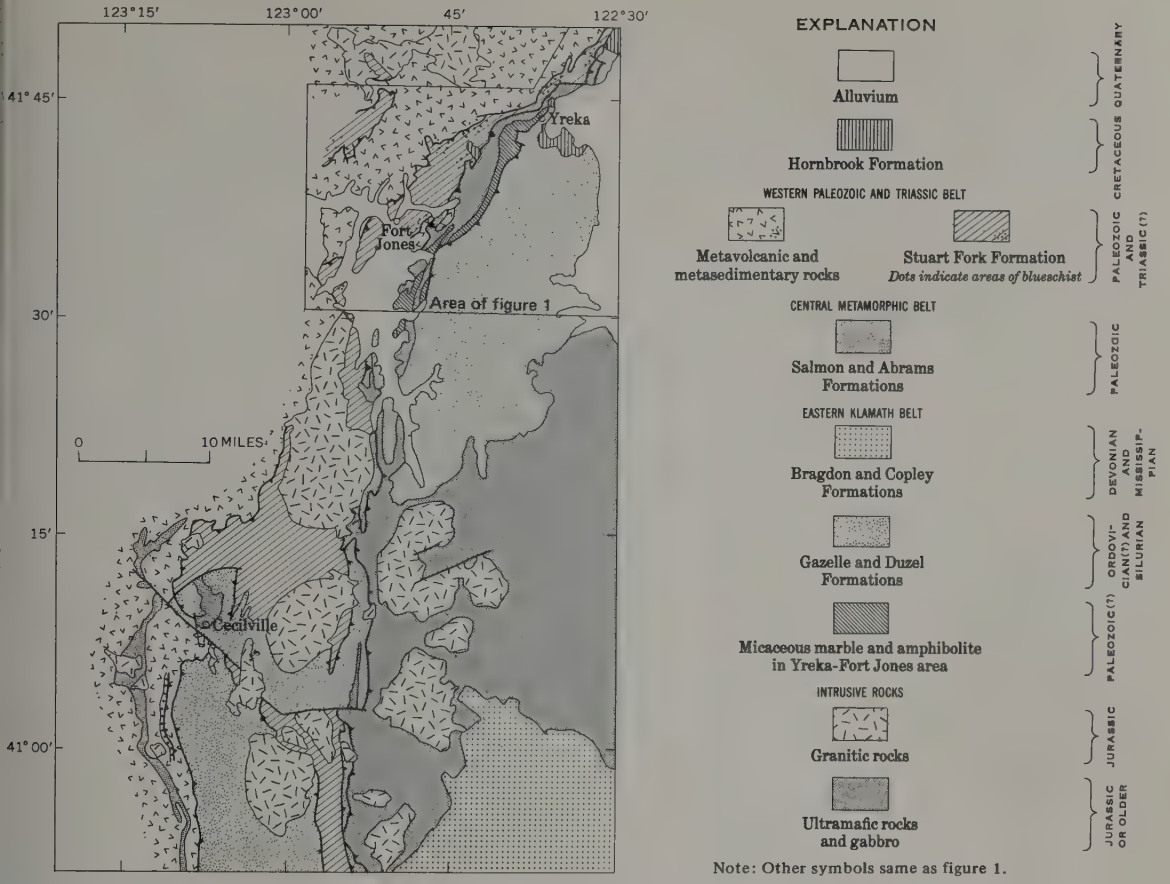

Figure 2.—Geologic map of the east-central Klamath Mountains, Calif.

Stuart Fork of the Trinity River between Deep and Van Matre Creek tributaries. In the Yreka–Fort Jones area the Stuart Fork Formation is composed predominantly of phyllitic quartzite. This rock is mainly light colored, thinly layered, and complexly deformed, even on a microscopic scale. The layering is conspicuous but is commonly discontinuous and extensively disrupted by close folding and transposition. Layers of fine-grained crystalloblastic quartz 1 to 5 mm thick alternate with micaceous lamellae composed of white mica and pale-green chlorite. A distinctive variety of phyllitic quartzite that is plentiful in the vicinity of Fort Jones has a pale-reddish coloration on cleavage surfaces owing to an abundance of microscopic hematite in the micaceous laminae.

Coarsely crystalline marble in small lenticular bodies constitutes an uncommon rock type in the Stuart Fork of this area.

Greenstone-chert assemblage

Metavolcanic rocks of basaltic composition predominate in the greenstone-chert assemblage. They are mainly massive, fine-grained flow rocks, but locally they show pillow structure. Breccias and agglomerates as well as vesicular and amygdaloidal metavolcanic rocks are less common varieties. Calcium carbonate commonly occurs in interstices as cavity fillings and as matrix material. Dike- and sill-like bodies of fine-grained diabase are recognizable in some places.

Original structures and textures of the metavolcanic rocks generally are well preserved. Common mineral phases are albite to sodic oligoclase + chlorite + actinolite + sphene ± calcite ± clinozoisite ± magnetite ± quartz, an assemblage characteristic of the greenschist metamorphic facies. Some specimens contain the assemblage albite + chlorite + unaltered clinopyroxene (augite), plus accessory epidote, sphene, calcite, and opaque minerals. The association of fresh clinopyroxene with albite and chlorite is typical of spilite.

Sedimentary rocks interbedded with the metavolcanic rocks range from thin beds a few feet thick to units several hundred feet thick that contain minor amounts of intercalated volcanic rock. Most of the sedimentary rock is very fine grained black argillite, slaty argillite, and phyllite. Chert is very common and

includes both the rhythmically bedded variety and the massive, poorly bedded type. The cherts are recrystallized to fine-grained quartzite. Other sedimentary rocks include minor amounts of fine-grained graywacke and occasional discontinuous, commonly lenticular bodies of marble.

DISTRIBUTION AND MODE OF OCCURRENCE OF THE BLUESCHIST

Blueschist of the Yreka–Fort Jones area is restricted to the Stuart Fork Formation, except for a few occurrences in rocks of the greenstone-chert assemblage very close to the contact with the Stuart Fork (fig. 1). All exposures found thus far have been close to either the contact with the serpentinite body or the contact of the Stuart Fork with the underlying greenstone-chert assemblage; however, this distribution may be more apparent than real, because most field traverses were near these contacts. The correlation between occurrences of blueschist and distribution of the Stuart Fork Formation is emphasized by the presence of blueschist minerals in a faulted outlier of the Stuart Fork in the Scott Bar Mountains, and their absence in the area between the outlier and the main Yreka–Fort Jones belt.

The blueschist occurs as isolated bodies that range in size from as much as 10 feet in many exposures to a few which may be 1,000 feet or more in length and several hundred feet in width. In some exposures, foliated blueschist is interlayered with fine-grained crossite-bearing quartzite and siliceous mica schist. Many schist bodies are ellipsoidal masses surrounded by siliceous schist, and one is enclosed by marble.

PETROGRAPHY OF THE BLUESCHIST

Blueschist in the Yreka–Fort Jones area contains the diagnostic metamorphic mineral assemblage lawsonite plus blue sodic amphibole. Common accessory minerals are white mica and sphene. Other accessory minerals, present in some rocks but not in others, are stilpnomelane, jadeite, aegerine, quartz, albite, pumpellyite, garnet, calcium carbonate, and chlorite. The blueschist formed from both basaltic and sedimentary rocks (table 1), with metabasalts apparently more common than metasedimentary varieties.

Metabasaltic rocks

The metabasalts commonly are very fine grained, hard, and massive, although some are phyllitic or schistose. Commonly, original structures and textures are obliterated by recrystallization, but in some thin sections faint relics of an ophitic or diabasic texture are visible. The specific gravity of these rocks ranges from 2.91 to 3.14; the average of 19 measurements is 3.08.

Glaucophane is plentiful in the metabasalts and is predominant in some. It is commonly very finely fibrous and may form a "mat" in which the other minerals occur, although in many specimens the fibers have a distinct parallelism.

Lawsonite commonly occurs as subhedral to strongly euhedral stubby prisms which may be scattered through a mat of glaucophane, or as crystals in glaucophane-lawsonite lamina with the glaucophane fibers wrapping around the lawsonite crystals (fig. 3*A*). In some specimens monomineralic folia and lenses of lawsonite alternate with layers in which glaucophane predominates (fig. 3*B*). Uncommonly, in some unsheared nonfoliated specimens, lawsonite is pseudomorphic after original plagioclase laths.

Sphene is a ubiquitous accessory mineral. It occurs as scattered anhedral grains and clusters and trains of granules. Commonly it is partly altered to a gray, opaque substance, presumably leucoxene.

Minor amounts of white mica are usually present in these rocks, as well as a little quartz. Small amounts of chlorite and stilpnomelane are also present. X-ray patterns of whole-rock powders indicate that some samples contain small quantities of albite, although none was positively identified under the microscope.

Jadeitic pyroxene was recognized in a few thin sections, but it is not a common constituent of blueschists in the Yreka–Fort Jones area. Where present it is a plentiful accessory, occurring as colorless to pale-brown anhedral, commonly radiating, masses. Some metabasalts contain a green pyroxene identified as aegerine from its optical properties and X-ray pattern (fig. 3*C*).

Pumpellyite was found in only a few thin sections.

Calcium carbonate is not abundant, but small amounts occur in some specimens. X-ray data indicate that it is calcite, not the aragonite which is commonly reported from blueschist terranes.

Pyrite is a common minor constituent, although there seldom is more than a percent or so. Magnetite, ilmenite, and hematite appear to be absent, a fact noted by Coleman and Lee at Cazadero, Calif. (1963, p. 275), and attributed to a relatively high sulfur fugacity for the metamorphic environment.

In figure 4 the analyzed metabasaltic rocks of table 1 are plotted in an Alk-F-M diagram and compared with analyzed metavolcanic rocks from the greenstone-chert assemblage of the Condrey Mountain and Hornbrook quadrangles. The similarity in composition is apparent.

Metasedimentary rocks

Siliceous metasedimentary rocks containing lawsonite and a sodic amphibole are less plentiful than the metabasaltic blueschist facies rocks. Probably they originally were impure quartzites or graywackes (table 1), for composition of relatively pure quartzite and chert is not suitable for formation of lawsonite. The specific gravity of eight samples was measured; it averaged 2.71.

Table 1.—*Chemical, semiquantitative spectrographic, and modal analyses of blueschist facies rocks*

[Tr., trace]

	Metabasalt						Metasedimentary rocks		
	FJ-4-66	FJ-3C-67	H-1-69	H-7-71	Y-3-65	Y-37-71	FJ-3B-67	H-6-71	Y-2-65
Chemical analyses[1] (weight percent)									
SiO_2	48.7	48.7	49.1	47.4	47.5	51.4	89.7	83.7	85.9
Al_2O_3	17.0	14.2	15.6	17.4	13.9	16.5	2.2	6.6	4.0
Fe_2O_3	1.6	3.8	3.6	4.8	5.8	2.3	2.1	1.2	1.6
FeO	6.8	7.3	8.0	5.9	6.5	6.9	.92	1.3	2.1
MgO	7.7	6.5	4.7	4.6	6.2	6.1	.89	1.3	1.4
CaO	5.6	9.0	7.5	8.3	9.3	6.5	.99	1.6	1.6
Na_2O	2.8	2.3	4.0	3.3	2.3	4.2	.78	.46	1.1
K_2O	.54	.18	.29	.15	.51	.11	.22	1.3	.23
H_2O+	5.9	5.6	4.4	6.0	5.7	4.1	.85	1.9	1.3
H_2O-	.32	.14	.08	.20	.32	.07	.02	.05	.03
TiO_2	2.0	1.5	1.6	1.5	.51	.94	.11	.27	.26
P_2O_5	.29	.11	.33	.20	.24	.02	.16	.00	.06
MnO	.14	.19	.13	.11	.26	.16	.14	.07	.07
CO_2	<.05	<.05	<.05	<.05	<.05	<.05	<.05	<.05	<.05
Total	99.39	99.52	99.33	99.86	99.04	99.03	99.08	99.75	99.65
Specific gravity	2.91	3.08	3.09	3.08	3.11	3.11	2.69	2.73	2.74
Semiquantitative spectrographic analyses[2] (parts per million)									
B	.....	.....	.....	.....	.....	.....	.....	.....	100
Ba	150	70	300	20	200	20	300	300	500
Co	30	50	30	50	30	30	5	7	3
Cr	500	300	.....	500	200	500	10	30	10
Cu	70	100	15	50	70	70	70	50	7
Ga	20	20	20	15	20	20	3	10	7
Nb	15	.....	.....	.....	.....	.....	.....	.....	7
Ni	150	100	10	100	70	70	50	20	15
Sc	20	70	30	50	70	50	5	10	7
Sr	500	70	200	150	100	300	15	50	50
V	150	300	150	300	300	300	70	50	30
Y	50	50	50	50	50	30	15	15	15
Yb	3	5	5	5	5	3	2	2	2
Zr	100	50	100	70	70	20	30	50	100
Modal analyses (volumetric percent)									
Crossite	.....	.....	.....	.....	.....	.....	10	8	17
Glaucophane	6	42	53	57	61	57	.....	.....	.....
Lawsonite	26	49	27	34	31	40	6	11	11
Sphene	10	4	6	7	6	3	.....	2	1
Aegerine	.....	3	10	1.5	.....	.....	.....	.....	.....
Jadeite	13	Tr.	.....	.....	.....	.....	.....	.....	.....
Muscovite	.....	.5	4	.3	Tr.	.....	Tr.	13	3
Quartz	8	1	.....	.....	1	.....	83	66	68
Chlorite	37	.....	Tr.	.....	1	.....	.....	.....	.....
Stilpnomelane	.....	.....	.....	.....	.....	.....	Tr.	.....	Tr.
Garnet	.....	.....	.....	.....	.....	.....	Tr.	.....	.....

[1] Methods used are those described by Shapiro and Brannock (1962), supplemented by atomic absorption. Analysts: P. L. D. Elmore, James Kelsey, H. Smith, J. L. Glenn.
[2] Analyst: Chris Heropoulos.

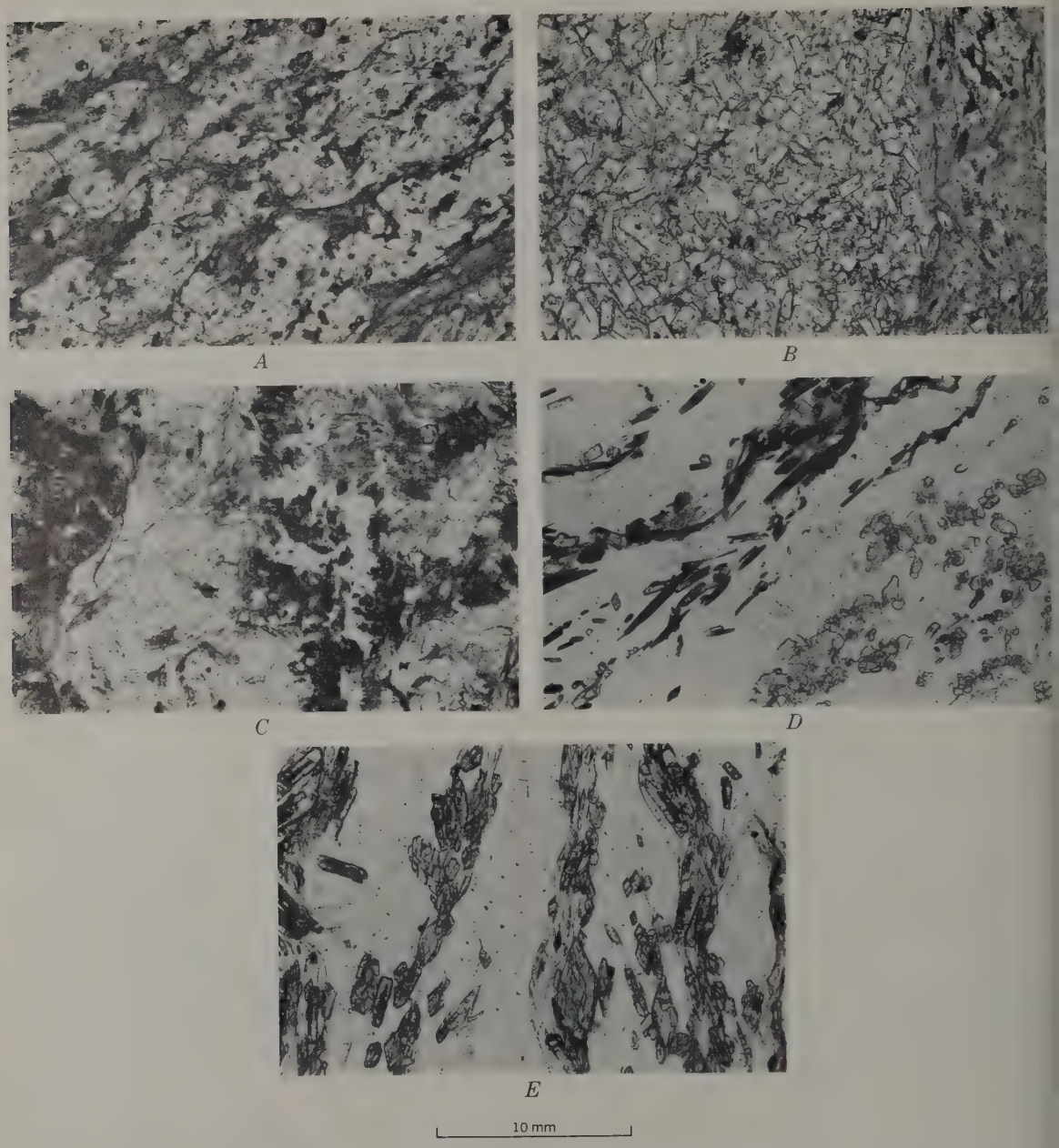

Figure 3.—Photomicrographs of blueschist facies rocks from Yreka–Fort Jones area.

A. Glaucophane-lawsonite schist. Gray is fibrous glaucophane; light gray, prismatic lawsonite; small dark grains, sphene.

B. Glaucophane-lawsonite phyllite. Gray is wispy glaucophane; light gray, lawsonite; dark scattered granules, sphene.

C. Glaucophane-lawsonite rock with aegerine. Light-gray masses are lawsonite; gray, fibrous glaucophane; white, irregular patches of muscovite; dark areas in left and right central parts of figure, aegerine.

D. Crossite-lawsonite quartzite. Low-relief light matrix is quartz; dark-gray blades, crossite, accompanied by stubby, prismatic lawsonite; light-gray high-relief grains in lower right part of figure are mostly colorless garnet (grossular) accompanied by a few prismatic lawsonite crystals.

E. Lawsonite-crossite-quartz-muscovite schist. Light-gray matrix is quartz; gray mineral with amphibole cross section (cleavage), crossite; lighter gray, moderate relief, muscovite; darker gray prisms, lawsonite. Crossite, muscovite, and lawsonite intergrown in close-spaced micaceous folia. Central parts of lawsonite crystals commonly cloudy with dustlike inclusions.

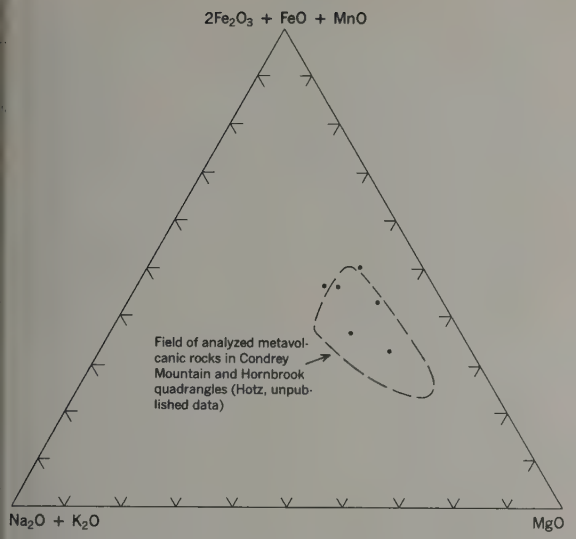
$2Fe_2O_3$ + FeO + MnO
Field of analyzed metavolcanic rocks in Condrey Mountain and Hornbrook quadrangles (Hotz, unpublished data)
Na_2O + K_2O
MgO

Figure 4.—Alk-F-M plot comparing blueschists of basaltic composition with metavolcanic rocks of the greenstone-chert assemblage.

Recrystallization destroyed the original fabric, and in hand specimens the rocks are fine grained and foliated with thin, alternating dark and light laminae parallel to the cleavage. Under the microscope the crystalloblastic texture of these rocks is clear. Anhedral interlocking quartz with irregular to sutured boundaries predominates. In some, the quartz grains are equidimensional, but in others they are somewhat elongate with nearly parallel orientation.

Dark-blue acicular crossite crystals in parallel arrangement and accompanied by strongly idioblastic prismatic lawsonite are concentrated in thin laminae (fig. 3*D*). In some specimens the laminae are fairly continuous; in others they are discontinuous wispy streaks and lenses. Amphibole needles commonly wrap around and enclose the lawsonite crystals. In some rocks, the laminae are highly contorted by microfolds. Crossite is the common soda amphibole in the metasedimentary rocks, but in some, presumably of lower original iron content, pale-blue glaucophane was formed instead.

White mica, although common, is a minor constituent (fig. 3*E*), but in some specimens it is more plentiful than the soda amphibole. Traces of chlorite and stilpnomelane are not uncommon. Minor quantities of colorless garnet occur as small grains in a few specimens (fig. 3*D*).

STRUCTURE

The contact of the Stuart Fork Formation with the underlying metavolcanic rocks, chert, and argillite is not exposed, but it can be placed within narrow limits because of the contrasting lithologies and structural styles. The metavolcanic and sedimentary rocks dip moderately to steeply southeast and northwest. They are deformed, but not as intensely as the overlying highly contorted and crumpled rocks of the Stuart Fork Formation. At several places near the contact, however, the underlying rocks are intensely deformed: chert beds are closely folded, siliceous argillites strongly sheared and crumpled, and greenstone sheared and brecciated. The sinuous trace of the contact at many places in areas of moderate to steep topography indicates a gentle dip. At other places the trace is straight and steep. This contact is interpreted as an east-dipping, undulatory, low-angle fault, modified by steeply dipping faults, on which a plate of Stuart Fork Formation has overridden the greenstone-chert assemblage (fig. 1). The partly mapped patch of Stuart Fork in the Scott Bar Mountains may be an outlier of this thrust plate. The moderate to steep eastward-dipping contact of the serpentinite with the Stuart Fork is interpreted to be a thrust fault on which the serpentinite and overlying metamorphic and lower Paleozoic sedimentary rocks overrode rocks of the western Paleozoic and Triassic belt.

CONCLUSIONS

In mineralogy, texture, and density the blueschists of the Yreka–Fort Jones area are comparable to the low-grade, Cazadero type III blueschists of Coleman and Lee (1963). The occurrences of blueschist in the Yreka–Fort Jones area are restricted to the Stuart Fork Formation and to greenstone of the underlying greenstone-chert assemblage immediately beneath the thrust plate of Stuart Fork Formation. Although many of the occurrences of blueschist of basaltic composition quite obviously are discontinuous bodies within the metasedimentary rocks, some of the metasedimentary blueschists are interlayered with siliceous phyllites that contain no critical blueschist facies minerals. Greenstones interfinger with the siliceous Stuart Fork Formation in its type area (Davis and others, 1965; Davis and Lipman, 1962) and may have had a similar relationship in the Yreka–Fort Jones area but became isolated by tectonic disruption. The similarity between the chemical composition of the metavolcanic rocks in the greenstone-chert assemblage and that of the basaltic blueschist supports the concept that some of the blueschist now within the plate of Stuart Fork rocks is metamorphosed greenstone from the greenstone-chert assemblage of the underlying plate.

The high-pressure and low-temperature conditions under which blueschist facies metamorphism takes place are reasonably well established (Coleman and Lee, 1962; Coleman, 1967; Ernst and others, 1970). Pressures on the order of 5–8 kb and temperatures of 200°–300°C are appropriate for the formation of low-grade blueschists of the kind that occur in the Yreka–Fort Jones area. The tectonic environment under which such temperature-pressure conditions are attained, however, is somewhat obscure and under dispute. Rapid, deep burial followed by rapid uplift (Bailey and others, 1964; Ernst

and others, 1970), and development of tectonic overpressures at the sole of overthrusts (Blake and others, 1967; Coleman, 1967) are two radically different models which have been proposed to satisfy the peculiar conditions of blueschist metamorphism. Regardless of the tectonic circumstances under which blueschists form, the terranes in which they occur throughout the world have many features in common. These include narrow, elongate belts that have developed along continental margins. Characteristically they are closely associated with elongate, parallel belts of alpine-type ultramafic rocks. In terms of plate tectonic theory, these tectonic environments can be regarded as suture zones marking the collision site between plates, the blueschists having been formed in the subduction zone between a descending oceanic plate and a continental plate (Blake and others, 1969; Ernst, 1970; Coleman, 1971).

Blueschist metamorphism in the Yreka–Fort Jones area may have been synchronous with metamorphism of the Stuart Fork Formation at its type area. A Middle or Late Jurassic age has been postulated for this event, on the basis of limited isotopic age determinations ranging from 133 to 158 m.y. (Lanphere and others, 1968). In the Scott Barr Mountains (fig. 1) and their northern extension in the Condrey Mountain quadrangle (Hotz, 1967), klippen composed of the Stuart Fork are intruded by Middle or Late Jurassic (145 to 155 m.y.) granitic plutons, while to the south in the Trinity Alps and Salmon Mountains granitic plutons 127 to 140 m.y. old intrude the Stuart Fork (Lanphere and others, 1968). Metamorphism probably occurred during the Nevadan orogeny, before the multiple Cretaceous deformations (Irwin, 1964) that produced the regional blueschist metamorphism in the Coast Ranges of California and southwestern Oregon (Suppe, 1969; Suppe and Armstrong, 1972).

The Yreka–Fort Jones blueschist belt probably developed along thrust faults that separate two tectonic plates. The phyllitic quartzite and siliceous phyllite of the Stuart Fork Formation may represent fine siliceous sediments deposited in a trench on late Paleozoic and Triassic(?) oceanic crust. These rocks collided with a continental plate composed of early Paleozoic metamorphic and sedimentary rocks. Underthrusting of the oceanic plate could account for the extreme deformation of the Stuart Fork Formation and for its blueschist metamorphism that developed as the sedimentary and volcanic rocks were scraped off against the landward plate and rapidly buried in the subduction zone. The serpentinite belt that now separates the two plates may be the basement (oceanic crust and upper mantle) of the eastern plate against which the younger oceanic plate collided.

REFERENCES CITED

Bailey, E. H., Irwin, W. P., and Jones, D. L., 1964, Franciscan and related rocks and their significance in the geology of western California: California Dept. Nat. Resources Div. Mines Bull. 183, 171 p.

Blake, M. C., Jr., 1969, Blueschist facies metamorphism related to regional thrust faulting: Tectonophysics, v. 8, p. 237–246.

Blake, M. C., Jr., Irwin, W. P., and Coleman, R. G., 1967, Upside-down metamorphic zonation, blueschist facies, along a regional thrust in California and Oregon, *in* Geological Survey Research 1967: U.S. Geol. Survey Prof. Paper 575-C, p. C1–C9.

Churkin, Michael, Jr., 1965, First occurrence of graptolites in the Klamath Mountains, California, *in* Geological Survey Research 1965: U.S. Geol. Survey Prof. Paper 525-C, p. C72–C73.

Churkin, Michael, Jr., and Langenheim, R. L., Jr., 1960, Silurian strata of the Klamath Mountains, California: Am. Jour. Sci., v. 258, no. 4, p. 258–273.

Coleman, R. G., 1967, Glaucophane schists from California and New Caledonia: Tectonophysics, v. 4, p. 479–498.

—— 1971, Plate tectonic emplacement of upper mantle peridotites along continental edges: Jour. Geophys. Research, v. 76, p. 1212–1222.

Coleman, R. G., and Lanphere, M. A., 1971, Distribution and age of high-grade blueschists, associated eclogites, and amphibolites from Oregon and California: Geol. Soc. America Bull., v. 82, p. 2397–2412.

Coleman, R. G., and Lee, D. E., 1962, Metamorphic aragonite in the glaucophane schists of Cazadero, California: Am. Jour. Sci., v. 260, no. 8, p. 577–595.

—— 1963, Glaucophane-bearing metamorphic rock types of the Cazadero area, California: Jour. Petrology, v. 4, no. 2, p. 260–301.

Cox, D. P., 1956, Geology of the Helena quadrangle, Trinity County, California: Stanford, Calif., Stanford Univ., unpub. Ph. D. thesis, 123 p.

Davis, G. A., 1968, Westward thrust faulting in the south-central Klamath Mountains, California: Geol. Soc. America Bull., v. 79, p. 911–934.

Davis, G. A., Holdaway, J. J., Lipman, P. W., and Romey, W. D., 1965, Structure, metamorphism, and plutonism in the south-central Klamath Mountains, California: Geol. Soc. America Bull., v. 76, no. 8, p. 933–966.

Davis, G. A., and Lipman, P. W., 1962, Revised structural sequence of pre-Cretaceous metamorphic rocks in the southern Klamath Mountains, California: Geol. Soc. America Bull., v. 73, p. 1547–1552.

Elliott, M. A., 1971, Stratigraphy and petrology of the Late Cretaceous rocks near Hilt and Hornbrook, Siskiyou County, California, and Jackson County, Oregon: Corvallis, Oreg., Oregon State Univ., unpub. Ph.D. thesis, 171 p.

Ernst, W. G., 1970, Tectonic contact between the Franciscan mélange and the Great Valley sequence–Crustal expression of a late Mesozoic Benioff zone: Jour. Geophys. Research, v. 75, p. 886–901.

Ernst, W. G., Seki, Y., Onuki, H., and Gilbert, M. C., 1970, Comparative study of low-grade metamorphism in the California Coast Ranges and the outer metamorphic belt of Japan: Geol. Soc. America Mem. 124, 276 p.

Hotz, P. E., 1967, Geologic map of the Condrey Mountain quadrangle and parts of the Seiad Valley and Hornbrook quadrangles, California: U.S. Geol. Survey Geol. Quad. Map GQ-618, scale 1:62,500.

Irwin, W. P., 1960, Geological reconnaissance of the northern Coast Ranges and Klamath Mountains, California, with a summary of the mineral resources: California Div. Mines Bull. 179, 80 p.

—— 1964, Late Mesozoic orogenies in the ultramafic belts of northwestern California and southwestern Oregon, *in* Geological Survey Research 1964: U.S. Geol. Survey Prof. Paper 501-C, p. C1–C9.

—— 1966, Geology of the Klamath Mountains province, *in* Bailey, E. H., ed., Geology of northern California: California Div. Mines and Geology Bull. 190, p. 19–38.

Lanphere, M. A., Irwin, W. P., and Hotz, P. E., 1968, Isotopic age of the Nevadan orogeny and older plutonic and metamorphic events in the Klamath Mountains, California: Geol. Soc. America Bull., v. 79, p. 1027–1052.

Masson, P. H., 1949, Geology of the Gunsight Peak district, Siskiyou County, California: Berkeley, Calif., California Univ., unpub. M.A. thesis, 74 p.

Potter, A. W., and Boucot, A. J., 1971, Ashgillian, Late Ordovician brachiopods from the eastern Klamath Mountains of northern California: Geol. Soc. America Abs. with Programs, v. 3, no. 2, p. 180.

Shapiro, Leonard, and Brannock, W. W., 1962, Rapid analysis of silicate, carbonate, and phosphate rocks: U.S. Geol. Survey Bull. 1144-A, 56 p.

Suppe, John, 1969, Times of metamorphism in the Franciscan terrain of the northern Coast Ranges, California: Geol. Soc. America Bull., v. 80, no. 1, p. 135–142.

Suppe, John, and Armstrong, R. L., 1972, Potassium-argon dating of Franciscan metamorphic rocks: Am. Jour. Sci., v. 272, no. 3, p. 217–233.

Wells, F. G., Walker, G. W., and Merriam, C. W., 1959, Upper Ordovician (?) and Upper Silurian formations of the northern Klamath Mountains, California: Geol. Soc. America Bull., v. 70, no. 5, p. 645–649.

Zdanowicz, Ted, 1971, The folded mallethead thrust, eastern Klamath Mountains, California: Geol. Soc. America Abs. with Programs, v. 3, no. 2, p. 223.

Jour. Research U.S. Geol. Survey
Vol. 1, No. 1, Jan.—Feb. 1973, p. 63—78

DOLOMITIZATION MODEL FOR UPPER CAMBRIAN AND LOWER ORDOVICIAN CARBONATE ROCKS IN THE EASTERN UNITED STATES

By LEONARD D. HARRIS, Knoxville, Tenn.

Abstract.—Existing models for dolomitization emphasize that penecontemporaneous dolomitization can occur in both subtidal and supratidal environments if the necessary chemical and physical factors favorable for the development of magnesium-rich hypersaline waters exist. Holocene shallow-water hypersaline environments that have the potential to produce dolomite without deposition of more soluble evaporite minerals are found in Shark Bay, Australia, and on the Great Bahama Bank. These hypersalinity systems are characterized by near-vertical isosalinity layers of increasing concentration landward from the open ocean and show little or no relationship to bottom topography. I suggest that a similar but larger scale epicontinental salinity system covering the Late Cambrian and Early Ordovician carbonate continental shelf produced a broad wedge of subtidally deposited dolomite in the eastern half of the United States from Mexico to Canada. The distribution of limestone and dolomite in this region is closely keyed to the salinity gradient and accounts for the natural progression from a normal marine limestone facies through a transition zone to a highly saline dolomite facies phase. Algal stromatolite mats and domes occupied low-energy niches in both the limestone and dolomite facies, whereas stratiform algal stromatolites were confined to the areas of moderate energy within the dolomite facies.

In the past, construction of environmental models that account for the large-scale deposition of dolomite in ancient widespread carbonate environments has defied resolution because the feasibility of the suggested processes could not be confirmed experimentally nor compared to natural modern sedimentary conditions. Recently some progress concerning the origin of dolomite has been gained through the discovery of dolomite in Holocene carbonate rocks and the subsequent study of its environmental parameters. The major contribution from these studies is the general acceptance of the idea that penecontemporaneous dolomitization is common where sediments in high intertidal or supratidal areas contain pore fluids consisting of concentrated magnesium-rich brines, as for example along wide salt flats, termed "sabkhas" in the Persian Gulf (Illing and others, 1965) and carbonate mudflats in the Bahamas (Shinn and others, 1965). The model of supratidal penecontemporaneous dolomitization has been widely used in interpreting ancient carbonate environments; however, it seems to be most applicable to relatively restricted geographic areas (commonly less than 10,000 sq mi) where thin carbonate units can be demonstrated to change from subtidal and intertidal limestone to supratidal dolomite. It is less applicable as a principal site of dolomitization in regionally extensive megacarbonate environments (approximately 1 million square miles) such as the Late Cambrian and Early Ordovician, where nearly 90 percent of the carbonate is dolomite. Some widespread uniform process, other than the supratidal model, must have been operating to have dolomitized thousands of square miles of carbonate as much as 3,000 feet thick. This report questions the currently popular usage of the intertidal and supratidal environments as exclusive sites for large-scale regional dolomitization, and offers an alternate hypothesis involving a magnesium-rich subtidal environment.

UPPER CAMBRIAN AND LOWER ORDOVICIAN CARBONATE ROCKS

A paleogeographic and lithofacies map of the Late Cambrian and Early Ordovician shows that during this time a vast continental shelf, about 2,000 miles long and from 100 to 1,000 miles wide, occupied much of the eastern half of the United States (fig. 1). Maximum development of the shelf and its attendant epicontinental sea occurred late in Cambrian time and persisted with apparent continuous sedimentation until late in Early Ordovician time. Facies of Late Cambrian and Early Ordovician age show an almost classic relationship to near-shore clastic sediments containing subordinate dolomite interfingering with offshore carbonate rocks. A multitude of stratigraphic names has been used to subdivide this ancient sequence of strata into stratigraphic units of differing ranks. Because the nomenclatural complexities are not critical to this study the reader is referred to the latest summary report (Holland, 1971). One major subdivision, the Knox Group, has been widely recognized in the southern and central Appalachians within the predominantly carbonate sequence, and I suggest that many of the general features of the Knox can be applied on a shelf-wide basis.

The Knox Group, as much as 3,000 feet thick, occupies most of the middle segment of the offshore carbonate sequence, crops out in Georgia, Alabama, eastern Tennessee, and southwestern Virginia, and lies in the subsurface of middle

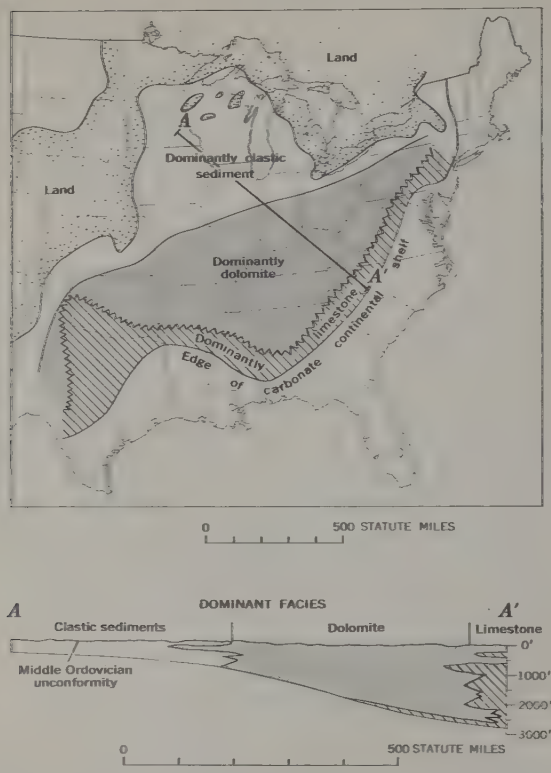

Figure 1.—Generalized paleogeographic map of Late Cambrian and Early Ordovician time, showing regional distribution of facies of the Knox Group and equivalent rocks on the ancient continental shelf. Based on Chenoweth (1968), Donaldson and Page (1964), Folk (1959), Lochman-Balk (1971), Perry (1964), Rodgers (1968), Swartz (1948), and Williams (1969).

and western Tennessee, Kentucky, West Virginia, Ohio, and parts of Indiana and Illinois. Throughout most of this area the Knox is dolomite, but in easternmost Tennessee and southwestern Virginia it is divided into a western dolomite facies and an eastern limestone facies. Recently Laporte (1971) summarized the view of sedimentologists concerned with the change of limestone to dolomite in Upper Cambrian and Lower Ordovician carbonate strata in the eastern United States. They suggest that the change is a response to the environment of deposition and indicate that the limestone has a subtidal origin, whereas the dolomite had an intertidal and supratidal origin. In their view each facies characteristically contains recognizable stratigraphic criteria imposed by environmental controls: subtidal limestone units, although exhibiting regional change and variation, tend to be uniform and may commonly show great lateral persistence. In contrast, variable conditions of sedimentation in the intertidal and supratidal dolomite regime produce abrupt and frequent changes in lithologic units, so that correlation of dolomite beds even between adjacent outcrops is nearly impossible. These apparent clear-cut differences between limestone and dolomite facies of Cambrian and Ordovician age as summarized by Laporte have not been corroborated by the studies of economic geologists in eastern Tennessee, who concentrated on details of stratigraphy without preconceived ideas of environmental constraints.

More than 40 years ago, when geologists realized that commercial quantities of zinc were confined regionally to a 200-foot zone in the upper part of the dolomite phase of the Knox Group of eastern Tennessee, zinc mining companies initiated intensive foot-by-foot stratigraphic studies in search of key beds to aid in exploration and in mine development. Detailed studies of mine workings demonstrated that, rather than a series of laterally discontinuous lithologic units, almost any distinctive stratum, such as a 1-inch sandstone or shale bed, a chert nodule zone, minor bedding or color variation, and so on, could be correlated from mine to mine in the Mascot-Jefferson City zinc district. Continuing surface and subsurface studies of approximately the upper 900 feet of the Knox in Tennessee have resulted in the careful documentation of an average of one key bed per approximately 11 feet of vertical section, many of which have regional significance (Oder and Miller, 1945; Crawford, 1945; Oder and Ricketts, 1961; Harris, 1969; Stagg and Fischer, 1970). In the past 20 years thousands of core holes have penetrated parts of the predominantly dolomite facies of the Knox in search for economic zinc deposits throughout much of Tennessee and in parts of Kentucky, Alabama, and Virginia. In every area, where enough closely spaced drilling has been done to develop a stratigraphic sequence, laterally extensive key beds can be recognized and can be correlated for considerable distances. In central and northern Virginia, far removed from the Tennessee zinc district, Young and Wedow (1962) and Herbert and Young (1956) experienced no difficulty in recognizing and using thin key units in rocks of the Beekmantown Dolomite, the lateral equivalent of the upper part of the Knox. The widespread uniformity of multiple key units in the dolomite facies of the Knox Group and equivalent rocks, rather than being characteristic of discontinuous intertidal-supratidal sedimentation, is more characteristic of the uniform subtidal sedimentation of Laporte (1971). Consequently many of the criteria summarized by Laporte and used to distinguish between subtidal, intertidal, and supratidal environments need to be critically analyzed.

PRIMARY FEATURES AS ENVIRONMENTAL INDICATORS

Identification of ancient intertidal and supratidal sediments is based on the recognition of features similar to those found on modern carbonate tidal flats. Unfortunately, there is a tendency to ignore the possibility that many of the primary features found on Holocene tidal flats may not necessarily be

limited to that environment. In fact, few primary features are infallible. Both shrinkage cracks and algal stromatolites are excellent examples of "infallible guides" used to identify positively the intertidal and supratidal environments. Shrinkage cracks are common features of modern intertidal and supratidal areas; however, Burst (1965) has experimentally confirmed that shrinkage cracks can form subaqueously, in response to an increase in salinity, in mud that contains a small quantity of swelling clay. In the Knox Group, shrinkage cracks are found in about equal abundance in both the limestone and dolomite facies. Detailed facies studies and insoluble residue contents suggest that cracked beds show a close affinity for niches within a subtidal environment where clay-mineral abundance, usually greater than 5 percent, is sufficient to react to major fluctuations in salinity. Major changes in salinity are undoubtedly common along the transition zone between masses of normal marine and penesaline water. Consequently, shrinkage cracks, although useful in many places as indicators of subaerial exposure, may just as commonly indicate fluctuations in salinity within subtidal environments.

Holocene algal stromatolites

Algal stromatolites are laminated structures formed by the trapping and binding of sediment by an algal film. They are organosedimentary features in which only the gross structure of the algal films is preserved; cellular and other detailed structure are not preserved. Logan, Rezak, and Ginsburg (1964) suggested that the form of a Holocene stromatolite is related to environmental conditions, and does not lend itself to the limited definition of form genera or form species. They proposed to abandon all generic and specific names, substituting a descriptive nomenclature based on the arrangement of certain geometric forms. Their classification contains two basic forms—the hemispheroid and the spheroid in three major arrangements: (1) laterally linked hemispheroids (LLH), (2) discrete, vertically stacked hemispheroids (SH), and (3) discrete spheroids (SS). Usefulness of algal stromatolites as environmental indicators was stressed by their suggesting that LLH and SH forms were restricted to intertidal areas and SS forms restricted to subtidal areas of shallow agitated water. Other studies of Holocene algal stromatolites (Ginsburg, 1960; Monty, 1965; Kendall and Skipwith, 1968; Gebelein, 1969; and G. R. Davis, 1970) have not fully confirmed either the form distribution or environmental parameters proposed by Logan, Rezak, and Ginsburg (1964), but generally all agree that there are three dominant geometric forms—mats, hemispheroids, and spheroids. Investigations of intertidal algal stromatolites by Kendall and Skipwith (1968) in the Persian Gulf and by G. R. Davis (1970) in Shark Bay, Western Australia, indicate that the dominant geometric growth form is a subparallel mat rather than a hemispheroid or a spheroid. The mat may be altered mechanically to many subforms depending upon its position within the intertidal and supratidal area. A summary of Holocene stromatolite reports suggests that the intertidal and supratidal areas can be subdivided into as many as five distinct zones (fig. 2).

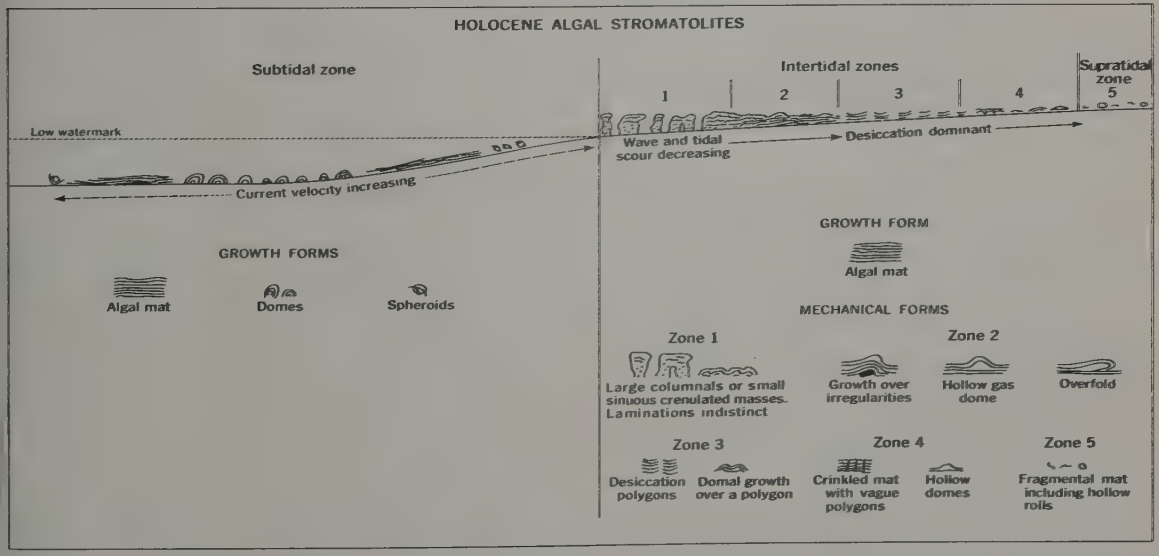

Figure 2.—Form distribution of Holocene algal stromatolites. Based on Black (1933); Ginsburg (1960); Logan, Rezak, and Ginsburg (1964); Kendall and Skipwith (1968); Gebelein (1969); and G. R. Davis (1970).

Zone 1.—A continuous algal mat may develop almost to the low watermark in a protected intertidal mudflat environment, but varieties of forms ranging from sinuous domes or ridges to columnar structures result where waves and tides have increased erosive force. Logan (1961) attributed the development of columnar forms to upward growth of algal stromatolites by progressive stacking of hemispheroidal laminae (SH-V). However, their development seems much more complex, and, as suggested by Logan (1961, figs. 2 and 3) and G. R. Davis (1970, p. 199), they appear to result from scour and beach-rock formation in conjunction with algal growth. Active algal mats are not mechanically resistant to moderate erosive forces (Gebelein, 1969, p. 56) and a slight increase in erosive energy scours the mat irregularly. Once the mat is breached, beach rock, which results from cementation caused by alternate wetting and drying in the intertidal zone, may begin to line the walls of channels. The protection on the walls afforded by the beach-rock formation causes erosion to proceed in a dominantly vertical direction, thereby inducing the development of characteristic SH-V columnar forms of Logan, Rezak and Ginsburg (1964). Along the low watermark, beach rock is sculptured by erosion into columnar structures that grade toward the high watermark into sinuous mounds or ridges, which may or may not be indurated, and finally into unbroken algal mat. Within the beach-rock environment the growth of algal mat is restricted to the top of structures where erosive forces are less. Continued growth of the mat adds to the development of sculptured forms, but its effect is minimal as suggested by the restriction of crudely defined laminations to the upper part of the structures.

Zone 2.—Smooth, nearly flat algal mats characteristically occupy diurnally flooded intertidal areas of low energy. Irregular domelike structures result from growth over irregularities, obstructions, or from erosion and slight desiccation. Superficially these domelike structures resemble the laterally linked hemispheroidal (LLH) structures of Logan, Rezak, and Ginsburg (1964), but they lack symmetry, and their mechanical origin is clearly discernible.

Zone 3.—Desiccation of the algal mat produces a typical polygonal pattern in which individual polygons are saucer shaped and exhibit a wide range in size depending upon the grain size of local sediment and the moisture distribution.

Zone 4.—The algal mat in this zone has a poorly defined polygonal pattern but exhibits abundant hollow domes and a crinkled surface produced by trapped gases. Locally this zone may change to a relatively flat mat similar to that of zone 2.

Zone 5.—Above the high watermark, in the supratidal zone, algal growth is inhibited, as shown by detrital fragments and spheroidally coiled pieces of algal mat.

Subtidal Holocene algal stromatolites have not received the same amount of study as the intertidal forms because they are more difficult to observe and classify. Although these forms were noted by Ginsburg (1960) and Monty (1965) in Florida and the Bahamas, a thorough study of their distribution and environmental parameters did not emerge until Gebelein (1969) published a paper on subtidal algal stromatolites of Bermuda. Gebelein found that algal development is favored in the lee of islands and on wide, shallow shelf areas where reduced wave and current scour takes place. Form distribution is closely keyed to current velocity and sediment supply (fig. 2). Areas of moderate current velocity and ample sediment supply develop algal mats, similar to those described in zone 2 of the intertidal zone, in water as much as 35 feet deep. In areas of reduced velocity where sediment supply is small, algal mats differentiate into discrete small domes; where sediment supply is large, they differentiate into large domes. Both domes tend to elongate in the direction of current movement. Lamination within small domes is distinct, convex, regular, and symmetrical; in contrast, lamination within domes is convex, indistinct, and irregular in thickness.

To summarize, Logan, Rezak, and Ginsburg (1964) based their classification of algal stromatolites on the assumption that hemispheroids or spheroids were the basic growth forms of algal stromatolites. Other studies (Kendall and Skipwith, 1968; Gebelein, 1969; G. R. Davis, 1970) indicated that there are three growth forms—mats, hemispheroids, and spheroids. The basic structural element of each form is a simple lamina. Logan, Rezak, and Ginsburg (1964) showed that development of laminae and form differentiation are controlled by physical, chemical, and biological constraints of the environment. Thus, wide variation in type and intensity of environmental constraints between subtidal and intertidal settings results in the development of distinctive algal stromatolite forms keyed to the particular environment (fig. 2). Natural growth of hemispheroidal forms is favored in subtidal areas where sediment supply is ample and current velocity is low. Spheroidal forms are more likely to develop in subtidal areas where current velocity alternates between low and moderate. Algal mats grow in both subtidal and intertidal environments because the controlling physical constraints of moderate current velocity and sediment supply are similar. The distinguishing characteristic between subtidal and intertidal algal mats is the greater diversity of forms mechanically produced in the intertidal zone in conjunction with erosion, beach rock formation, gas generation, and desiccation. Because Logan, Rezak, and Ginsburg (1964) did not recognize the algal mat as a distinct form and did not distinguish between intertidally mechanically produced forms and subtidal growth forms, they unintentionally limited the usefulness of algal stromatolites as environmental indicators of ancient carbonate depositional environments.

Algal stromatolites of the Knox Group

Preservation of algal stromatolites in the Knox Group of Tennessee and southwestern Virginia ranges from vague outlines in dolomite to minute detailed structures in chert. Because of intense weathering, the residuum from the Knox contains vast quantities of chertified algal stromatolites. On the basis of detailed study of bedrock and residual products,

ancient algal structures in the Knox are limited to algal mats, stratiform layers, and growth domes, with only a rare spheroidal structure (fig. 3). By analogy with Holocene algal stromatolite zonation (fig. 2) the absence of mechanically produced structures, such as polygonal forms and mechanical domes, suggests that intertidal and supratidal environments were absent or poorly developed during deposition of the Knox.

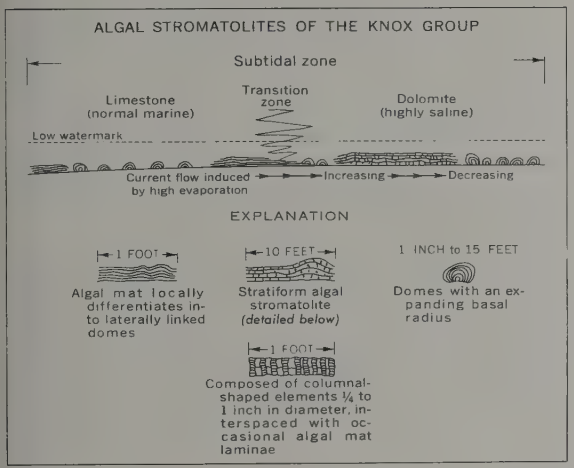
ALGAL STROMATOLITES OF THE KNOX GROUP
Subtidal zone
Limestone (normal marine)
Transition zone
Dolomite (highly saline)
Low watermark
Current flow induced by high evaporation
Increasing
Decreasing
EXPLANATION
1 FOOT
Algal mat locally differentiates into laterally linked domes
10 FEET
Stratiform algal stromatolite (detailed below)
1 INCH to 15 FEET
Domes with an expanding basal radius
1 FOOT
Composed of columnal-shaped elements ¼ to 1 inch in diameter, interspaced with occasional algal mat laminae

Figure 3.—Forms and distribution of Late Cambrian and Early Ordovician algal stromatolites in the Knox Group. Comparison of the small-scale algal mat structure with the large-scale stratiform algal structures suggests many similarities; the main difference is size.

Beds consisting of near-parallel paper-thin laminae, similar to those described (Black, 1933, p. 170–171) as the result of rhythmic alternation of Holocene carbonate sediments and dark algal films, are common in the Knox Group. Unfortunately, rhythmic alternation in organic content does not in itself identify laminated algal structures. Periodic changes in salinity, which are not unlikely in the highly saline environment suggested for the Knox, could cause mass mortality in phytoplankton (Emery and Stevenson, 1957, p. 687), which in turn would result in the deposition of a lamina high in organic matter, resembling a primary algal lamina. The lack of suitable criteria to differentiate between laminated algal sediments and organic lamination from other processes limits the number of such beds that can be assigned to an algal origin.

Paper-thin laminated beds in the Knox Group without exception have been found to have a clay content ranging from 10 to more than 25 percent, strongly suggesting that the lamination primarily resulted from rhythmic changes in clay content. That rhythmic changes in amounts of clay alternate with algal mat development is implied by the fact that locally some paper-thin laminated beds are found to differentiate into LLH structures.

The most abundant algal stromatolite in the Knox Group is in regionally persistent stratiform units in which the basic structural element is a crude column exhibiting paper-thin and vertically stacked hemispheroidal laminae. Thousands of the individual basic columnar elements, from ¼ inch to 1 inch in diameter, are in laterally continuous layers from 1 inch to 3 feet thick. Silicified specimens in which many primary structures are preserved in detail, suggest that the layering results from periodic interruption in upward growth of individual columnal elements. These interruptions are recorded as laminae which form natural partings that present-day weathering tends to accentuate. In all respects the growth layers imitate algal mat development—they form laterally continuous subparallel stratiform layers that locally differentiate into a series of hemispheroids several feet in height and more than 10 feet in diameter. The major difference between the laminae of an algal mat and the layers in the columnar structures is a matter of scale, plus the fact that each growth layer is composed of thousands of individual units (fig. 3).

Stratiform algal stromatolites in massive units from 3 to 140 feet thick are confined to the dolomite facies of the Knox Group of eastern Tennessee and southwestern Virginia. Detailed studies indicate that many of these thick stratiform zones persist laterally for more than 50 miles. Intercalated within these zones are thin beds of oolite, intraformational round-pebble conglomerate, and dololutite. Lateral facies changes from algal to nonalgal material involving individual beds within the zone can be transitional or abrupt. Where transitional, the stratiform algal beds change laterally to algal debris, then to oolite and dololutite, and finally to dololutite containing abundant growth domes; where abrupt, they change directly to dololutite with thin beds of oolite, intraformational round-pebble conglomerate, and growth domes. Distribution of insoluble residues across the facies boundaries shows a direct relationship between the amount of clay residue and rock type. Clay content of stratiform algal stromatolites, oolite, and some debris beds is less than 1 percent; in contrast, the clay content of all dololutite beds exceeds 5 percent. The low clay content of the algal beds, oolites, and algal debris suggests that these rocks were deposited in an environment where the energy level was sufficiently great to prevent the mechanical accumulation of clay, whereas dololutite with higher clay content accumulated in areas of lower energy.

The laterally continuous nature of stratiform algal stromatolite deposits suggests that uniformly widespread subtidal environmental conditions must be responsible for their development. Low clay content and presence of oolite and round-pebble intraformational conglomerate implies that stratiform algal deposits developed in areas of moderate current activity where scouring action of the current prevented growth between columnals. Periodic reduction in current velocities encouraged limited growth of laterally continuous algal laminae. Exceptional conditions exist in present-day hypersaline environments where water lost to high evaporation is

continuously replaced by oceanic water (Emery and Stevenson, 1957, p. 686). The continuous inflow of marine water to replace water lost to evaporation in hypersaline environments may be the mechanism which accounts for the widespread development of laterally persistent stratiform algal zones and their restriction to the dolomite facies of the Knox Group.

Unlike the SH-C domes of Logan, Rezak, and Ginsburg (1964), which are defined as discrete structures in which succeeding hemispheroidal laminae develop without an increase in the basal radius, algal growth domes in the Knox Group develop with an increasing basal radius. Growth domes are distinct and nearly symmetrical structures markedly different from the randomly disposed and asymmetrical mechanical domes developed in Holocene intertidal settings. Normally, growth domes in the Knox are arranged in laterally continuous layers composed of hundreds or thousands of individual domes. The size of individual domes within a layer ranges from a few inches up to 15 feet in diameter. The initial spacing of individual domes within a layer is critical and determines the ultimate size and configuration of the mature structures. If growth is initiated at widely spaced intervals, individual elements develop without interference into large, wide-spaced domes; but if development starts at more closely spaced intervals, the growing domes soon impinge on one another and compound forms with complex growth patterns develop.

That both limestone and dolomite facies contain domes demonstrates that their growth was not dependent on variations in salinity. However, their growth does appear to be keyed to subtidal zones with low current velocities, where they are associated with low-energy lithologies such as calcilutite and dololutite containing more than 5 percent insoluble clay.

MODELS OF DOLOMITIZATION

Studies of Holocene massive carbonate deposits have emphasized that dolomite is formed as a penecontemporaneous replacement of calcium carbonate and that the process of dolomitization is operative in supratidal areas in which magnesium-rich hypersaline solutions are developed (Illing and others, 1965; Shinn and others, 1965). Similarly, studies of ancient evaporite deposits have emphasized that subtidal dolomite can be an early primary deposit (Irwin, 1965) or can form late in the evaporite cycle as a consequence of refluxion of magnesium-rich brines (Adams and Rhodes, 1960). The unifying theme emerging from these studies is that dolomitization can occur in both supratidal and subtidal environments, where high evaporation rate and low fresh-water dilution produce magnesium-rich brines. Salinity systems with the potential to develop and maintain the necessary chemical and physical factors favoring widespread subtidal dolomitization through a considerable time span have been described for the deepwater barred basin and the shallow epicontinental sea model (fig. 4).

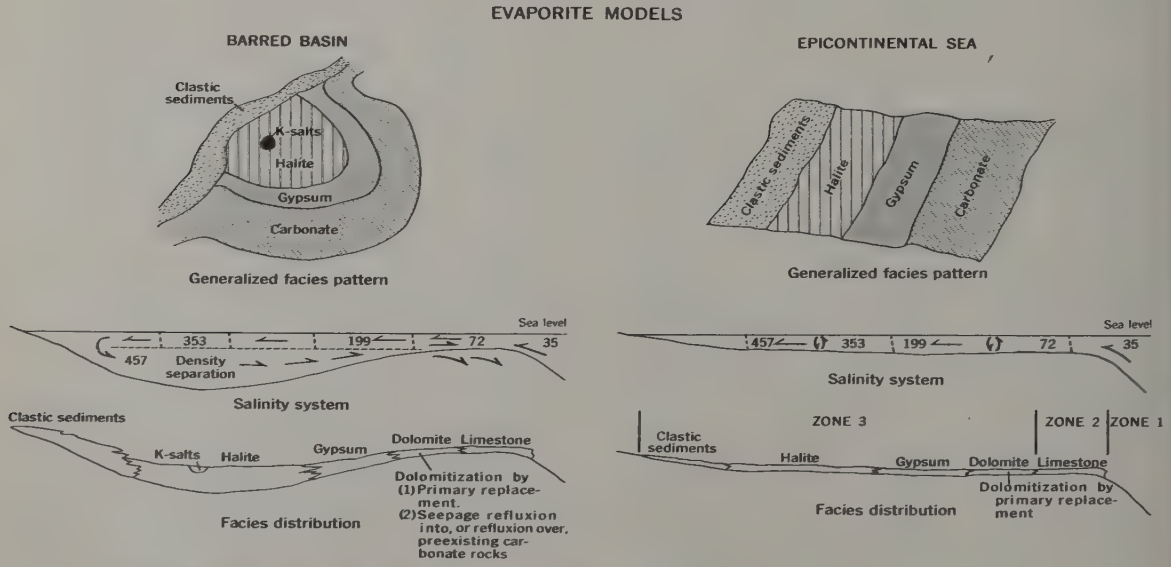

Figure 4.—The salinity systems, facies distributions, and generalized facies patterns of the barred-basin and epicontinental sea evaporite models. Based on data from King (1947), Scruton (1953), Adams and Rhodes (1960), Shaw (1964), Irwin (1965), and Hite (1968, 1970). The values given in the salinity systems are parts per thousand.

Barred basin

The barred-basin evaporite model (Ochsenius, 1877; King, 1947), which is operative in warm arid areas where evaporation exceeds dilution by fresh and oceanic water, is generally a relatively deep topographic depression separated from the open ocean by a shallower physical barrier. Commonly the barrier has been a shelf covering thousands of square miles (Hite, 1970, p. 50) that nearly or completely surrounds the basin. As sea water moves across the shallow shelf toward the basin, a strong horizontally increasing salinity gradient is produced in response to high evaporation rates (Lang, 1937). Continued evaporation establishes a circulatory system in the basin because of density stratification and density flow. Dense brine in the farthest reaches of the basin sinks and flows back beneath the less dense influxing current toward the bottom of the basin; some of this brine is refluxed back over the barrier to the sea (King, 1947, p. 474). The combination of chemical and physical factors controlling the circulation in a barred basin produces a distinctive and somewhat circular facies pattern in which chemical and biochemical carbonates occur on the fringing shelf and the more soluble salts occur near the center (fig. 4). A large part of the shelf carbonate is thought to have been dolomitized by seepage refluxion through permeable beds (Adams and Rhodes, 1960) or by refluxion of the brines over the carbonate shelf (Hite, 1970, p. 53).

Continental shelf

Although several shallow-water sedimentation models have been proposed to explain sedimentary patterns in a variety of carbonate and evaporite sequences, only relatively recently has it been recognized that certain elements were common to all shallow-water models, enabling Shaw (1964) and Irwin (1965) to describe a generalized model for epicontinental sedimentation. Shaw and Irwin emphasize that an epicontinental sea environment is characterized by the great width of the shelf (hundreds of miles) where bottom depositional slopes are on the order of less than 1 foot per mile, and where circulation, except near the edge, is restricted by the shallow depth of the sea. According to Shaw and Irwin, lateral variation in biochemical, chemical, and physical factors from shore to deeper water results in the development of three major zones of sedimentation. These sedimentary zones, in contrast to the nearly circular sedimentary pattern of a barred basin, tend to form a series of broad bands roughly parallel to the shore (fig. 4). Their three zones include:

1. An open ocean zone of low energy, hundreds of miles wide, where the depth of water restricts the hydraulic energy. Sediments are largely derived from zone 2 (see below) and consist of fine-grained organic debris. Bottom conditions tend to be reducing, thus preserving introduced organic matter and producing dark sediments.
2. A zone of high energy, tens of miles wide extending from the point where waves first strike the bottom to the limit of tidal action. Physical, chemical, and organic activity within this zone causes an orderly shoreward progression of facies ranging from biogenetic sediments to oolites and coated grains to pellets to mud.
3. A zone of low energy, free from the effects of oceanic waves and tides, extending from zone 2 to shore. In areas of high evaporation and low fresh-water runoff, salinities should increase progressively shoreward, initiating chemical precipitation keyed to that gradient. Precipitation begins with calcium carbonate and progresses consecutively through dolomite to gypsum, halite, and other more soluble salts.

Wind-generated currents within a shallow epicontinental sea tend to homogenize the water mass to a depth of at least 65 feet, thereby preventing the development of vertical density stratification. Instead, a horizontal gradient is established with increasing salinity and density toward the shore (fig. 4). The higher density water mass is prevented from free refluxion to the open ocean by the lack of sufficient hydrologic head to overcome the frictional resistance of the gently sloping sea bottom (Scruton, 1953). This frictional entrapment of highly saline water is in contrast to the hydrologic system of the deeper barred basin, where circulation is dependent upon a density differential between influxing surface currents and refluxing bottom currents. The existence at the present time of hydrologic condition similar to the epicontinental sea model but on a smaller scale seems well established (Emery and Stevenson, 1957), particularly by the long-term measurements (13 years) in Shark Bay, Western Australia (Logan and Cebulski, 1970), and the consistencies in data obtained through a 29-year time span for the Great Bahama Bank (Black, 1933; Smith, 1940; Newell and others, 1959; Cloud, 1962).

Shark Bay, Western Australia, with a semiarid subtropical climate is a shallow-water embayment open to the ocean, whereas the Great Bahama Bank with a humid subtropical climate is a shallow-water carbonate shelf surrounded by the open ocean. Despite these environmental differences, the hydrologic systems of both areas are similar in that high salinities are formed in response to high evaporation, small tidal influx, and low fresh-water dilution. Surface and bottom salinity in Shark Bay shows a gradient from normal marine salinity at the bay mouth to hypersalinity in the bay head (Logan and Cebulski, 1970, fig. 6). Cross sections drawn through the long axis of the bay show no horizontal density stratification, nor do isohalines show any relationship to bottom topography (fig. 5). Instead, the structure of the high-salinity water mass is nearly vertical, with increasing salinity and density toward the bay head. The vertical isosalinity zones, which are uniformly oxygenated from top to bottom, result from continuous homogenization by currents and wave action (Logan and Cebulski, 1970, p. 14). Surface

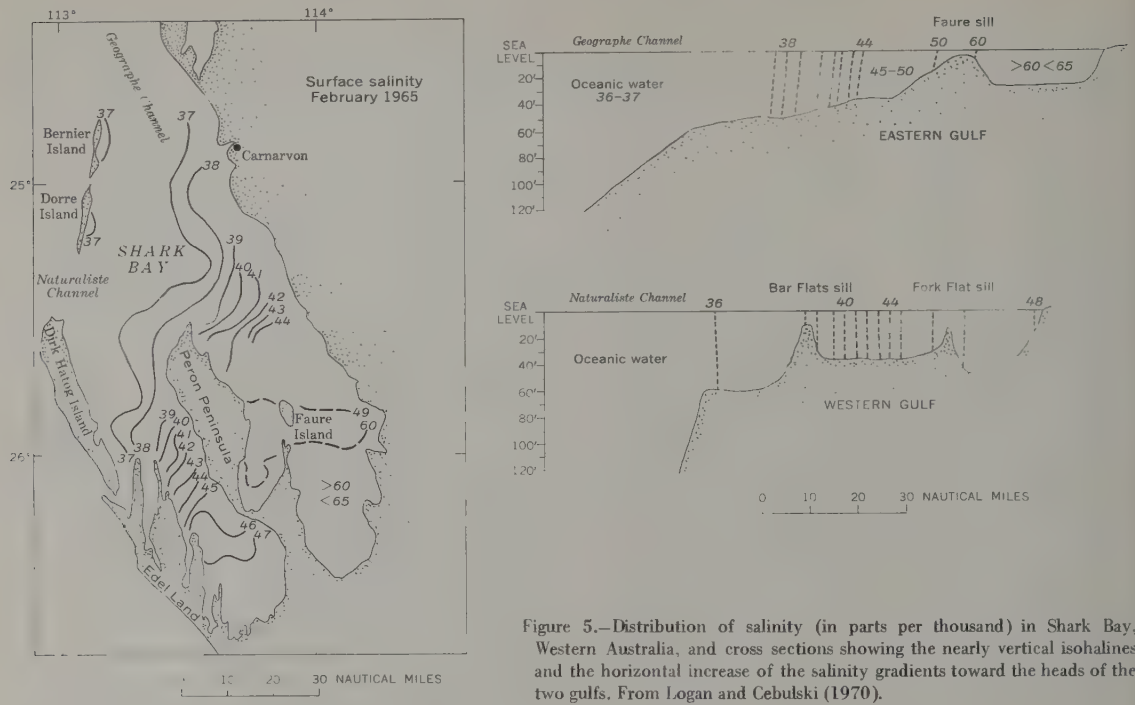

Figure 5.—Distribution of salinity (in parts per thousand) in Shark Bay, Western Australia, and cross sections showing the nearly vertical isohalines and the horizontal increase of the salinity gradients toward the heads of the two gulfs. From Logan and Cebulski (1970).

and bottom salinity gradients (Cloud, 1962, table 25) for part of the Great Bahama Bank show that the structure of the Bahama high-salinity mass is defined by steeply inclined isohalines, similar to the configuration at Shark Bay (fig. 6).

Circulation in Shark Bay and on the Great Bahama Bank is sluggish, having an estimated residual time for a particular water mass to complete a circuit from open ocean and back to be on the order of 5 months in Shark Bay (Logan and Cebulski, 1970, p. 21) and 3 months in the Bahamas (Smith, 1940, p. 156). An equilibrium condition between evaporation rate and oceanic exchange has been accomplished in Shark Bay by the constant slow movement of tidal currents bringing oceanic water in on east-facing shores and a reflux of higher salinity water out along west-facing shores (Logan and Cebulski, 1970, p. 21). Tidal currents play a minor role as a controlling factor in the circulation on the Great Bahama Bank. The direction of tidal flooding is such that its effect is largely canceled out; thus, residual current directions are determined by seasonal changes in prevailing winds (Smith, 1940, p. 15). During the summer months when prevailing winds are from the east, continuing evaporation results in the development of a high-salinity water mass with its apex off the northwest shore of Andros Island (fig. 6). Water with salinities greater than 39 parts per thousand is carried westward by persistent residual currents to cover much of the bank. Apparently, 40 to 60 inches of rain, mainly during the summer months, tends to prevent the salinity of the Bahama water mass from attaining concentrations greater than 45 parts per thousand. During the winter months the wind shifts to the northwest and oceanic water of lower salinity is carried shoreward to dilute the high-salinity mass. Thus, the salinity system developed on the bank is dynamic and tends to move and deteriorate seasonally.

DOLOMITIZATION

Studies of Holocene dolomitization, especially that of Illing, Wells, and Taylor (1965), emphasize that magnesium-ion concentrations are sufficiently great early in the evaporite cycle to initiate dolomitization before large concentrations of gypsum or anhydrite are deposited. The relationship is well illustrated by a plot of Illing, Wells, and Taylor's data from the Persian Gulf (fig. 7). Incipient dolomitization begins subtidally as suggested by the combination of minor dolomite and abundant magnesian calcite. Supratidally, where dolomitization is more complete, dolomite is abundant and magnesian calcite is sparse. The mole Mg-Ca ratio of pore water increases to about 19 at the seaward edge of the supratidal area, where gypsum first appears in the sediments; thereafter it decreases as magnesium is subtracted by the process of dolomitization. The relatively slight increase in chlorinity across the supratidal sabkha suggests that the system is near equilibrium and that

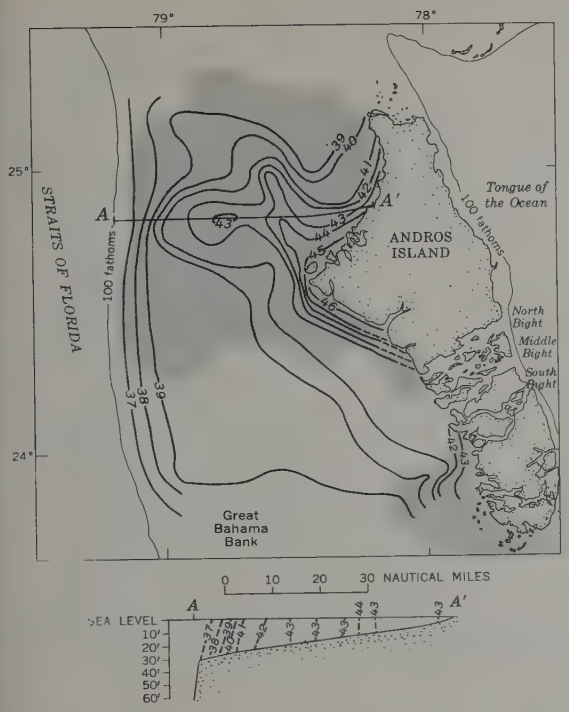

Figure 6.—Distribution of salinity (in parts per thousand) on the Great Bahama Bank, and cross section showing the nearly vertical isohalines and the horizontal increase of the salinity gradient shoreward. Shaded areas contain more than 3 percent magnesium carbonate. Data from Newell and Rigby (1957) and Cloud (1962).

dolomitization is proceeding rapidly, accompanied by deposition of small amounts of gypsum. Accordingly, dolomitization occurs early in the evaporite cycle during the transition from deposition of calcium carbonate to gypsum. Significantly, many ancient evaporite deposits have a marked deficiency of magnesium relative to its abundance in sea water (Stewart, 1963, p. 40), lending support to the concept that magnesium in ancient evaporite basins was extracted early in the process of dolomitization, thereby depleting residual brines so that only small quantities of magnesium salts were available for precipitation and refluxion. The natural progression of facies from limestone to dolomite to gypsum to halite to potassium salt is simply a reflection of the varying concentration of salts within a salinity system.

The process of magnesium concentration in sediments appears to be operative subtidally within a present-day shallow carbonate environment. This is suggested by the comparison of the distribution of salinity on the Great Bahama Bank (Cloud, 1962, table 25) to distribution of magnesium (Newell and Rigby, 1957, fig. 13). Areas of greatest magnesium in the bottom sediment appear to be closely allied to the configuration of the Bahama salinity system; in contrast, sediments with low magnesium content are deposited where oceanic water with lower salinities circulates more freely, such as north of and southwest of Andros Island and in the area of the bights near the center of Andros (figs. 6, 8). Cloud (1962, p. 94) suggests that most high-magnesium calcite in the bottom sediment of the bank is probably related to the skeletal content of the sediment. However, the amount of magnesium in skeletal material is thought to be dependent upon temperatures and salinity of the environment as well as the genetic effect of the organism (Chave, 1954; Lowenstam, 1954; Chilingar, 1962). Magnesium in the Bahamas may well be all concentrated in skeletal material, but this simply reflects the high-salinity environment within which the material formed. Magnesium distribution superimposed on a facies map of the Great Bank (Imbrie and Purdy, 1962, fig. 10) demonstrates that no clear-cut relation exists between facies and magnesium content (fig. 8). The lack of control by facies lends credence to the inference that the distribution of magnesium in the bottom sediments is related to the configuration of the salinity system on the Great Bahama Bank.

The epicontinental-sea salinity system of Shaw (1964) and Irwin (1965) and its shoreward horizontally increasing salinity gradient has the potential to develop the necessary chemical and physical factors to promote widespread subtidal dolomitization. I believe that such a system is responsible for the regional development of subtidal dolomite during Late Cambrian and Early Ordovician time.

LATE CAMBRIAN AND EARLY ORDOVICIAN SEDIMENTATION MODEL

Massive evaporite deposits attributed to deepwater deposition have not been described in the Knox Group. Minor amounts of anhydrite in vugs, small veins, and thin laminae have been observed in Tennessee and also in Lower Ordovician carbonate rocks in Texas (Barnes, 1959, p. 57) and Illinois (Saxby and Lamar, 1957, p. 14). The limited amounts of anhydrite and the broad-band facies distributions (figs. 1 and 4) tend to rule out the barred-basin model as a means of explaining deposition of dolomite in the Knox. Instead, the epicontinental-sea salinity system of Shaw (1964) and Irwin (1965) and its shoreward increasing salinity gradient is postulated as a more likely environment for the deposition of this facies. Characteristically, the deposition of limestone and dolomite in the Knox was related to the epicontinental salinity gradient, so that a shoreward succession exists from normal marine limestone on the east through a transitional zone to a highly saline dolomite phase on the west (fig. 9). Subsurface information (summarized by Lochman-Balk, 1971) shows that the Knox gradually thins northwestward toward Illinois and is replaced by a dominantly clastic sequence (fig. 1). Primary characteristics of outcropping Upper Cambrian and Lower Ordovician rocks of Wisconsin (Ostrom, 1970; R. A. Davis, 1970) compared to the primary characteristics of equivalent

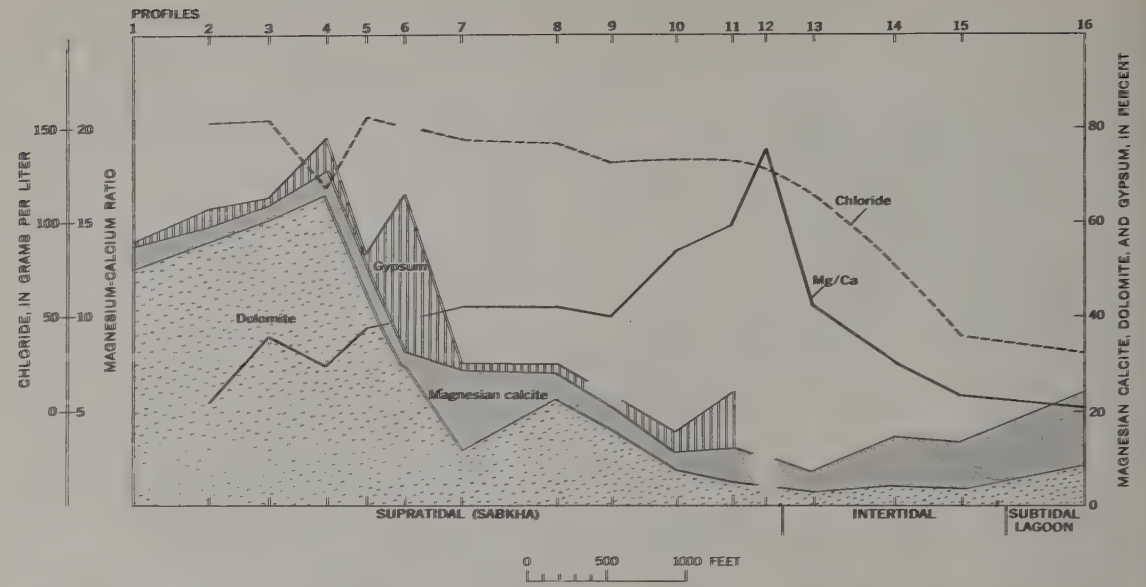

Figure 7.—Profiles to a depth of 58 cm across the Sabkha Faishakh on the Persian Gulf, showing changes in chlorinity, Mg-Ca ratio, and percentage of magnesian calcite, dolomite, and gypsum. The process of dolomitization appears to intensify progressively from incipient dolomitization subtidally to massive dolomitization in the high supratidal area. Adapted from Illing, Wells, and Taylor (1965).

age rocks of the Knox Group suggest that in near-shore areas the ancient salinity system did not continue to increase (fig. 10). Apparently fresh-water dilution from the bordering land lowered salinities to the point that a more diverse fauna developed, as well as contributed toward the preservation of minor amounts of limestone.

Reconstruction of the configuration of the original carbonate shelf of the Knox Group is hampered by numerous thrust faults of regional extent in eastern Tennessee (fig. 11). These faults with displacements on the order of miles obscure regional facies trends by burying large segments of the original depositional shelf and bringing into juxtaposition the facies which accumulated on separate parts of the shelf. This is especially true in regard to the limestone facies. Before faulting, the original width of the area of limestone deposition was on the order of 100 miles (fig. 1). Mass transport by faults has buried the easternmost edge of the original shelf where sediments reflecting high energy were deposited. Consequently, only that part of the limestone sequence deposited under a low-energy condition is preserved in eastern Tennessee. Despite the fact that parts of the record are obscure, generalized facies trends can be ascertained in a series of stratigraphic sections extending from the easternmost outcrop belt in eastern Tennessee to deep wells in eastern Kentucky (fig. 9). A summary of selected primary features of the limestone facies, the transition zone, and the dolomite facies clearly indicates that many of the same primary elements are found throughout all facies of the Knox Group (fig. 12), emphasizing the regional impress of the overall subtidal environment. However, physical and chemical differences within the subtidal environment tended to restrict the abundance and even the presence of few elements to particular facies.

Where the limestone facies is present, it is characterized by dark-gray calcilutite containing thin zones of paper-thin laminated beds, angular intraclasts, oolite, arenite, and domal algal stromatolites. This combination of lithologies and algal domes suggests that the eastern limestone facies was deposited in water of normal salinity near wave base but not below the zone of photosynthesis. The energy level as suggested by the abundance of dark-gray calcilutite was normally low, although intraclasts and arenite beds record an occasional short-term increase in energy from strong storm currents. That a low-energy level was maintained throughout deposition of the limestone sequence is probably related to the fact that much of the ocean's energy from tides and wave action was largely dissipated before reaching that part of the facies now preserved in eastern Tennessee.

The transition zone between the dominantly limestone facies on the east and the dolomite facies on the west is confined to a relatively narrow geographic belt (fig. 9). Prouty (1947; 1948, p. 1618) thought that this abrupt facies change was related to a structural barrier, but my stratigraphic work shows no unusual thickening or thinning across the so-called

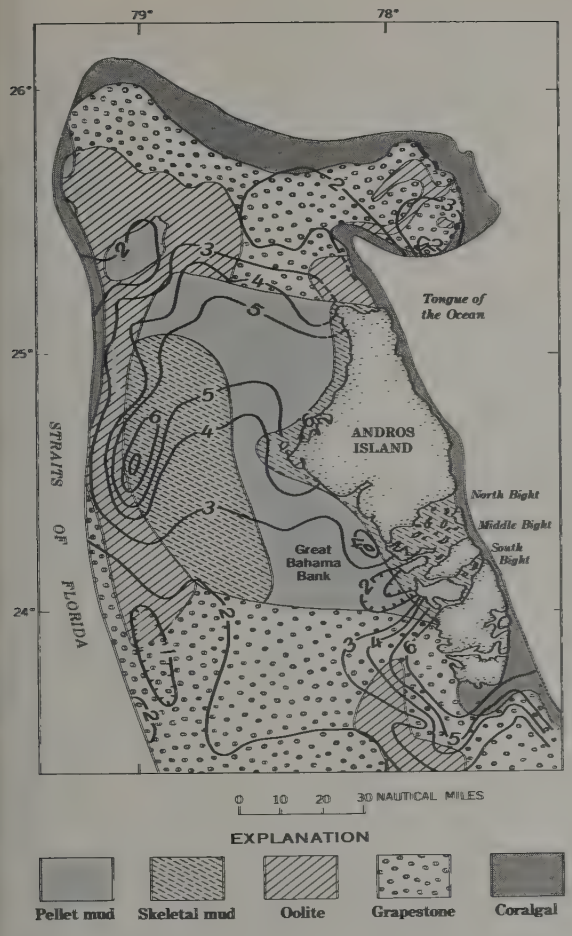

Figure 8.—Map of part of the Great Bahama Bank, showing the distribution of facies and magnesian carbonate content of sediments, in percent. From Newell and Rigby (1957) and Imbrie and Purdy (1962).

barrier. I believe that the transition zone, which has been partly telescoped by Appalachian thrusting, marks the location of a relatively constant geographic zone of change from normal marine water to penesaline water within an epicontinental sea. Surface and subsurface studies (Swartz, 1948; Donaldson and Page, 1964; Perry, 1964; Barnes, 1959; Chenoweth, 1968; Williams, 1969) suggest that this same transition zone within carbonate rocks equivalent to the Knox Group persists from New York to Texas (fig. 1), thus implying that the change from normal marine water to penesaline water existed completely around the edge of the ancient continental shelf.

The transition zone characteristically contains about equal proportions of dolomite and limestone, apparently reflecting the gradual lateral shift of the eastern part of the high-salinity water mass where magnesium concentration was large enough to promote dolomitization. The facies within the transition zone contains a higher proportion of oolite in relation to intraclasts and records the first stratiform algal stromatolites in dolomite. The transition facies apparently accumulated near the limit of oceanic wave and tidal effect, but under the influence of induced currents produced by water loss to evaporation.

The dolomite facies of the Knox Group contains a diversity of rock types ranging from dololutite to oolite, produced by widely different levels of depositional energy within a high-salinity environment. Forcefully emphasizing that although dolomitization may be controlled by the concentration of magnesium ions within an epicontinental sea, it does not follow that concentration of magnesium can only occur in low-energy environments. Despite the fact that a dolomite facies was deposited largely beyond the reach of oceanic waves and tidal currents, circulation within the high-salinity water mass was not static. Instead, high evaporation induced a constant shoreward current flow, which had a profound effect upon the kind and lateral distribution of facies. These induced currents were uniform and widespread, and caused the deposition of laterally persistent lithologic units as little as 1 inch thick. Where these currents were moderate, oolite and massive-bedded stratiform algal stromatolite as much as 140 feet thick accumulated; where current velocities were low, dololutite with domal algal stromatolites accumulated. Because of the similarity in energy levels, the distribution of dololutite, oolite, and stratiform algal stromatolite of the highly saline environment closely resembles the distribution pattern of like lithologic elements in the normal marine limestone phase of Shaw (1964) and Irwin (1965), where oolite and reefs accumulated in the higher energy zones at the shelf edge and calcilutite accumulated in areas of lower energy.

SUMMARY

Approximately 90 percent of the Upper Cambrian and Lower Ordovician carbonate strata is dolomite. This is in sharp contrast to Holocene carbonate deposition sites where most of the carbonate strata are limestone and only a small percentage of the total sediment is dolomite, mainly confined to the supratidal area. The epicontinental-sea sedimentation model and its shoreward increasing salinity gradient is postulated to be the likely mechanism responsible for widespread subtidal dolomitization during Late Cambrian and Early Ordovician time. Comparison of the epicontinental sedimentation model to present-day carbonate depositional sites suggests that Holocene sites represent only the normal marine limestone phase of the epicontinental model.

Present-day examples of the epicontinental salinity system, although measured only by tens of miles, illustrate that appreciable salinity increase can occur without physical

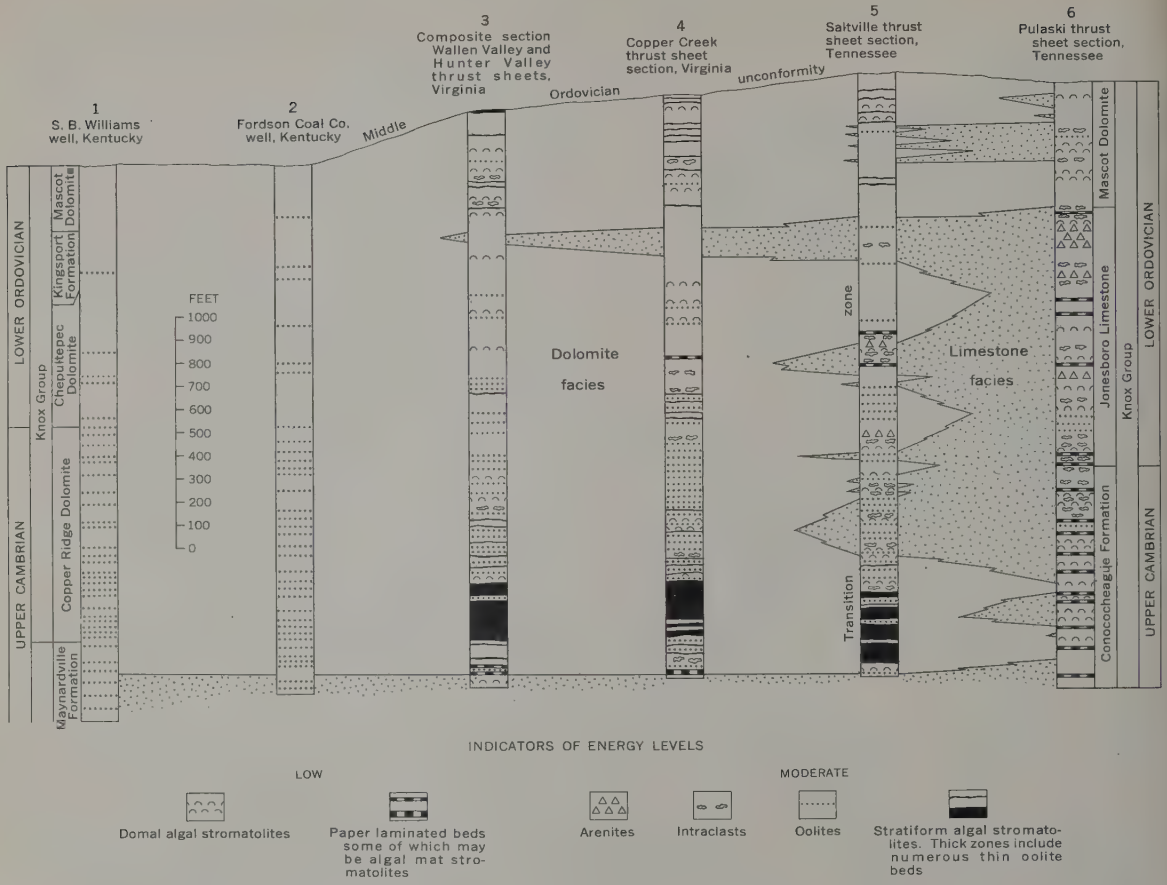

Figure 9.—Sections showing the distribution of energy-indicative beds in the Upper Cambrian and Lower Ordovician carbonate strata in wells in Kentucky and surface sections in Virginia and Tennessee. Algal stromatolites could not be identified in well cuttings from Kentucky. (See fig. 11 for line of section.)

barriers. Such a system developed on an ancient, shallow continental shelf, hundreds of miles wide, could easily concentrate sea water to the point of gypsum saturation. This would result in the development of subtidal dolomite on a regional scale. Increased fresh-water runoff from land or seasonal shifts in wind direction, as in the Bahamas, would contribute to a seasonal deterioration of the ancient salinity system. Resolution of calcium sulfate during the period of lower salinity would account for only trace amounts of gypsum now found in the rocks of Late Cambrian and Early Ordovician age.

Sedimentation within an epicontinental sea, as typified by the Knox Group of Late Cambrian and Early Ordovician age in the southern Appalachians, is closely related to a westward-increasing salinity gradient, so that a lateral transition from normal marine limestone facies to a transition zone to a dolomite facies exists. Domal algal stromatolites are abundant throughout both the limestone and dolomite facies of the Knox, indicating that variation in salinity has little effect on their growth, but that water depth during deposition of either facies was not below the zone of photosynthesis. Limestone deposition was restricted to a rather narrow band at the oceanic bordering edge of the epicontinental sea, where continual flushing by wave and tidal currents prevented extensive buildup in salinity. The transition zone developed near the limit of tidal exchange, thus it occupies a relatively fixed geographic position throughout deposition of the Knox. Although the dolomite facies was deposited in high-salinity water beyond the reach of oceanic and tidal currents, energy levels within that environment were not uniformly low. Instead, the diversity in rock type, from dololutite to oolite, suggests that energy levels ranged from low to moderate. The

EPICONTINENTAL-SEA SEDIMENTATION MODEL

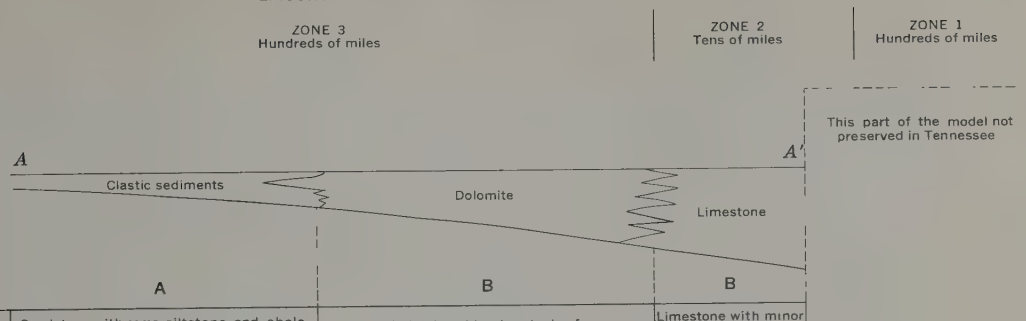

	A	B	B
Lithology	Sandstone with some siltstone and shale. Carbonate rocks increasing upward and to the southeast. Glauconite	Dolomite with minor beds of sandstone and shale	Limestone with minor beds of sandstone and shale
Crossbedding and ripple marks	Abundant	Rare	
Oolite content	Locally abundant in carbonate rocks	Low to abundant	Low
Shrinkage cracks	Generally rare in sequence, but can be locally abundant		
Intraclast content	Abundant	Low to moderate	Moderate
Laminations	Few	Locally abundant	Abundant
Burrows	Common	Locally common	
Algal stromatolites	Abundant in carbonate rocks	Abundant	
Other fossils	Diverse to restricted	Restricted to a few forms	Diverse
Salinity	Fluctuating from normal to high because of fresh water dilution from land	High	Normal ← Increasing
Dominant energy level	High → Low to moderate	Low to moderate	Low
Source of energy	← Wind; Longshore currents due to density differential produced by fresh water runoff; Induced currents →	→ Induced current flow from high rate of evaporation ←	Oceanic wave and tidal
Environment	Intertidal to subtidal	Subtidal	

Figure 10.—Summary of primary characteristics and interpretive environments of the rocks of the Knox Group of Tennessee (B) compared with similar parameters of equivalent age rocks in Wisconsin (A). Cross section is line A–A' of figure 1. (Wisconsin data from Ostrom, 1970, and R. A. Davis, 1970).

distribution of the different rock types was related to circulatory patterns induced where a constant shoreward current flow developed from replacement of water by evaporation loss. Where velocities of the induced current were moderate, oolite and stratiform algal stromatolite development is favored; where velocities were low, dololutite with domal algal stromatolites accumulated.

REFERENCES CITED

Adams, J. E., and Rhodes, M. L., 1960, Dolomitization by seepage refluxion: Am. Assoc. Petroleum Geologists Bull., v. 44, no. 12, p. 1912–1920.

Barnes, V. E., 1959, Stratigraphy of the pre-Simpson Paleozoic subsurface rocks of Texas and southeast New Mexico, V. 1–2: Texas Univ. Pub. no. 5924, 836 p.

Black, Maurice, 1933, The algal sedimentation of Andros Island, Bahamas: Royal Soc. London Philos. Trans. ser. B, vol. 222, p. 165–192.

Burst, J. F., 1965, Subaqueously formed shrinkage cracks in clay: Jour. Sed. Petrology, v. 35, no. 2, p. 348–353.

Chave, K. E., 1954, Aspects of the biochemistry of magnesium–[Pt.] 1, Calcareous marine organisms: Jour. Geology v. 62, no. 3, p. 266–283.

Chenoweth, P. A., 1968, Early Paleozoic (Arbuckle) overlap, southern Mid-continent, United States: Am. Assoc. Petroleum Geologists Bull. v. 52, no. 9, p. 1670–1688.

Chilingar, G. V., 1962, Dependence on temperature of Ca/Mg ratio of skeletal structure of organisms and direct chemical precipitation out of sea water: Southern California Acad. Sci. Bull., v. 61, p. 45–60.

Cloud, P. E., Jr., 1962, Environment of calcium carbonate deposition west of Andros Island, Bahamas: U.S. Geol. Survey Prof. Paper 350, 138 p.

Crawford, Johnson, 1945, Structural and stratigraphic control of zinc deposits in East Tennessee: Econ. Geology, v. 40, p. 408–415.

Davis, G. R., 1970, Algal-laminated sediments, Gladstone embayment, Shark Bay, Western Australia, *in* Carbonate sedimentation and environments, Shark Bay, Western Australia: Am. Assoc. Petroleum Geologists Mem. 13, p. 169–205.

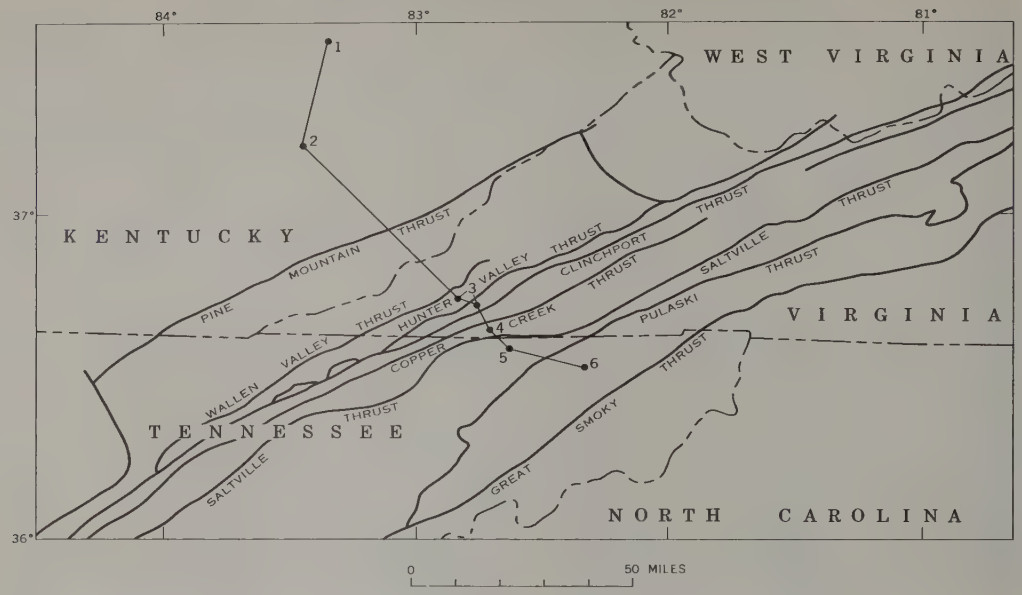

Figure 11.—Map showing the location of wells and measured sections in figure 9 and the trace of major thrust faults in the area.

Davis, R. A., Jr., 1970, Prairie Du Chien Group in the Upper Mississippi Valley, *in* Field trip guidebook for Cambrian-Ordovician geology of western Wisconsin—Geol. Soc. America, Ann. Mtg., Milwaukee, Wis., 1970: Wisconsin Geol. and Nat. History Survey Inf. Circ. 11, p. 35–44.

Donaldson, Alan, and Page, Ronald, 1964, Stratigraphic reference sections of Elbrook and Conococheague Formations (Middle and Upper Cambrian) and Beekmantown Group (Lower Ordovician) in Berkeley and Jefferson Counties, West Virginia: West Virginia Acad. Sci. Proc., v. 35, p. 149–171.

Emery, K. O., and Stevenson, R. E., 1957, Estuaries and lagoons—[Pt.] 1, Physical and chemical characteristics, *in* Chap. 23 *of* Hedgpeth, J. W., ed., Ecology: Geol. Soc. America Mem. 67, p. 673–693.

Folk, R. L., 1959, Thin-section examination of pre-Simpson Paleozoic rocks, *in* V. 1 *of* Barnes, V. E., Stratigraphy of the pre-Simpson Paleozoic subsurface rocks of Texas and southeast New Mexico: Texas Univ. Pub., no. 5924, p. 95–130.

Gebelein, C. D., 1969, Distribution, morphology, and accretion rate of Recent subtidal algal stromatolites, Bermuda: Jour. Sed. Petrology, v. 39, no. 1, p. 49–69.

Ginsburg, R. N., 1960, Ancient analogues of Recent stromatolites: Internat. Geol. Cong., 21st, Copenhagen, 1960, Rept., pt. 22, p. 26–35.

Harris, L. D., 1969, Kingsport Formation and Mascot Dolomite (Lower Ordovician) of East Tennessee, *in* Papers on the stratigraphy and mine geology of the Kingsport and Mascot Formations (Lower Ordovician) of East Tennessee: Tennessee Div. Geology Rept. Inv. 23, p. 1–39.

Herbert, Paul, Jr., and Young, R. S., 1956, Sulfide mineralization in the Shenandoah Valley of Virginia: Virginia Div. Geology Bull. 70, 58 p.

Hite, R. J., 1968, Distribution and geologic habitat of marine halite and associated potash deposits, *in* Seminar on sources of mineral raw materials for the fertilizer industry in Asia and the Far East: U.N. ECAFE Mineral Resources Devel. Ser. 32, p. 307–326.

——1970, Shelf carbonate sedimentation controlled by salinity in the Paradox basin, southeast Utah, *in* Rau, J. L., and Dellwig, L. F., eds., Third symposium on salt, V. 1: Cleveland, Ohio, Northern Ohio Geol. Soc., p. 48–66.

Holland, C. H., ed., 1971, Cambrian of the New World, V. 1: New York and London, Interscience Publishers, 456 p.

Illing, L. V., Wells, A. J., and Taylor, J. C. M., 1965, Penecontemporary dolomite in the Persian Gulf, *in* Dolomitization and limestone diagenesis—A symposium: Soc. Econ. Paleontologists and Mineralogists Spec. Pub. 13, p. 89–111.

Imbrie, John, and Purdy, E. C., 1962, Classification of modern Bahamian carbonate sediments, *in* Classification of carbonate rocks—A symposium: Am. Assoc. Petroleum Geologists Mem. 1, p. 253–272.

Irwin, M. L., 1965, General theory of epeiric clear water sedimentation: Am. Assoc. Petroleum Geologists Bull., v. 49, no. 4, p. 445–459.

Kendall, C. G., and Skipwith, P. A., 1968, Recent algal mats of a Persian Gulf lagoon: Jour. Sed. Petrology, v. 38, no. 4, p. 1040–1058.

King, R. H., 1947, Sedimentation in Permian Castile Sea: Am. Assoc. Petroleum Geologists Bull. v. 31, no. 3, p. 470–477.

Lang, W. T. B., 1937, The Permian formation of the Pecos Valley of New Mexico and Texas: Am. Assoc. Petroleum Geologists Bull., v. 21, p. 833–898.

Laporte, L. F., 1971, Paleozoic carbonate facies of the central Appalachian shelf: Jour. Sed. Petrology, v. 41, no. 3, p. 724–740.

Lochman-Balk, Christina, 1971, The Cambrian of the craton of the United States, *in* Cambrian of the New World, V. 1: New York and London, Interscience Publishers, p. 79–167.

Logan, B. W., 1961, Cryptozoon and associate stromatolites from the Recent Shark Bay, Western Australia: Jour. Geology, v. 69, no. 5, p. 517–533.

Logan, B. W., and Cebulski, D. E., 1970, Sedimentary environments of Shark Bay, Western Australia, *in* Carbonate sedimentation and environments, Shark Bay, Western Australia: Am. Assoc. Petroleum Geologists Mem. 13, p. 1–37.

Logan, B. W., Rezak, Richard, and Ginsburg, R. N., 1964, Classification and environmental significance of algal stromatolites: Jour. Geology, v. 72, no. 3, p. 68–83.

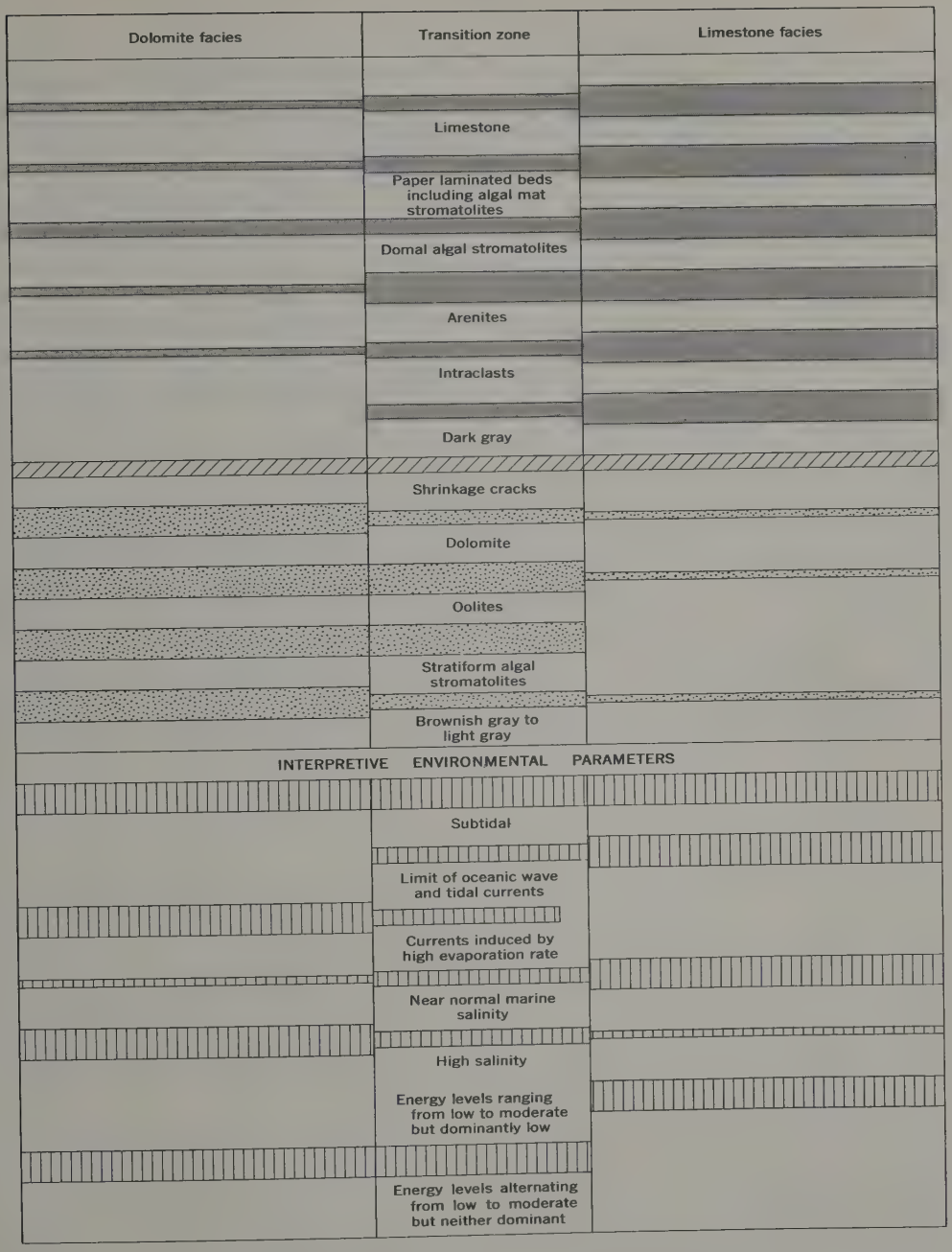

Figure 12.—The distribution of common elements of the dolomite, transition, and limestone facies of the Knox Group, and interpretive environmental parameters. Thickness of the bar emphasizes the relative importance of each element within each facies.

Lowenstam, H. A., 1954, Factors affecting the aragonite-calcite ratios in carbonate-secreting marine organisms: Jour. Geology v. 62, p. 284–322.

Monty, Claude, 1965, Recent algal stromatolites in the Windward Lagoon, Andros Island, Bahamas: Soc. Géol. Belgique Annales, v. 88, p. 269–276.

Newell, N. D., Imbrie, John, Purdy, E. G., and Thurber, D. L., 1959, Organism communities and bottom facies, Great Bahama Bank: Am. Mus. Nat. History Bull. v. 117, p. 177–228.

Newell, N. D., and Rigby, J. K., 1957, Geological studies on the Great Bahama Bank, *in* Regional aspects of carbonate deposition—A symposium: Soc. Econ. Paleontologists and Mineralogists Spec. Pub. 5, p. 15–72.

Ochsenius, Karl, 1877, Die Bildung der Steinsalzlager und ihrer Mutterlaugensalze: Halle, C. E. M. Pfeffer, 172 p.

Oder, C. R. L., and Miller, H. W., 1945, Stratigraphy of the Mascot-Jefferson City zinc district [Tenn.]: Am. Inst. Mining Metall. Engineers Tech. Pub. 1818, 9 p.; A.I.M.E. Trans., v. 178, p. 223–231 (1948).

Oder, C. R. L., and Ricketts, J. E., 1961, Geology of the Mascot-Jefferson City zinc district, Tennessee: Tennessee Div. Geology Rept. Inv. 12, 29 p.

Ostrom, M. E., 1970, Sedimentation cycles in the Lower Paleozoic rocks of western Wisconsin, *in* Field trip guidebook for Cambrian-Ordovician geology of western Wisconsin—Geol. Soc. America, Ann. Mtg., Milwaukee, Wis. 1970: Wisconsin Geol. and Nat. History Survey Inf. Circ. 11, p. 10–34.

Perry, W. J., Jr., 1964, Geology of Ray Sponaugle well, Pendleton County, West Virginia: Am. Assoc. Petroleum Geologists Bull., v. 48, no. 5, p. 659–669.

Prouty, C. E., 1947, Relationship of Cambro-Ordovician dolomites to facies barriers in Tennessee and Virginia [abs.]: Geol. Soc. America Bull., v. 58, no. 12, pt. 2, p. 1218–1219.

——1948, Trenton and sub-Trenton stratigraphy of northwest belts of Virginia and Tennessee, *in* Appalachian Basin Ordovician symposium: Am. Assoc. Petroleum Geologists Bull., v. 32, no. 8, p. 1596–1626.

Rodgers, John, 1968, The eastern edge of the North American Continent during the Cambrian and Early Ordovician, Chap. 10 *in* Zen, E-an, and others, eds., Studies of Appalachian geology, northern and maritime: New York and London, Interscience Publishers, p. 141–149.

Saxby, D. B., and Lamar, J. E., 1957, Gypsum and anhydrite in Illinois: Illinois State Geol. Survey Circ. 226, 26 p.

Scruton, P. C., 1953, Deposition of evaporites: Am. Assoc. Petroleum Geologists Bull., v. 37, no. 11, p. 2498–2512.

Shaw, A. B., 1964, Time in stratigraphy: New York, McGraw-Hill Book Co., 365 p.

Shinn, E. A., Ginsburg, R. N., and Lloyd, R. M., 1965, Recent supratidal dolomite from Andros Island, Bahamas, *in* Dolomitization and limestone diagenesis—A symposium: Soc. Econ. Paleontologists and Mineralogists Spec. Pub. 13, p. 112–123.

Smith, C. L., 1940, The Great Bahama Bank—[Pt.] 1, General hydrographical and chemical features: Jour. Marine Research, v. 3, no. 2, p. 147–170.

Stagg, A. K., and Fischer, F. T., 1970, Upper Knox stratigraphy of Middle Tennessee [abs.]: Geol. Soc. America Abstracts with Programs, v. 2, no. 7, p. 693.

Stewart, F. H., 1963, Marine evaporites, Chap. Y *of* Data of Geochemistry, 6th ed.: U.S. Geol. Survey Prof. Paper 440-Y, 52 p.

Swartz, F. M., 1948, Trenton and sub-Trenton of outcrop areas in New York, Pennsylvania, and Maryland, *in* Appalachian Basin Ordovician symposium: Am. Assoc. Petroleum Geologist Bull., v. 32, no. 8, p. 1493–1595.

Williams, C. H., Jr., 1969, Cross section from Mississippi-Tennessee State line to Horn Island in Gulf of Mexico: Jackson, Miss., Mississippi Geol. Survey, map.

Young, R. S., and Wedow, Helmuth, Jr., 1962, Geologic setting of the Myers zinc prospect, Smyth County, Virginia [abs.]: Geol. Soc. America Spec. Paper 68, p. 82.

Jour. Research U.S. Geol. Survey
Vol. 1, No. 1, Jan.—Feb. 1973, p. 79—80

DETERMINATION OF GOLD IN PHOSPHATES BY ACTIVATION ANALYSIS USING EPITHERMAL NEUTRONS

By JACK J. ROWE, Washington, D.C.

Abstract.—A simple method is described for determining gold in phosphates and phosphatic materials. Samples in a cadmium container are irradiated with epithermal neutrons to minimize the formation of ^{32}P, while permitting the formation of adequate amounts of ^{198}Au. Fire assay-radiochemical methods are used to separate the ^{198}Au. Concentrations as low as 0.1 ppb can be determined readily while maintaining low radiation levels.

The routine determination of gold in geologic materials using the method of Rowe and Simon (1968) provides for a 10-hour irradiation at a flux of 5×10^{12} n per cm^2 per sec and 10 days of cooling to permit the decay of 15-hour ^{24}Na, the principal source of matrix radioactivity in rocks and minerals. When this procedure is applied to phosphatic materials, high levels of 16-day ^{32}P are formed. Because of its biological effect, it is undesirable to expose personnel to the hazards of radioactive phosphorus. It is not practical to wait for the decay of ^{32}P because the 2.7-day ^{198}Au decays much more rapidly than the 16-day ^{32}P. The use of epithermal neutron irradiation permits the determination of gold while reducing the amount of ^{32}P formed.

The "advantage factor" obtained by using epithermal neutrons for irradiations rather than the entire reactor spectrum (thermal plus epithermal) can be defined by the ratio R_{Cd}^{m}/R_{Cd}^{a} where R_{Cd} is the cadmium ratio, m is the matrix, and a is the element being studied. The cadmium ratio can be determined experimentally or by calculation. If the cadmium ratio of a standard isotope, usually ^{198}Au, has been determined, the corresponding R_{Cd} for another nuclide can be calculated from the following formula given by Brunfelt and Steinnes (1969):

$$R_{Cd} = 1 + \frac{\sigma_o}{\sigma_o^{Au}} \cdot \frac{0.44\,\sigma_o^{Au} + I^{Au}}{0.44\,\sigma_o + I} \quad (R_{Cd}^{Au} - 1),$$

where σ_o = the thermal neutron cross section and I = the resonance activation integral excluding the $1/v$ contribution for the nuclide.

Experimentally, the cadmium ratio (R_{Cd}) can be defined as:

$$R_{Cd} = \frac{A_{th} + A_r}{A_r},$$

where A_{th} and A_r are the activities produced from thermal and epithermal neutrons, respectively. Hence the cadmium ratio is a measure of the decrease in activity of an isotope irradiated by epithermal neutrons compared to irradiation with the total neutron flux.

Brunfelt and Steinnes (1969) have shown that the calculated values for the cadmium ratio agree with experimentally determined values for many elements. Table 1 shows the cadmium ratio and the gold advantage factor for some of the nuclides observed in studies of rocks and phosphatic materials. The advantage factors are favorable not only for the determination of gold in a phosphorus matrix, but also for matrices containing Na, Fe, Co, Cr, and Ca. Hence epithermal neutron irradiations can be applied to many materials.

IRRADIATION PROCEDURE

Approximately 1 g of each sample was weighed into $^2/_5$-dram polyethylene vials. Monitors containing 50 ng of gold were prepared by accurately pipetting 0.2 ml of a solution containing 250 ng of gold per ml onto 0.2 g of spectrographic grade silica in a $^2/_5$-dram vial. Usually 10 samples plus four monitors were irradiated together. Vials were heat sealed and placed in a cadmium cylinder (1 mm thick) fitted with cadmium caps at top and bottom and formed to fit inside the usual irradiation polybucket. The cadmium absorbed neutrons below 0.4 eV, hence the induced activity in the samples was due to epithermal neutrons.

Samples and monitors were irradiated for 30 minutes in the U.S. Naval Research Laboratory reactor (thermal flux = 5×10^{12} n per cm^2 per sec; $R_{Cd}^{Au} = 3.2$). After cooling overnight, the overall radioactivity of the samples was generally less than 2 mr per hour at 6 inches. unshielded. This low amount reduced the hazards involved in handling the irradiated samples.

Table 1.—*Cadmium ratio and gold advantage factor for various nuclides*

Nuclide	Half-life[1]	R_{Cd}	Advantage factor R^{m}_{Cd}/R^{Au}_{Cd}
^{198}Au	2.7 d	3.2	----
^{86}Rb	18.6 d	3.1	0.97
^{122}Sb	2.8 d	2.5	.8
^{124}Sb	60 d	1.6	.5
^{134}Cs	2.3 y	3.3	1.03
^{131}Ba	12 d	2.5	.8
^{153}Sm	47 h	3.3	1.03
^{160}Tb	73 d	2.7	.8
^{181}Hf	46 d	21	6.6
^{182}Ta	111 d	2.3	.7
^{233}Pa(Th)	27 d	4.0	1.25
^{24}Na	15 h	60	18.7
^{47}Ca	150 d	27	8.4
^{46}Sc	85 d	74	23
^{59}Fe	45 d	32	10
^{60}Co	5.3 y	18	5.6
^{140}La	40 h	26	8
^{152}Eu	12 y	45	14
^{152m}Eu	9.5 h	34	10.6
^{32}P	16 d	39	12.1
^{51}Cr	27 d	26	8.4

[1] Abbreviations: h, hour; d, day; y, year.

RADIOCHEMISTRY

Because of the low concentrations of gold in the samples being analyzed, it was necessary to perform a radiochemical separation of the gold. The procedure used was the fire assay-radiochemical method of Rowe and Simon (1968). Samples were processed through fire assay with gold carrier. The final gold bead was weighed for yield determination. Samples were counted in a 3- by 3-inch well-type NaI(Tl) detector coupled to a multichannel analyzer. The 0.413-MeV peak of ^{198}Au was used for the calculations.

DISCUSSION

Epithermal neutron irradiations have been applied by de Lange and others (1968) and Lobanov and others (1966) to reduce the interferences from ^{24}Na and ^{59}Fe in the instrumental determination of gold in ores. Brunfelt and Steinnes (1969) showed an improvement in the instrumental neutron activation determination of many elements through the use of epithermal irradiations. It can be seen from table 1 that the technique is applicable to the determination of Ta, Ba, Sb, Rb, Cs, Sm, Tb, and Th to overcome interferences from Na, Fe, Co, Eu, Sc, Ca and P.

Gamma-ray spectra obtained after fire assay radiochemistry of phosphates were virtually free of other nuclides. The only isotope observed was ^{144}Ce (31-hour). It has a peak at 0.296 MeV, which does not interfere with the 0.413-MeV peak for ^{198}Au. The ^{198}Au activity was sufficient to provide 150 counts per min per ng of gold in the photopeak using Covell's (1959) method for calculating peak area. Samples of phosphates were irradiated one afternoon, processed the next morning, and counted by the close of the day, providing for rapid analyses with only negligible exposure of analysts to radioactivity.

This method was applied to the determination of gold in Florida phosphates where the gold content ranged from 0.4 to 5 ppb. It was also used for the determination of gold in deer antlers in connection with a study by Jones (1970, p. 12) of the gold content of animals. Gold in the ash of deer antlers ranged from 0.3 to 28.3 ppb. Each irradiation included at least one 0.1-g sample of gold quartz standard GQS-1 (Millard and others, 1969). Results for this standard agree with the published values.

ACKNOWLEDGMENTS

The author wishes to acknowledge the assistance and cooperation of L. P. Harris, of the U.S. Naval Research Laboratory, and the helpful suggestions of L. P. Greenland.

REFERENCES CITED

Brunfelt, A. O., and Steinnes, E., 1969, Instrumental activation analysis of silicate rocks with epithermal neutrons: Anal. Chim. Acta, v. 48, no. 1, p. 13–24.

Covell, D. F., 1959, Determination of gamma-ray abundance directly from total absorption peak: Anal. Chemistry, v. 31, p. 1785–1790.

deLange, P. W., deWet, W. J., Turkstra, J., and Venter, J. H., 1968, Nondestructive neutron activation analysis of small samples of Witwatersrand ore for gold: Anal. Chemistry, v. 40, no. 2, p. 451–454.

Jones, R. S., 1970, Gold content of water, plants, and animals: U.S. Geol. Survey Circ. 625, 15 p.

Lobanov, E. M., Miranskii, I. A., Pozychanyuk, V. F., Saifutdinova, D. G., and Khaidarov, A. A., 1966, A more effective determination of gold in ores by activation analysis, *in* Lobanov, E. M., ed., Activation analysis; Proceedings of First All-Union Coordinating Conference, Tashkent, Oct. 24–28, 1962: Jerusalem, Israel Program for Sci. Translation, p. 60–63, available from Natl. Tech. Inf. Service, U.S. Dept. Commerce, Springfield, Va.

Millard, H. T., Jr., Marinenko, John, and McLane, J. E., 1969, Establishment of gold-quartz standard GQS-1: U.S. Geol. Survey Circ. 598, 6 p.

Rowe, J. J., and Simon, F. O., 1968, The determination of gold in geologic materials by neutron-activation analysis using fire assay for the radiochemical separations: U.S. Geol. Survey Circ. 599, 4 p.

Jour. Research U.S. Geol. Survey
Vol. 1, No. 1, Jan.–Feb. 1973, p. 81–84

RAPID DETERMINATION OF SULFUR IN ROCKS

By LEONARD SHAPIRO, Washington, D.C.

Abstract.—Sulfur is determined turbidimetrically as barium sulfate after an aqua regia attack. The turbidity is formed in an ammoniacal solution from which R_2O_3 has been centrifuged. Reproducibility of turbidity is obtained by adding barium chloride as a solid rather than as a solution. Sulfur is determined in the range 0.01–4 percent within ±0.02 absolute, or approximately 5 percent of the amount present, whichever is larger. A 100-mg sample is used for sulfur concentrations of up to 0.50 percent S, a 20-mg sample for higher levels. A determination requires about 5 minutes.

Conventional chemical procedures for the determination of sulfur in rocks are generally based on an oxidizing sodium carbonate fusion to decompose the sample, followed by a separation of the sulfur from possible interferences and the subsequent precipitation and weighing of barium sulphate. An excellent summary of currently used procedures for sulfur determinations is given by Maxwell (1968). All the procedures described can give excellent results, but they are lengthy. An excellent summary of methods for sulfur in materials other than rocks is given by Patterson (1958), who also gives a general review of turbidimetric methods for sulfur.

The precipitation of sulfur with barium is probably the most widely used turbidimetric determination (Fisher, 1966, p. 277–282). The precision of this determination is dependent on the reproducibility of the turbidity which is itself dependent on the conditions at the time of initiation of precipitation. Fisher refers to the complexity and irreproducibility of nucleation and crystal growth. Solid barium chloride has been used in water and soil analysis (American Public Health Association, 1965, p. 291–292; Bardsley and Lancaster, 1965) to obtain reproducible turbidity, and in our laboratory it was found that when barium chloride is introduced as a solid and the precipitation made in ammoniacal solution, reproducibility is remarkably better than when it is added as a solution.

The method described in this paper is a chemical technique which is more rapid and simple than previous chemical techniques and requires no complex instrumentation. To a solution made by attacking a 100-mg sample with aqua regia in a test tube, calcium chloride is added. The solution is boiled, made ammoniacal, and the precipitate centrifuged off. About 5 ml of the clear supernatant liquid is transferred by pipet to a dry test tube to which a small spike of sulfate has been added. The sulfate is precipitated by adding powdered barium chloride, and the absorbance of the resultant turbidity is measured in a spectrophotometer after a few minutes. A solution prepared from pure sodium sulfate is used as a reference standard. The result obtained represents all the sulfide which has been converted to sulfate plus all the acid-soluble sulfate.

The procedure may be repeated using hydrochloric acid in place of aqua regia to obtain a value for the acid-soluble sulfate. Samples containing as much as 4 percent S can be analyzed.

REAGENTS AND APPARATUS

Reagents

Barium chloride: Crush the crystals with a mortar and pestle.
HNO_3, concentrated.
HCl, concentrated.
Dilute HNO_3, 1+3 dilution with water.
NH_4OH, 1+1 dilution with water.
Standard sulfate solution: Dissolve 177.5 mg Na_2SO_4 in 250 ml H_2O. One ml contains 0.4 mg SO_3 or 0.16 mg S.
Calcium chloride solution: Dissolve 5 g $CaCl_2 \cdot 2H_2O$ in 100 ml H_2O.

Apparatus

Spectrophotometer, fitted for test tubes.
Centrifuge.
Test tubes, 18 by 150 mm.
Bunsen burner.
Pipets, squeeze type, 2-ml and 5-ml capacities.
Dipper, about 2 mm deep and 5 mm in diameter capable of measuring 30±10 mg of the powdered barium chloride.

PROCEDURE

Transfer 100-mg samples (100 mesh or finer) through a funnel to each of a series of test tubes. To an additional test tube add 2 ml of standard sulfate solution. Another test tube serves as a blank. Add 0.2 ml of concentrated HNO_3 to all test tubes with a squeeze-type pipet. Pass each test tube contain-

ing a sample over a flame for several seconds to bring the solution to a boil. Allow each test tube to cool for at least a minute, then repeat the heating after adding 0.4 ml of concentrated HCl. Add 1 ml of $CaCl_2$ solution to all test tubes. Add 5 ml of water to the first sample with the squeeze-type pipet, bring to a boil over a burner and maintain at or near boiling for 30 seconds, and then add 2 ml of (1+1) NH_4OH by squeeze pipet and agitate briefly. Add 5 ml of water and agitate briefly. Repeat this treatment with each of the samples. Add 2 ml (1+1) NH_4OH to the blank and standard. Add 10 ml of water to the blank and 8 ml to the standard test tube and agitate the blank and standard. Centrifuge all the samples at about 1,200 rpm for 1½ minutes.

To each of a second set of dry test tubes add 0.1 ml of the standard sulfate solution to serve as a spike, and then transfer 5 ml of the supernatant liquids previously prepared, using a squeeze pipet, to this second set of test tubes.

Set the spectrophotometer to read 0 absorbance at 650 nm using a test tube containing water. Record the absorbance of each test tube of the second set. These readings provide a means of correcting for any color, cloudiness, or tube variations. By use of the dipper transfer approximately 30 mg of powdered $BaCl_2$ to each tube, without agitation. Note the time and then agitate each tube for a few seconds. It is not necessary to dissolve all the barium chloride. Two minutes after the first tube has been agitated start reading absorbance. The addition and agitation steps should be done with not more than 10 tubes at a time.

Calculate sulfur concentrations by subtracting the absorbance readings prior to precipitation from those after precipitation for each tube and then subtracting the value for the blank from those of the samples and the standard. The standard corresponds to 0.32 percent S, and its absorbance should be about 0.400.

If the sulfur is higher than 0.5 percent, the procedure should be repeated with a 20-mg sample, and a standard curve should be made using 0, 1, 2, 3, 4, and 5 ml of the standard sulfate solution. The curve is linear to 3 ml of standard sulfate solution, but is usable to 5 ml which corresponds to 4 percent S in a sample.

DISCUSSION AND RESULTS

The results shown in table 1 illustrate the greater reproducibility obtained when $BaCl_2$ is added by dipper as powder than that obtained when 0.2 ml of 30-percent $BaCl_2$ is added by pipet.

The variation in weight of 10 dipperfuls was found to be about 20 percent when a spatula was used to level the powder in the dipper. The turbidity was then measured using a 1-ml aliquot of the sulfate standard solution (equivalent to 0.16 percent S) in the described procedure and 20, 40, and 80 mg of powdered $BaCl_2$. The turbidity produced by 20 mg and 40 mg was the same, whereas that produced by 80 mg was about

Table 1.—*Comparison of absorbances produced by* $BaCl_2$ *added as a solid and as a solution*

30 mg of solid	*0.2 ml of 30-percent solution*
0.170	0.205
.170	.170
.170	.155
.160	.130
.165	.115
.165	.105

10 percent less. The tests were done in triplicate. In the procedure described, a 30-mg dipper is used which allows considerable variation in the amount dispensed without noticeable effect on the resultant turbidity.

The stability and the time required for the turbidity to reach a maximum vary with the sulfate level. When 0.5 mg S is used, the maximum for which linearity is obtained, maximum absorbance occurs in several seconds and is stable for about 5 minutes; after this it begins to decline. At low levels of sulfate the maximum absorbance is reached in 2–3 minutes and is stable for a much longer time than that obtained from the high levels of sulfate. Adding some known stabilizers tends to have an adverse effect on the rate of turbidity formation.

At very low levels of sulfur, equivalent to a few hundredths of a milligram, the initiation of turbidity is variable and sometimes fails to occur. This problem is eliminated by the addition of a spike of 0.016 mg S to all solutions. This ensures that enough sulfur is always present to initiate turbidity. If the standards and samples are measured 2–4 minutes after dissolving the powdered barium chloride, the standards show a near linearity, beginning to fall off slightly above 0.5 mg S.

The slope of the absorbance-concentration curve is steeper (about 15 percent) when aqua regia instead of hydrochloric acid is used in decomposing the sample. This is of concern if one were to determine soluble sulfate where hydrochloric acid alone would be used. The difference can be eliminated if a small amount of nitric acid is added to the hydrochloric acid solution along with the sulfate spike prior to the addition of barium chloride. When 0.2, 0.4, and 0.6 ml (1+3) HNO_3 is used the turbidity obtained is nearly the same. For determining acid-soluble sulfate, 0.4 ml was chosen. Three times this amount perceptibly reduces the turbidity.

When the procedure was applied to several hundred rocks, some of them, particularly those with organic matter, inhibited the formation of turbidity, even that which would normally occur from the spike. Inhibition was sufficient at times to prevent precipitation in the presence of three times the concentration of the spike. This effect is completely eliminated by the addition of calcium prior to ammonium hydroxide addition. The mechanism for this is not understood by the author but probably involves a chelating effect between barium and organic matter which is displaced by calcium.

After the R_2O_3 has been precipitated by ammonium hydroxide, the solution, which is strongly alkaline, is used for the sulfate precipitation. When attempts are made to acidify the solution prior to precipitation, the pH becomes a critical

factor because the turbidity characteristics vary with acidity. In addition, at low pH readings the slope is about half of that found when precipitation is made from alkaline solutions. The only drawback to working on the alkaline side is that the determination must be completed within three hours after ammonium hydroxide has been added or sufficient carbon dioxide will be absorbed to initiate precipitation of barium carbonate.

To evaluate the procedure a series of samples was run by the described method. Table 2 shows that results of the new procedure compare favorably with those of existing methods. Data are not shown here on the discrimination between sulfide and sulfate by the use of an aqua regia attack and a hydrochloric acid attack. It may sometimes be useful to determine whether the sulfur in a sample is predominantly sulfide or sulfate for the purpose of reporting a value in one form or the other, but the accuracy of this discrimination has not been ascertained.

The method of attack is based on the assumption that a rock consists of an assemblage of minerals from which the aqua regia will effectively dissolve all but a few rare sulfur minerals. Aqua regia does not attack, to a significant degree, most silicate minerals present. The procedure therefore fails with obsidian and other glasses where the sulfur may be enclosed within a protective siliceous shield. It also fails if barium is present in excess of about half a percent When iron is present up to about 15 percent calculated as Fe_2O_3 no noticeable loss of sulfur is observed with the R_2O_3. Above this and especially at iron ore levels, some percentage of the sulfur goes with the R_2O_3 precipitate. In iron ores a fairly good result can still be obtained if a similar material is used as a reference standard so that approximately the same proportion of sulfur is absorbed with both the standard and sample. A similar situation prevails with phosphate rocks. Sulfur, which is frequently high in phosphate rocks, tends to be absorbed to some extent on the calcium phosphate precipitated so that the results are about 10 percent too low. This is easily corrected if a standard phosphate rock is carried through the procedure and used as the comparison standard when analyzing phosphate rocks.

Organic matter, which may contain sulfur, is not decomposed by the attack described. Organic matter found in such materials as shale, carbonates, and phosphates generally contains about 1 percent S, and the rocks rarely contain more than 5 percent organic matter so that a potential error as great as 0.05 percent S could occur. If a substantially greater amount of organic matter is present, one of the conventional oxidizing fusion procedures should be used. The yellow coloration produced where 5 percent or less of organic matter is present has such little absorbance at 650 nm that it does not interfere with the determination. Elemental sulfur present in small amounts will go into solution; it rarely occurs in amounts in excess of that which can go into solution by the decomposition procedure.

Table 2.—*Sulfur content of silicate rocks determined by turbidimetry and other methods*

Sample	Sulfur (percent)	Other methods	
		Sulfur (percent)	Source of data
Granite, G-2	0.01	0.01, 0.08, 0.01, 0.02	Flanagan (1969, p. 84–89).
Granodiorite, GSP-1	.03	.03, .02, .21	Do.
Andesite, AGV-1	.00	.01, .01, .02	Do.
Peridotite, PCC-1	.01	.02	Do.
Dunite, DTS-1	.00	.00, .00, .00	Do.
Basalt, BCR-1	.05	.04, .02, .04, .05	Do.
Bauxite, NBS-69A	.03	.02	National Bureau of Standards certificate value.
Dolomite, NBS-88	.03	.02	Do.
Fleet clay, NBS-97	.02	.02	Do.
Plastic clay, NBS-98	.03	.03	Do.
Limestone, NBS-1A	.30	.28	Do.
Phosphate rock, NBS-56	2.5	2.7	Do.
Portland cement, NBS-117	.62	.64	Do.
Portland cement, NBS-1013	.72	.72	Do.
Granite, G-1	.02	.01, .01, .02, .01	Stevens (1960, table 1).
Diabase, W-1	.01	.02, .02, .03	Stevens (1960, table 2).
Lab sample 1	1.8	1.7	Shapiro, gravimetric analysis.
2	1.5	1.4	Do.
3	.60	.55	Do.
4	.33	.28	Do.

REFERENCES CITED

American Public Health Association, 1965, Standard method for the examination of water and waste water: New York, Am. Public Health Assoc., 769 p.

Bardsley, C. E. and Lancaster, J. D., 1965, Sulfur, *in* Black, C. A., ed. Methods of soil analysis: Madison, Wis., Am. Soc. Agronomy, p. 1102–1116.

Fisher, R. B., 1966, Turbidimetry and nephelometry, *in* Welcher, F. J., ed., Standard methods of chemical analysis, v. 3: Princeton, N.J., D. Van Nostrand Co., 974 p.

Flanagan, F. J., 1969, U.S. Geological Survey Standards–[Pt.] 2, First compilation of data for new U.S.G.S. rocks: Geochim. et Cosmochim. Acta, v. 33, no. 1, p. 81–120.

Maxwell, J. A., 1968, Rock and mineral analysis: New York, Interscience Publishers, 584 p.

Patterson, G. D., Jr., 1958, Sulphur *in* Boltz D. F., ed., Colorimetric determination of nonmetals: New York, Interscience Publishers. p. 261–308.

Stevens, R. E., and others, 1960, Second report on a cooperative investigation of the composition of two silicate rocks: U.S. Geol. Survey Bull. 1113, 126 p.

Jour. Research U.S. Geol. Survey
Vol. 1, No. 1, Jan.–Feb. 1973, p. 85–87

ANTIMONY-BEARING ORPIMENT, CARLIN GOLD DEPOSIT, NEVADA

By ARTHUR S. RADTKE, CHARLES M. TAYLOR[1], and CHRIS HEROPOULOS,
Menlo Park, Calif., Stanford, Calif., Menlo Park, Calif.

Abstract.—Orpiment, As_2S_3, containing up to 1.5 percent antimony has been recognized in carbonaceous arsenic-rich gold ores in the unoxidized East ore body of the Carlin gold deposit. Associated hydrothermal minerals include realgar (AsS) and quartz. Stibnite, commonly associated with realgar in the ores, has not been observed associated with this type of orpiment.

Orpiment, As_2S_3, has been recognized in several disseminated replacement-type gold deposits in the Western United States. These include the Getchell deposit in Nevada (Joralemon, 1951; Weissberg, 1965), the White Caps deposit at Manhattan, Nev. (Ferguson, 1924), the Carlin deposit in Nevada (Radtke and Scheiner, 1970), and the Mercur deposit in Utah (Gilluly, 1932). Deposits of this general type are usually in limestones from which significant amounts of carbonate have been removed and silica added. The characteristic hydrothermal mineral assemblage includes fine-grained metallic gold, quartz, pyrite, pyrrhotite, arsenopyrite, cinnabar, stibnite, realgar, orpiment, sphalerite, galena, and several other sulfide and sulfosalt minerals. Barite is also an important hydrothermal mineral in the Carlin ores.

Although no data are available on the content of antimony in orpiment from the other deposits, samples of the mineral from the Carlin deposit were found to contain significant amounts of the element. To the best of the writers' knowledge, there have been no reports of antimony substituting for arsenic in the mineral orpiment.

Acknowledgments.—We wish to thank Richard C. Erd, U.S. Geological Survey, for his assistance in X-ray diffraction studies and Mel Essington, mine geologist, Carlin Gold Mining Co., for his help in sampling within the mine. Permission to publish information on the Carlin deposit was kindly given by Newmont Mining Corp.

OCCURRENCE AND ASSOCIATIONS

The Carlin gold deposit is in northern Eureka County, Nev., about 33 miles northwest of the town of Elko (fig. 1). Host rocks for the gold ore bodies are dark- to medium-gray, thin-bedded, siliceous, argillaceous, dolomitic limestone of the Silurian Roberts Mountains Formation. The gold ores probably were formed from a low-temperature, acid, hydrothermal solution which transported silica, iron, barium, sulfur, gold, mercury, and other elements. After ore deposition the upper parts of the ore bodies were altered by oxygen-bearing meteoric waters. Important chemical and mineralogical changes that took place during ore deposition and subsequent oxidation are summarized in Radtke and others (1972).

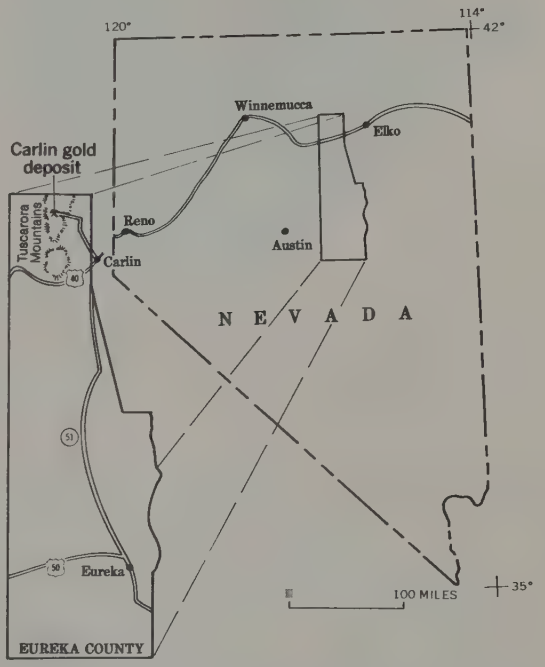

Figure 1.—Index map showing the location of the Carlin gold deposit in north-central Nevada.

The primary unoxidized gold ores of the Carlin deposit may be classified into several types according to (1) the amount of silica and organic carbon, (2) the form and associations of

[1] Stanford University.

gold, and (3) the ratios and abundance of the various hydrothermal minerals.

Although all the primary ores contain significant amounts of arsenic, one variety contains a very large concentration of the element, most of which is present as realgar (AsS) (fig. 2). The arsenic content may exceed 10,000 ppm, and more than 1

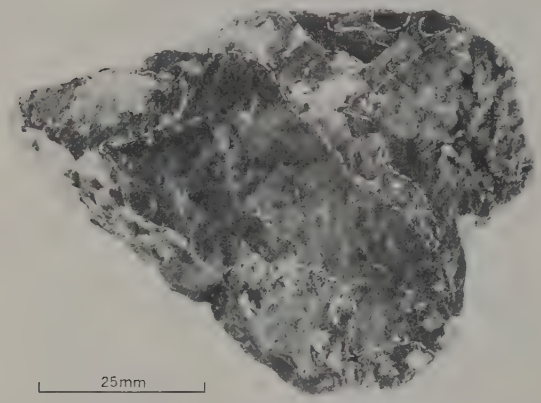

Figure 2.—Specimen of carbonaceous gold ore, showing small veinlets (outlined) of realgar and barite cutting host rock (limestone). Realgar appears dark gray, similar to the limestone, and barite is light gray.

percent of the rock commonly is made up of arsenic sulfide. Most of the realgar occurs with barite in narrow veinlets that fill small fractures and cut the gold-bearing limestones. The realgar-barite veinlets may contain fine-grained metallic gold, pyrite, and other sulfide minerals, including stibnite, interlocked with quartz. Physical relations and textural features indicate that the realgar may have been deposited from the hydrothermal solution after the gold and most of the quartz and pyrite had been precipitated.

Locally, the veinlets contain large amounts of orpiment and small amounts of realgar. Foliated and columnar crystals of orpiment as much as 8 mm long are interlocked with fragments of the dark-gray silicified limestone host rock (fig. 3). Only small amounts of fine-grained quartz and realgar are scattered through and intergrown with the orpiment, and no other hydrothermal minerals, including those usually associated with realgar, have been recognized.

CHEMICAL COMPOSITION

Orpiment in this particular type of occurrence in arsenic-rich gold ores at the Carlin deposit usually contains significant amounts of antimony. A semiquantitative spectrographic analysis of hand-picked fragments of orpiment is given in table 1. High values for silica and calcium shown in table 1 reflect the presence of minor amounts of hydrothermal quartz

Figure 3.—Specimens of antimony-bearing orpiment. Light-gray shiny areas are orpiment crystals. Dark areas are limestone fragments.

Table 1.—*Semiquantitative spectrographic analysis of antimony-bearing orpiment*

[Sought but not found: Ag, Au, B, Be, Bi, Cd, Ce, Co, Eu, Ga, Ge, Hf, In, K, La, Li, Mn, Mo, Na, Nb, Ni, P, Pb, Pd, Pt, Re, Sc, Sn, Sr, Ta, Te, Th, Ti, Tl, U, V, W, Y, Yb, Zr. Values are in weight percent. Analyst: Chris Heropoulos]

Si	1.5	Ca	0.5	Cu	0.0002
Al	.007	As	>20	Sb	1
Fe	.005	Ba	.002	Zn	.03
Mg	.0015	Cr	.0002		

inclusions in orpiment as well as quartz and calcite from small limestone fragments.

Eight small grains of orpiment were mounted and polished for electron microprobe analysis. Qualitative spectral scans and quantitative analyses were made using the Applied Research Laboratory EMX-SM model electron microprobe in the Department of Geology, Stanford University, California.

Arsenic, sulfur, and antimony were the only elements detected from spectral scans. Five grains were selected for quantitative analysis, and 10 to 15 points on each grain were analyzed for these three elements. Analytical conditions used were: (1) arsenic, $K\alpha$ characteristic line, LiF crystal, 25 kV, and realgar (AsS) standard; (2) sulfur, $K\alpha$ characteristic line, ADP crystal, 15 kV, and realgar standard; and (3) antimony, $L\alpha_1$ characteristic line, LiF crystal, 15 kV, and stibnite (Sb_2S_3) standard.

Although the content of antimony varied from grain to grain (0.10 to 1.50 percent Sb), the amount present within individual grains was generally uniform. The composition of five grains is shown in table 2.

Table 2.—*Chemical analyses of antimony-bearing orpiment*

Grain No.	As	Sb	S	Total
1	59.6	1.1	39.2	99.9
2	59.4	1.5	39.1	100.0
3	60.1	.5	39.3	99.9
4	59.2	1.2	39.4	99.8
5	59.7	1.0	39.2	99.9

It is apparent that under certain conditions antimony may substitute for arsenic in orpiment. Some experimental study to determine the solubility of antimony in As_2S_3 is justified.

REFERENCES CITED

Ferguson, H. G., 1924, Geology and ore deposits of the Manhattan district, Nevada: U.S. Geol. Survey Bull. 723, 163 p.

Gilluly, James, 1932, Geology and ore deposits of the Stockton and Fairfield quadrangles, Utah: U.S. Geol. Survey Prof. Paper 173, 171 p.

Joralemon, Peter, 1951, The occurrence of gold at the Getchell mine, Nevada: Econ. Geology, v. 46, no. 3, p. 267–310.

Radtke, A. S., Heropoulos, Chris, Fabbi, B. P., Scheiner, B. J., and Essington, Mel, 1972, Data on major and minor elements in host rocks and ores, Carlin gold deposit, Nevada: Econ. Geology. [In press]

Radtke, A. S., and Scheiner, B. J., 1970, Studies of hydrothermal gold deposition (I). Carlin gold deposit, Nevada—The role of carbonaceous materials in gold deposition: Econ. Geology, v. 65, no. 2, p. 87–102.

Weissberg, B. G., 1965, Getchellite, $AsSbS_3$, a new mineral from Humboldt County, Nevada: Am. Mineralogist, v. 50, nos. 11–12, p. 1817–1826.

Jour. Research U.S. Geol. Survey
Vol. 1, No. 1, Jan.–Feb. 1973, p. 89–98

ACCESSORY APATITE FROM HYBRID GRANITOID ROCKS OF THE SOUTHERN SNAKE RANGE, NEVADA

By DONALD E. LEE, RICHARD E. VAN LOENEN, and ROBERT E. MAYS, Denver, Colo.; Menlo Park, Calif.

Abstract.—Analytical data, optical properties, and unit-cell parameters are presented for 24 samples of accessory apatites recovered from hybrid granitoid rocks of the southern Snake Range, Nev. A complete chemical analysis is given for one. In the Snake Creek–Williams Canyon outcrop area, where the hybrid rocks grade from granodiorite with 63 percent SiO_2 to a quartz monzonite with 76 percent SiO_2 within a horizontal distance of about 3 miles, abundance and crystal habit of the apatite change with rock chemistry. The apatite probably is slightly more than 90 mole percent fluorapatite in the most felsic rocks, slightly less in the most mafic. The range of F⇌OH substitution in apatite from this outcrop area is much smaller than in the coexisting biotites. Except for manganese, strontium, sodium, and the rare earths, there is very limited substitution for calcium in the crystal structure of these apatites. Apatites from the more mafic rocks tend to contain a lighter, more basic assemblage of rare earths, in agreement with results obtained for coexisting allanites, monazites, and zircons.

Granitoid rocks of Jurassic age crop out a few miles north of the Mount Wheeler mine in the southern part of the Snake Range, about 50 miles southeast of Ely, Nev. (Lee and Van Loenen, 1970, fig. 1; 1971). The many well-defined differences in the chemistry and mineralogy of these granitoid rocks within an outcrop area of about 20 square miles are believed by Lee and Van Loenen (1971) to have resulted mainly from assimilation of chemically distinct host rocks. The 1971 report is a comprehensive field and laboratory study and includes a geologic map and sample locality data. The present paper describes the chemical and physical properties of 24 samples of accessory apatite recovered from these granitoid rocks and associated aplites.

Petrologically and structurally, the hybrid granitoid rocks from which these apatites were recovered fall into three separate study units: the Snake Creek–Williams Canyon area, the Pole Canyon–Can Young Canyon area, and the Young Canyon–Kious Basin area. The 18 samples of apatite from the Snake Creek–Williams Canyon area are discussed first, and then the six apatites from the other areas, including two apatites from aplitic phases.

Special care was taken to recover apatite fractions having a high degree of purity. After the preliminary concentration described by Lee and Dodge (1964), the apatite was centrifuged in a mixture of methylene iodide and bromoform, the specific gravity of the liquid being controlled by means of a Christian Becker specific gravity balance before each operation. Specific gravity of the apatite was determined by the suspension method during centrifuging. Each fraction analyzed was centrifuged on either side of a very narrow specific gravity range. This method, often with repeated processing of a given fraction, enabled us to reject (heavier) apatite grains having relatively abundant inclusions of zircon, or (lighter) apatite grains having relatively abundant inclusions of quartz. After exposure to heavy liquids, each fraction was cleaned by ultrasonic vibration in 25 ml of distilled water for about an hour; the effectiveness of the cleaning action was evident from the fact that the water surrounding the mineral became milky. Finally, apatite grains with tiny inclusions of biotite were drawn away from the main fraction by means of the Frantz isodynamic separator.

Indices of refraction were determined by the immersion method, by use of a spindle stage (Wilcox, 1959) and focal masking technique (Wilcox, 1962). Cell parameters were obtained by least-squares refinement of powder diffractometer data, with an internal standard of CaF_2 and a self-indexing computer program developed by Evans, Appleman, and Handwerker (1963).

Quantitative spectrographic analyses have an overall accuracy of ±15 percent except near limits of detection, where only one digit is reported. Semiquantitative spectrographic results are based on their identity with geometric brackets whose boundaries are 1.2, 0.83, 0.56, 0.38, 0.26, 0.18, 0.12 percent, and so forth; and the results are reported arbitrarily as midpoints of these brackets, 1.0, 0.7, 0.5, 0.3, 0.2, 0.15, and 0.1 percent, respectively. The precision of a reported value is approximately one bracket at 68-percent or two brackets at 95-percent confidence.

APATITE OCCURRENCE AND ANALYSES

Apatites from Snake Creek–Williams Canyon area

The influence of host rock on chemistry and mineralogy of intrusive rocks of the southern Snake Range is most clearly

shown in the Snake Creek–Williams Canyon area. There the intrusive is undeformed, probably has not been eroded to a depth of much more than 1,000 feet, and is well exposed in contact with limestone, shale, and quartzite. Within a horizontal distance of 3 miles the intrusive grades from a granodiorite (63 percent SiO_2, 4.5 percent CaO) where the host rock is limestone to quartz monzonite (76 percent SiO_2, 0.5 percent CaO) where the host rock is quartzite. The amount of apatite present in the intrusive increases rather systematically from less than 0.02 weight percent in the most felsic rocks to about 0.3 weight percent in the most mafic rocks. The apatite tends to be associated with biotite, although in the more mafic rocks (CaO>2.5 percent) euhedra of apatite are readily found in all the essential minerals.

Crystal habit of the apatite changes with rock chemistry (fig. 1). The sparse apatite in the most felsic rocks is present as relatively large grains with a stubby habit; length-to-width ratio seldom exceeds 2:1. Apatite recovered from the more mafic rocks tends to be more acicular, and where the CaO content of the rock is 2.5 percent or more, the apatite crystals commonly have a length-to-width ratio that exceeds 4:1. In the more mafic rocks tiny euhedral apatite needles about 25μ long were found to be intimately intergrown with biotite crystals (Lee and Van Loenen, 1970, p. D199).

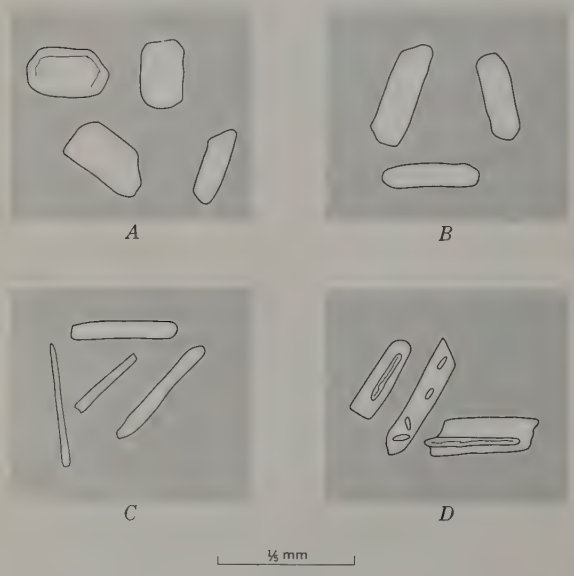

Figure 1.–Representative apatite crystals recovered from the Snake Creek–Williams Canyon area. Broken fragments of larger grains, especially abundant in *A* and *B*, not sketched.

A. Sample 238-MW-61, 0.78 percent CaO in rock. The apatite in this rock is so sparse that we were unable to recover enough for analytical work.

B. Sample 174-MW-61, 1.5 percent CaO in rock.

C. Sample 40B-MW-60, 3.5 percent CaO in rock.

D. Types of inclusions found in some apatite crystals. The middle grain contains some colorless inclusions with index of refraction (n)> apatite (probably zircon), and some with $n <$ apatite (probably quartz). The other two grains contain biotite inclusions and could easily be separated from biotite-free apatite by means of the Frantz isodynamic separator.

Many observers, the earliest being Harker (1895), have recorded the relative abundance and acicular form of apatite crystals in the more contaminated parts of hybrid rocks. Nockolds (1933, p. 563) wrote:

> This conclusion was based partly on the relative abundance of apatite found in the xenoliths and more contaminated portions of the magma when compared with the amount present in the invaded or invading rock. This apatite is characteristically present as thin needles penetrating the other minerals and often of exceedingly small dimensions.

Moreover, Nockolds cited 14 reports describing the relative abundance of apatite in hybrid rocks. Many of these authors mentioned "apatite needles" or otherwise referred to the acicular habit of the apatite.

Results of experimental work bear on these relations. Wyllie, Cox, and Biggar (1962) found that apatite crystals coexisting with liquid or with vapor are equant, whereas crystals precipitated from a liquid during a quench are greatly elongated parallel to the *c* axis. If the material added to a magma is nearer the high-temperature end of the solid solution series than the crystals with which the magma is saturated (as happened in the more mafic parts of the Snake Creek–Williams Canyon area), the reaction is exothermic and decreases the amount of liquid (Bowen, 1922, p. 531). This in effect is a quenching action, and according to the findings by Wyllie, Cox, and Biggar would be expected to lead to the development of elongated apatite crystals. Bowen showed that if the material added to a magma is nearer the lower end of the solid solution series than the crystals with which the liquid is saturated (as happened in the most felsic parts of the Snake Creek–Williams Canyon rocks), the reaction is endothermic and increases slightly the amount of liquid. This would allow the apatite crystals to coexist longer with the liquid or vapor and might be expected to result in larger apatite crystals with a more equant habit.

We note that the occurrence of zircon (also a tetragonal mineral) in some hybrid rocks is similar to that just described for apatite. After studying the Monadhliath granite in Scotland, Wyatt concluded (1954, p. 988) that "the evidence indicated that very elongated zircon is produced only in granite which has been contaminated * * *." Taubeneck (1957) and Huang (1958) emphasized the greater elongation ratio of zircon from hybrid rocks. In the Snake Creek–Williams Canyon area, zircon is both more acicular and more abundant in the more mafic parts of the exposure (Lee and others, 1968).

A wet chemical analysis of apatite 40A-MW-60 (table 1) is calculated on the basis of 26 (O, OH, Cl, F) to the apatite formula $Ca_5(PO_4)_3(F,Cl,OH)$, by use of the computer

Table 1.—*Chemical analysis and physical properties of apatite 40A-MW-60*

[Chemical analysis by Elaine L. Munson]

Chemical analysis (weight percent)	
SiO_2	0.18
Al_2O_3	.08
Fe_2O_3	.06
FeO	.04
CaO	54.87
Na_2O	.06
K_2O	.01
P_2O_5	41.97
MnO	.13
Cl	.02
F	3.36
R_2O_3	[1].45
Insoluble	[2].23
Subtotal	101.46
Less O≡Cl,F	1.41
Total	100.05

Number of ions, on basis of 26 (O,OH,F,Cl)		
P	6.001	6.031
Si	.030	
Al	.016	10.025
Fe^{+3}	.008	
Fe^{+2}	.006	
Mn	.019	
Ca	9.928	
Na	020	
K	.002	
Ce^{+3}*	.026	
F	1.795	1.801
Cl	.006	

Optical and other properties	
Specific gravity observed	3.215±0.005
Density calculated	3.210 g/cm³
Cell volume measured	523.6±0.1 A³
Cell volume calculated	522.8 A³
ϵ	1.631±0.001
ω	1.633±0.001
$\omega-\epsilon$	.002
a	9.373±0.001 A
c	6.881±0.001 A
c/a	.7342

[1] Rare-earth oxide precipitate. See table 2 for analysis.

[2] Insoluble in 1:1 HCl at 100°C. From X-ray diffraction study this material is estimated to be 40 percent quartz, 40 percent zircon, and 20 percent zoisite.

*For simplicity, entire rare-earth oxide precipitate calculated as Ce_2O_3.

program described by Jackson, Stevens, and Bowen (1967). The analysis shows 0.23 weight percent material insoluble in 1:1 HCl at 100°C, and thus the material analyzed was 99.77 percent pure. The 0.23-percent impurity is estimated to be 40 percent quartz, 40 percent zircon, and 20 percent zoisite; probably all of it was present as inclusions in the apatite grains. The analysis also shows 0.45 weight percent rare-earth oxide precipitate. An X-ray spectrographic analysis of this precipitate was calculated to atomic percent of total rare earths in the apatite (table 2); the low rare-earth oxide total probably results from the presence of filter-paper ash in the precipitate.

Table 2.—*Analysis of rare-earth precipitate and calculation of* Σ(La+Ce+Pr) *for apatite 40A-MW-60*

[X-ray spectrographic analysis by Frank Cuttitta, Ralph Christian, and Harry J. Rose, Jr. Sc_2O_3 not detected. Low total probably due to presence of filter-paper ash in precipitate]

X-ray spectrographic analysis (weight percent)			
Y_2O_3	22.9	Tb_2O_3	1.01
La_2O_3	7.04	Dy_2O_3	3.32
CeO_2	22.1	Ho_2O_3	1.21
Pr_2O_3	3.52	Er_2O_3	1.76
Nd_2O_3	15.6	Tm_2O_3	.55
Sm_2O_3	5.03	Yb_2O_3	1.71
Eu_2O_3	2.01	Lu_2O_3	.65
Gd_2O_3	3.27	Total	91.68

Atomic percent of total rare earths in apatite			
Y	33.77	Dy	2.96
La	7.19	Ho	1.07
Ce	21.38	Er	1.53
Pr	3.56	Tm	.47
Nd	15.44	Yb	1.44
Sm	4.81	Lu	.54
Eu	1.91	Total	100.00
Gd	3.01	Σ(La+Ce+Pr)	32.5
Tb	.92		

The fluorine content of 40A-MW-60 shows it to be about 90 mole percent fluorapatite. Virtually all of the remaining 10 mole percent must be hydroxylapatite, for the chlorine content of the mineral is negligible, and no effervescence occurred when the mineral was immersed in 1:1 HCl, indicating absence of CO_2 in the structure. The amount of material was not sufficient for direct determination of H_2O.

Analytical and physical data for 18 apatites (including 40A-MW-60) from the Snake Creek–Williams Canyon area are shown in table 3. The major-element data and physical properties (tables 1, 3) indicate that all 18 minerals are hydroxyl-fluorapatites, and despite certain variations in physical properties (discussed below) they indicate a narrow range of major-element composition. The large and complex variations in composition within the apatite group make accurate correlation of physical properties difficult. Generally, however, cell parameters and indices of refraction of hydroxyl-fluorapatites depend mostly on the extent of substitution of

Table 3.—*Analytical data and physical properties for accessory apatites from*

[Samples arranged in order of increasing CaO content of whole rock. Sample localities are shown on plate 1 of Lee and Van Loenen (1971). elements by Robena Brown and H. J. Rose, Jr. Spectrographic analyses by R. E. Mays. Results for Si, Na, and Pb are semiquantitative; all

	Sample No.	147-MW-61	151-MW-61	190-DL-62	14-MW-60	36-DL-62	8-DL-62	31-DL-62	40A-MW-60	
	CaO in rock (weight percent)	1.5	1.8	2.0	2.2	2.2	2.3	2.4	2.4	
	Specific gravity (±0.005)	3.221	3.220	3.220	3.211	3.210	3.212	3.215	3.215	
	Indices of refraction									
1	ϵ(±0.001)	1.629	1.630	1.629	1.630	1.630	1.630	1.630	1.631	1
2	ω(±0.001)	1.631	1.632	1.631	1.632	1.632	1.632	1.632	1.633	2
3	$\omega-\epsilon$	.002	.002	.002	.002	.002	.002	.002	.002	3
	Cell parameters									
4	a(±0.001 A)	9.369	9.370	9.370	9.374	9.374	9.368	9.376	9.373	4
5	c(±0.001 A)	6.881	6.880	6.881	6.881	6.882	6.879	6.883	6.881	5
6	c/a	.7344	.7343	.7343	.7341	.7342	.7344	.7341	.7342	6
7	Volume (±0.1 A^3)	523.2	523.1	523.2	523.7	523.7	523.2	523.9	523.6	7
	Major elements (weight percent)[2]									
8	CaO	.....	54.0	.....	54.4	.....	53.9	53.8	[3]54.87	8
9	P_2O_5	.....	41.6	.....	41.7	.....	41.8	41.3	[3]41.97	9
10	F	.....	.....	.....	.....	.....	.....	.....	[3]3.36	10
11	Cl	.....	<.02	[4].02	<.02	[4].02	<.02	<.02	[3].02	11
	Spectrographic analyses (weight percent)									
12	Al	0.130	0.042	0.038	0.020	0.016	0.023	0.014	.....	12
13	Ba	.0006	<.0005	<.0005	<.0005	<.0005	<.0005	<.0005	<.0005	13
14	Cu	.0004	.0005	.0006	.0002	.0003	.0005	.0005	.0003	14
15	Fe	.044	.042	.036	.028	.022	.030	.034	.....	15
16	Mg	.0060	.0050	.0050	.0030	.0020	.0050	.0060	.0050	16
17	Mn	.25	.25	.29	.11	.13	.14	.13	.....	17
18	Na	.15	.1	.1	.07	.05	.05	.07	.....	18
19	Pb	.0015	.002	.002	.001	0	.001	.001	.001	19
20	Si	.3	.15	.15	.07	.2	.1	.1	.....	20
21	Sr	.050	.042	.038	.050	.040	.060	.050	.036	21
22	Ti	.014	.014	.026	.0055	.0060	.013	.010	.014	22
23	V	.002	.002	.004	.002	.0022	.002	.002	.002	23
24	Zr	.020	.040	.026	.012	.021	.020	.016	.014	24

[1] Apatite from xenolith. [2] X-ray fluorescence analyses performed on 25-mg samples.

OH for F. Cell parameters indicate slightly increased substitution of OH for F in apatites from the more mafic rocks. Thus the a dimension tends to increase with CaO content of the whole rock (Deer and others, 1962, p. 324). The rising indices of refraction (table 3) with increased CaO content of the whole rock also indicate slightly increased substitution of OH for F (Deer and others, 1962, p. 331) in apatites from the more mafic rocks. (Admittedly, the 3.53 percent F in apatite 16-MW-60 does not conform.)

In terms of fluorapatite-hydroxylapatite end members, the total range of composition deduced from the physical properties just discussed is on the order of 10–15 mole percent. Chemical analyses of biotites coexisting with most of the apatites listed in table 3 show a similar but much sharper change in the F:OH ratio, with fluorine ranging from 0.33 percent in biotite from mafic rocks to 1.13 percent in biotite from felsic rocks (Lee and Van Loenen, 1970). Stormer and Carmichael (1971) calculated the distribution of F and OH between apatite and biotite for various temperatures of crystallization by using free-energy data for the simple fluorides and hydroxides; but our data do not fit their hypothetical distribution diagram. That is, plotting F/(F+OH) in biotite against F/(F+OH) in apatite gives points that fall near or below the 127°C temperature curve.

Analytical results for apatite 40A-MW-60 (table 1) provide a good indication of the amount (0.23 percent) and type (quartz, zircon, and zoisite) of impurity to be expected in the other samples included in table 3. We conclude that all the zirconium values listed therein are due to tiny inclusions of zircon in the analyzed apatites. Also, the titanium found might result from inclusions of sphene, closely associated with apatite in these rocks; however, we were unable to detect any sphene peaks during X-ray diffraction work on the insoluble residue of apatite 40A-MW-60. The copper values probably come from heavy liquids used, despite the subsequent ultrasonic cleaning of each apatite fraction, for these liquids are

the Snake Creek–Williams Canyon area, southern Snake Range, Nev.

Determination of specific gravity, indices of refraction, and cell parameters explained in text. X-ray fluorescence analysis for major other results are quantitative. General limitations of the two methods given in text]

	38-MW-60	25-DL-61	152-MW-60	21A-MW-60	40B-MW-60[1]	126-MW-60[1]	43-DL-61	27-DL-61[1]	16-MW-60	98-DL-62[1]	
	2.5 3.215	3.1 3.210	3.2 3.206	3.4 3.205	3.5 3.205	3.5 3.221	3.9 3.210	4.1 3.211	4.3 3.202	4.5 3.215	
					Indices of refraction						
1	1.630	1.630	1.630	1.630	1.631	1.629	1.631	1.630	1.630	.....	1
2	1.632	1.632	1.633	1.632	1.633	1.632	1.634	1.633	1.632	.....	2
3	.002	.002	.003	.002	.002	.003	.003	.003	.002	.....	3
					Cell parameters						
4	9.375	9.375	9.376	9.371	9.373	9.369	9.377	9.376	9.370	9.367	4
5	6.882	6.882	6.882	6.883	6.882	6.882	6.882	6.880	6.881	6.879	5
6	.7340	.7341	.7341	.7345	.7342	.7346	.7340	.7338	.7344	.7345	6
7	523.8	523.9	523.9	523.5	523.6	523.2	524.1	523.8	523.2	522.7	7
					Major elements (weight percent)[2]						
8	53.3	54.3	.....	54.0	54.9	54.0	54.3	.....	53.9	54.4	8
9	41.3	41.4	.....	42.0	42.1	42.0	42.1	.....	41.3	41.6	9
10	.....	.....	.....	.....	.....	.....	.....	.....	[4]3.53	.....	10
11	<.02	<.02	.....	<.02	<.02	<.02	<.02	.....	[4].00	[4].01	11
					Spectrographic analyses (weight percent)						
12	0.042	0.02	0.026	0.060	0.024	0.046	0.020	0.022	0.024	0.014	12
13	<.0005	<.0005	<.0005	.0006	<.0005	<.0005	.0026	<.0005	.0006	<.0005	13
14	.0003	.0004	.0005	.0006	.0004	.0012	.0005	.0005	.0006	.0007	14
15	.034	.036	.044	.055	.050	.014	.036	.028	.030	.028	15
16	.0060	.0070	.0090	.013	.0010	.0070	.010	.0060	.0070	.0050	16
17	.15	.10	.11	.055	.10	.18	.075	.075	.050	.060	17
18	.1	.1	.07	.1	.07	.1	.05	.1	.07	.07	18
19	.001	.001	.001	.0015	0	.001	0	.001	.001	.001	19
20	.15	.15	.15	.15	.1	.15	.15	.2	.15	.15	20
21	.075	.070	.050	.060	.036	.026	.085	.050	.050	.036	21
22	.014	.014	.014	.0090	.0070	.015	.013	.013	.0048	.012	22
23	.001	.003	.002	.002	<.001	.002	.002	.002	.002	.007	23
24	.022	.022	.016	.030	.024	.030	.018	.016	.014	.003	24

[3]See table 1. [4]Wet chemical determination by E. L. Munson.

kept standing over copper foil to prevent their breakdown. Although silicon-bearing apatites have been recognized (for example, Cruft, 1966, p. 379), and the analysis of 40A-MW-60 (table 1) does show 0.18 percent SiO_2, we conclude that the silicon values in table 3 result mainly from inclusions of quartz and silicates. We attribute the aluminum values mostly to the presence of zoisite and possibly other aluminosilicates.

The tiny amounts of barium, lead, and vanadium listed are probably present in the crystal structure of the apatites. The values for sodium are equivalent to the range (of Na_2O) for apatites from plutonic rocks of the Odenwald Mountains, Germany, reported by Taborszky (1962), who found Na_2O content of apatite to be unrelated to rock type. Scatter diagrams based on table 3 show a slight tendency for sodium to decrease with whole-rock CaO. A similar trend for biotites from these rocks was found to relate to activity of albite in the system (Lee and Van Loenen, 1970, p. D199). The amounts of iron and magnesium listed are so small that they might have been trapped in the crystal structure of apatite (Cruft, 1962, p. 391), or they might be in inclusions.

Cruft noted that the strontium content is highest in apatite from the ultrabasic rocks, decreasing with increasing acidity of the rocks. The same trend is apparent in our data but is not pronounced, probably because strontium in these rocks is concentrated in epidote, a mineral that is well developed in the more mafic parts of the Snake Creek–Williams Canyon exposure (Lee and others, 1971).

Several observers, including Otto (1935), have noted that larger amounts of manganese are likely to be found in apatites from more felsic rocks. This is well illustrated by the data in table 3—those apatites that are richer in manganese tend to have higher specific gravities. In general, however, these same apatites contain a heavier assemblage of rare-earth elements, as described later in this paper.

Apatites from other areas, and from aplites

Most of the Young Canyon–Kious Basin area intrusive was sheared and deformed by Miocene movement on a regional thrust fault (Lee and others, 1971, fig. 2). The undeformed part of this intrusive outcrop is a quartz monzonite that is petrologically similar to, though not identical with, some of the more felsic parts of the Snake Creek–Williams Canyon exposure.

The Pole Canyon–Can Young Canyon area intrusive is an unusual hybrid rock that has developed through assimilation of argillite. It is distinguished in part by the presence of large muscovite phenocrysts, many of which contain euhedral crystals of biotite. The apatite in this rock is present in large (+150 mesh), poorly formed grains, and almost all the zircon in the rock is present as acicular inclusions within the apatite grains (fig. 2).

Analytical data and physical properties are presented (table 4) for four apatites from granitoid rocks (two from the Young Canyon–Kious Basin area and two from the Pole Canyon–Can Young Canyon area) and for two apatites from aplites. We

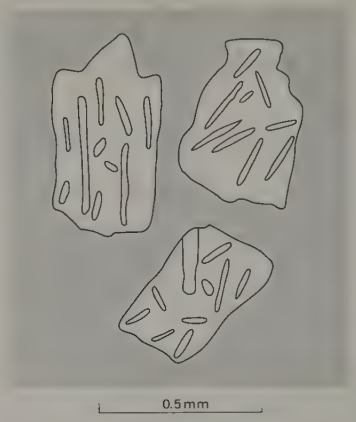

Figure 2.–Representative apatite from the Pole Canyon–Can Young Canyon area. Sample 135-DL-62, fragments of apatite crystals containing many inclusions of zircon. Almost all the zircon in the rock is present as inclusions in the apatite.

Table 4.–*Analytical data and physical properties for accessory apatites from the Young Canyon–Kious Basin area, the Pole Canyon–Can Young Canyon area, and from aplites, southern Snake Range, Nev.*

[Sample localities are shown on plate 1 of Lee and Van Loenen (1971). Determination of specific gravity, indices of refraction, and cell parameters explained in text. Spectrographic analyses by R. E. Mays. Results for Si, Na, and Pb are semiquantitative; all other results are quantitative. General limitations of the two methods given in text]

	Young Canyon–Kious Basin area		Pole Canyon–Can Young Canyon area		Aplites	
Sample No.	190-MW-61	234-MW-61	135-DL-62	120-MW-60	119-MW-60	121-MW-60
CaO in rock, (weight percent)	1.2	1.6	0.98	1.3	0.63	0.70
Specific gravity (±0.005)	3.225	3.225	3.210	3.220	3.215	3.230
Indices of refraction						
ϵ(±0.001)	1.629	1.629	1.629	1.630	1.629	1.629
ω(±0.001)	1.631	1.631	1.631	1.632	1.631	1.631
$\omega-\epsilon$	.002	.002	.002	.002	.002	.002
Cell parameters						
a(±0.001 A)	9.366	9.367	9.369	9.367	9.365	9.366
c(±0.001 A)	6.878	6.878	6.881	6.879	6.878	6.878
c/a	.7343	.7344	.7345	.7343	.7345	.7343
Volume (±0.1 A^3)	522.5	522.6	523.0	522.7	522.5	522.5
Spectrographic analyses (weight percent)						
Al	0.034	0.050	0.026	0.070	0.26	0.022
Ba	<.0005	<.0005	<.0005	<.0005	.0008	<.0005
Cr	<.0002	<.0002	<.0002	<.0002	.0008	<.0002
Cu	.0004	.0004	.0005	.0004	.0011	.0003
Fe	.055	.048	.044	.055	.055	.060
Mg	.0030	.0040	.0030	.0035	.0070	.0030
Mn	.50	.38	.19	.34	.50	.80
Na	.15	.15	.1	.1	.07	.07
Ni	<.0004	<.0004	.0024	<.0004	<.0004	<.0004
Si	.15	.1	.15	.15	.5	.02
Sr	.024	.036	.042	.042	.019	.006
Ti	.025	.017	.012	.010	.028	.0090
V	.002	.002	<.0010	<.0010	.001	.001
Zr	.015	.022	.17	.013	.018	.010

were unable to obtain major-element data for these six samples, but values for indices of refraction and cell parameters suggest that all are hydroxyl-fluorapatites. The minor-element data in table 4 require no comment beyond the previous discussion of similar data for apatites from the Snake Creek–Williams Canyon area (table 3).

DISTRIBUTION OF RARE-EARTH ELEMENTS

Distribution of rare earths in the hybrid granitoid rocks of the southern Snake Range has proved to be one of the most interesting features of the geochemistry of these rocks. In the Snake Creek–Williams Canyon area, where the equivalent of a large part (63–76 percent SiO_2) of the classic differentiation sequence is exposed, analyses of 87 rocks show an increase in total rare-earth content from the more felsic toward the more mafic parts of the exposure. Moreover, the rare-earth assemblage is increasingly enriched in the lighter, more basic lanthanides in the more mafic parts of the exposure (Lee and Van Loenen, 1971, table 5, fig. 6).

In treating rare-earth analyses of minerals recovered from these hybrid rocks, we have followed the procedure devised by Murata, Rose, and Carron (1953), who sought to denote the composition of each sample by means of a single number. They proposed the quantity $\Sigma(La + Ce + Pr)$ in atomic percent of total rare-earth elements as a numerical index of the composition and the stage of fractionation attained by the rare-earth elements. Thus, higher values of $\Sigma(La + Ce + Pr)$ represent greater enrichment of the lighter, more basic rare-earth elements. In the following discussion, this quantity $\Sigma(La + Ce + Pr)$ is referred to simply as sigma.

The quantitative data for 40A-MW-60 (table 2) and the semiquantitative data for other apatites from the Snake Creek–Williams Canyon area (table 5) are calculated to atomic percent of rare-earth elements, and the sigma value is given for each apatite. Values of sigma range from 17 to 48 atomic percent, representing an appreciable range of composition in terms of the rare-earth elements; obviously, apatites from the more mafic rocks tend to have the higher sigma values.

Results for apatites from the Young Canyon–Kious Basin area and the Pole Canyon–Can Young Canyon area (table 6) fit this trend; they were recovered from felsic rocks, and they contain a relatively heavy assemblage of rare-earth elements. Results for two apatites recovered from aplites (table 6) also fit this trend.

Fleischer and Altschuler (1969) have summarized available data on the rare-earth contents of apatites from different geological environments. Our data (tables 5, 6) would plot within the field that Fleischer and Altschuler (1969, p. 729, fig. 3) have outlined for apatites from "granitic" rocks.

Quantitative data for 20 allanites and 13 monazites, many of which coexist with the apatites listed in tables 2, 5, and 6, show sigma values ranging from 61 to 81 atomic percent (Lee and Bastron, 1967), with higher values found in those minerals from the more mafic rocks. Semiquantitative data for 25 zircons from these rocks show the same trend (Lee and others, 1968). However, although sphenes from these rocks contain significant amounts of rare-earth elements, their sigma values are not very obviously related to whole-rock chemistry (Lee and others, 1969). Under the conditions of formation of these hybrid rocks, crystallochemical selection was perhaps more important than the chemistry of the rock-forming medium in determining fractionation of rare earths in sphene. Only minor amounts of rare-earth elements were found in the epidotes analyzed.

Therefore, apatites recovered from the more mafic rocks tend to contain a lighter, more basic assemblage of rare earths, in agreement with results obtained for coexisting allanites, monazites, and zircons. The distribution of rare earths in these hybrid rocks and in their constituent allanites, apatites, monazites, and zircons has been cited (Lee and Bastron, 1967; Lee and Van Loenen, 1971, p. 20, 21) as evidence that the chemical processes once operative in these rocks might be similar to processes which contribute to the formation of alkalic rocks and carbonatites.

SUMMARY

In the Snake Creek–Williams Canyon area, where the hybrid rocks grade from granodiorite with 63 percent SiO_2 to quartz monzonite with 76 percent SiO_2 within a horizontal distance of 3 miles, the following relations have been found:

1. Abundance of apatite increases from less than 0.02 weight percent in the most felsic rocks to about 0.3 weight percent in the most mafic.
2. Crystal habit of the apatite relates to rock chemistry. In the most felsic rocks the apatite has a stubby habit, whereas in the most mafic rocks the mineral has an acicular habit and a length-to-width ratio that commonly exceeds 4:1.
3. In terms of the fluorapatite-hydroxylapatite end members, the span of composition deduced from analytical data and physical properties is 10–15 mole percent. The mineral probably is slightly more than 90 mole percent fluorapatite in the most felsic rocks, slightly less in the most mafic. The range of $F \rightleftharpoons OH$ substitution in apatite from this outcrop area is much smaller than in the coexisting biotites.
4. Except for manganese, strontium, sodium, and the rare earths, there is very limited substitution for calcium in the crystal structure of these apatites.
5. Apatites recovered from the more mafic rocks tend to contain a lighter, more basic assemblage of rare earths, corresponding to results obtained previously for coexisting allanites, monazites, and zircons.
6. In the Pole Canyon–Can Young Canyon area, where a distinctive muscovite-rich granitoid rock has resulted from assimilation of argillite, almost all the zircon in the rock is present as acicular inclusions in large, equant apatite crystals.

Table 5.—*Rare-earth contents of accessory apatites from the Snake*

[Samples arranged in order of increasing CaO content of whole rock. Sample localities are shown on plate 1 of Lee and Van Loenen (1971). General limitations of the two methods given in text. Looked for but

	Sample No.	147-MW-61	151-MW-61	190-DL-62	14-MW-60	36-DL-62	8-DL-62	31-DL-62	
	CaO in rock (weight percent)	1.5	1.8	2.0	2.2	2.2	2.3	2.4	
	Rare earths in apatite (weight percent)								
1	Y	0.21	0.25	0.23	0.06	0.1	0.08	0.065	1
2	La	.036	.034	.026	.03	.044	.032	.036	2
3	Ce	.15	.1	.1	.1	.15	.1	.1	3
4	Pr	.015	.02	.02	.015	.03	.02	.02	4
5	Nd	.15	.15	.15	.1	.15	.1	.07	5
6	Sm	.05	.07	.03	.05	0	.05	.015	6
7	Eu	.005	.003	0	.003	0	.003	0	7
8	Gd	.05	.07	0	.02	.02	.02	.015	8
9	Dy	.05	.05	.05	.003	.015	.007	.015	9
10	Ho	.01	.01	.007	.003	.005	.003	.005	10
11	Er	.03	.015	.015	0	0	0	0	11
12	Tm	0	.003	0	.001	0	.0015	0	12
13	Yb	.017	.021	.017	.0055	.007	.008	.0046	13
14	Lu	0	.005	0	0	0	0	0	14
15	Total	.773	.801	.645	.3905	.521	.4195	.3456	15
	Total rare-earth elements in apatite (atomic percent)[2]								
16	Y	38.2	43.1	47.9	22.9	27.6	26.1	27.2	16
17	La	4.2	3.8	3.5	7.4	7.9	7.2	9.7	17
18	Ce	17.3	10.9	13.2	23.9	26.4	22.1	26.5	18
19	Pr	1.8	2.2	2.6	3.7	5.4	4.4	5.3	19
20	Nd	16.9	15.9	19.2	23.2	25.5	21.5	18.3	20
21	Sm	5.4	7.2	3.7	11.1	0	10.3	3.7	21
22	Eu	.5	.3	0	.7	0	.6	0	22
23	Gd	5.2	6.9	0	4.4	3.2	4.1	3.7	23
24	Dy	5.0	4.8	5.7	.7	2.2	1.2	3.4	24
25	Ho	1.0	.9	.7	.7	.8	.6	1.1	25
26	Er	2.9	1.4	1.7	0	0	0	0	26
27	Tm	0	.3	0	.3	0	.3	0	27
28	Yb	1.6	1.8	1.8	1.0	1.0	1.6	1.1	28
29	Lu	0	.5	0	0	0	0	0	29
30	Total	100.0	100.0	100.0	100.0	100.0	100.0	100.0	30
31	Σ(La+Ce+Pr)	23.3	16.9	26.2	35.0	39.7	33.7	41.5	31

[1] Apatite from xenolith.

[2] Results of conversion to atomic percent are given in more significant figures than justified by

REFERENCES CITED

Bowen, N. L., 1922, The behavior of inclusions in igneous magmas: Jour. Geology, v. 30, supp. to no. 6, p. 513–570.

Cruft, E. F., 1966, Minor elements in igneous and metamorphic apatite: Geochim. et Cosmochim. Acta, v. 30, no. 4, p. 375–398.

Deer, W. A., Howie, R. A., and Zussman, J., 1962, Rock-forming minerals—v. 5, Non-silicates: New York, John Wiley and Sons, Inc., 371 p.

Evans, H. T., Jr., Appleman, D. E., and Handwerker, D. S., 1963, The least squares refinement of crystal unit cells with powder diffraction data by an automatic computer indexing method [abs.]: Am. Crystallog. Assoc. Program and Abs. 1963 Ann. Mtg., p. 42–43.

Fleischer, Michael, and Altschuler, Z. S., 1969, The relationship of the rare-earth composition of minerals to geological environment: Geochim. et Cosmochim. Acta, v. 33, no. 6, p. 725–732.

Harker, Alfred, 1895, Carrock Fell—A study in the variation of igneous rock masses; Pt. 2, The Carrock Fell Granophyre: Geol. Soc. London Quart. Jour., v. 51, p. 125–139.

Huang, W. W. T., 1958, Zircons in the Precambrian igneous rocks, Wichita Mountains, Oklahoma [abs.]: Geol. Soc. America Bull., v. 69, no. 12, pt. 2, p. 1589.

Jackson, E. D., Stevens, R. E., and Bowen, R. W., 1967, A computer-based procedure for deriving mineral formulas from mineral analyses, *in* Geological Survey Research 1967: U.S. Geol. Survey Prof. Paper 575-C, p. C23–C31.

Lee, D. E., and Bastron, Harry, 1967, Fractionation of rare-earth elements in allanite and monazite as related to geology of the Mt. Wheeler mine area, Nevada: Geochim. et Cosmochim. Acta, v. 31, no. 3, p. 339–356.

Lee, D. E., and Dodge, F. C. W., 1964, Accessory minerals in some granitic rocks in California and Nevada as a function of calcium content: Am. Mineralogist, v. 49, nos. 11–12, p. 1660–1669.

Lee, D. E., Mays, R. E., Van Loenen, R. E., and Rose, H. J., Jr., 1969, Accessory sphene from hybrid rocks of the Mount Wheeler mine area, Nevada, *in* Geological Survey Research 1969: U.S. Geol. Survey Prof. Paper 650-B, p. B41–B46.

—— 1971, Accessory epidote from hybrid granitoid rocks of the Mount Wheeler mine area, Nevada, *in* Geological Survey Research

Creek—Williams Canyon area, southern Snake Range, Nev.

Spectrographic analyses by R. E. Mays. Results for Y, La, and Yb are quantitative; results for all other elements are semiquantitative. not found: Tb (limit of detection 0.005 percent). Σ discussed in text]

	38-MW-60 2.5	25-DL-61 3.1	152-MW-60 3.2	21A-MW-60 3.4	40B-MW-60[1] 3.5	126-MW-60[1] 3.5	43-DL-61 3.9	27-DL-6[1] 4.1	16-MW-60 4.3	98-DL-62[1] 4.5	
					Rare earths in apatite (weight percent)						
1	0.12	0.11	0.07	0.03	0.085	0.13	0.06	0.09	0.034	0.055	1
2	.032	.03	.032	.03	.019	.038	.03	.044	.019	.036	2
3	.1	.1	.15	.1	.07	.15	.15	.15	.1	.15	3
4	.015	.02	.015	.015	.015	.02	.015	.02	.015	.015	4
5	.1	.07	.15	.1	.05	.15	.1	.1	.1	.1	5
6	.015	.07	.015	.01	.07	.05	0	.02	0	.015	6
7	0	.003	.003	.003	.003	.003	.003	.005	0	.003	7
8	.015	.05	.03	.01	.02	.05	.02	.03	0	.01	8
9	.015	.05	.015	.005	.007	.015	.005	.015	.0015	.007	9
10	.005	.005	.003	.0015	.003	.007	.0015	.005	0	.0015	10
11	0	.01	0	0	.015	0	0	0	0	0	11
12	0	.0015	0	0	.001	0	0	0	0	0	12
13	.012	.009	.007	.0025	.009	.01	.004	.006	.0025	.004	13
14	0	0	0	0	0	0	0	0	0	0	14
15	.429	.5285	.490	.307	.367	.623	.3885	.485	.272	.3965	15
					Total rare-earth elements in apatite (atomic percent)[2]						
16	38.8	30.5	21.4	15.0	33.4	30.2	22.8	27.1	18.6	20.6	16
17	6.6	5.4	6.2	9.7	4.9	5.6	7.4	8.6	6.8	8.7	17
18	20.4	17.5	29.0	31.3	17.4	22.1	35.9	28.7	34.6	35.7	18
19	3.2	3.5	3.0	4.9	3.9	2.9	3.7	3.8	5.4	3.7	19
20	19.8	12.0	28.1	30.4	12.2	21.5	23.1	18.4	33.6	23.0	20
21	2.9	11.5	2.7	3.1	16.4	6.8	0	3.5	0	3.3	21
22	0	.5	.5	.9	0	.4	.7	.8	0	.7	22
23	2.8	7.9	5.1	2.6	4.5	6.6	4.4	5.1	0	2.0	23
24	2.6	7.6	2.4	1.3	1.4	1.9	1.0	2.4	.5	1.3	24
25	.9	.7	.5	.4	.7	.8	.3	.8	0	.3	25
26	0	1.5	0	0	3.1	0	0	0	0	0	26
27	0	.2	0	0	.4	0	0	0	0	0	27
28	2.0	1.2	1.1	.4	1.7	1.2	.7	.8	.5	.7	28
29	0	0	0	0	0	0	0	0	0	0	29
30	100.0	100.0	100.0	100.0	100.0	100.0	100.0	100.0	100.0	100.0	30
31	30.2	26.4	38.2	45.9	26.2	30.6	47.0	41.1	46.8	48.1	31

precision of original data.

1971: U.S. Geol. Survey Prof. Paper 750-C, p. C112–C116.

Lee, D. E., Stern, T. W., Mays, R. E., and Van Loenen, R. E., 1968, Accessory zircon from granitoid rocks of the Mount Wheeler mine area, Nevada, *in* Geological Survey Research 1968: U.S. Geol. Survey Prof. Paper 600-D, p. D197–D203.

Lee, D. E., and Van Loenen, R. E., 1970, Biotites from hybrid granitoid rocks of the southern Snake Range, Nevada, *in* Geological Survey Research 1970: U.S. Geol. Survey Prof. Paper 700-D, p. D196–D206.

—— 1971, Hybrid granitoid rocks of the southern Snake Range, Nevada: U.S. Geol. Survey Prof. Paper 668, 48 p.

Murata, K. J., Rose, H. J., Jr., and Carron, M. K., 1953, Systematic variation of rare earths in monazite: Geochim. et Cosmochim. Acta, v. 4, no. 6, p. 292–300.

Nockolds, S. R., 1933, Some theoretical aspects of contamination in acid magmas: Jour. Geology, v. 41, no. 6, p. 561–589.

Otto, Helmut, 1935, Die Rolle des Mangans in den Mineralien: Tschermaks Mineralog. u. Petrog. Mitt., v. 47, p. 89–140.

Stormer, J. C., and Carmichael, I. S. E., 1971, Fluorine-hydroxyl exchange in apatite and biotite—A potential igneous geothermometer: Contr. Mineralogy and Petrology, v. 31, no. 2, p. 121–131.

Taborszky, F. K., 1962, Geochemie des Apatits in Tiefengesteinen am Beispiel des Odenwaldes: Beitr. Mineralogie u. Petrographie, v. 8, no. 5, p. 354–392.

Taubeneck, W. H., 1957, Zircons in the metamorphic aureole of the Bald Mountain batholith, Elkhorn Mountains, northwestern Oregon [abs.]: Geol. Soc. America Bull., v. 68, no. 12, pt. 2, p. 1803–1804.

Wilcox, R. E., 1959, Use of the spindle stage for determination of principal indices of refraction of crystal fragments: Am. Mineralogist, v. 44, nos. 11–12, p. 1272–1293.

—— 1962, Cherkasov's "focal screening" for determination of refractive index by the immersion method, *in* McCrone, W. C., ed., Internat. Microscopy Symposium, Chicago, 1960 [1962], Proc.: p. 160–165.

Wyatt, Michael, 1954, Zircons as provenance indicators: Am. Mineralogist, v. 39, nos. 11–12, p. 983–990.

Wyllie, P. J., Cox, K. G., and Biggar, G. M., 1962, The habit of apatite in synthetic systems and igneous rocks: Jour. Petrology, v. 3, pt. 2, p. 238–243.

Table 6.—*Rare-earth contents of accessory apatites from the Young Canyon–Kious Basin area, the Pole Canyon–Can Young Canyon area, and from aplites, southern Snake Range, Nev.*

[Sample localities are shown on plate 1 of Lee and Van Loenen (1971). Spectrographic analyses by R. E. Mays. Results for Y, La, and Yb are quantitative; results for all other elements are semiquantitative. General limitations of two methods given in text. Looked for but not found: Tb (limit of detection 0.005 percent). Σ discussed in text]

	Young Canyon–Kious Basin area		Pole Canyon–Can Young Canyon area		Aplites	
Sample No.	190-MW-61	234-MW-61	135-DL-62	120-MW-60	119-MW-60	121-MW-60
CaO in rock (weight percent)	1.2	1.6	0.98	1.3	0.63	0.70
Rare earths in apatite (weight percent)						
Y	0.20	0.30	0.15	0.16	0.2	0.1
La	.046	.050	.026	.026	.032	.034
Ce	.2	.15	.15	.07	.1	.15
Pr	.03	.02	.015	.015	.02	.03
Nd	.2	.15	.1	.1	.15	.15
Sm	.07	.05	.15	.015	.05	.07
Eu	.005	.005	.003	.005	.005	.005
Gd	.07	.07	.07	.03	.05	.1
Dy	.07	.05	.07	.02	.03	.03
Ho	.015	.007	.01	.01	.005	.005
Er	.05	.03	.015	0	0	0
Tm	0	0	.002	0	0	0
Yb	.021	.023	.007	.0095	.005	.002
Lu	.005	.015	0	0	0	0
Total	.982	.920	.768	.4605	.647	.676
Total rare-earth elements in apatite (atomic percent)[1]						
Y	29.9	44.7	29.4	46.8	42.5	22.3
La	4.4	4.8	3.3	5.0	4.3	4.9
Ce	19.0	14.2	18.7	13.0	13.4	21.1
Pr	2.8	1.9	1.9	2.9	2.6	4.1
Nd	18.4	13.8	12.0	18.0	19.6	20.5
Sm	6.2	4.4	17.4	2.6	6.2	9.3
Eu	.4	.4	.4	.8	.6	.6
Gd	6.0	5.9	7.9	4.9	6.0	12.6
Dy	5.7	4.1	5.4	3.1	3.6	3.8
Ho	1.2	.5	1.1	1.6	.6	.6
Er	4.0	2.4	1.6	0	0	0
Tm	0	0	.2	0	0	0
Yb	1.6	1.7	.7	1.3	.6	.2
Lu	.4	1.2	0	0	0	0
Total	100.0	100.0	100.0	100.0	100.0	100.0
Σ(La+Ce+Pr)	26.2	20.9	23.9	20.9	20.3	30.1

[1] Results of conversion to atomic percent are given in more significant figures than justified by precision of original data.

Jour. Research U.S. Geol. Survey
Vol. 1, No. 1, Jan.–Feb. 1973, p. 99–103

NEW DATA ON CUPROBISMUTITE

By CHARLES M. TAYLOR[1]; ARTHUR S. RADTKE, and
C. L. CHRIST, Stanford, Calif.; Menlo Park, Calif.

Abstract.—Cuprobismutite from Tunnel Extension Number Two mine, Ohio mining district, Utah, was chemically analyzed using the electron microprobe. Its empirical formula was determined to be $Cu_{20.8}Ag_{0.97}Pb_{0.35}Mn_{0.22}Bi_{26.7}Sb_{0.06}Te_{0.05}Se_{0.55}S_{50.4}$. The tentative conclusion is that unsubstituted cuprobismutite has the chemical formula $5Cu_2S{\cdot}6Bi_2S_3$ rather than the previously ascribed formula $6Cu_2S{\cdot}6Bi_2S_3$ and that cuprobismutite is therefore not dimorphous with emplectite.

Microscopic examination of polished sections of gold- and silver-bearing sulfide ore from the Tunnel Extension Number Two mine, Ohio mining district, Utah, showed that the ore contains a variety of bismuth-bearing minerals, including cuprobismutite, bismuthinite, emplectite, and tetradymite. Electron microprobe studies also indicate the presence of a secondary hydrated bismuth sulfate mineral, the data for which will be given separately. This paper presents data on the micromineralogy of the ore minerals and defines the chemical composition of cuprobismutite.

The Ohio mining district is located along the east flank of the Tushar Range, about 6 miles southwest of Marysvale (fig. 1) in Piute County, Utah. Most of the sulfide ore bodies in the Tunnel Extension Number Two mine are tabular and occur within steeply dipping shear or fault zones. Locally, small amounts of ore replace the wallrocks which are latite and agglomerate units of the Bullion Canyon Volcanics of Oligocene age.

The ore bodies in the Tunnel Extension Number Two mine, as well as other deposits in the Ohio district described by Butler, Loughlin, Heikes, and others (1920), were mined principally for their high content of gold and silver. Although the other deposits in the district may contain the same suite of bismuth-bearing minerals, the only specimens used in this study came from the 400-foot level of the Tunnel Extension Number Two mine.

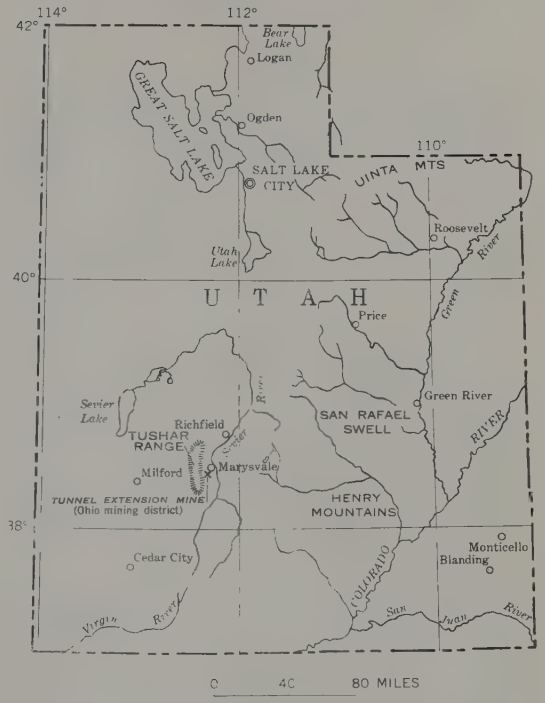

Figure 1.—Index map of Utah, showing location of the Tunnel Extension mine (Ohio mining district) (Radtke and others, 1967).

Acknowledgments.—All electron microprobe analyses were done on the Model 400 electron microprobe analyzer at Materials Analysis Co., Palo Alto, Calif., which is now a division of ETEC Corp. We wish to thank Richard Wolf of Microspec Corp., Palo Alto, Calif., for the use of his computer program for electron microprobe quantitative data reduction, and the following members of the U.S. Geological Survey: Richard C. Erd and Joan R. Clark for critical review of the manuscript; Richard C. Erd for assistance in X-ray diffraction analysis; Chris Heropoulos for spectrographic analyses; Brent P. Fabbi for X-ray fluorescence analyses; and W. W. Brannock for specific gravity determinations. The ore specimens were generously provided by John E. Frost, Mineral Department Manager, Esso Eastern, Inc., Houston, Texas.

[1] School of Earth Sciences, Stanford University.

ORE CHEMISTRY AND MINERALOGY

The chemical and mineralogical associations in this ore were described previously by Radtke, Taylor, and Frost (1967). Results of this earlier work and more recent study of these ores as they apply to the detailed study of the bismuth-bearing minerals are summarized below.

The fine-grained siliceous sulfide ores are composed mainly of cuprobismutite, quartz, and bismuthinite. The approximate percentage by volume of these and other minerals is shown in table 1. Primary ore minerals are cuprobismutite, bismuthinite, tetrahedrite, tetradymite, chalcopyrite, and native gold. Secondary or alteration minerals are chalcocite, covellite, and a hydrated bismuth sulfate. Quartz makes up most of the gangue. Other gangue minerals include significant amounts of cassiterite (Radtke and others, 1967) and small amounts of calcite. The three most abundant minerals, cuprobismutite, bismuthinite, and quartz, are intergrown and interlocked in the ore (fig. 2).

Table 1.—*Mineralogy of massive sulfide ores*

[Abundance, in percentage by volume of total sample, was estimated visually. (From Radtke and others, 1967.)]

Mineral	Abundance	Mineral	Abundance
Cuprobismutite	40	Tetrahedrite	1
Bismuthinite	30	Cassiterite	1
Quartz	20	Tetradymite	<1
Hydrated bismuth sulfate	5	Chalcopyrite	<1
Covellite	1	Gold	<1
Chalcocite	1	Calcite	<1

A semiquantitative spectrographic analysis of a typical specimen of ore is given in table 2. This analysis, plus several other spectrographic analyses performed by Taylor and Radtke on other ore samples indicate that the principal elements in the ore are bismuth (>20 percent), silicon (7–10 percent), copper (5–7 percent), tin (1–1.5 percent), and silver (0.3–1 percent). Although the ore contains small amounts of selenium and tellurium, data on these elements are not given in table 2. Owing to poor sensitivity and spectral interference, selenium is not sought in the standard method used. However,

Table 2.—*Semiquantitative spectrographic analysis of massive sulfide ore*

[Sought but not found: As, B, Be, Cd, Ce, Co, Eu, Ga, Ge, Hf, Hg, In, K, La, Li, Na, Nb, P, Pd, Pt, Re, Sc, Sr, Ta, Te, Th, Tl, U, Y, Yb, Zn, and Zr. Values are in weight percent. Analyst: Chris Heropoulos. (From Radtke and others, 1967.)]

Element	Amount	Element	Amount	Element	Amount
Si	10	Ag	1	Ni	0.001
Al	.02	Au	.003	Pb	.3
Fe	.015	Ba	.001	Sb	.1
Mg	.0003	Bi	>10	Sn	1.5
Ca	.001	Cr	.0002	V	.005
Ti	.007	Cu	7	W	.01
Mn	.07	Mo	.001		

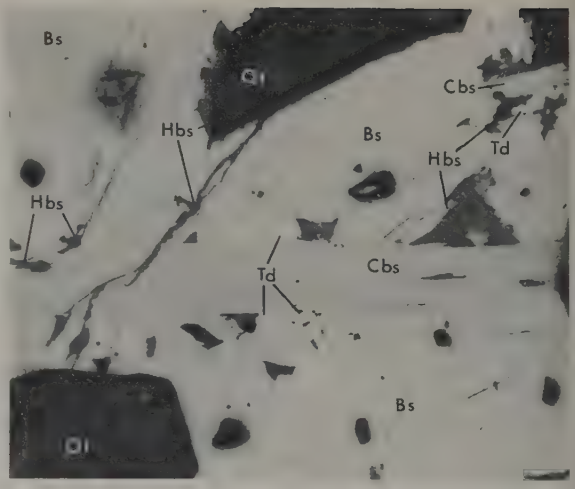

Figure 2.—Photomicrograph showing intergrowths of medium-gray bladed cuprobismutite (Cbs) and small white grains of tetradymite (Td) in pale-gray bismuthinite (Bs). Darkest areas are euhedral quartz (Qt) grains. Note alteration of primary bismuth minerals to a hydrous bismuth sulfate (Hbs) along fractures and grain boundaries. X 340. (From Radtke and others, 1967.)

X-ray fluorescence analysis shows the content of selenium to be approximately 0.2–0.3 weight percent; the content of tellurium is <0.1 percent.

CUPROBISMUTITE

Because one of the purposes of this paper is to establish the composition of cuprobismutite and because the validity of this mineral as a distinct species has been questioned in the past, a brief review of the literature is necessary. Hillebrand (1884) reported the presence of "a sulpho-bismuthite of copper and silver in ore specimens" from the Missouri mine, Halls Valley, Park County, Colo. He recognized this as "a probably new mineral" and proposed the formula $3(Cu,Ag)_2S{\cdot}4Bi_2S_3$. Dana (1892) listed the data collected by Hillebrand and named the mineral cuprobismutite. Schneiderhöhn and Ramdohr (1931) presented some data on the physical and optical properties of cuprobismutite and indicated that the mineral also occurred at Arnsberg, Westphalia.

On the basis of study of polished sections of specimens from the type locality, Halls Valley, Colo., Short (1931) reported that cuprobismutite was identical with emplectite ($Cu_2S{\cdot}Bi_2S_3$) and listed cuprobismutite as a discredited or doubtful mineral. Palache (1940) examined the type specimen, USNM 92902, from Halls Valley, identified bismuthinite (Bi_2S_3) and emplectite, and concluded (p. 611) "since a mixture of these two phases would give the composition revealed by Hillebrand's analysis, the species has no validity." Palache, Berman, and Frondel (1944) also classified cuprobismutite as a discredited species.

Nuffield (1952) examined the type specimen and showed that cuprobismutite was a valid species and not a mixture of bismuthinite and emplectite. Because of the presence of several intergrown phases, Nuffield was not able to determine the exact chemical formula. However, he argued that since the Bi-Cu ratio was close to 1:1, it was reasonable to suggest that its chemical formula was $Cu_2S{\cdot}Bi_2S_3$ and that cuprobismutite was dimorphous with emplectite. Ramdohr (1969, p. 707) stated that the composition was "presumably $3Cu_2S{\cdot}4Bi_2S_3$, but in the classic occurrence according to the structure probably $CuBiS_2$, i.e., dimorphous with emplectite."

Electron microprobe analysis

Polished sections of the ore were prepared for microscopic examination and electron microprobe analysis following the method outlined by Taylor and Radtke (1965). The polished section containing the standards for electron microprobe analysis and the section for analysis were simultaneously carbon coated to uniform thicknesses. Numerous grains of cuprobismutite were analyzed by spectral scans, and all elements detected were subsequently analyzed quantitatively.

Corrections in electron microprobe intensity data were made taking into account: (1) drift of the incident electron beam, (2) background from the continuous spectrum, (3) characteristic fluorescence by other radiations, (4) absorption effects, and (5) atomic number effects. $K\alpha$ characteristic lines were used for S, Se, Cu, and Mn; $L\alpha$ characteristic lines were used for Te, Sb, and Ag; and $M\alpha$ characteristic lines were used for Bi and Pb. Operating voltages were 20 kV for S, Ag, Te, and Bi; 25 kV for Sb and Pb; and 30 kV for Mn, Cu, and Se. Standards used for the quantitative analyses include Mn, Cu, Se, Ag, Sb, Te, PbS, and Bi_2S_3. The quantitative data were reduced at the Stanford University Computing Center according to a program developed by Richard Wolf, of Microspec Corp. Results of the analysis of numerous grains of cuprobismutite showed the composition to be remarkably uniform. The chemical analysis of a typical grain is given in table 3.

These analytical results yield the complex empirical formula $Cu_{2.0.8}Ag_{0.97}Pb_{0.35}Mn_{0.22}Bi_{2.6.7}Sb_{0.06}Te_{0.05}Se_{0.55}S_{5.0.4}$

Table 3.—*Electron microprobe analysis of cuprobismutite*

Element	Weight percent	Precision[1]	Atomic percent
S	18.5	±0.20	50.38
Se	.50	±.04	.55
Te	.07	±.02	.05
Bi	63.8	±.30	26.66
Sb	.08	±.02	.06
Cu	15.1	±.20	20.75
Ag	1.19	±.03	.97
Pb	.84	±.03	.35
Mn	.14	±.02	.22
Total	100.2		99.99

[1] Precision is calculated from the standard counting error from an average of 18 points in two separate but near-together grains. The values of precision listed indicate that the elements are distributed uniformly within and between the two grains. The values listed in the weight percentage column are considered to be accurate to ±2 percent.

for cuprobismutite. For this formula, the total charge for the anions is −102.0, taking S, Se, and Te as −2, and that for the cations is +103.2, taking Cu and Ag to be +1, Pb and Mn to be +2, and Bi and Sb to be +3. This agreement, which is within 1.2 percent, is entirely satisfactory, considering the errors of analysis and the complex chemistry of the mineral. The charge-balance calculation is, of course, based on the assumption that the valence rule is valid and that cuprobismutite is a "sulfosalt" and not a "complex sulfide" (such as binnite, $Cu_{12}As_4S_{13}$), as defined by Nowacki (1971).

X-ray data

From single-crystal X-ray diffraction studies of type specimen cuprobismutite, Nuffield (1952) found that the mineral is monoclinic with cell constants a=17.65, b=3.93, c=15.24 A, and β=100.5°. He observed that the phase gave systematic X-ray extinctions for the general class of hkl reflections for which $h+k\neq 2n$, and he correctly stated that this result is consistent with the space group $C2/m$. Actually, these extinction conditions are also consistent with the space groups $C2$ and Cm.

In the present study, X-ray powder data were obtained from four different grains of the Tunnel Extension Number Two cuprobismutite, each of which had the same chemical composition, within limits of error. The measured d spacings and intensities did not differ significantly from pattern to pattern. The measured data from a typical pattern are listed in table 4 for the specimen designated as MU-1. Starting with the cell constants of Nuffield (1952), the d_{hkl} values for MU-1 were treated by the computer program of Evans, Appleman, and Handwerker (1963) to index the pattern and to obtain a least-squares refinement of the cell constants. The cell constants obtained for MU-1 are a=17.628±0.01, b=3.911±0.002, c=15.190±0.01 A, and β=101°16′; the volume of the unit cell is 1,027.0±0.8 A^3, and the errors given represent 1 standard error. The calculated d spacings and indices are listed in table 4, as are the data for cuprobismutite from the type specimen (USNM 92902) reported by Berry and Thompson (1962).

Mineral chemistry

As shown by the quantitative electron microprobe analysis (table 3), the cuprobismutite studied here has as major constituents copper, bismuth, and sulfur and also contains a significant amount of silver and minor amounts of selenium, tellurium, antimony, lead, and manganese. Starting with the empirical formula, $Cu_{2.0.8}Ag_{0.97}Pb_{0.35}Mn_{0.22}Bi_{2.6.7}Sb_{0.06}Te_{0.05}Se_{0.55}S_{5.0.4}$, and summing the atomic percentages of the elements as (Cu+Ag+Pb+Mn)=22.3, (Bi+Sb)=26.8, and (S+Se+Te)=51.0, the ratio of (Bi+Sb) to (Cu+Ag+Pb+Mn) is 12 to 10. This result suggests that the correct chemical formula for unsubstituted cuprobismutite is $5Cu_2S{\cdot}6Bi_2S_3$, or

Table 4.—*X-ray powder diffraction data for cuprobismutite from the Ohio mining d*

Calculated[1]		Cuprobism Tunnel Ext Number Tw Ohio mining district, Utah		Cuprobismutite[3] Missouri mine, Halls Valley, Park County, Colo.	
		Observed		Observed	
hkl	d_{hkl} (A)	d_{hkl} (A)	I/I_0	d_{hkl} (A)	I/I_0
001	14.898	.....	....	.....	....
200	8.644	.....	....	.....	....
201	8.204	.....	....	.....	....
002	7.449	.....	....	.....	....
201	6.914	6.94	12	.....	....
202	6.282	6.28	35	6.24	20
202	5.166	.....	....	.....	....
003	4.966	4.96	15	.....	....
$\bar{2}03$	4.723	.....	....	.....	....
401	4.386	.....	....	.....	....
400	4.322	4.32	40	4.31	30
$\bar{4}02$	4.102	.....	....	.....	....
203	3.983	.....	....	.....	....
401	3.950	3.941	10	.....	....
110	3.814	.....	....	.....	....
$\bar{1}11$	3.734	.....	....	.....	....
004	3.724	.....	....	.....	....
$\bar{2}04$	3.693	.....	....	.....	....
111	3.658	.....	....	3.65	40B
$\bar{4}03$	3.630	3.632	70		
$\bar{4}02$	3.457	.....	....	3.47	10
$\bar{1}12$	3.456	3.452	45		
112	3.338	.....	....	.....	....
$\bar{3}11$	3.237	.....	....		
310	3.236	3.220	70	3.23	40
204	3.201	.....	....		
$\bar{4}04$	3.141	.....	....	.....	....
$\bar{3}12$	3.095	.....	....		
311	3.093	.....	....	3.10	100
$\bar{1}13$	3.090	3.090	100		
205	3.003	.....	....	.....	....
403	2.984	.....	....	.....	....
005	2.980	.....	....		
$\bar{1}13$	2.964	2.971	12	2.96	5B
$\bar{6}01$	2.938	.....	....		
$\bar{6}02$	2.883	.....	....		
600	2.881	.....	....	2.86	10B
$\bar{3}13$	2.858	2.860	30		
$\bar{3}12$	2.856	.....	....		
$\bar{6}03$	2.735	.....	....		
601	2.731	.....	....	2.73	60
$\bar{1}14$	2.724	2.721	80		
$\bar{4}05$	2.713	.....	....		
		2.580	40	2.58	10
		2.501	10	2.49	5
		2.291	12	2.30	5
		2.160	35	2.17	20
		2.091	30	2.09	20
		1.995	25	2.00	5
		1.955	40	.....	....
		1.862	12	.....	....
		1.825	15	.....	....

Table 4.—*X-ray powder diffraction data for cuprobismutite from the Ohio mining district, Utah.*—Continued

Calculated[1]		Cuprobismutite[2] Tunnel Extension Number Two mine, Ohio mining district, Utah		Cuprobismutite[3] Missouri mine, Halls Valley, Park County, Colo.	
		Observed		Observed	
hkl	d_{hkl} (A)	d_{hkl} (A)	I/I_0	d_{hkl} (A)	I/I_0
		1.722	30	.....	....
		1.669	15	.....	....
		1.610	5B	.....	....
		1.485	7	.....	....
		1.454	10	.....	....
		1.435	10	.....	....

[1] Calculated from least-squares refinement of the observed X-ray powder data from specimen MU-1 (see footnote 2) by use of the computer program of Appleman, Evans, and Handwerker (1972).

[2] Specimen MU-1, private collection of C. M. Taylor, School of Earth Sciences, Stanford University; film ASR-1, 1968; Cu/Ni; radiation Cu$K\alpha$ = 1.5418 A; camera diameter 114.6 mm.

[3] Specimen 92902, U.S. National Museum, type specimen of cuprobismutite; Cu/Ni; radiation Cu$K\alpha$ = 1.5418 A; data from Berry and Thompson (1962, p. 143).

$Cu_{10}Bi_{12}S_{23}$. For this formula, and adjusting for the abundances of the other elements present, the formula weight of the cuprobismutite is 3,933. Using a unit-cell weight of 3,933 and the calculated unit-cell volume of 1,027 A^3, the calculated density is 6.36 g cm^{-3}. Unfortunately, no single crystals of the specimen studied were available, so that no direct measurement could be made to check this calculated density. However, it was possible to arrive at a specific gravity value in the following way: The specific gravity of a sample containing about 50 percent cuprobismutite was measured. A small sample of ore was crushed to −225 mesh and treated with hydrochloric acid to remove any carbonates. The heavy minerals were separated from the quartz using methylene iodide, and the concentrate was cleaned and dried. The specific gravity of the heavy-media concentrate was determined to be 6.35.

The contents of copper, bismuth, silica, and tin in the heavy-media concentrate were determined using standard X-ray fluorescence methods. By solving two simultaneous equations set up on the basis of the weight balance and the copper balance in the sample, it was determined that the heavy-mineral concentrate contained 53.2 percent cuprobismutite and 44.2 percent bismuthinite. Chemical analysis showed that the concentrate contained 2.4 percent quartz and 0.1 percent cassiterite. Covellite, the only other mineral identified, was estimated at 0.1 percent. The specific gravity of cuprobismutite was then calculated by setting up an equation in which the weight percent of each mineral divided by its

specific gravity was added and the summation made equal to 100 divided by the specific gravity of the bulk concentrate. The specific gravity of cuprobismutite was determined to be 6.36.

Obviously, the excellent agreement between the calculated density and measured specific gravity of cuprobismutite is somewhat fortuitous, considering the assumptions made, but it does tend to confirm the cell contents of the unsubstituted mineral to be $5Cu_2S{\cdot}6Bi_2S_3$ (or some integral multiple of this formula) and indicates that cuprobismutite is not dimorphous with emplectite, $6Cu_2S{\cdot}6Bi_2S_3$.

A unit-cell content of $Cu_{10}B_{12}S_{23}$ is not consistent with the *C*-centered cell found by Nuffield (1952) if all crystallographically equivalent sites are occupied. A *C*-centered cell must, of necessity, contain equivalent atoms in at least multiples of 2 (in special positions). For *Cm* or *C*2, general positions are fourfold, and for *C*2/*m*, general positions are eightfold. A unit-cell content of 23 atoms of sulfur is not in agreement with these requirements. Thus, the possibility exists that some of the equivalent sites are vacant and that cuprobismutite forms a defect structure if the data of Nuffield (1952) are correct. On the other hand, it is quite possible that the unit cell determined by Nuffield (1952) is actually a submultiple of the true unit cell, or that the symmetry assigned to the structure is incorrect, or that a combination of all of these possibilities exists. Obviously, further work is necessary to resolve this problem. Ideally, this would involve a complete crystal structure determination on chemically well-characterized single crystals. Short of a structure determination, it would be considerably helpful to redetermine the symmetry and unit-cell constants by modern single-crystal X-ray techniques, such as the precession camera method. As pointed out in the foregoing, single crystals suitable for X-ray study are not available in the specimens studied.

BISMUTHINITE

Large amounts of bismuthinite are also present in the sulfide ores of the Tunnel Extension Number Two mine. Microscopic examination of polished sections shows that the bulk ore contains approximately 30 percent bismuthinite by volume and may in some samples contain as much as 45 percent.

Although the composition of bismuthinite is, in essence, Bi_2S_3, analyses summarized in Palache, Berman, and Frondel (1944) indicate that small amounts of lead, copper, iron, and tellurium, and larger amounts of antimony and selenium may be present in the structure. Quantitative electron-microprobe analyses of numerous grains of bismuthinite show that in these ores, this mineral contains 0.43–0.47 weight percent Cu, 0.93–0.98 weight percent Pb, 0.12–0.15 weight percent Sb, 0.68–0.73 weight percent Se, and 0.05–0.07 weight percent Te.

REFERENCES CITED

Appleman, D. E., Evans, H. T., Jr., and Handwerker, D. S., 1972, Job 9214; Indexing and least-squares refinement of powder diffraction data, U.S. Geol. Survey Computer Contr. 20: Springfield, Va., Natl. Tech. Inf. Service.

Berry, L. G., and Thompson, R. M., 1962, X-ray powder data for ore minerals—the Peacock atlas: Geol. Soc. America Mem. 85, 281 p.

Butler, B. S., Loughlin, G. F., Heikes, V. C., and others, 1920, The ore deposits of Utah: U.S. Geol. Survey Prof. Paper 111, 672 p.

Dana, E. S., 1892, The system of mineralogy of James Dwight Dana, 1837–1868, 6th ed.: New York, John Wiley and Sons, Inc., 1,134 p.

Hillebrand, W. F., 1884, On an interesting variety of löllingite and other minerals: Am. Jour. Sci., v. 27, p. 349–358.

Nowacki, W., 1971, Introductory talk: Japan Mining Geol. Soc., Spec. Issue 2, p. 3–9.

Nuffield, E. W., 1952, Studies of mineral sulpho-salts—[Pt.] 16, Cuprobismuthite: Am. Mineralogist, v. 37, nos. 5–6, p. 447–452.

Palache, Charles, 1940, Cuprobismutite—a mixture: Am. Mineralogist, v. 25, no. 9, p. 611–613.

Palache, Charles, Berman, Harry, and Frondel, Clifford, 1944, The system of mineralogy of James Dwight Dana and Edward Salisbury Dana, v. 1, Elements, sulfides, sulfosalts, oxides, 7th ed., rev.: New York, John Wiley and Sons, Inc., 834 p.

Radtke, A. S., Taylor, C. M., and Frost, J. E., 1967, Bismuth and tin minerals in gold- and silver-bearing sulfide ores, Ohio mining district, Marysvale, Utah, *in* Geological Survey Research 1967: U.S. Geol. Survey Prof. Paper 575-D, p. D127–D130.

Ramdohr, Paul, 1969, The ore minerals and their intergrowths, 3d ed.: London, Pergamon Press, 1,174 p.

Schneiderhöhn, Hans, and Ramdohr, Paul, 1931, Lehrbuch der Erzmikroskopie, 2d ed.: Berlin, Germany, Verlag von Gebrüder, 714 p.

Short, M. N., 1931, Microscopic determination of the ore minerals: U.S. Geol. Survey Bull. 825, 204 p.

Taylor, C. M., and Radtke, A. S., 1965, Preparation and polishing of ores and mill products for microscopic examination and electron microprobe analysis: Econ. Geology, v. 60, no. 6, p. 1306–1319.

Jour. Research U.S. Geol. Survey
Vol. 1, No. 1, Jan.–Feb. 1973, p. 105–111

CHEMICAL COMPOSITION OF A SALINE LAKE ON ENDERBURY ISLAND, PHOENIX ISLAND GROUP, PACIFIC OCEAN

By DAVID W. BROWN and ROBERT A. GULBRANDSEN,
Menlo Park, Calif.

Abstract.—Ion activity products for the dissolution of calcite, aragonite, gypsum, monetite, brushite, dolomite, magnesite, hydroxyapatite, and fluorapatite were calculated for a South Pacific guano island brine with an ionic strength of 6.4. Environmental conditions for the brine at the time of analysis and of sampling indicated saturation with respect to calcite, aragonite, gypsum, hydroxyapatite and fluorapatite; a comparison of the ion activity products and equilibrium constants indicated saturation or supersaturation with respect to most minerals found in lake sediments or elsewhere on the island. The results suggest that chemical thermodynamic calculations for brines may have some usefulness despite the many assumptions and estimations that must be made.

Enderbury Island is one of the atolls of the Phoenix Island Group in the central equatorial Pacific Ocean (fig. 1). It is a small island about 3 miles in length and about a mile in greatest breadth. The highest point is 33 feet, the top of an old phosphate stockpile. The surface of the island in cross section is concave, and most drainage is to the interior. Because of the great porosity of the surface material, all drainage is underground. The climate is arid, even though the mean annual rainfall is around 25 inches (Hutchinson, 1950, p. 166), and vegetation is sparse.

The bulk of the island is coral, but many kinds of shells and other skeletal material are incorporated in the coral reefs and mixed with coral fragments in the sands of the beaches and of much of the interior of the island. Phosphate, as guano and guano-derived phosphate rock and sediment, is widespread on the island but not now abundant. Hutchinson (1950, p. 180) estimated that about 100,000 tons of phosphate ore was shipped from Enderbury in the latter half of the nineteenth century.

A shallow saline lake is located in the southern half of the island (fig. 1) and occupies the site of a former lagoon that became filled with sediment. The depth of the lake probably never exceeds a few feet. The small islands within the lake are old reefs, now above sea level. The water of the lake is derived directly from rain on its surface, from rainwater drained from the island, from sea-water spray, and possibly from beach-ridge overwash during large storms. Ground water under the lake may be sea water. Because the drainage terrain is of restricted composition, composed almost entirely of calcium and magnesium carbonates and phosphates, and because of the existence of an evaporitic environment, a sample was collected from the lake to determine the composition of the water. One of the purposes of this study is to relate the existence of any remaining phosphate deposits to the water composition. Mineral equilibria calculations were attempted in order to assess the extent of saturation in the water of phosphate and other minerals found on the island and in the lake sediment. These calculations also serve to illustrate the applicability of chemical thermodynamic calculations to brines of very high dissolved solids content.

Acknowledgments.—The water sample was collected in the course of an investigation of the economic potential of phosphate deposits on the island. This work was a joint effort of the United Kingdom and the United States, and it was performed by Brian D. Hackman, on behalf of the United Kingdom, and by Joshua I. Tracey, Jr., and the junior author of this paper on behalf of the United States. We are grateful to the U.S. Air Force for the opportunity to make this study.

WATER ANALYSIS

The water sample was collected on the eastern edge of the lake (fig. 1). Temperature of the water at the time of collection was 40°C.

All chemical species were measured according to accepted procedures (Brown and others, 1970). In these procedures, all cation concentrations were determined by atomic absorption spectrophotometry. Alkalinity was measured by acid titration. Total halides (excluding fluoride) were determined by the Mohr method. Bromide and iodide were measured iodometrically after appropriate oxidation to bromate and iodate. Sulfate was determined by the thorin barium titration method by use of a spectrophotometrically determined end point. Silica and phosphate concentrations were determined colorimetrically by use of their respective molybdate complexing methods. Boron and fluoride concentrations were also determined colorimetrically, with the dianthrimide and Zirconium-Eriochrome Cyanide R methods, respectively.

The composition of the water is presented in table 1. The lake is highly saline, about 10 times more concentrated with

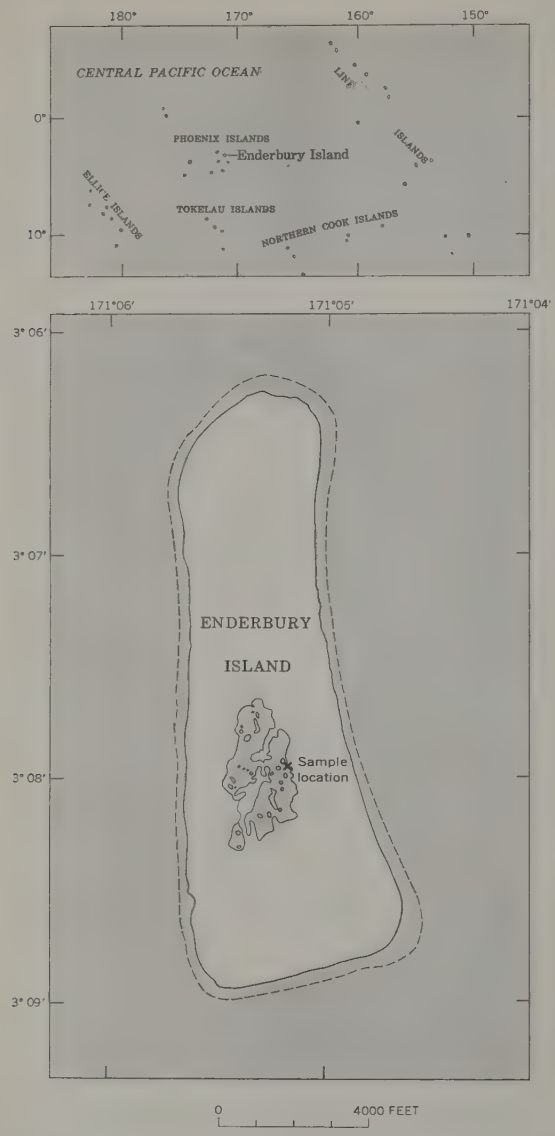

Figure 1.—Map showing outline of Enderbury Island and saline lake in southern part of island. Dashed line around island marks the approximate position of low tide.

Table 1.—*Analysis of Enderbury lake water*

Species	Method	Concentration		
		Mg/l	Molarity (Major ions only)	Normality (Major ions only)
Neutral:				
SiO_2	Colorimetric (molybdate).	0.5	.....	.....
Cations:				
Cu	Atomic absorption.	3.6	.....	.....
Ca	..... do.....	885	0.022	0.044
Mg	..... do.....	7,800	.32	.64
Sr	..... do.....	42	.....	.....
Na	..... do.....	104,000	4.52	4.52
K	..... do.....	2,000	.051	.051
Li	..... do.....	1.0	.....	.....
Anions:				
HCO_3	Acid titration.	442	.0072	.0072
CO_3	..... do.....	0	.....	.....
OH	..... do.....	0	.....	.....
SO_4	Ba^{+2} titration (thorin).	14,100	.147	.294
Cl	Ag^{+} titration (Mohr).	176,000	4.96	4.96
F	Colorimetric (cyanine).	10	.....	.....
Br	Hypochlorite oxidation, titration with thiosulfate.	104	.001	.001
I	Bromine oxidation, titration with thiosulfate.	[1]19±7	.....	.....
PO_4	Colorimetric (molybdate).	1.6	.....	.....
B	Colorimetric (1, 1-dianthrimide).	30	.....	.....

Normality total cations: 5.26 *N*
Normality total anions: 5.27 *N*
Total dissolved solids: 305,000 mg/l
pH: 7.70
Density: 1.202 g/ml
Appearance: Light pink with some suspended solids.
Mg/Ca molar ratio: 14.5

[1] Inadequate sample for accurate determination.

respect to sodium chloride than sea water. The sodium and chloride contents show well the contribution of sea water to the present composition of the lake. Magnesium is more concentrated relative to calcium in the lake water than in sea water; the Mg/Ca molar ratios are 14.5 and 5.4 (Goldberg, 1965, p. 164), respectively. A ratio of 35.7 was found for a brine pool on Jarvis Island, east of Enderbury in the southern Line Islands, by Schlanger and Tracey (1970, p. 676). They also found calcium-rich dolomite in the nearby evaporitic sediments. Bottom sediment of the Enderbury lake has not been sampled, but two sediment cores, collected by Joshua Tracey, Jr., and Brian Hackman, one on the east edge and one on the west edge of the lake, both contain high-magnesium calcite (about 35–40 mol percent $MgCO_3$) 2 to 3 feet below the surface. A study of these cores that is in progress shows that gypsum and bassanite layers are also present and that aragonite, low-magnesium calcite, and gypsum are the principal minerals in the upper few inches of the cores. Apatite, probably a carbonate hydroxyfluorapatite, is present in all of the sediment in small amounts.

The copper content of the water, 3.6 mg/l, is of special interest. It is more than 1,000 times greater than the amount

reported in sea water, 0.003 mg/l (Goldberg, 1965, p. 164), and much more than can be accounted for by the contribution of sea water to the lake's composition. A source for the copper, however, is not difficult to explain. A sample of guano spectrographically analyzed by R. E. Mays contains 20 ppm Cu, and skeletal parts of a number of organisms, including corals, contain from 11 to 25 ppm Cu (Bowen, 1966, p. 72). The island's drainage of rainwater into the lake, therefore, should provide an adequate supply of copper. The fact that copper can occur in such a high amount in saline water may help to explain the copper deposits in evaporitic sequences such as in the Permian Flowerpot Shale in Oklahoma (Ham and Johnson, 1964).

THEORETICAL CONSIDERATIONS

The fact that a closed-basin lake on a phosphate-rich island contains only 1.6 mg total phosphate (as PO_4) per liter may possibly be explained by assuming the phosphate to be in equilibrium with the large concentrations of calcium and (or) magnesium. Since there are primarily three types of phosphate ions present in any orthophosphate solution, there are several possible combinations of equilibrium species.

In a solution of known ionic strength, hydrogen ion activity, and extent of complex ion formation, the relative activities of the three phosphate ions $H_2PO_4^{-1}$, HPO_4^{-2}, and PO_4^{-3} may be calculated. If the activities of the ions which are suspected of being in equilibrium with phosphate are also calculated, one may determine whether the appropriate cation–phosphate ion activity products are characteristic of a system in chemical equilibrium with respect to these ions.

With regard to complex ion formation we first estimated the complexing effect of sulfate on the major cations to determine the cation activities, then we calculated the complexing effect of those cations on bicarbonate, fluoride, and finally phosphate. It was assumed that only sulfate significantly affects the cation activities because it is the only strongly complexing anion present in quantities comparable to the cation concentrations.

From the four cation-sulfate complex dissociation relations,

$$K_{CaSO_4} = \frac{[Ca^{+2}][SO_4^{-2}]}{[CaSO_4^{0}]}, K_{MgSO_4} = \frac{[Mg^{+2}][SO_4^{-2}]}{[MgSO_4^{0}]},$$

$$K_{NaSO_4} = \frac{[Na^{+}][SO_4^{-2}]}{[NaSO_4^{-}]}, \text{ and } K_{KSO_4} = \frac{[K^{+}][SO_4^{-2}]}{[KSO_4^{-}]}.$$

For the $CaSO_4^0$, $MgSO_4^0$, $NaSO_4^-$, and KSO_4^- complex ions and the concentration relations

$$C_{Ca} = \frac{[Ca^{+2}]}{\gamma_{Ca}} + \frac{[CaSO_4^{0}]}{\gamma_{CaSO_4}}, C_{Mg} = \frac{[Mg^{+2}]}{\gamma_{Mg}} + \frac{[MgSO_4^{0}]}{\gamma_{MgSO_4}},$$

$$C_{Na} = \frac{[Na^{+}]}{\gamma_{Na}} + \frac{[NaSO_4^{-}]}{\gamma_{NaSO_4}}, C_{K} = \frac{[K^{+}]}{\gamma_{K}} + \frac{[KSO_4^{-}]}{\gamma_{KSO_4}}, \text{ and}$$

$$C_{SO_4} = \frac{[SO_4^{-2}]}{\gamma_{SO_4}} + \frac{[CaSO_4^{0}]}{\gamma_{CaSO_4}} + \frac{[MgSO_4^{0}]}{\gamma_{MgSO_4}} + \frac{[NaSO_4^{-}]}{\gamma_{NaSO_4}} + \frac{[KSO_4^{-}]}{\gamma_{KSO_4}},$$

it can be shown that

$$[Ca^{+2}] = \frac{C_{Ca}}{\frac{1}{\gamma_{Ca}} + \frac{[SO_4^{-2}]}{K_{CaSO_4}\gamma_{CaSO_4}}}, \text{ with similar relations for}$$

$[Mg^{+2}]$, $[Na^{+}]$, and $[K^{+}]$, or more generally,

$$[i^{+z}] = \frac{C_i}{\frac{1}{\gamma_i} + \frac{[SO_4^{-2}]}{K_{iSO_4}\gamma_{iSO_4}}}, \text{ where } i \text{ represents Ca, Mg, Na, or}$$

K, and z is the ionic charge. It can also be shown that

$$[SO_4^{-2}] = \frac{C_{SO_4}}{\left\{\frac{1}{\gamma_{SO_4}} + \sum_{i = Ca, Mg, Na, K} \left(\frac{\frac{C_i}{K_{iSO_4}\gamma_{iSO_4} + [SO_4^{-2}]}}{\gamma_i}\right)\right\}}$$

This equation can be solved by several successive iterations, with $[SO_4^{-2}] = C_{SO_4}\gamma_{SO_4}$ (no complexing) as the first approximation. Bracketed terms are the molal thermodynamic activities of the particular ions in brackets. K_{CaSO_4}, K_{MgSO_4}, K_{NaSO_4}, and K_{KSO_4} are the ion complex dissociation constants. The total molal cation and sulfate concentrations are represented by C_{Ca}, C_{Mg}, C_{Na}, C_K, and C_{SO_4}, respectively. The terms γ_{Ca}, γ_{Mg}, γ_{Na}, γ_K, γ_{CaSO_4}, γ_{MgSO_4}, γ_{NaSO_4}, γ_{KSO_4}, and γ_{SO_4} are the activity coefficients of Ca^{+2}, Mg^{+2}, Na^+, K^+, $CaSO_4^0$, $MgSO_4^0$, $NaSO_4^-$, KSO_4^-, and SO_4^{-2}, respectively, and are a function of the solution's ionic strength. The ionic strength, a measure of the total dissolved electrolytes, can be calculated from the molal concentrations of the major ionic species in solution by the relation

$$\mu = \frac{\Sigma m_i z_i^2}{2},$$

where μ is the molal ionic strength, m_i is the molality of the

ith ion, and z is the unit charge on that ion. In dilute solutions, molarity can be substituted for molality, introducing only negligible error, but in solutions such as ours having very high total dissolved solids concentrations, the difference between molality and molarity is no longer negligible. Molality can be expressed by the relation

$$m = \frac{M}{\rho - S},$$

where M is molarity, ρ is the density of the solution in grams per milliliter, and S is the total grams dissolved solids per milliliter solution. In our specific case the relation is

$$m = \frac{M}{\rho - S} = \frac{M}{(1.202 - 0.305)\text{g/ml}} = 1.115\,M.$$

The major ionic species present in our sample are listed in table 2 with their molarities, molalities, and contributions to total ionic strength.

At this very high ionic strength, the original assumptions used in deriving the Debye-Hükel and Davies equations (Butler, 1964, p. 437) are no longer valid. These equations cannot be used to calculate ion activity coefficients in this solution. Such coefficients must be estimated from experimentally determined mean activity coefficients. Polzer and Roberson (1967, p. C117) have calculated such activity coefficients for various species at an ionic strength of 6.3. For most uncharged species ($CaSO_4^0$, $MgSO_4^0$), the activity coefficient is 3.0. For most monovalent cations and anions (K^+, $NaSO_4^-$, KSO_4^-), it is taken as 0.8 (1.3 for Na^+), for divalent anions (SO_4^{-2}) as 0.03, and for Ca^{+2} and Mg^{+2} ions as 0.9 and 2.2, respectively. Given this data and the following dissociation constants (Garrels and Thompson, 1962, p. 58), summarized below, we can solve for the cation and sulfate activities:

$$C_{SO_4} = 0.164\,m;\ \gamma_{SO_4} = 0.03$$

i	C_i (molal)	K_{iSO_4} at 25°C	γ_i	$\gamma_i SO_4$
Ca	0.024	$10^{-2.31}$	0.9	3.0
Mg	.36	$10^{-2.36}$	2.2	3.0
Na	5.04	$10^{-0.72}$	1.3	.8
K	.057	$10^{-0.96}$	.8	.8

Substituting into the appropriate aforementioned relations, we obtain activities and p values as follows:

Species	Activity (molal)	p[ ]
SO_4^{-2}	0.0013	2.89
Ca^{+2}	.020	1.70
Mg^{+2}	.65	.19
Na^+	6.45	−.81
K^+	.045	1.35

Table 2.—*Molarities, molalities, and ionic strength contributions of major ions*

Ion	Molarity (M)	Molality (m)	$\frac{m_i z_i^2}{2}$
Ca^{+2}	0.022	0.024	0.048
Mg^{+2}	.32	.36	.72
Na^+	4.52	5.04	2.52
K^+	.051	.057	.028
HCO_3^-	.007	.008	.004
SO_4^{-2}	.147	.164	.328
Cl^-	4.96	5.53	2.76
		Total ionic strength $= \frac{\Sigma m_i z_i^2}{2} = 6.4$	

In examining the bicarbonate complex ion system, we note that no potassium-bicarbonate complex ion is thought to exist. We need only consider the complexes $CaHCO_3^+$, $MgHCO_3^+$, and $NaHCO_3^0$. We write the concentration and equilibrium dissociation relations:

$$K_{CaHCO_3} = \frac{[Ca^{+2}][HCO_3^-]}{[CaHCO_3^+]},\ K_{MgHCO_3} = \frac{[Mg^{+2}][HCO_3^-]}{[MgHCO_3^+]},$$

$$K_{NaHCO_3} = \frac{[Na^+][HCO_3^-]}{[NaHCO_3^0]},$$

$$\text{and } C_{HCO_3} = \frac{[HCO_3^-]}{\gamma_{HCO_3}} + \frac{[CaHCO_3^+]}{\gamma_{CaHCO_3}} + \frac{[MgHCO_3^+]}{\gamma_{MgHCO_3}} + \frac{[NaHCO_3^0]}{\gamma_{NaHCO_3}},$$

from which can be derived the relation

$$[HCO_3^-] = \frac{C_{HCO_3}}{\left\{\frac{1}{\gamma_{HCO_3}} + \sum_{i\,=\,Ca,Mg,Na}\left(\frac{[i^{+z}]}{K_{iHCO_3}\,\gamma_{iHCO_3}}\right)\right\}}$$

Substituting C_{HCO_3}, the previously calculated cation activities, and the appropriate activity coefficients (Polzer and Roberson, 1967, p. C117) and dissociation constants (Garrels and Thompson, 1962, p. 58),

$$C_{HCO_3} = 0.0077\,m;\ \gamma_{HCO_3} = 0.8$$

i	$[i]$ (molal)	K_{iHCO_3} at 25°C	$\gamma_i HCO_3$
Ca	0.020	$10^{-1.26}$	0.8
Mg	.65	$10^{-1.16}$	.8
Na	6.45	$10^{+0.25}$	3.0

we obtain $[HCO_3^-] = 0.00052\,m$, or $pHCO_3 = 3.28$. Carbonate-bicarbonate equilibrium dictates that

$\frac{[CO_3^{-2}][H^+]}{[HCO_3^-]} = 10^{-10.33}$ at 25°C (Sillén and Martell, 1964, p. 135).

Therefore $pCO_3 + pH - pHCO_3 = 10.33$, or $pCO_3 = 10.33 + pHCO_3 - pH = 5.91$, for our pH of 7.70 at 25°C.

We may calculate the fluoride activity in the same manner, taking into consideration the ion complexes CaF^+ and MgF^+, for which the activity coefficients are assumed to be 0.8. The activity coefficient for F^- is estimated at 1.2 from mean activity coefficients for KF (Harned and Owen, 1967, p. 732). Sillén and Martell (1964, p. 257–258) report dissociation constants at 25°C for CaF^+ and MgF^+ as $>10^{-1.04}$ and $10^{-1.82}$, respectively. Substituting this data, and also $C_F = 0.00059$, $[Ca^{+2}] = 0.020\ m$, and $[Mg^{+2}] = 0.65\ m$ into the relation

$$[F^-] = \frac{C_F}{\left\{\frac{1}{\gamma_F} + \sum_{i = Ca, Mg}\left(\frac{[i]}{K_{iF}\,\gamma_{iF}}\right)\right\}},$$

we obtain $[F^-] = 0.000011\ m$, or pF = 4.96.

In calculating the activities of the three orthophosphate ions $H_2PO_4^-$, HPO_4^{-2}, and PO_4^{-3}, we shall consider the known complex ions $CaH_2PO_4^+$, $CaHPO_4^0$, $CaPO_4^-$, $MgHPO_4^0$, $MgPO_4^-$, $NaHPO_4^-$, and $KHPO_4^-$. Our equilibrium and concentration relations are

$$K_2 = \frac{[HPO_4^{-2}][H^+]}{[H_2PO_4^-]} \text{ and } K_3 = \frac{[PO_4^{-3}][H^+]}{[HPO_4^{-2}]} \quad \text{(second and third dissociation constants of phosphoric acid).}$$

$$K_{CaH_2PO_4} = \frac{[Ca^{+2}][H_2PO_4^-]}{[CaH_2PO_4^+]}, K_{CaHPO_4} = \frac{[Ca^{+2}][HPO_4^{-2}]}{[CaHPO_4^0]},$$

$$K_{CaPO_4} = \frac{[Ca^{+2}][PO_4^{-3}]}{[CaPO_4^-]}, K_{MgHPO_4} = \frac{[Mg^{+2}][HPO_4^{+2}]}{[MgHPO_4^0]},$$

$$K_{MgPO_4} = \frac{[Mg^{+2}][PO_4^{-3}]}{[MgPO_4^-]}, K_{NaHPO_4} = \frac{[Na^+][HPO_4^{-2}]}{[NaHPO_4^-]},$$

$$K_{KHPO_4} = \frac{[K^+][HPO_4^{-2}]}{[KHPO_4^-]}, \text{ and}$$

$$C_{PO_4} = \frac{[H_2PO_4^-]}{\gamma_{H_2PO_4}} + \frac{[HPO_4^{-2}]}{\gamma_{HPO_4}} + \frac{[PO_4^{-3}]}{\gamma_{PO_4}} + \frac{[CaH_2PO_4^+]}{\gamma_{CaH_2PO_4}} + \frac{[CaHPO_4^0]}{\gamma_{CaHPO_4}} + \frac{[CaPO_4^-]}{\gamma_{CaPO_4}} + \frac{[MgHPO_4^0]}{\gamma_{MgHPO_4}} + \frac{[MgPO_4^-]}{\gamma_{MgPO_4}} + \frac{[NaHPO_4^-]}{\gamma_{NaHPO_4}} + \frac{[KHPO_4^-]}{\gamma_{KHPO_4}}.$$

From these relations it may be shown that

$$\frac{C_{PO_4}}{[PO_4^{-3}]} = \frac{1}{\gamma_{PO_4}} + \frac{[H^+]}{K_3\gamma_{HPO_4}} + \frac{[H^+]^2}{K_2K_3\gamma_{H_2PO_4}} + \frac{[Ca^{+2}][H^+]^2}{K_2K_3\gamma_{CaH_2PO_4}K_{CaH_2PO_4}} + \frac{[Ca^{+2}][H^+]}{K_3\gamma_{CaHPO_4}K_{CaHPO_4}} + \frac{[Ca^{+2}]}{\gamma_{CaPO_4}K_{CaPO_4}} + \frac{[Mg^{+2}][H^+]}{K_3\gamma_{MgHPO_4}K_{MgHPO_4}} + \frac{[Mg^{+2}]}{\gamma_{MgPO_4}K_{MgPO_4}} + \frac{[Na^+][H^+]}{K_3\gamma_{NaHPO_4}K_{NaHPO_4}} + \frac{[K^+][H^+]}{K_3\gamma_{KHPO_4}K_{KHPO_4}}.$$

Activity coefficients are estimated as earlier:

Uncharged species: ($CaHPO_4^0$, $MgHPO_4^0$) $\gamma = 3.0$.

Monovalent cations, anions: ($H_2PO_4^-$, $CaH_2PO_4^+$, $MgH_2PO_4^+$, $NaHPO_4^-$, $KHPO_4^-$) $\gamma = 0.8$.

Divalent anions: (HPO_4^{-2}) $\gamma = 0.03$.

Using the assumption (from the Debye-Hückel equation) that the negative logarithm of the activity coefficients for divalent and trivalent ions is proportional to the square of the unit ionic charge (z) by the same constant, we may arrive at a fairly reasonable value for γ_{PO_4}. If

$$\frac{-\log \gamma_{HPO_4}}{-\log \gamma_{PO_4}} = \frac{\log 0.03}{\log \gamma_{PO_4}} = \frac{(-2)^2}{(-3)^2} = \frac{4}{9},$$

then

$$\log \gamma_{PO_4} = -3.43, \text{ and } \gamma_{PO_4} = 10^{-3.43} = 0.0004.$$

However, the accuracy of this term is not critical, for the term $\frac{1}{\gamma_{PO_4}}$ will be negligible as compared to other terms in the denominator of our phosphate concentration relation.

We have the following dissociation constants: $K_2 = 10^{-7.2}$; $K_3 = 10^{12.2}$ (Roberson, 1966, p. D181), $K_{CaH_2PO_4} = 10^{1.41}$, $K_{CaHPO_4} = 10^{-2.74}$, $K_{CaPO_4} = 10^{6.46}$, $K_{MgHPO_4} = 10^{2.5}$, $K_{MgPO_4} = 10^{6.46}$ (estimated), $K_{NaHPO_4} = 10^{1.15}$, and $K_{KHPO_4} = 10^{1.04}$ (R. A. Gulbrandsen and C. E. Roberson, written commun., 1972).

Most thermodynamic data is referenced at 25°C, but the temperature of our sample at the time of collection was 40°C. However, it can be thermodynamically shown that for most reactions between ions that concern us, the change in the pK value is small over a 15°C temperature range. Where the heat of reaction, ΔH_R°, valid within the 25°–40°C temperature range, is expressed in kilocalories, the change in pK is equal to $-0.035\ \Delta H_R^\circ$. For the reactions of the dissociation of phosphoric acid these changes are seen as quite small, for at 25°C pK_2 and pK_3 are 7.2 and 12.2, and at 40°C they are 7.2 and 12.1. Owing to the many approximations we are forced to make in our treatment, our margins of error will often exceed small differences such as these; therefore we may still use data valid at 25°C. Substituting this data, our cation activities, and a total phosphate concentration (C_{PO_4}) of $10^{-4.72}$ m (1.6 mg/l), we obtain $[PO_4^{-3}] = 10^{-11.69}$, or $pPO_4 = 11.69$.

Since phosphate-hydrogen ion equilibrium dictates that

$$\frac{[PO_4^{-3}][H^+]}{[HPO_4^{-2}]} = 10^{-12.2} \text{ and } \frac{[HPO_4^{-2}][H^+]}{[H_2PO_4^-]} = 10^{-7.2},$$

then

$$pPO_4 + pH - pHPO_4 = 12.2 \text{ and } pHPO_4 + pH - pH_2PO_4 = 7.2,$$

which yield

$$pHPO_4 = 7.19 \text{ and } pH_2PO_4 = 7.69.$$

The activity of water was estimated as 0.75 ($pH_2O = 0.12$) by Polzer and Roberson (1967, p. C118) from data for the NaCl-H_2O system listed by Robinson and Stokes (1959). (All ion activities calculated in this paper are summarized in table 3.)

The appropriate ion activities may be multiplied to determine whether our sample is saturated with respect to various species. Our calculated ion activity products are compared in table 4 with values calculated for 25° and 40°C from heats of formation and entropy values (Garrels and Christ, 1965; Robie and Waldbaum, 1968; and Sillén and Martell, 1964). This comparison points to the conclusion that our sample is near equilibrium with respect to gypsum, aragonite, and calcite, and supersaturated with respect to dolomite, magnesite, and apatite. Such calculations are only suggestive for solutions of this nature, because the calculations involve the following assumptions: (1) the activity and ion complex dissociation constants for all ions are reasonably accurate, and (2) the sample's pH as measured by a pH electrode is accurate (such accuracy decreases with increasing ionic strength). The electrode method for determining ion activities depends on the assumed constancy of the reference electrode's liquid-junction potential for the unknown and for the calibrating standard. If there is a large difference in ionic strength between the unknown and the standard, the liquid-junction potential (caused by differences in mobility between cations and anions of the same absolute charge as they migrate across a membrane from one solution to the other) is probably not constant, and

Table 3.—*Ion activities*

Ion	Activity (molal)	p[ ]
Ca^{+2}	0.020	1.70
Mg^{+2}	.65	.19
Na^+	6.45	−.81
K^+	.045	1.35
H^+	$10^{-7.70}$	7.70
HCO_3^-	.00052	3.28
CO_3^{-2}	($pCO_3 = 10.33 + pHCO_3 - pH$ at 25°C)	5.91
OH^-	(pOH = 14.00 − pH at 25°C)	6.30
SO_4^{-2}	.0013	2.89
F^-	.000011	4.96
PO_4^{-3}	$10^{-11.69}$	11.69
HPO_4^{-2}	($pHPO_4 = pPO_4 - 12.2 + pH$ at 25°C)	7.19
$H_2PO_4^-$	($pH_2PO_4 = pHPO_4 - 7.2 + pH$ at 25°C)	7.69

Table 4.—*Comparison of solubility products and experimental ion activity products*

Species	pK_{s0} at 25°C	pK_{s0} at 40°C	ΔH_f°, S_f° source	p (ion activity product)	Comments
Aragonite ($CaCO_3$)	8.16	8.26	1	$pCa + pCO_3 = 7.61$	Present in lake sediments.
Calcite ($CaCO_3$)	8.35	8.45	1	$pCa + pCO_3 = 7.61$	Do.
Gypsum ($CaSO_4 \cdot 2H_2O$)	4.63	4.64	1	$pCa + pSO_4 + 2pH_2O = 4.83$	Do.
Monetite ($CaHPO_4$)	5.71	5.88	1	$pCa + pHPO_4 = 8.89$	Present on island, not in lake.
Brushite ($CaHPO_4 \cdot 2H_2O$)	5.62	5.64	1	$pCa + pHPO_4 + 2pH_2O = 9.13$	Do.
Dolomite ($CaMg(CO_3)_2$)	18.43	18.63	2	$pCa + pMg + 2pCO_3 = 13.71$	High-magnesium calcite present in lake sediments.
Magnesite ($MgCO_3$)	8.00	8.21	1	$pMg + pCO_3 = 6.10$	
Hydroxyapatite ($Ca_{10}(PO_4)_6(OH)_2$)	113.99	115.3	5	$10pCa + 6pPO_4 + 2pOH = 99.74$	Hydroxyfluorapatite present in lake sediments (no thermodynamic data available for this mineral).
Fluorapatite ($Ca_{10}(PO_4)_6F_2$)	120.86	121.82	3, 4	$10pCa + 6pPO_4 + 2pF = 97.06$	

Sources: 1. Garrels and Christ (1965, p. 408, 416).
2. Robie and Waldbaum (1968, p. 20, 22).
3. Roberson (1966, p. D180).
4. Sillén and Martell (1964, p. 183).
5. Kramer (1964, p. 637). (pK_{s0} at 40°C obtained by extrapolation of values at 0, 5, 15, 25, and 30°C)

the measured activity could be in error. The use of a saturated KCl solution as a salt bridge between the reference electrode and the test solution minimizes this problem unless the test solution's ionic strength is very high, as ours is.

With the admission that all of the above assumptions are suspect, the calculations, along with geological evidence (the physical presence of various minerals in lake sediment samples and elsewhere on the island), indicate that crude calculations for equilibrium in highly saline systems may have some merit.

REFERENCES CITED

Bowen, H. J. M., 1966, Trace elements in biochemistry: New York, Academic Press, 241 p.

Brown, Eugene, Skougstad, M. W., and Fishman, M. J., 1970, Methods for collection and analysis of water samples for dissolved minerals and gases: U.S. Geol. Survey Techniques Water Resources Inv., book 3, chap. A1, 160 p.

Butler, J. N., 1964, Ionic equilibrium—a mathematical approach: Reading, Mass., Addison-Wesley, 547 p.

Garrels, R. M., and Christ, C. L., 1965, Solutions, minerals, and equilibria: New York, Harper and Row, 450 p.

Garrels, R. M., and Thompson, M. E., 1962, A chemical model for sea water at 25°C and one atmosphere total pressure: Am. Jour. Sci., v. 260, no. 1, p. 57–65.

Goldberg, E. D., 1965, Minor elements in sea water, *in* Riley, J. P., and Skirrow, G., eds., Chemical oceanography, v. 1: New York, Academic Press, p. 163–196.

Ham, W. E., and Johnson, K. S., 1964, Copper in the Flowerpot Shale (Permian) of the Creta area, Jackson County, Oklahoma: Oklahoma Geol. Survey Circ. 64, 32 p.

Harned, H. S., and Owen, B. B., 1967, The physical chemistry of electrolytic solutions: New York, Reinhold, 803 p.

Hutchinson, G. E., 1950, The biogeochemistry of vertebrate excretion: Am. Museum Nat. History Bull., v. 96, 594 p.

Kramer, J. R., 1964, Sea water: Saturation with apatites and carbonates: Science, v. 146, no. 3644, p. 637–638.

Polzer, W. L., and Roberson, C. E., 1967, Calculation of ion activity products for a brine from the Bonneville Salt Flats, Utah, *in* Geological Survey Research 1967: U.S. Geol. Survey Prof. Paper 575-C, p. C116–C119.

Roberson, C. E., 1966, Solubility implications of apatite in sea water, *in* Geological Survey Research 1966: U.S. Geol. Survey Prof. Paper 550-D, p. D178–D185.

Robie, R. A., and Waldbaum, D. R., 1968, Thermodynamic properties of minerals and related substances at 298.15°K (25.0°C) and one atmosphere (1.013 bars) pressure and at high temperatures: U.S. Geol. Survey Bull. 1259, 256 p.

Robinson, R. A., and Stokes, R. H., 1959, Electrolyte solutions: London, Butterworths, 559 p.

Schlanger, S. O., and Tracey, J. I., Jr., 1970, Dolomitization related to recent emergence of Jarvis Island, Southern Line Islands (Pacific Ocean): Geol. Soc. America Abs. with Programs, v. 2, no. 7, p. 676.

Sillén, L. G., and Martell, A. E., 1964, Stability constants of metal-ion complexes: London, The Chemical Society, 754 p.

Jour. Research U.S. Geol. Survey
Vol. 1, No. 1, Jan.–Feb. 1973, p. 113–115

A RAPID METHOD FOR THE DETERMINATION OF RADIOACTIVE CESIUM ISOTOPES IN WATER

By V. J. JANZER, Lakewood, Colo.

Abstract.—Radioactive cesium in water is concentrated by ion-exchange on finely divided ammonium hexacyanocobalt ferrate (NCFC), and then determined by beta counting. No carrier is added, and the method can be used to determine beta-emitting cesium isotopes at the 10-pCi/l level using a 100-ml sample. Five samples can be prepared for counting in approximately 3 hours, and the method is applicable to fresh and saline waters.

Eleven radioactive cesium isotopes, and stable cesium-133, which yields radioactive cesium-134 by a neutron-gamma reaction, are produced by the slow neutron fission of uranium-235. Most of the radiocesium isotopes have such short half lives that they are of little importance in natural waters. The longer lived isotopes, cesium-134 and cesium-137, have been deposited over most of the earth's surface primarily as the result of nuclear weapons use and testing.

Cesium-137 is produced in excess of 6-percent yield by thermal neutron fission of uranium-233, uranium-238, plutonium-239, and thorium-232 (Finston and Kinsley, 1961). Owing to a 30-year half life, cesium-137 and daughter barium-137m account for approximately 8 percent of the total activity of 2-year-old fission products (U.S. Public Health Service, 1960).

Detectable quantities of cesium-137 may consequently be found in most surface water, in surficial soil, and in most land plants and animals. The relatively high fission yield of cesium-137 combined with a half life of 30 years and a physiological similarity to potassium account for its importance as a potential water pollutant and a biological hazard. Measurements of the cesium-137 concentrations which occur in natural waters are necessary to evaluate its movement and fate in the hydrologic environment.

Many techniques for the separation and determination of radiocesium are given by Finston and Kinsley (1961). Most of these techniques, however, are time consuming or are not satisfactory for the determination of cesium at the picocurie per liter levels in relatively small-volume samples.

Prout, Russell, and Groh (1965) reported the determination of cesium-137 by gamma counting methods, using the inorganic salt, potassium hexacyanocobalt(II) ferrate(II) (KCFC), as a highly specific ion exchanger.

Boni (1966) described the use of KCFC for the rapid determination of radiocesium in milk, urine, sea water, and environmental samples by various gamma counting techniques. He reported a detection limit of 3 pCi/l, using a 1-gallon water sample and a 9- by 9-inch sodium iodide crystal with 3- by 6-inch well in a gamma spectrometer system. Direct concentration of radiocesium from water samples was hindered by absorption of ruthenium, zirconium, niobium, cobalt, and zinc.

With the exception of cobalt, these interferences were eliminated by preparing the sample in 1 *N* HCl and 0.5 *N* HF. Elimination of all radionuclide interferences including cobalt was reported when the hydrochloric acid concentration was increased to 10 *N*. No cobalt or zinc radioactivity was detected by gamma spectrum analyses of the samples which Boni analyzed by this technique.

Ellenburg and McCown (1968) described a batch technique in which KCFC was used to separate cesium-137 from a mixture of fission products in normal reactor fuel solutions. They reported that 50 mg of 60-mesh KCFC in contact with 50 ml of solution for more than 5 minutes was sufficient to enable complete recovery of all cesium-137 present. Samples ranging in activity from approximately 2×10^4 to 2×10^6 cpm were analyzed by use of a 3- by 3-inch NaI (Tl) crystal and a multichannel analyzer.

Petrow and Levine (1967) reported the use of ammonium hexacyanocobalt ferrate (NCFC) as an improved inorganic exchange material for the determination of cesium-137. The use of the ammonium-ion-exchange salt rather than the potassium salt resulted in much purer gamma spectra and enabled the measurement of exchanged cesium at lower detection levels.

Batch exchange of cesium-137 from dilute solutions by means of NCFC, and subsequent beta counting by the use of low background proportional counting systems has been used by this laboratory to rapidly determine cesium-137 at levels as low as 1–5 pCi/l.

APPARATUS AND REAGENTS

Beta counter, low-background. Sharp Widebeta automatic proportional counter, thin-window, flowing-gas.

Filtration apparatus:
Ring and disk assemblies to accommodate 47-mm filters.
Millipore Sterifil plastic 47-mm filter holder.
Nitrocellulose membrane filters, 0.45 μm, 47-mm diameter.
Plastic film, kitchen-wrap type.
Teflon beakers, 100- to 800-ml capacity.
Ammonium hexacyanocobalt ferrate (NCFC). Prepared as described by Petrow and Levine (1967) and sieved to pass 100-mesh screen.
Cesium-137 standardized solution. Obtained commercially. Contains about 100 pCi/ml of cesium-137.

PROCEDURE

1. Transfer a measured volume of sample to a Teflon beaker of suitable size. A sample of 100 to 500 ml is usually adequate.
2. Filter the sample through a 0.45-μm nitrocellulose membrane filter if turbid.
3. Add concentrated hydrochloric and hydrofluoric acids to adjust the acidity to 1.0 *N* in HCl and 0.5 *N* in HF, respectively. Handle samples in hood, and use plastic gloves and appropriate precautions required with hydrofluoric acid. For a 500-ml sample, add 45 ml of concentrated HCl and 10 ml of concentrated HF; this results in a final volume of approximately 550 ml. For smaller samples, use proportionately smaller volumes of acid.
4. Stir to mix.
5. Add 100 mg (±1 mg) of NCFC fines, and stir for 5 to 10 minutes on a stir plate.
6. Remove from stir plate, allow fines to settle, and filter through a 0.45-μm, 47-mm diameter nitrocellulose filter by using suction. By means of liquid still remaining in the beaker in the last stages of filtration, transfer the major part of the NCFC fines to the filter to produce a uniform deposit, then release suction and transfer the clear filtrate to the Teflon beaker.
7. Filter the solution through the NCFC pad a second time, and quantitatively transfer all the NCFC remaining in the beaker to the filter.
8. Rinse the beaker with several small volumes of distilled water; rinse down the funnel sides, and wash the filter and retained NCFC several times. To maintain a uniform deposit do not disturb the filter pad.
9. Apply suction until the pad is free of wash water, and then mount on a ring and disk assembly and dry under a heat lamp.
10. Cover with a single layer of plastic film, and count in the beta counter. Three 50-minute counts are generally adequate.
11. Prepare blank NCFC planchets by slurrying 100 mg of NCFC fines in a volume of 0.5 *N* HF–1.0 *N* HCl equal to the volume of the samples to be analyzed and prepared in the same manner as the samples.
12. Prepare cesium-137 standards in triplicate, each with 100 mg of NCFC in the same volume of mixed hydrochloric-hydrofluoric acids as the samples plus 5-ml parts of approximately 100 pCi/ml of cesium-137 standard solution. The ring-and-disk standards can be used repeatedly if the plastic covers are not torn and NCFC is not lost.

CALCULATIONS

Cesium-137 concentrations in the samples analyzed are determined by the following calculations:

1. Determine the standard deviation of the net counting rate, as described by Barker and Robinson (1963), from the equation:

$$\sigma_N = \left(\frac{B}{t_b} + \frac{R}{t_s}\right)^{1/2},$$

where

σ_N = standard deviation of the net counting rate,
B = blank counting rate, in counts per minute,
t_b = time, in minutes, that blank was counted,
R = gross sample counting rate, in counts per minute, and
t_s = time, in minutes, that sample was counted.

2. If the net counting rate is equal to or in excess of two standard deviations of the net counting rate, that is, $R - B \geq 2\sigma_N$, calculate the cesium-137 concentration in the sample from the equation:

$$\text{Cesium concentration, in picocuries per liter} = \frac{1{,}000}{V}\left[\frac{(R-B)\pm 2\sigma_N}{E}\right],$$

where

E = counting efficiency of system, in counts per minute per picocurie, and
V = volume of sample analyzed, in milliliters.

Counting efficiency (E) of the system is determined by:

$$E = \frac{(R_s - B)}{V_s C_s},$$

where

R_s = gross counting rate of standard, in counts per minute,
V_s = volume of standard solution used, in milliliters, and
C_s = concentration of cesium-137 standard, in picocuries per milliliter.

3. If the net counting rate does not exceed two standard deviations of the net counting rate, report the result as less than the minimum detection level (MDL). The MDL is calculated from the equation

$$\text{Cs-137 MDL} = \frac{2\sigma_N\,(1{,}000)}{EV}.$$

Precision data for this method based on replicate analysis of duplicate samples are not available. However, based only on counting statistics, the 95-percent confidence limit, that is, two standard deviations of the net counting rate for 1 pCi of cesium-137 determined in 100 ml of sample and yielding a net count of 0.6 cpm, could be calculated as follows:

$$2\sigma_N = 2\left(\frac{2.2}{100}+\frac{2.8}{100}\right)^{1/2}$$

$$= 2(0.224)$$

$$= 0.448 \text{ cpm.}$$

The net counting rate 0.6 cpm exceeds 0.448 cpm ($2\sigma_N$), and a value and error is calculated and reported as follows:

$$\text{Cs-137 pCi/l} = \frac{1{,}000}{V}\,\frac{(2.8-2.2)\pm 2\sigma_N}{E}$$

$$= 10\,\frac{0.6\pm 0.45}{0.6}$$

$$= 10\pm 7.5 \text{ pCi/l.}$$

DISCUSSION

Strontium-90 present in some of the samples was found to interfere in the determination of cesium by the NCFC method. The short-lived daughter of strontium-90, yttrium-90, as well as cesium was absorbed by the NCFC exchanger. Boni (1966) reported the elimination of zirconium-95, niobium-95, ruthenium-103, and ruthenium-106 fission product interference when using gamma counting to determine cesium absorbed on KCFC by preparing the sample in 1 *N* HCl and 0.5 *N* HF prior to ion exchange. Similar acidification of the samples analyzed in this study using NCFC, eliminated the yttrium-90 interference. No other interfering fission product activity detectable by gamma spectroscopy was present in the samples tested.

If cesium-134 as well as cesium-137 is present in the sample, and the ratio of the concentrations of these two nuclides is desired, other techniques such as those described by Yamamoto (1966) must be used.

A plastic filtration apparatus is necessary for filtering the mixed hydrochloric-hydrofluoric acidified samples. The fritted glass filter support in the usual vacuum filter apparatus disintegrates rapidly when used with hydrofluoric acid solutions.

A lower recovery and counting efficiency was obtained for 500-ml than for 100-ml standards. Counting efficiency for standards prepared in volumes of 100 and 500 ml using 100 mg of NCFC mounted and counted in the matter described has ranged from 0.56 to 0.69 cpm/pCi of cesium-137. The results shown in table 1 were calculated by using an average counting efficiency of 0.64 and 0.60 cpm/pCi of cesium-137 for sample volumes of 100 and 500 ml, respectively.

All standards listed in table 1 were counted for 100 minutes. Blank planchets prepared in the same manner but without added cesium-137 counted an average of 2.21 cpm.

To minimize variations in the cesium-absorption efficiency of NCFC with variations in solution volumes, all samples are adjusted to the same volume or a set of standards is prepared that spans the volume range of the samples to be analyzed. The samples are stirred with the NCFC and filtered, and the filtered solution is refiltered through the exchanger bed to further increase the degree of contact and improve the precision of the method.

Table 1.—*Recovery of cesium-137 from standard solutions*

Sample No.	Standard volume (ml)	Cesium-137	
		Added (pCi)	Found (pCi)
1	100	11	10.5
2	100	11	11.5
3	100	23	21.9
4	100	23	22.6
5	100	56	58.6
6	100	56	57.8
7	100	113	108
8	100	113	115
9	500	11	12.6
10	500	11	11.0
11	500	56	56.9
12	500	56	54.1
13	500	113	107.4
14	500	113	105.5

REFERENCES CITED

Barker, F. B., and Robinson, B. P., 1963, Determination of beta activity in water: U.S. Geol. Survey Water-Supply Paper 1696-A, 32 p.

Boni, A. L., 1966, Rapid ion exchange analysis of radiocesium in milk, urine, sea water and environmental samples: Anal. Chemistry, v. 38, no. 1, p. 89–92.

Ellenburg, E. J., and McCown, J. J., 1968, Rapid carrier-free method for the radiochemical determination of cesium-137: Anal. Letters, v. 1, no. 11, p. 697–706.

Finston, H. L., and Kinsley, M. T., 1961, The radiochemistry of cesium: U.S. Dept. Commerce Nuclear Sci. Ser. NAS-NS, no. 3035, 68 p.

Petrow, H. G., and Levine, H., 1967, Ammonium hexacyanocobalt ferrate as an improved inorganic exchange material for determination of cesium-137: Anal. Chemistry, v. 39, no. 3, p. 360–362.

Prout, W. E., Russell, E. R., and Groh, H. J., 1965, Ion exchange absorption of cesium by potassium hexacyanocobalt (II) ferrate (II): Jour. Inorganic and Nuclear Chemistry, v. 27, p. 473–479.

U.S. Public Health Service, 1960, Radiological health handbook: U.S. Dept. Health, Education and Welfare, 468 p.

Yamamoto, S., 1966, Analysis of cesium-134–cesium-137 mixtures by gamma ray spectrometric methods: Anal. Chemistry, v. 38, no. 9, p. 1261–1264.

Jour. Research U.S. Geol. Survey
Vol. 1, No. 1, Jan.–Feb. 1973, p. 117–120

EFFECT OF SEPTIC-TANK WASTES ON QUALITY OF WATER, IPSWICH AND SHAWSHEEN RIVER BASINS, MASSACHUSETTS

By GEORGE B. MORRILL III and LARRY G. TOLER,
Boston, Mass.

Abstract.—Many housing projects in the metropolitan area of Boston are beyond the reach of municipal sewer systems. Waste water disposed of through septic-tank or cesspool systems percolates to ground-water reservoirs and eventually reaches the streams. The dissolved-solids load in the streams receiving septic-tank effluent is increased by an amount that can be predicted from the housing density. In the study area, highway deicing salts are the only materials other than septic-tank discharge that contribute to water-quality degradation. The effect of these salts on the relationship with housing density is eliminated by subtracting the specific conductance due to sodium chloride from the measured specific conductance of a water sample. The difference is called residual conductance and is proportional to the dissolved-solids content minus the concentration of sodium chloride.

Development of housing beyond the reach of municipal sewer systems of metropolitan areas has lowered the quality of the environment in many of the developments and has created health hazards in others. Waste-water disposal through septic tanks and cesspools is common practice in many developments in the Boston area. The purpose of this study is to determine if there is a relationship between the number of septic-tank disposal systems in a drainage basin and some parameter describing quality of water in streams draining the basin.

LOCATION AND DESCRIPTION

Seventeen small drainage basins, all but one less than 1 square mile in area, were selected for study. All are in the Ipswich and Shawsheen River basins (fig. 1), in the communities of Andover, Burlington, North Reading, Tewksbury, Wilmington, and Peabody, Mass. All the basins are served by public water supplies, but none have municipal sewer systems, and individual houses are served by on-site disposal systems. The basins differ considerably in size, stream gradient, topography, amount of drainage through culverts, and age of houses; housing density ranges from 0 to 900 units per sq mi.

Typically, the drainage basins are characterized by low rounded hills surrounded by swamp-dotted lowlands where drainage is generally poor. The low hills are underlain by

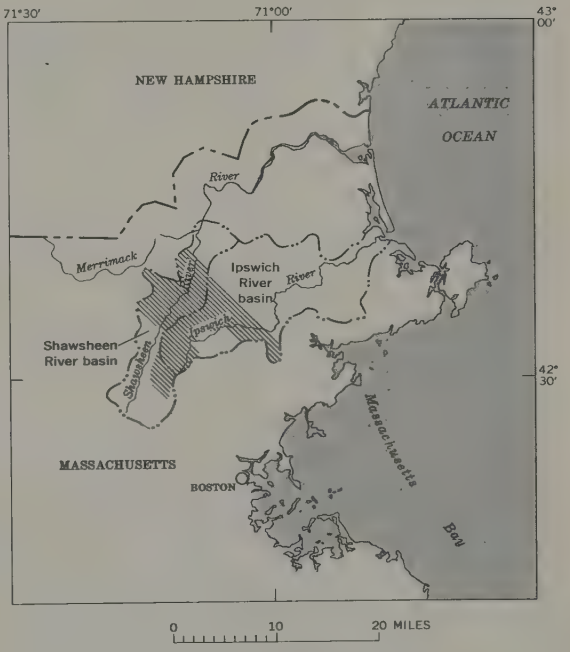

Figure 1.—Index map showing location of study area (patterned) in northeastern Massachusetts.

bedrock or glacial till—a relatively impermeable mixture of unsorted silt, sand, rounded to angular gravel, and boulders. The till forms a thin mantle overlying bedrock. In the lowlands the till is covered by permeable sand and gravel. Many of the housing developments are located in the lowlands because the level terrain is easy to develop and the good soil permeability permits installation of on-site disposal systems. The water table is only a few feet below land surface, and about one-fifth of the area is subject to seasonal flooding (Sammel and others, 1966, p. 6). The high water table and flooding make operations of on-site disposal systems inefficient at least part of the year.

Streams draining developed areas are frequently malodorous and support a luxuriant growth of weeds and brush. Residents with whom the problems have been discussed have expressed their concern about the sanitary and esthetic qualities of the streams, and some have prevailed upon public health officials to take action. The action, for the most part, has been to install culverts to convey the streams underground through the developments to swamps. Many of the swamps into which these streams flow contain foul-smelling stagnant water. The absence of other obvious sources of the foul smell suggests that it comes from domestic waste-water disposal systems by way of ground-water seepage into the streams.

The 17 small basins were chosen to meet two requirements: (1) that they were drained by a stream or ditch from which representative base-flow samples could be taken, and (2) that they had no apparent source of extraneous material other than septic-tank and cesspool wastes and highway deicing chemicals.

METHOD OF STUDY

Base runoff from ground-water discharge in the Ipswich River basin averages approximately 13 inches per year, or 6.2×10^5 gpd per sq mi (Sammel and others, 1966, p. 52). Although ground-water discharge can be expected to vary considerably in small basins having a wide range of terrain and ground cover, 13 inches per year is used as an average.

Average water consumption in east coast suburbs with metered water and septic tanks was determined by Linaweaver, Geyer, and Wolff (1967) to be 245 gpd per dwelling, of which 42 gpd was used for irrigation of lawns and gardens. Unmetered areas were found to use more water for lawns but about the same for household purposes. Septic-tank flow per house is estimated to be 200 gpd.

The 42 gpd or more used for watering gardens, lawns, and shrubs is applied during the growing season, a time when evapotranspiration normally exceeds precipitation. Most of this water is evaporated and transpired, so little reaches the water table and does not contribute significantly to base flow of streams. The water applied for irrigation, therefore, is not included in this analysis.

Samples of water from the streams were collected periodically during periods of base flow from March through August 1968. The samples were analyzed in the field for chloride concentration and specific conductance and the results averaged for each site.

The specific electrical conductance of water is a good indicator of its dissolved-solids content. Because the measurement is easy to make, specific conductance is widely used in geochemical studies of water. For natural water, the dissolved solids, in milligrams per liter, usually range from 0.55 to 0.75 times the specific conductance, in micromhos per centimeter at 25°C (Hem, 1959, p. 40).

Highway salting in most of the basins affects both chloride concentration and conductivity. To correct for this effect, a residual conductivity, the difference between the measured specific conductance and that calculated to be caused by sodium chloride, the principal highway deicing agent, was used for defining the quality of the water. The residual conductivity is proportional to the dissolved-solids content minus the sodium chloride concentration. The specific conductance of sodium chloride is approximately 3.5 times the chloride concentration, in milligrams per liter.

Average values of specific conductance and chloride concentration for natural water were obtained by sampling several small unpolluted streams in the basins during base flow. The average specific conductance was 48 μmhos, and the average concentration of chloride was 5 mg/l. The average residual conductance is 30 μmhos.

Almost no data are available defining septic-tank effluent in terms of the concentrations of its dissolved constituents. Published data on untreated sewage do not include specific conductance. An average residual conductivity of 785 μmhos was determined from analysis of two samples of septic-tank liquor from the project area. The concentration of chloride was about 50 mg/l higher than that of the tapwater entering the septic tank.

Tapwater contributes significant concentrations of some minerals to the ground water. Chloride concentrations of tapwater samples taken in the towns in the study area ranged from 17 to 54 mg/l and averaged about 35 mg/l. Residual conductance ranged from 87 to 150 μmhos and averaged 120 μmhos.

Base flow in the basins is derived from precipitation and imported municipal water. Some precipitation percolates to the water table, forming "natural" ground water, whereas the municipal water is used in homes and discharged to ground-water reservoirs by way of septic tanks and cesspools. If the storage of both water and dissolved solids in the aquifer is assumed to be constant, the dissolved-solids load, in excess of that of natural ground water, leaving the ground-water reservoir by way of base flow is the sum of the loads carried in by precipitation and septic-tank effluent.

Description of terms

A = Drainage basin area (sq mi).
n = Number of houses in the basin (houses).
d = Housing density = n/A (houses per sq mi).
q_b = Average annual base flow per unit area (gpd per sq mi).
q_n = Natural base flow per unit area derived from average annual infiltration of precipitation (gpd per sq mi).
q_s = Average combined septic-tank and cesspool flow per house (gpd per house).
C = Quality parameter, concentration in base flow.
C_n = Quality parameter, concentration in natural ground water.
C_s = Quality parameter, concentration in domestic septic-tank effluent.

Calculations

The average annual base flow of a specific drainage basin is equal to the sum of two components, one derived from precipitation and one derived from septic tank effluent, according to the equation

$$q_b A = q_n A + q_s n, \quad (1)$$

which may be made more general by eliminating the terms for area and restating equation 1 in terms of housing density as

$$q_b = q_n + q_s d. \quad (2)$$

This equation multiplied by the appropriate concentrations of the quality parameter yields

$$q_b C = q_n C_n + q_s d C_s. \quad (3)$$

When one combines equations 2 and 3 to express base-flow concentration, C, as a function of housing density, one obtains the working equation

$$C = \frac{C_n}{1+\frac{q_s d}{q_n}} + \frac{C_s}{1+\frac{q_n}{q_s d}}. \quad (4)$$

This equation for C gives the average annual base-flow concentration of any contaminant for which C_n and C_s can be determined.

The residual conductance in base flow (C_{RC}) in the study area in terms of housing density may be estimated by substituting the following in equation 4:

C_n = residual conductance in natural water (average 30 μmhos),
C_s = residual conductance in septic-tank effluent (average 785 μmhos),
q_s = 200 gpd per house, and
q_n = 6.2×10^5 gpd per sq mi,

which results in

$$C_{RC} = \frac{93{,}000 + 785d}{3{,}100 + d}. \quad (5)$$

Figure 2 was developed to evaluate sampling sites and to identify those with probable sources of extraneous material other than domestic waste water. The graph in figure 2 was developed for chloride but should be adaptable to other parameters. To use the graph, the specific conductance and concentration of chloride of a sample of water from a study site and the average concentration of chloride in public water serving the study site must be known.

A line from a point (X) representing the specific conductance and chloride concentration of a sample, drawn parallel to the housing-density lines, intercepts the horizontal specific-conductance scale at the value for residual conductance. The concentration of chloride contributed by domestic waste water is read on the vertical chloride scale at the intercept of a horizontal line from the point (O), where the line, previously drawn parallel to the housing-density lines, intersects a line representing average concentration of chloride in tapwater. The difference between the concentration of chloride in the sample and the concentration of chloride from domestic waste water represents chloride from other sources. The initial plot of specific conductance and chloride concentration should lie on or near the housing-density line, approximating the housing density in the basin. If this plot does not approximate the actual housing density, extraneous material other than domestic waste and sodium chloride is indicated.

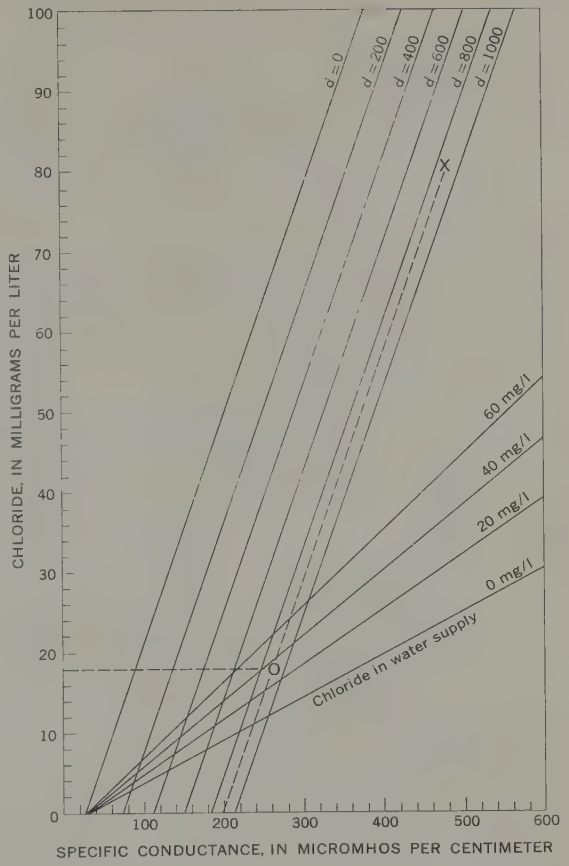

Figure 2.—Graph to evaluate sampling sites for sources of extraneous material in terms of residual conductance and chloride. See text for explanation of use.

RESULTS

The residual conductivity data from the 17 sites in table 1 generally agree with the relationship predicted by equation 5 (fig. 3) and indicate that most dissolved solids from septic-tank systems reach the streams. The dissolved-solids-accretion scale

Table 1.—*Sampling site data*

Site No.	Housing density in drainage basin (houses per sq mi)	Drainage basin area (sq mi)	Average specific conductance (μmhos at 25°C)	Average base-flow residual conductivity (μmhos)	Average chloride (mg/l)	Number of samples
	d	*A*	*C*	C_{RC}		
1.....	0	0.031	46	29	5	1
2.....	75	.120	94	59	10	3
3.....	105	.210	53	35	5	2
4.....	150	.040	52	34	5	3
5.....	170	.110	144	102	12	3
6.....	275	.215	187	124	18	2
7.....	325	.037	174	108	19	3
8.....	350	.210	170	128	15	6
9.....	360	.165	176	89	25	3
10.....	370	.165	127	78	14	5
11.....	440	.032	140	98	12	1
12.....	510	1.85	474	173	86	5
13.....	585	.075	292	128	47	4
14.....	590	.027	225	180	13	2
15.....	730	.115	225	155	20	8
16.....	830	.420	440	177	75	5
17.....	900	.525	434	210	64	4

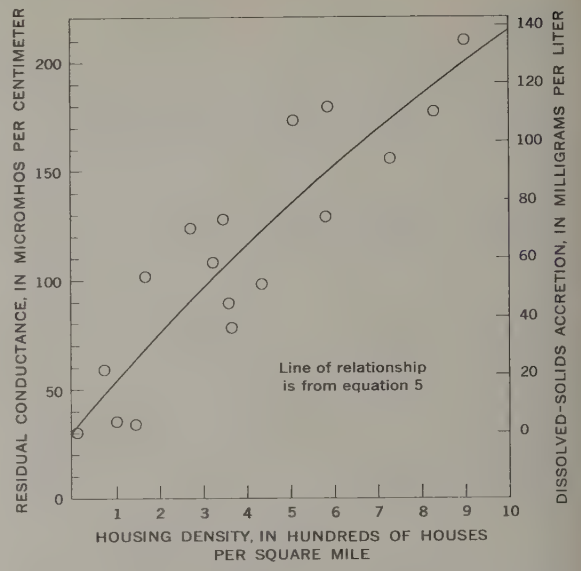

Figure 3.—Relationship of housing density to residual conductance and accretion of dissolved solids in base flow of streams.

on the right of figure 3 shows the estimated increase of dissolved solids in base runoff caused by various housing densities. Dissolved-solids accretion was calculated by multiplying the increase in residual conductance in base flow of a polluted stream over that of natural ground water by 0.65 (Hem, 1959, p. 40) and adding the increase in dissolved solids caused by domestic waste-water chloride (50 mg/l concentration of chloride in 200 gpd per house), which was excluded from residual conductance.

The scatter of the data points in figure 3 may be in large part due to deviations from the average values used for (1) volume of infiltration and subsequent ground-water discharge, (2) concentration of chloride in public water supplies, and (3) volume of septic-tank effluent. Undetected sources of extraneous material may also cause deviation from the line of relationship predicted from equation 5.

The graph indicates that the amount of dissolved solids in base flow of streams is dependent on housing density. In the range of housing densities observed, dissolved solids in stream base flow can be expected to increase 10 to 15 mg/l per 100 houses per sq mi.

REFERENCES CITED

Hem, J. D., 1959, Study and interpretation of the chemical characteristics of natural water: U.S. Geol. Survey Water-Supply Paper 1473, 269 p. [4th printing, 1967]

Linaweaver, F. P., Jr., Geyer, J. E., and Wolff, J. B., 1967, Summary report on the residential water use research project: Am. Water Works Assoc. Jour., no. 3, v. 59, p. 267–270.

Sammel, E. A., Baker, J. A., and Brackley, R. A., 1966, Water resources of the Ipswich River basin, Massachusetts: U.S. Geol. Survey Water-Supply Paper 1826, 83 p. [1967].

Jour. Research U.S. Geol. Survey
Vol. 1, No. 1, Jan.–Feb. 1973, p. 121–124

THE GREAT TUNISIAN FLOOD

By FRANK E. CLARKE, Washington, D.C.

Abstract.—In the autumn of 1969, unusual meteorological conditions over Europe and northern Africa caused an enormous persistent desert storm in Tunisia and eastern Algeria. Poorly developed drainage patterns and gypsum-encrusted surfaces of these desert regions intensified effects of the storm and contributed to the heavy loss of life and property. Destruction of Roman bridges suggests that such storms may have recurrence probabilities of several thousands of years. The event also suggests that, although desert storms are less frequent than those of temperate regions, they can be similar in magnitude.

Collection of field data for a U.S. Geological Survey report (Clarke and Jones, 1972) was brought to a close prematurely on September 25, 1969, by a desert storm and resulting flood of enormous proportions—an event with a presumed recurrence interval of thousands of years. This summary is provided to document the relatively few facts available on a rare type of meteorological phenomenon which undoubtedly has affected desert hydrology significantly through geologic time.

Meteorologists attribute the unusual storm to a shift in the Azores high-pressure pattern from lat 35° N., the normal center, to 45° N. This change reduced rainfall and resulted in unusually warm and sunny weather in most of Europe during the summer of 1969. Apparently, it also triggered movement of cool air from Europe toward the Mediterranean Sea, and meteorological conditions over North Africa directed the moisture-laden northern airmass across Tunisia to the Atlas Mountains, where it stalled on September 25, 1969, and created the persistent cyclonic pattern shown in figure 1.

FACTORS AFFECTING SEVERITY OF DAMAGE

Geologic and hydrologic factors.—The area of Tunisia and adjoining Algeria immediately south of the Atlas Mountains receives little rainfall, about 7.5 cm (3 inches) per year. Its surface drainage pattern is poorly developed, with a limited river (oued) network and many internal sinks (chotts).

The relatively high temperature and corresponding high evaporation rate, together with the abundance of calcium sulfate in both earth strata and ground waters, produce a gypsum-encrusted surface or subsurface which is highly impermeable to water. Windblown silt and sand which veneer the gypsum surface to shallow depths are relatively unstable and offer little resistance to wind and water.

Cultural factors.—Because of the dearth of precipitation, inhabitants of these semiarid and desert regions take little account of the possibility of occasional floods. Oueds and chotts, which are dry for the most part and gentle in grade, are systematically used for roads and other transportation routes. Villages encroach on ancient flood plains; buildings lack the substantial construction that predominates in more stormy climates, and they often occupy sites which can easily be isolated by high water. Pastures and related facilities involve the same hazards for livestock. Desert societies generally lack facilities for rapid response to natural disasters.

Precipitation.—Intense steady rainfall started late on the afternoon of September 25, after several hours of severe duststorms and intermittent thundershowers. Flooding in the relatively impermeable desert terrain was almost instantaneous over a wide area. In the study area near El Hamma, Tunisia, arroyos were raging torrents, and highways resembled oueds in less than 20 minutes. Forty centimeters (15 inches) of rain fell in the environs of Gabès, Tunisia, during the first 24-hour period—about 5 times the annual rainfall for the area. Figures 2, 3, 4, and 5 show the extent of early flooding. Intermittent heavy precipitation continued for 38 days. The author has been unable to obtain a figure for total rainfall or for variations in pattern over the 162,750 sq km (63,000 sq mi) affected.

FLOODING AND EFFECTS

Tunisia.—Nine of Tunisia's 13 provinces were seriously affected by overland runoff, filling of chotts, and flooding of oueds. Stages as much as 11 m (36 feet) above normal were recorded. The Zeroud and Marguelil oueds combined to form a single torrent 13 km (8 miles) wide. Innumerable flooded chotts, some as much as 13 km in diameter, existed at the end of the storm. The exceptional magnitude of flooding is indicated by the destruction of several massive Roman bridges which have stood the test of the elements for thousands of years.

The unique combination of meteorological, geologic, and cultural factors in the desert storm wreaked unbelievable

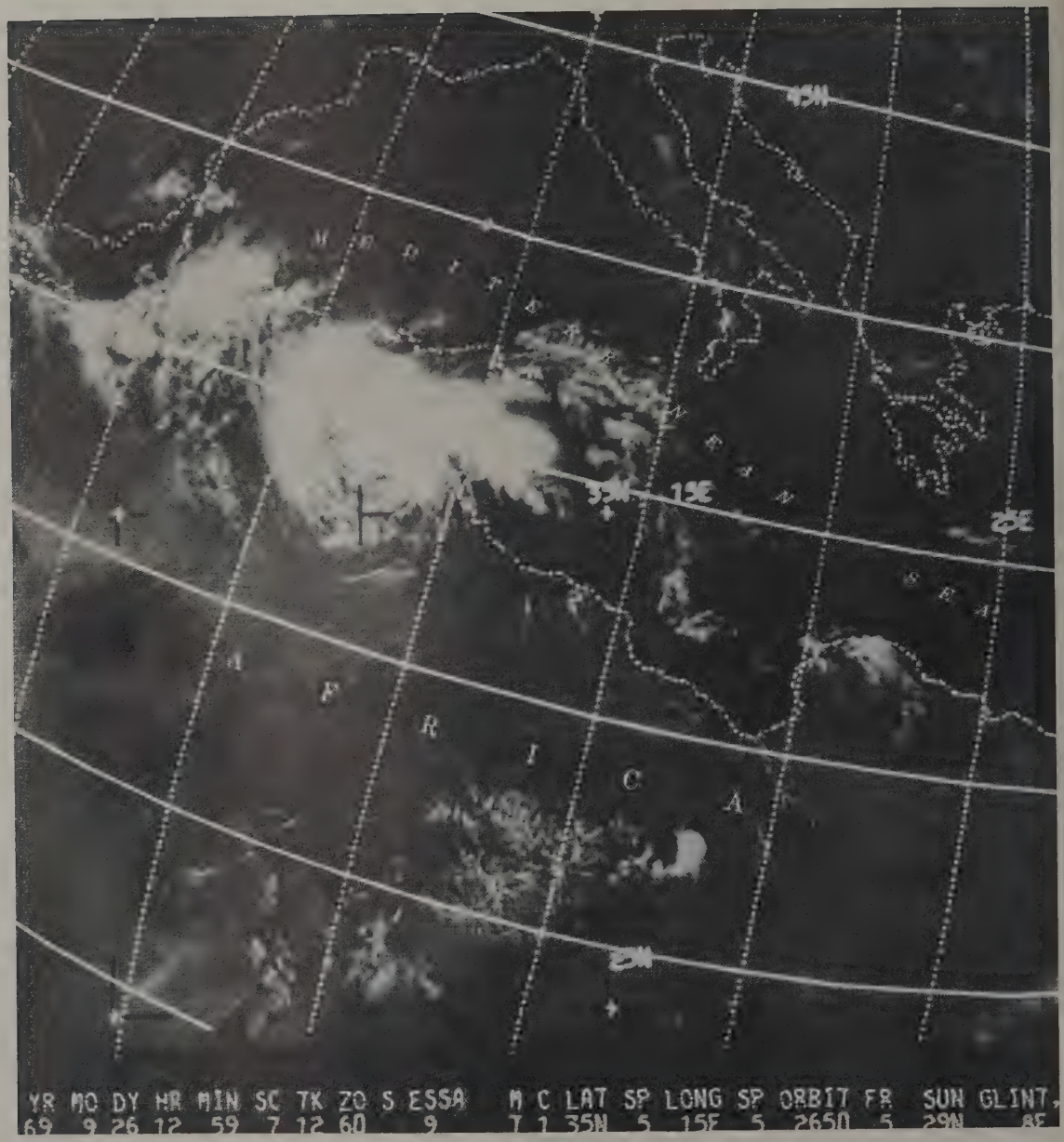
45N
35N
15E
25E
A F R I C A
25N
YR MO DY HR MIN SC TK ZO S ESSA M C LAT SP LONG SP ORBIT FR SUN GLINT
69 9 26 12 59 7 12 60 9 1 1 35N 5 15E 5 2650 5 29N 8E

Figure 1.—Storm pattern of record-breaking North Sahara flood. Photograph taken from Nimbus meteorological satellite.

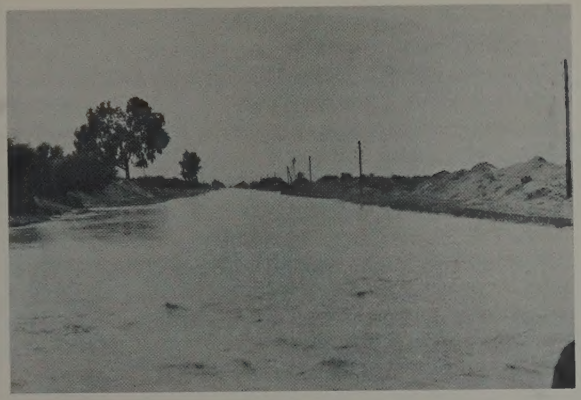

Figure 2.—Highway to Gafsa, 20 km (12.5 miles) west of Gabès, Tunisia, 18 hours after rain began.

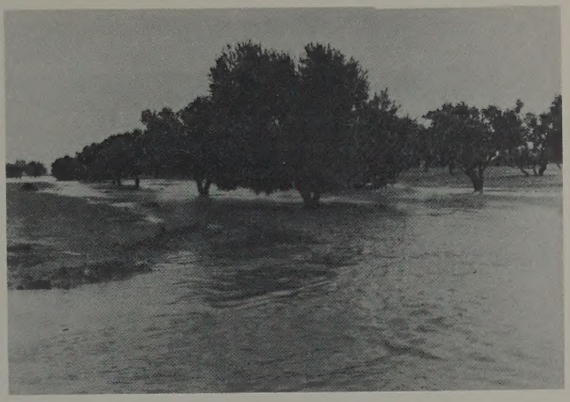

Figure 3.—Flooded olive grove, 20 km (12.5 miles) west of Gabès.

Figure 4.—Gabès-Sfax highway, 40 km (25 miles) north of Gabès, 42 hours after rain began.

havoc on Tunisia. The relatively small population of 4.5 million suffered 600 dead and 300,000 homeless. Other losses included an estimated 1 million livestock, 10,000 olive trees, 35 bridges, and virtually the entire network of highways and railroads in 80 percent of the country, including transportation links which serviced the vitally important phosphate industry at Gafsa. This disruption alone represented a loss to the country of $4.8 million weekly in mineral revenue during the time of outage.

The specific losses were accompanied by profound surface changes which literally revised the map of Tunisia. In the Kairouan Plain, 130 km (81 miles) south of Tunis, removal of 1 m (3 feet) of accumulated soil exposed a sizable Roman village. At the same time, the great flood deposited sediment

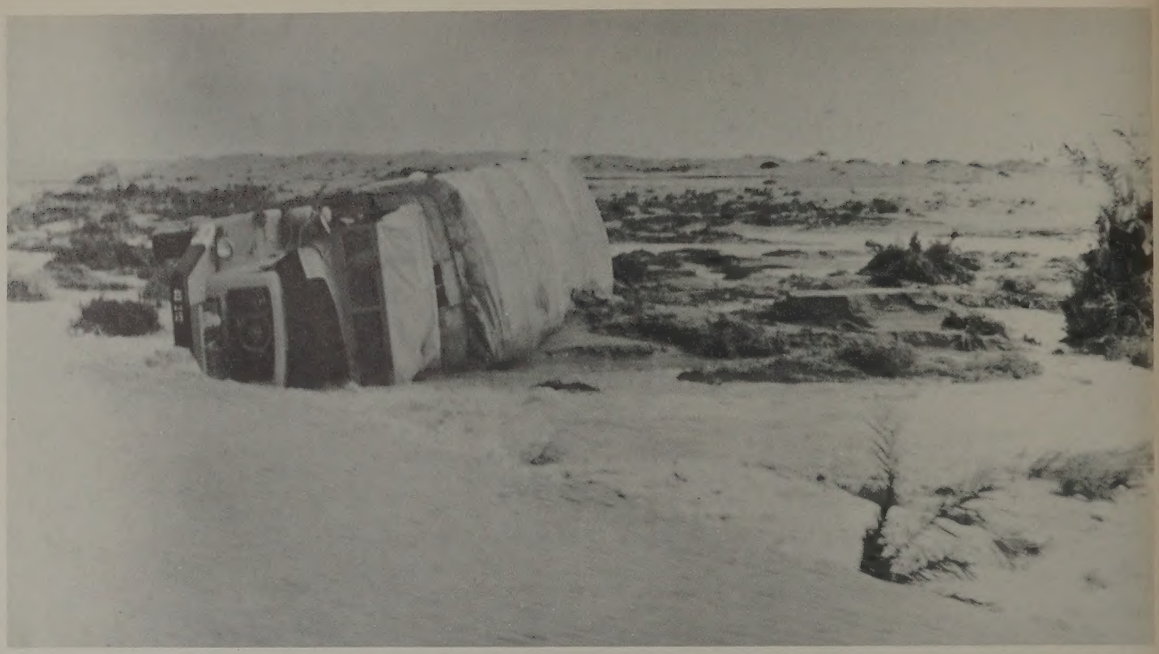

Figure 5.—Flood-damaged Gabès-Sfax highway, about 40 km (25 miles) north of Gabès. The highway followed an ancient broad, shallow drainage channel.

from 0.4 to 1.8 m (1 to 6 feet) in depth on a 14-km- (9-mile-) wide coastal plain between Gabès and Sfax, Tunisia, thereby converting the barren gypsum-encrusted area to fertile green pasture. Such alterations must have been widespread and highly significant. Similar changes undoubtedly have occurred at widely scattered intervals throughout time.

Algeria.—The somewhat smaller losses in neighboring Algeria are explained by the limited area affected. They included 60 dead (250 injured), 18,800 homes (13,000 damaged), 10,000 livestock, 2,000 hectares (5,000 acres) of crops, hundreds of trees, 50 km (31 miles) of rail line, and 2,600 wells. In final count, 91,000 people of Algeria were homeless, and total dollar value of damage in that country was approximately $96 million.

Response.—The Tunisian-Algerian flood was recognized from the beginning as an unusual natural disaster of international importance. At least 24 countries, including the United States, and a number of international organizations, sent prompt and substantial aid.

The U.S. Geological Survey worked with the United Nations Educational, Scientific, and Cultural Organization in an effort to document effects of the flood by aerial mapping and other remote-sensing techniques. Unfortunately, the plan could not be implemented.

Hydrologic significance.—Destruction of Roman bridges suggests a recurrence probability of thousands of years for desert storms of this kind. The long duration and great intensity of precipitation also suggest that, despite their infrequency, the magnitude of desert storms may equal that of temperate-zone storms.

REFERENCE CITED

Clarke, F. E., and Jones, B. F., 1972, Significance of ground-water chemistry in performance of North Sahara tube wells in Algeria and Tunisia: U.S. Geol. Survey Water-Supply Paper 1757-M. [In press]

RECENT PUBLICATIONS OF THE U.S. GEOLOGICAL SURVEY

(Books may be ordered from the Superintendent of Documents, Government Printing Office, Washington, D.C., 20402, to whom remittances should be sent by check or money order. Give title, series No., stock No. (shown in parentheses in this list), and catalog No. [shown in brackets])

Professional Papers

562-J. Summary of alluvial-channel data from Rio Grande conveyance channel, New Mexico, 1965–69, by J. K. Culbertson, C. H. Scott, and J. P. Bennett. 1972. p. J1–J49. 70¢. (2401-2184) [I 19:16:562-J]

599-J. The contributions of Ranger photographs to understanding the geology of the Moon, by N. J. Trask. 1972. p. J1–J16. 40¢. (2401-2111) [I 19:16:599-J]

689. Sedimentary processes and distribution of particulate gold in the northern Bering Sea, by C. H. Nelson and D. M. Hopkins. 1972. 27 p. 75¢. (2401-2107) [I 19:16:689]

698. Petrographic and chemical reconnaissance study of some granitic and gneissic rocks near the San Andreas fault from Bodega Head to Cajon Pass, Calif., by D. C. Ross. 1972. 92 p. $2.25. (2401-2090) [I 19:16:698]

707. Interpretation of an aeromagnetic survey of the Amchitka Island area, Alaska, by G. D. Bath, W. J. Carr, L. M. Gard, Jr., and W. D. Quinlivan. 1972. 25 p. $1.75. (2401-2087) [I 19:16:707]

714. Mineral resource evaluation of the U.S. Forest Service Sierra Demonstration Project area, Sierra National Forest, Calif., by J. P. Lockwood, P. C. Bateman, and J. S. Sullivan. 1972. 59 p. $1. (2401-2103) [I 19:16:714]

716-A. Geology and copper mineralization of the Saindak quadrangle, Chagai District, West Pakistan, by Waheeduddin Ahmed, S. N. Khan, and R. G. Schmidt. 1972. p. A1–A21. $1. (2401-2108) [I 19:16:716-A]

726-A. Aeromagnetic, Bouguer gravity, and generalized geologic studies of the Great Falls-Mission Range area, northwestern Montana, by M. D. Kleinkopf and M. R. Mudge. 1972. p. A1–A19. $1.75. (2401-2075) [I 19:16:726-A]

738. Silurian rugose corals of the Klamath Mountains region, California, by C. W. Merriam. 1972. 50 p.; 8 plates. $1. (2401-2077) [I 19:16:738]

739. Geology of Isla Desecheo, Puerto Rico, with notes on the great southern Puerto Rico fault zone and Quaternary stillstands of the sea, by V. M. Seiders, R. P. Briggs, and Lynn Glover III. 1972. 22 p. 45¢. (2401-2106) [I 19:16:739]

741. The quinary reciprocal salt system Na,K,Mg,Ca/Cl,SO_4–A review of the literature with new data, by J. J. Rowe, G. W. Morey, and C. S. Zen. 1972. 37 p. 50¢. (2401-2140) [I 19:16:741]

742. Characteristics of estuarine sediments of the United States, by D. W. Folger. 1972. 94 p. $1.25. (2401-2112) [I 19:16:742]

745. Geology and uranium deposits, Shirley Basin area, Wyoming, by E. N. Harshman. 1972. 82 p. $1.50. (2401-2138) [I 19:16:745]

749. Distribution of the Middle Ordovician Copenhagen Formation and its trilobites in Nevada, by R. J. Ross, Jr., and F. C. Shaw. 1972. 33 p.; 8 plates. 70¢. (2401-2109) [I 19:16:749]

751-A. Preliminary results of injecting highly treated sewage-plant effluent into a deep sand aquifer at Bay Park, N.Y., by John Vecchioli and H. F. H. Ku. 1972. p. A1–A14. 30¢. (2401-2181) [I 19:16:751-A]

753. Geophysical, geohydrological, and geochemical reconnaissance of the Luke salt body, central Arizona, by G. P. Eaton, D. L. Peterson, and H. H. Schumann. 1972. 28 p. 40¢. (2401-2161) [I 19:16:753]

755. Calorimeters for heat of solution and low-temperature heat capacity measurements, by R. A. Robie and B. S. Hemingway. 1972. 32 p. 40¢. (2401-2182) [I 19:16:755]

760. Paleomagnetism of some Lake Superior Keweenawan rocks, by K. G. Books. 1972. 42 p. 50¢. (2401-2180) [I 19:16:760]

Bulletins

1314-F. Trace-element contents of some plutonic rocks of the Sierra Nevada batholith, by F. C. W. Dodge. 1972. p. F1–F13. 55¢. (2401-2137) [I 19:3:1314-F]

1342. Massive sulfide deposits near Shellabarger Pass, southern Alaska Range, Alaska, by B. L. Reed and G. D. Eberlein. 1972. 45 p. $1. (2401-2088) [I 19:3:1342]

1372-B. Stratigraphic nomenclature of Cambrian and Lower Ordovician rocks of easternmost southern Arizona and adjacent westernmost New Mexico, by P. T. Hayes. 1972. p. B1–B21. 25¢. (2401-2183) [I 19:3:1372-B]

1377. Bibliography and index of U.S. Geological Survey publications relating to coal, 1882–1970, by Paul Averitt and Lorreda Lopez. 1972. 173 p. 75¢. (2401-2175) [I 19:3:1377]

Water-Supply Papers

1663-H. Origin of mineralized water in Precambrian rocks of the upper Paraíba basin, Paraíba, Brazil, by S. L. Schoff. 1972. p. H1–H38. 60¢. (2401-2143) [I 19:13:1663-H]

1798-K. Fluvial sediment in Salem Fork watershed, West Virginia, by R. F. Flint. 1972. p. K1–K29. 30¢. (2401-2165) [I 19:13:1798-K]

1938. Water supply for the Nuclear Rocket Development Station at the U.S. Atomic Energy Commission's Nevada Test Site, by R. A. Young. 1972. 19 p. $1.25. (2401-2069) [I 19:13:1938]

1939-D. Chemical quality of the water in the Tucson basin, Arizona, by R. L. Laney. 1972. p. D1–D46; plates in separate case. $4.25. (2401-2076) [I 19:13:1939-D]

2008. Sediment transport in a Mississippi River distributary–Bayou Lafourche, La., by W. H. Doyle, Jr. 1972. 48 p. 40¢. (2401-2197) [I 19:13:2008]

2016. Quality of surface waters of the United States, 1967–Parts 12–16, North Pacific slope basins, Alaska, and Hawaii and other Pacific areas. 1972. 431 p. $2. (2401-2174) [I 19:13:2016]

2021. Evaluation of yields of wells in consolidated rocks, Virginia to Maine, by D. J. Cederstrom. 1972. 38 p. 65¢. (2401-2159) [I 19:13:2021]

U.S. GOVERNMENT
PRINTING OFFICE
PUBLIC DOCUMENTS DEPARTMENT
WASHINGTON, D.C. 20402
OFFICIAL BUSINESS
PENALTY FOR PRIVATE USE $300

POSTAGE AND FEES PAID
U.S. GOVERNMENT
PRINTING OFFICE
375

U.S.MAIL